Optimisation of Autoselective Plasma Regeneration of Wall-Flow Diesel Particulate Filters

By

Karim Ladha (BEng Hons)

A doctoral thesis submitted in partial fulfilment of the requirements for the award of Doctor of Philosophy of Loughborough University

March 2010

Abstract

The increase in number of diesel powered vehicles has led to greater concern for the effects of their exhaust emissions. Engine manufacturers must now consider using diesel particulate filters to make their engines meet the legislated limits. Diesel particulate filters can remove more than 95% of the particulates from the exhaust flow but require cleaning, known as regeneration.

This thesis describes the research and optimisation of the Autoselective regeneration system for cordierite wall flow diesel particulate filters. The novel Autoselective technology uses an atmospheric pressure glow discharge plasma to selectively oxidise particulate matter (soot) trapped within the filter. The aim of this research was to produce a regeneration system that can operate under all exhaust conditions with a low energy demand and no precious metal dependence to compete with the numerous pre-existing technologies.

The effect of discharge electrode type and position on regeneration performance has been investigated in terms of regeneration uniformity, power requirement and regeneration rate. The results showed that the electrode orientation had a large effect on regeneration distribution and energy demand.

The electrode capacitance and breakdown voltage was shown to affect the choice of power supply circuit because not all power supply topologies were suitable for powering electrodes with >100 pF capacitance. A number of power supplies were designed and tested, a voltage driven resonant transformer type supply was shown to be optimal when used in conjunction with a swept frequency.

The current and frequency ranges of electrical discharges were continuously variable, and their effect on discharge regeneration performance was studied. The results showed that the discharge frequency had no effect on the regeneration process but did affect spatial distribution. An optimised resonant transformer power supply was designed that was ideally suited for the electrodes used. A novel power modulation strategy, which used a switching frequency phase locked to the

modulating frequency, was employed which extended the operating range of the discharge to below 10 mA for electrode separations > 7.5 mm.

The heat flows within the filter and discharge during regeneration were analysed and the filter damage process was linked to the heat released by the discharge inside the filter wall. Other filter materials were compared based on the findings and Mullite ceramic was identified as a potentially better filter material for Autoselective regeneration.

The filtration efficiency is important and was observed to be affected by the Autoselective process. The effect of the discharge on filtration efficiency was studied and the mechanism of particulate re-entrainment was identified as a combination of electrostatic and electro-acoustic forces.

The Autoselective technology was successfully implemented in both flow-rig and on-engine tests. Results showed significant reduction in back-pressure for power inputs of ~ 500 W. The understanding of the Autoselective regeneration system has been improved and the research resulted in a novel method of filter regeneration.

Table of Contents

Acknowledgements

Nomenclature

AC	Alternating Current
ADC	Analogue to Digital Converter
AFR	Air to Fuel Ration
b	Used as a generic variable type in some equations
Blow-off	PM ablated from the filter walls
Blow-through	PM that escapes through the filter
C	Capacitance
CCRT	Catalysed Continuously Regenerating Trap
CDPF	Catalysed Diesel Particulate Filter
CE	Characteristic Equation
Cerium	A rare earth metal
CF	Crest factor (the peak divided by the rms)
Channel spacing	Number of full channels between the electrodes
CLTF	Closed Loop Transfer Function
CO	Carbon monoxide
CO_2	Carbon dioxide
cpsi	Cells Per Square Inch
CRT	Continuously Regenerating Trap
DC	Direct Current
De-sulphation	Removal of sulphate compounds
DOC	Diesel Oxidation Catalyst
DPF	Diesel Particulate Filter
Duty cycle	proportion of the period that the measured parameter is active
Earth	Point of zero electrical potential
ECU	Electronic Control Unit
EGR	Exhaust Gas Re-circulation
EUROx	European emission standard
f	Frequency (Hz)
Ground	Point of zero electrical potential
HC	Hydro-Carbons
HDD	Heavy Duty Diesel
HV	High Voltage
I	Current
IUPAC	International Union of Pure and Applied Chemistry
j	Imaginary number equal to sqrt(-1)
J	Joules, unit of energy
K	Degrees Kelvin
k	Used as a generic variable type in some equations
L	Inductance
LHP	Left Hand Plane
LNT	Lean NOx trap
n	Used as a integer variable type in some equations
Nano-particle	Particulate with effective diameter < 50 nm
NEAR	Non-thermal Electro-Acoustic Regeneration
NH_3	Ammonia gas

Nm	Unit of torque
NO	Nitrogen monoxide
NO_2	Nitrogen dioxide
NO_3	Nitrate compounds
NOx	Nitrogen oxides including NO2, NO and N2O
NTE	Not To Exceed
O^-	Oxygen radical / ion
O_3	Ozone
Off-time	Duration discharge is off for during on/off modulation
On-time	Duration discharge is powered for during on/off modulation
PAH	Poly-cyclic Aromatic Hydro-carbons
PC	Personal Computer
PCB	Printed Circuit Board
Period	Inverse of frequency
PM	Particulate matter
PM loading	Volume of PM within the filter per unit volume
PPM	Parts Per Million
PWM	Pulse width modulation
Q	Amount of either heat flow or electrical charge in Coulombs
Q factor	Dimensionless measure that describes how under-damped a resonator is.
R	Resistance
RHP	Right Hand Plane
rms	Root Mean Square
Rn	The discharge steady state negative incremental impedance
Rp	The discharge positive high frequency resistance
rpm	Revolutions per minute
s	Laplace operator
SAE	Society of Automotive Engineers
SCR	Selective Catalytic Reduction
SiC	Silicon carbide
SO_2	Sulphur dioxide
SOF	Soluble Organic Fraction
Soot loading	Volume of PM within the filter per unit volume
STP	Standard temperature and pressure (273K, 100kPa, IUPAC)
T	Period (1/f)
t	Time (seconds if no units used)
TDC	Top Dead Centre (referring to piston position)
US	United States of America
USB	Universal Serial Bus
V	Voltage
X	Reactance (imaginary part of the impedance)
Z	Complex impedance
π	Constant Pi
ω	Angular frequency (rad.s-1)
Ω	Resistance ohms
ε	Value for permittivity

1. Introduction

The diesel engine has been an important prime mover for over a century since its invention. The engine offers many advantages over gasoline powered spark ignition engines including its better fuel economy and durability. The former is primarily due to the ability to operate un-throttled and with a higher compression ratio. These advantages are the primary reasons for the diesel engine being used for most of the world's heavy duty engine applications such as ships, trains, earth moving equipment and trucks. The developments in diesel engine technology have resulted in comparable power densities to gasoline engines which, together with the fuel economy benefits, have led to the acceptance of the diesel engine for passenger car applications. In 2004, more than half the passenger cars in Europe were diesel powered. The increasing numbers of diesel engines has resulted in more concern for the health of workers exposed to diesel exhaust emissions.

Studies have identified several harmful emissions which have been regulated since 1973. By 2010, the emission regulations will require a 99% reduction over uncontrolled levels. The diesel particulate emissions are of serious concern after recent studies identified them as a human carcinogen. Effective after-treatment of the exhaust is the only way to meet the current regulations to continue to take advantage of the diesel engines merits. This thesis describes the development of a new technology for diesel particulate emission control. This chapter introduces the diesel engine, emission control and diesel exhaust after-treatment. The final section of this chapter describes the Autoselective regeneration technology, electrical plasmas and gives a summary of the subsequent chapters.

1.1 Cleaner Diesel Engines

Diesel engines are regulated by laws governing the amount of harmful exhaust products they can release into the atmosphere. The regulated level of each exhaust product differs between countries, applications and year of engine manufacture. Emission legislation across the world is becoming increasingly stringent resulting in the need for new engine and exhaust after-treatment technologies. The main

pollutants from diesel engines are particulate matter and nitrogen oxides, these pollutants provide the biggest challenge to engineers since combustion technology that reduces one usually increases the levels of the other.

The diesel emission legislation before 2000 was met without after-treatment in most cases. Advances combustion improvement technologies were used to make the fuel burn more cleanly and produce less by-products. By 2004 the changes in emission legislation made further combustion quality improvements unable to meet the levels required in many heavy duty diesel (HDD) applications and after-treatment systems were routinely fitted (Blakeman, 2003).

Figure 1.1 shows the heavy duty diesel emission legislation for Europe since 1991 for nitrogen oxides (NOx) and particulate matter (PM). To meet the legislation criteria, an engine must operate within the area bound by the maximum allowable PM and NOx levels. This is sometimes referred to as 'operation within the box'. As the legislation becomes more stringent, the area of the box becomes smaller and operation within it becomes more difficult. By 2011 operation within the box will probably require both PM and NOx after-treatment. Previous technologies for combustion improvements will no longer be sufficient to meet the targets.
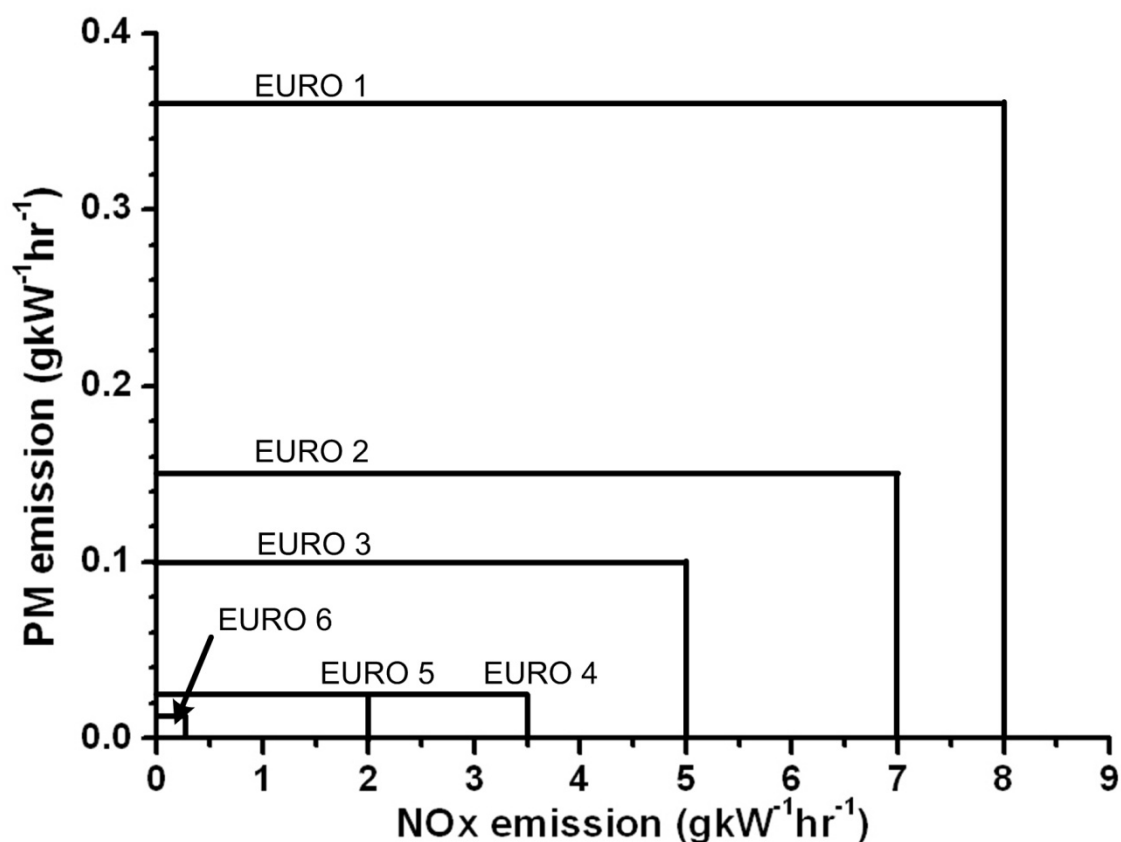
Figure 1.1 The European emission legislation 1991 (EURO 1) to 2011 (EURO 6) for particulates and NOx

The diesel particulate filter (DPF) is the best way to remove PM from the exhaust flow and is used on most light and heavy duty diesel engines being manufactured in 2009. The leading type of DPF technology is the wall flow filter (WFF) which routinely achieves 99% PM removal by mass (Mizutani, 2007). Although some DPFs are designed to be replaced when they become clogged with PM, the majority require cleaning known as regeneration. The process of filter regeneration presents the main design challenge for engineers, the various approaches will be discussed later.

1.2 Health Implications of Diesel Exhaust

Modern diesel engines produce comparable levels of NOx to their gasoline fuelled equivalents and are responsible for most vehicle particulate emissions. NOx has

relatively minor health implications in the concentrations found near roadsides, it is most harmful following reactions with other chemicals in the atmosphere. NOx is one of the chemicals responsible for photochemical smog which is linked to many respiratory illnesses and was the main reason for first implementing emission legislation on automobiles in California in the late 1960s. The presence of high concentrations of ground level ozone is also attributed to NOx, ozone is known to cause respiratory harm in very low concentrations. NOx can combine with water in the atmosphere to produce nitric acid which falls as acid rain which has been linked to deforestation.

Particulate matter (PM) is noticeable when it exits the exhaust at high concentrations, such as during vehicle acceleration. However, the visual warning is often misleading since the production of PM occurs across the operating range of the engine and is often invisible to the naked eye. Recently public buses in many countries have been retrofitted with diesel particulate filters, see for example Figure 1.2, following increased public awareness of the dangers.

Figure 1.2 The known dangers of particulate inhalation has led to the retrofitting of DPF technology (*right*) on vehicles such as school buses

The PM becomes suspended in the atmosphere in, for example, towns and along roads, and these particulates are readily deposited in the lungs. Epidemiological evidence shows truck drivers occupationally exposed to particulates are 20 - 40% more likely to develop lung cancer according to the review of literature by Kagawa (2002). This review revealed that both the International Agency for Research on

Cancer (IARC) and the National Institute of Occupational Safety and Health (NIOSH) both identified PM as a probable or potential carcinogen respectively. Many studies have been conducted to try to establish the extent of its carcinogenicity, most studies show a 20 - 50% increase in the risk of contracting lung cancer when occupationally exposed.

One study on healthy volunteers by Salvi *et al* (1999) used concentrations of diesel exhaust comparable to bus stations and ferry decks. They concluded that it causes an acute cellular inflammatory response despite not significantly reducing pulmonary function (i.e. the effects were asymptomatic). This type of reaction could have implications for members of the community with pre-existing circulatory or pulmonary dysfunction because of the increased risk of stroke and cardiovascular morbidity. A study into the effect of particulates on bronchial epithelial cells by Baulig *et al* (2003) show that there is a marked decrease in the ability of cells to proliferate when exposed to airborne particulates. Their conclusion was that the effect on bronchial epithelial cells was a combination of the chemicals contained within the particulates and the physical interaction of the particulates with the cell membranes. This justifies why the 10 nm PM fraction is considered by many organisations to be the most harmful since small particulates have the highest surface area to volume ratio.

In summary, PM and NOx emissions are harmful to humans and the environment. The amount of PM presently being produced is enough to cause significant harm those routinely exposed to it. The reduction of NOx and PM emissions is essential to improve air quality and to avoid environmental harm. A reliable particulate after-treatment system is therefore needed and is presently a requirement in many applications.

1.3 Diesel Combustion

This section summarises the way the diesel fuel is oxidised during engine operation with emphasis on the way harmful emissions are produced. The fuel is injected just before the top of the piston stroke into the compressed air trapped by the piston. The air temperature is increased to several hundred (e.g. 500 – 600 °C) degrees Celsius

as a result of being compressed by a factor of typically 50 times, it is hot enough to spontaneously begin oxidation of the fuel spray without an additional ignition source. The burning fuel spray is described as an 'unsteady turbulent diffusion flame' (Heywood, 1988) which is a good description of the combustion appearance. The air and fuel are not pre-mixed, there is a continuously varying air to fuel ratio (AFR) throughout the cylinder which changes during combustion. The ratio of fuel to air can be expressed as the equivalence ratio which is a measure how the fuel to oxygen ratio deviates from stoichometric. The lowest equivalence ratio is furthest from the fuel spray which is essentially just air and exhausts gas residuals. The highest is at the orifice of the injector where the equivalence ratio is essentially infinite (purely fuel). Dec (1999) revealed the structure of the combusting fuel jet as illustrated in Figure 1.3.
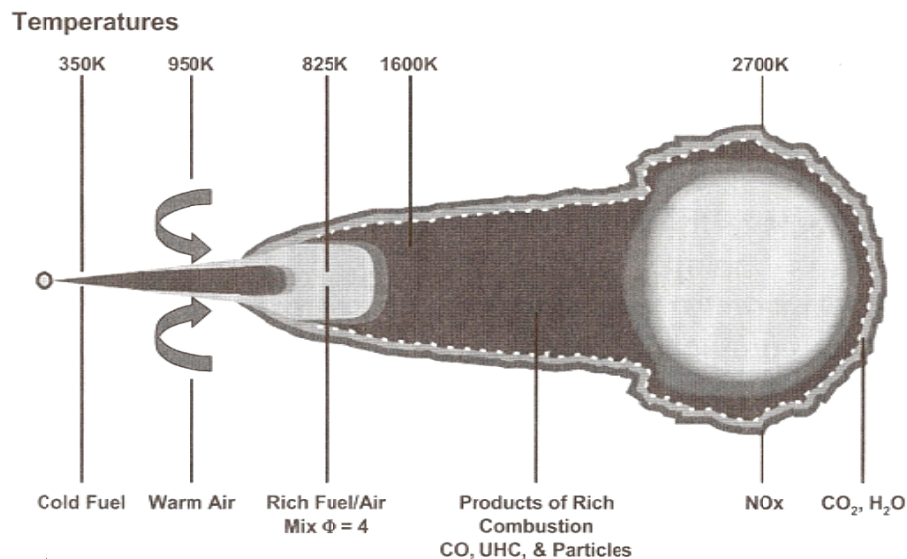
Figure 1.3 Structure of the combusting fuel spray, Dec (1999)

After the injection starts, the fuel begins to vaporise and diffuse into the hot air forming regions around the outside of the fuel spray to have an equivalence ratio close to unity (stoichometric). Pyrolisis, decomposition and oxidation reactions within these zones release heat which leads to rapidly increasing combustion rates. The burning of the fuel is now limited by the rate that the fuel vaporises and mixes with the available oxygen, this is known as mixing-controlled combustion. Most of the heat release comes from this mode of fuel burning during normal diesel combustion, it

leads into the late combustion phase where most of the residual traces of fuel and incomplete combustion products are oxidised.

The main products of combustion are water and CO_2 which are generally accepted as being ideal combustion products for hydrocarbons fuels. The residual hydrocarbon (HC) and carbon monoxide (CO) emissions are low because there is always an overall excess of oxygen unlike most gasoline engines. HC emission is mostly from unburned fuel, this occurs in regions of very low and high equivalence ratio such as from the fuel trapped within injector nozzle or from the 'lean flame-out' regions at the spray periphery, respectively. NOx and PM production is a function of temperature and equivalence ratio as shown in Figure 1.4 where an example of a normal combustion event is shown. The fuel is injected at high equivalence ratio from the injector nozzle, the equivalence ratio decreases locally as the fuel vaporises. After ignition the temperature increases rapidly resulting in particulate production, the plume of particulates in the centre of the fuel spray mixes with the air around the edge and begins to oxidise increasing the gas temperature further. The higher temperatures and low equivalence ratio result in NOx production and PM oxidation. The expansion stroke of the piston rapidly cools the remaining mixture halting further reactions. Combustion improvement technologies attempt to steer the combustion route around the PM and NOx producing zones.
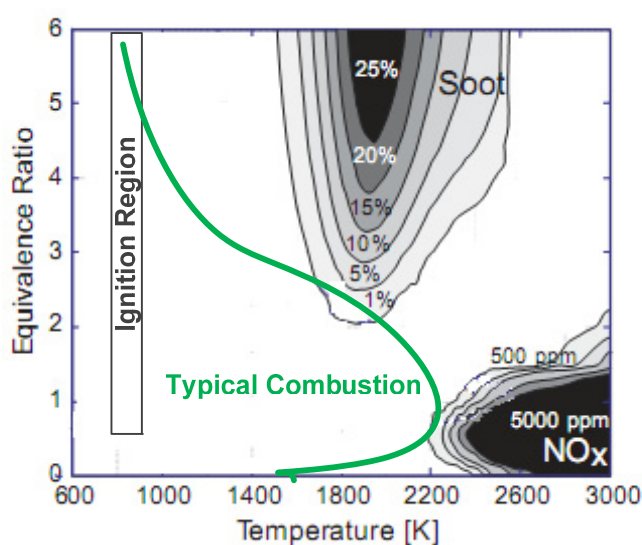
Figure 1.4 Particulate and NOx formation maps (Kook, 2005)

_____

Particulate emissions (PM) make up a small fraction of the mass of fuel burned (typically 0.1% for modern heavy duty engines) and are made up of small particles of a variety of diameters from 10^{-8} m to 10^{-5} m. Particulates form in the regions close to the fuel spray where high temperature oxygen depleted gases contact the liquid fuel droplets. Over 90% of all PM formed during the combustion is then oxidised before entering the exhaust system due to the high cylinder temperatures and excess oxygen (Heywood, 1988). The mechanism by which PM is produced changes for different temperatures and combustion conditions summarised in Figure 1.5 (Setten *et al,* 2001).
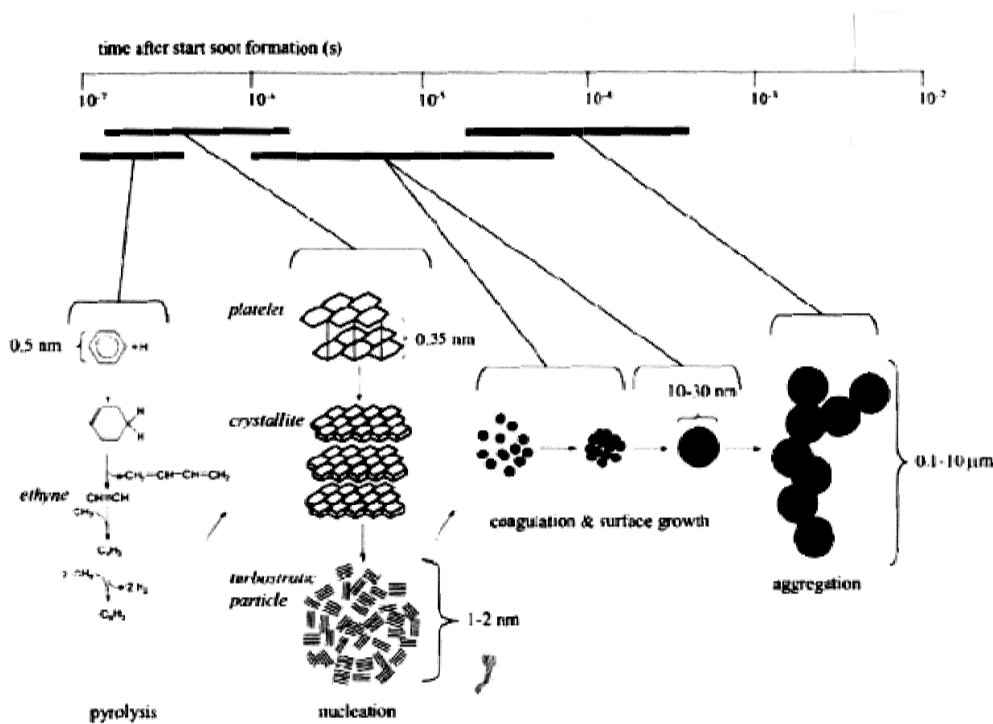
Figure 1.5 Particulate formation (Setten *et al,* 2001)

In general, the first stage of PM production starts with aromatic hydrocarbons, particularly polycyclic aromatic hydrocarbons (PAH), undergoing condensation and fragmentations reactions and aliphatic hydrocarbons undergoing fragmentation reactions similar to hydrocarbon cracking. The condensed aromatics form large molecules and then undergo surface growth to form PM nuclei as other smaller molecules bond with them (nucleation). The smaller fragmentation products, especially alkynes, polymerise and produce larger molecules with low hydrogen to carbon ratios which attach to the surfaces of growing nuclei. As the particles grow, nucleation comes to a halt. The existing particulates continue to grow via surface growth until they become known as spherules (10 – 80 nm). The spherules then undergo agglomeration to form chains or clusters known as particles, as shown in Figure 1.6, which are the largest form of PM. Most of the solid particulate mass is carbon, although a large fraction may be absorbed organic and inorganic matter (mainly adsorbed HC, sulphates and ash).
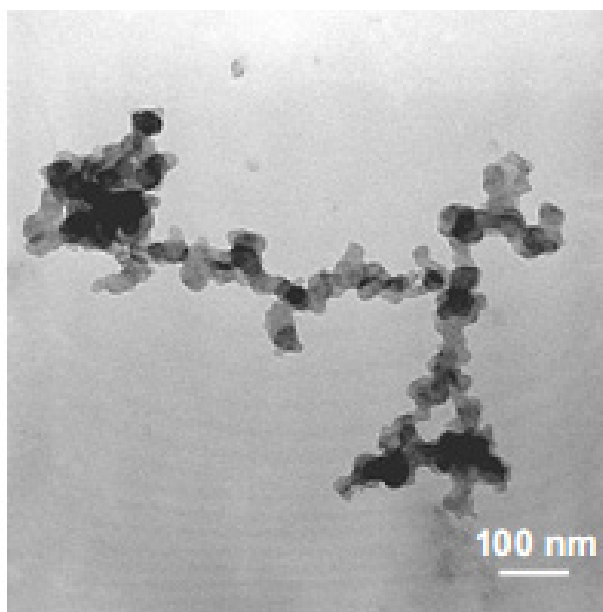
Figure 1.6 Particulate structure (Song, 2004)

The PM in the exhaust has a range of sizes as shown in Figure 1.7. Future emission legislation will likely use number based systems which will make control of the nano-particle (< 50 nm) class of particulates difficult. Present emission legislation used a mass based measurement which does not limit the nano-particles effectively since the majority of the PM mass is emitted as agglomerated larger particles. Smaller

particles have a higher surface area and cause more health problems but detection of particulates below 5 nm is difficult using current techniques since the particle diameter is of a molecular scale (for example, a single hexagon of graphite is roughly 0.25 nm across) and future emission legislation may still be inadequate.
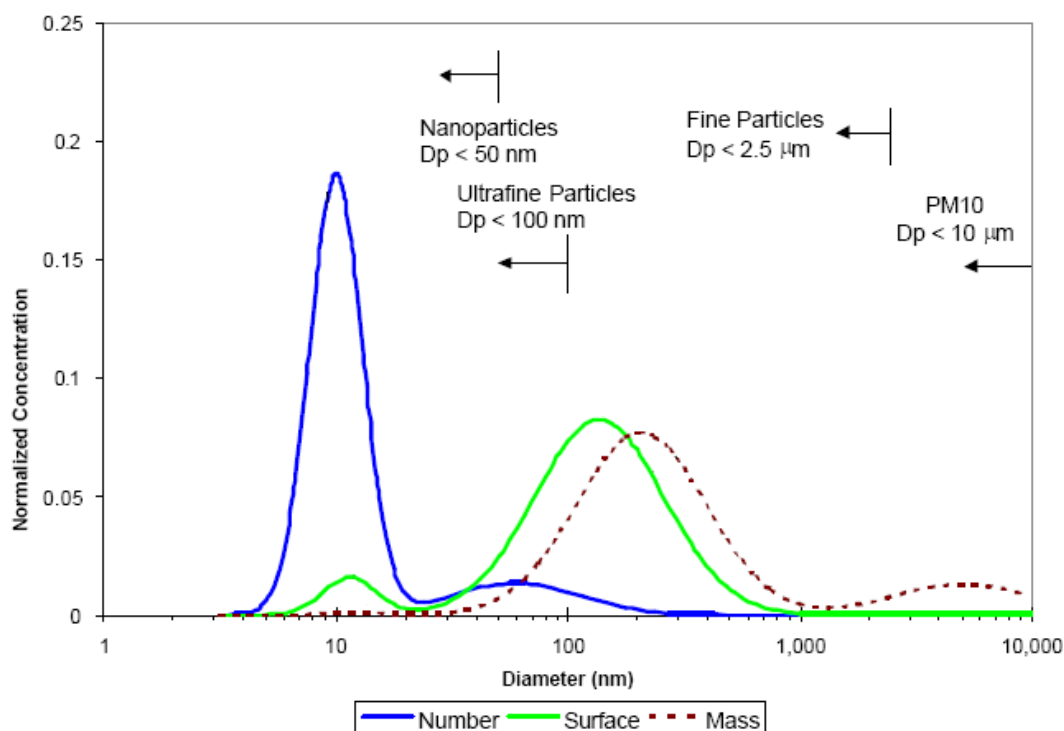
Figure 1.7 Typical soot size distribution (Kittelson, 2002). (D_p = Particle diameter)

1.4 Pre-Combustion Emission Control

It is possible to reduce both NOx and PM emissions by altering the fuel composition and this can be achieved using different chemical fuel blends. Oxygen-rich fuels produce less PM than standard diesel fuel. However, oxygen enrichment usually involved the addition of more expensive chemicals into the fuel such as alcohols (Kitamura, 2001). This has not gained acceptance from the automotive industry yet since it significantly increases fuel cost. There are some more practical ways of reducing diesel engine emissions using fuel composition changes, these include low sulphur fuel and some bio-diesel fuels.

Low sulphur fuel is especially successful when reducing PM emissions since a major constituent of diesel PM is inorganic sulphates. Low sulphur gasoline and diesel fuel

is also essential to preserve the life of various catalytic after-treatment systems. After-treatment systems using oxidation catalysts show an increase in particulate mass as the exhaust gas passes through them as a result of sulphate formation on the catalyst surface. Low sulphur fuels have replaced ordinary diesel in many countries between 2000 and 2005 reducing the 350 ppm sulphur level to 50 ppm.

A practical way of reducing PM emissions is to reduce the PAH levels of the fuel. Reducing concentrations of these has been shown to effectively reduce the PM output of the engine by reducing nucleation (Richter, 2000). However the process of diesel production by hydrocarbon cracking produces large amounts of PAH. It is expensive to reduce the PAH content after cracking and there is insufficient diesel fuel produced via normal distillation methods to meet demand. An alternative to further expensive chemical refinement is bio-diesel which contains lower concentrations of PAH and sulphur, bio-diesel generally results in lower PM levels than petroleum derived diesel fuel (Durbin *et al*, 2000).

The particulate production mechanism during fuel combustion is very complex and there are many routes by which soot is formed. In general, lower levels of PAH in the fuel can reduce the numbers of particulates by reducing nucleation. Small quantities of oxygen in the fuel reduces the levels of alkynes formed during incomplete combustion which reduces surface growth of the nuclei and the total mass of emitted particulate. Sulphur in the fuel forms sulphur dioxide in the exhaust which is oxidised to sulphate compounds on oxidation catalysts. Sulphates can make up a significant proportion of particulate mass (Salvat, 2000) when operating with more than 350 ppm sulphur fuels in conjunction with oxidation catalysts.

1.5 In-Cylinder Emission Reduction

Particulate formation occurs at the points where hot burned gasses contact unburned fuel in the rich parts of the flame. Particulate production may be reduced by increasing the injection pressures to increase fuel spray volume and atomisation, this improves fuel air mixing during and prior to the combustion. Other methods of PM reduction include increasing swirl and using multiple orifice injectors. PM reduction

may also be accomplished by increasing the amount of oxygen available during combustion. This can be accomplished by ensuring the overall equivalence ratio is low, such as at low engine load, or by increasing the oxygen available within the cylinder during combustion. Charge coolers and turbo chargers increase the mass of air in the cylinder which has this effect.

Most methods of reducing the PM result in a higher peak cylinder temperature which is partially responsible for their effectiveness. More than 90% of the total PM formed during combustion is oxidised before entering the exhaust system (Heywood, 1988). This is due to the particulate being oxidized as it mixes with the hot oxygen rich gasses in the cylinder. By increasing the temperature or pressure of the cylinder gases (or by adding more oxygen to the cylinder) the amount of PM burned before the exhaust may be increased. PM reduction techniques that increase cylinder temperatures by even a small amount will produce far higher levels of NOx because its formation is an exponential function of temperature (Charlton, 2005). This factor is known as the 'NOx-Particulate trade-off'. Methods that reduce the amount of PM produced early in the combustion are better than those that increase the amount that is burned later because lower temperature and pressure combustion can be used. This includes increasing the injection pressures which have been steadily increased to well over 2000 bar.

Reduction of NOx is possible by lowering the peak cylinder temperature during combustion. This reduces the percentage of PM that is oxidised before the exhaust and therefore increases PM emissions. Increasing the injection pressures improves the distribution of the combustion within the cylinder and lowers the volume of premixed combustion which lowers the peak temperatures. Using a later injection timing (retarded injection) also lowers the peak cylinder temperatures due to less heat release before the piston reaches the top dead centre (TDC). Using a lower compression ratio would also have a similar effect at the expense of lower engine thermal efficiency.

Adding inert gases with a high thermal capacity to the cylinder can absorb some of the heat released during combustion and hence lower the peak temperatures and NOx levels. This is achieved practically using exhaust gas recirculation (EGR). EGR has at least two other mechanisms for reducing NOx. The ignition delay is increased which retards the ignition and the inert molecules chemically slow down the formation of NOx. Engines running with EGR can produce very low NOx levels although the reduction of the peak combustion temperature increases PM emissions. This is because more of the PM produced during combustion will remain unburned, due to the lower temperatures. The main difficulties with EGR are durability and implementation. The induction of the EGR directly into the intake is difficult with turbo charged engines due to the adverse pressure difference between the compressor and the turbine inlet. Adding the exhaust gases before the compressor causes problems with additional wear, and corrosion. Ideally the EGR is cooled, increasing the size of the vehicles cooling system and causing problems with fouling of heat exchangers with PM deposits. The EGR gasses from sulphur containing fuels contain sulphuric acid that corrodes engine components. Present EGR technology is effective for reducing NOx levels although it still has durability issues and a typical 6% fuel economy penalty compared to normal combustion (Lambert, 2004).

In conclusion, in cylinder emission reduction is achievable by many ways of which the lowest cost and most reliable are presently used. The production of NOx and PM are closely linked and reducing one generally increases the production of the other, this is known as the NOx-Particulate trade-off. An after-treatment system that can remove either NOx or PM may be used to reduce both of the emissions by changing the engine combustion characteristics. To meet current emission legislation at least one after-treatment system for either NOx or PM is needed.

1.6 Diesel Exhaust NOx After-treatment

NOx after-treatment of diesel exhaust is difficult due mainly to the presence of excess oxygen (Frost, 2005). The reducing CO found in gasoline engine exhaust is also in much lower concentrations. A three-way catalyst is not effective for the treatment of oxygen rich diesel exhaust. Highly selective reductants such as ammonia gas can be

used in conjunction with a catalyst to reduce the NOx (selective catalytic reduction). NOx storage catalysts can be used to trap NOx temporarily (lean NOx traps, LNTs) before being reduced during periods of rich engine combustion. NOx after-treatment is often expensive due to the catalysts used, this makes in cylinder NOx control more attractive. If NOx control is implemented in-cylinder, an effective PM after-treatment method will be essential to meet legislation. A more detailed account of NOx after-treatment is covered in the next chapter.

1.7 Particulate After-treatment

Diesel engine particulate matter consists of carbonaceous matter, sulphates, adsorbed HC, ash and a soluble organic fraction (SOF). The particle size range is over several orders (typically 10 nm to 10 µm) and changes with engine speed and load (Muramatsu, 2006). In general, particulates can be removed by electrostatic precipitators, cyclones or filters, the most effective way to remove the particulates from the exhaust, however, is to use a ceramic wall flow filter (WFF). The idea of a particulate filter is to force some or all of the exhaust flow through a porous or fibrous material that retains some or most of the particulates. Filters made from woven fibres, ceramics, metal foams and various other inventive substrates have all proven effective. The most widely accepted and optimised filter is the ceramic wall-flow filter (WFF). The ceramic WFF offers the minimum back-pressure to volume ratio for a >90% mass filtration efficiency. The filter needs to exhibit a low back-pressure to reduce engine pumping losses. The filter should also be able to hold as much PM as possible to reduce the need for frequent cleaning (regeneration).

1.7.1 Filtration Mechanisms

The smallest particles emitted from a typical diesel engine (~ 10 nm diameter) can be effectively filtered by a ceramic wall flow filter with pores 3000 times their diameter. The particulates are not being 'sieved' out of the flow, the filtration mechanism is more complex.

The filtration method of a wall flow filter changes depending on particle size as shown by Ohara (2007) illustrated in Figure 1.8. Larger particles and debris may simply be

sieved from the flow. Smaller particles are removed by impaction, interception and diffusion. The removal of the particles from the exhaust always involves the contact of these particles onto a surface. Once on the surface, the forces trying to return it to the flow must be smaller than the forces holding it on the surface. A trapped particle on the surface of a filter has strong bond to the surface that prevents its return to the flow, this is set up by the interactions of intermolecular forces, bonding and friction.
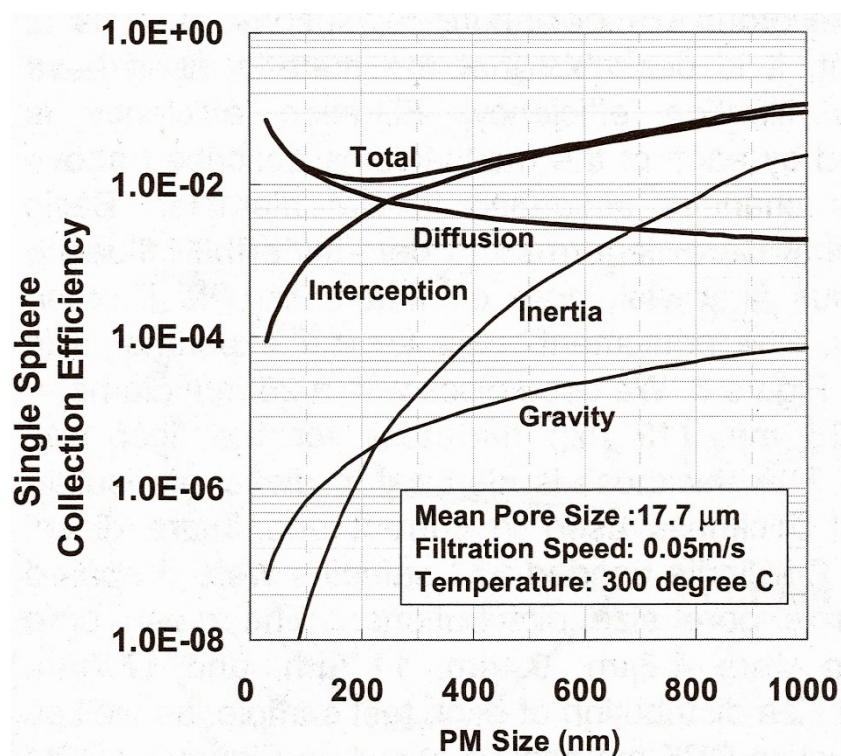
Figure 1.8 Predictions of single sphere collection efficiencies for a wall flow filter for each collection mechanism (Ohara, 2007)

A particle may reach the surface of the filter if the direction of gas flow changes suddenly close to an obstruction. The momentum of the particle forces it out of the gas flow and into the obstacle where it is trapped which is known as impaction (Figure 1.9 refers to it as 'inertial filtration'). Smaller particles will not experience the same path since they have a lower momentum and more easily follow the direction of gas flow. If a particle flowing in a gas follows a path that within one particle radius from the filter surface it will contact the surface and be trapped, this is known as interception. Particles under 0.1 μm diameters are unlikely to follow such paths and are not affected by sudden changes in flow direction like heavier particles. These

particles interact strongly with the gas molecules and follow random paths (i.e. Brownian motion) due to the frequent collisions. This random motion allows the tiny particles to diffuse rapidly over large distances and this movement often brings the particles in contact with the filter walls where they are trapped which is known as diffusion filtration. Diffusion filtration may be polarised by a temperature gradient which is known as thermophoresis. Ohara (2007) also describes filtration by the forces of gravity, his predictions are that this is a negligible mechanism for the expected particle size range. The mechanisms of filtration are illustrated in Figure 1.9.
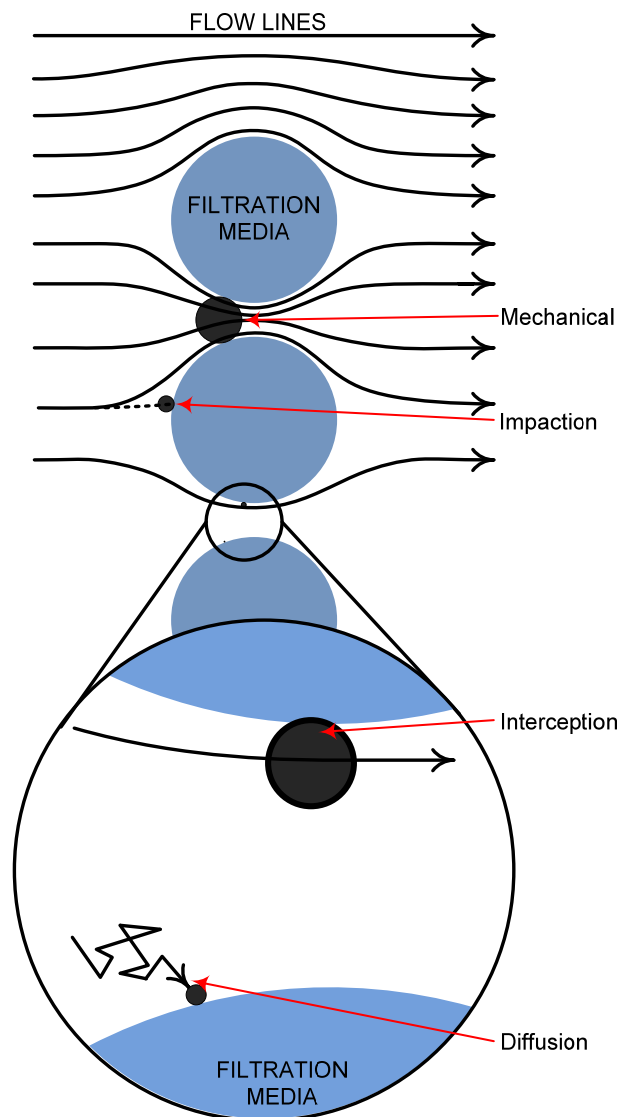
Figure 1.9 Filtration mechanisms

As the porous filtration media becomes gradually filled with PM, a thick layer of particulate matter forms on the outer surfaces of the filter. Up until the formation of this layer, the particles were filtered within the porous or fibrous substrate, know as deep bed filtration which is characterised by a steady rate of loading throughout a significant depth of filter section. Once the filter becomes loaded with soot to about 1 g.litre^{-1}, the filtered PM is deposited on this outside caked layer (cake filtration). In wall flow filters, the thick layer of particulates on the filter surface improves the typical filtration efficiency of the filter from 90% to 99% (Mizutani, 2007) due to the larger filter surface area and stronger adhesion forces experienced between particles. Most of the PM holding capacity of a wall flow filter is in the caked layer.

1.7.2 Partial Filters

For some applications, the removal of 40 - 90 % of the PM from the exhaust may be acceptable and in these cases a partial filter may be used. A partial filter allows some of the exhaust gas to pass through unfiltered. The advantage of this is that the back-pressure drop is often less and the maximum back-pressure is limited. Some partial filters have been used successfully on retrofitted vehicles (Jacobs, 2006), they usually rely on passive regeneration by NO_2 during high load operation, this process is explained in a later section. If the engine is not operated at full load for some time, the particulate filtration efficiency falls and the back-pressure increases until no particulates are being filtered. Partial filters presently used for some retrofit applications especially on city buses.

1.7.3 Wall Flow Filters

Wall flow filters (WFF) can be made of several types of substrate of which silicon carbide and cordierite are the two most popular, examples of WFFs are shown in Figure 1.10. The wall flow filter works by forcing the exhaust flow through a thin section of porous ceramic. The WFF has a ceramic honeycomb structure similar in appearance to the catalytic converter used with most gasoline engines, however, in the WFF the channels are plugged alternately at each end so that there is no direct path from one side to the other. This structure is finished into a cylindrical package that can be fitted into an exhaust system. The only path through the filter is through

the porous ceramic walls where the filtration takes place. The WFF represents the best filtration area to volume ratio available and is widely accepted in the automotive world. For this reason, the WFF has been chosen for the application of Autoselective technology presented in this thesis. One of the aims of this research is to produce a workable regeneration system that is applicable to present WFF technology.

(a)   (b)
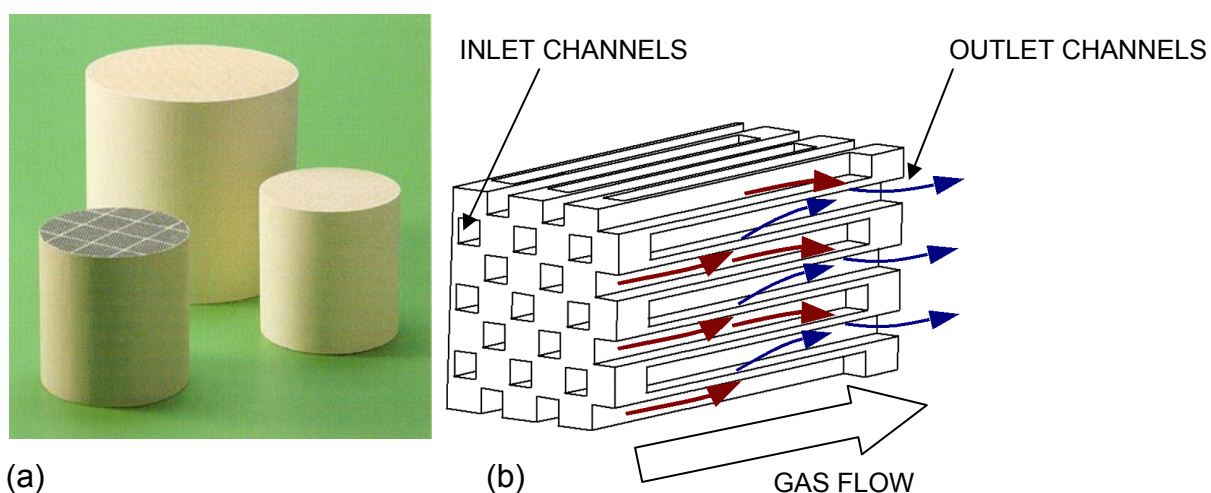
Figure 1.10 (a) Examples of the wall flow filter (product literature, Corning Inc.) (b) Principle of operation (Williams, 2007)

1.8 Auto Selective Filter Regeneration

Autoselective regeneration is a novel diesel particulate filter regeneration method that has been developed at Loughborough University which uses an electric glow discharge. It can be used to oxidise the particulate matter from a diesel particulate filter, regenerating it. The key enabler to the technology is that PM is conductive and can pass electric current whereas cordierite filter substrate is non-conductive. An electric discharge current prefers to flow through the PM which causes the discharge to seek out regions of high soot concentrations. The glow discharge burns the PM away leaving the non-conductive ceramic behind before moving to a region of higher soot concentration. In this way the discharge automatically selects the PM laden parts of the filter and regenerates them.

Early work by Proctor (2007) confirmed that the glow discharge could effectively regenerate soot from a large portion of the filter using inserted electrodes. Tests also

showed that the regeneration process was more efficient compared to other electrical regeneration methods and many non-electrical regeneration methods.

1.9 Electric Discharges

Electric discharges occur when an electric current passes through a gas forming a plasma consisting of free electrons and ions. Plasma is generally accepted as a separate state of matter and indeed most of the matter in the universe exists as plasma. It is normally a conductive gas in which the charge carriers are electrons and positive ions present as a result of ionisation of the gas molecules (or atoms).

Plasmas are usually characterised by their temperature and pressure, they naturally self extinguish as they cool. Extinguishing is the process of recombination of ions and electrons which leaves the gas non-conductive. This happens rapidly for electrically sustained plasma under atmospheric conditions ($\approx$ 1 ms) once the electric current is interrupted. Common plasma applications sustain the plasma using an electric current between conductive electrodes, the resulting plasma is termed an 'electric discharge'.

Common forms of electric discharge plasmas are tube-lights, welding arcs, sodium lamps, plasma torches and lightning. These are all electrical discharges that vary in current level, temperature and pressure. Tube-lights use a low pressure, low current glow discharge in mercury vapour. The current is usually of the order of a few hundred milliamps. Arc welders and plasma torches use a high pressure (atmospheric) arc of the order of 100 amps. Discharges are often classified by their electron density and mean electron speed. The following plot illustrates a wide range of plasma encountered by science, Figure 1.11.
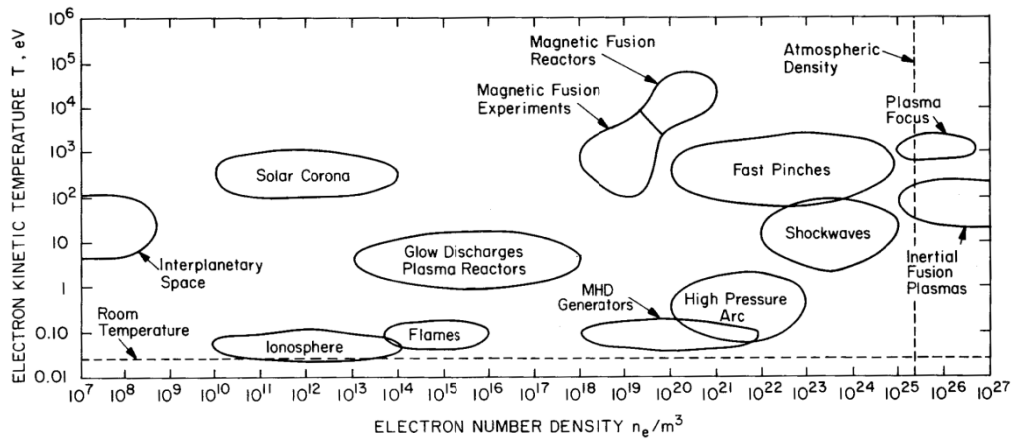
Figure 1.11 Plasma characterisation from Roth (1995)

The plasma used in this research is a non-thermal atmospheric pressure glow discharge. The discharge is characterised by its low current and relatively high voltage. The temperature of the discharge is much less than an electrical arc but is still thousands of degrees Kelvin. The electron temperature is usually higher than the ion temperature due to the low electron mass (compared to the ions), high electric fields and the ion collision rate. Plasma with this characteristic is known as non-equilibrium. The high electron temperature allows some energetic chemical reactions to take place at lower temperatures such as the production of ozone and nitrogen oxides. Electric discharges are discussed further in Chapters 3, 4 and 6.

1.10 Thesis Outline

This thesis presents the research carried out in optimising the Autoselective regeneration technology for wall flow filters. All aspects of the technology were considered and key variables were identified and tested in order to produce an Autoselective regeneration system for a heavy duty diesel application.

Chapter 2 describes the prior DPF regeneration systems and other important aspects of diesel exhaust after-treatment.

Chapter 3 explains the many considerations required when designing discharge power supplies. A key requirement of this research was to design and build several

novel discharge power supplies. This chapter describes some of these and discusses the difficulties encountered when powering electric discharge loads.

Chapter 4 summarises the optimisation of the glow discharge used for Autoselective regeneration and presents the results and conclusions from this part of the research.

Chapter 5 presents the research into implementing the Autoselective technology on a cordierite wall flow filter. This section focuses in particular on the results from the filter damage and electrode geometry testing.

Chapter 6 summarises the filter damage process and the discharge energy balance analysis. The filter damage heat flows are discussed and other filter substrates are compared based on the measured transient heat flows.

Chapter 7 presents the investigative work and results regarding particulate re-entrainment. The results and observations led to the identification of a new method of filter regeneration, distinctly different to Autoselective regeneration, which uses an electric discharge to non-thermally regenerate a filter.

Chapter 8 summarises the development of the research in terms of engine testing performance and key conclusions. This chapter presents the flow-rig and engine testing results and the corresponding conclusions that were made.

Chapter 9 presents the major conclusions that can be made from the research with a summary of the contribution to knowledge this research has made. A list of suggested further research is also given.

1.11 Summary of Research

This research investigated the process of Autoselective regeneration with the view of adapting it to regenerate a wall flow filter. The glow discharge was studied to determine the optimum current waveform to use in terms of frequency and current level, amongst other variables. The electrode geometry was investigated in terms of

placement and type. The regeneration performance was characterised into key variables of effectiveness, rate, distribution and damage threshold. An ideal operating window was found for the current waveform for the cordierite wall flow filter. This was used with the optimum electrode geometry settings on a full-filter on-engine test. The new settings required the use of a novel power supply which can sustain a glow discharge beyond its stability limit by applying a novel quasi-pulsed current waveform.

The engine test results were compared with previous results and conclusions were made. A thorough investigation of the thermal balances within a regenerating discharge was undertaken and a model was made to describe the transient heat flows within the Autoselective discharge. In addition to the Autoselective research, a novel non-thermal method of filter regeneration was found and investigated. Its performance was shown to exceed that of the Autoselective system in preliminary tests.

1.12 Contribution to Knowledge

The main contribution to knowledge has been the improvement of the Autoselective technology and new understanding of the process. This research has exhaustively and scientifically shown the limitations of the technology with respect to the identified key performance variables. The effect of electrode type, spacing, orientation and capacitance has on regeneration performance has been determined. The effect the discharge current waveform has on the regeneration performance has been determined across more than three decades of frequency and two decades of current as well as other identified variables. The research also included extensive damage testing which identified the damage threshold for cordierite.

The research has also provided valuable thermal transient model of the discharge being applied specifically to the damage observed during Autoselective regeneration. The model is particularly useful for investigating the suitability of new materials for the regeneration technology, as they become available, without the need to make filter samples.

An understanding for the mechanism of particulate re-entrainment has been made and this was applied to create a novel filter regeneration method which exceeds the performance of the Autoselective system. A promising start point for a new branch of research has been established.

Publications arising from this research include:

SAE paper - 'Low Power Autoselective Regeneration of Monolithic Wall Flow Diesel Particulate Filters', SAE-2009-01-1927, A. M. Williams, C. P. Garner, J. E. Harry, D. W. Hoare, D. Mariotti, K. S. Ladha, J. W. Proctor, Y. Yang, J. G. P. Binner

and

Patent application - for Electro-Acoustic DPF regeneration (by Caterpillar Inc), due to be published in 2010

2. Literature Review

Chapter 1 introduced the diesel engine, its benefits and disadvantages with respect to the harmful levels of exhaust pollutants. This chapter describes previous after-treatment systems with emphasis on the methods of DPF regeneration. The purpose of this chapter is to identify a set of requirements for a regeneration system and to provide a measure by which the Autoselective system can be compared.

After-treatment describes the process by which exhaust products are processed after they leave the engine combustion chamber in order to reduce the concentrations of harmful exhaust components. This is used whenever improvements to in-cylinder combustion are insufficient to meet emission legislation.

2.1 NOx After-treatment Methods

This section briefly outlines the key technologies used to reduce the total NOx output from diesel engines. This research focuses on a PM after-treatment technology but it is important to consider NOx treatment due to the NOx-PM trade-off. It is possible to reduce PM emissions to low values by changing the combustion characteristics at the expense of a larger NOx output. NOx production represents efficient combustion and better fuel economy therefore applications where fuel economy is important may favour a NOx after-treatment strategy. Unfortunately, conventional catalytic converter type after-treatment systems that are commonly found with gasoline engines cannot be used with diesel engines mainly because they rely on the production of CO to reduce the NOx (typical diesel engines produce low CO emissions by comparison). In addition, PM build up on the catalyst surface lowers the active area of the catalyst reducing its activity. It should also be noted here that reduction of NOx in an oxidising environment such as diesel exhaust is difficult. The NOx after-treatment of diesel exhaust is very different to the technologies used with modern gasoline engines.

2.1.1 Selective Catalytic Reduction of NOx

Since there is little CO or other reductants readily available to react with and remove the NOx from the exhaust gas stream, a separate reducing agent needs to be added. The reducing agent must be selectively oxidised by the NOx since there are a large quantity of other oxidising substances present in the exhaust, including oxygen. This is the basis of the selective catalytic reduction (SCR) of NOx. The accepted reducing agent used in modern SCR systems is ammonia gas (NH_3), but this is difficult to store and is toxic. NH_3 can be safely stored in solution or as urea (carbamide) which reacts with water in the high exhaust temperatures by thermo-hydrolysis to produce NH_3 and CO_2. The NH_3 reacts with the NOx on the SCR catalytic converter which is often the alumino-silicate mineral zeolite. Zeolite has a much lower cost compared to precious metal catalysts.

The conversion efficiency is improved by converting the nitrogen oxide NO to nitrogen dioxide NO_2 before the SCR catalyst and it has been found that slightly less than 50% NO_2:NO ratio is optimal (Blakeman, 2003). For this reason, the SCR system is usually preceded by an oxidation catalyst. Oxidation catalysts oxidise SO_2, produced by the combustion of sulphur in the fuel, to sulphate particulates which add to the PM emissions from the engine. The sulphur also gradually poisons precious metal oxidation catalysts. For these reasons, the use of an oxidation catalyst requires the use of low sulphur fuels which are more expensive.

SCR has recently increased in popularity due to the availability of low sulphur fuel and the low cost of the SCR catalyst. Low NH_3 dosing systems require little control and can get 60% reductions of NOx levels (Seher, 2003). Increasing the dosing can be used to achieve up to 90% reductions (Geishoff, 2000 and Blakemen, 2003) but NOx and NH_3 slip present emission problems during parts of most engine test cycles. The catalytic solution to reducing NH_3 slip uses a hydrolyser upstream to encourage low temperature urea conversion in combination with a downstream diesel oxidation catalyst (DOC) to remove un-reacted NH_3. However, the extra catalysts increase system cost, packaging sizes and add further sensitivity to fuel sulphur levels. Seher (2003) showed that complex control methods could be used to achieve comparable results without these extra catalysts.

In general, SCR has many advantages for heavy duty on highway vehicles which require high fuel economy and where the fuel savings offered by SCR can offset the cost of implementation. SCR produces only about 0.2 % fuel economy penalties for typical installations (Lambert, 2004) and the effective NOx removal allows engines to run with higher engine-out NOx levels offering significant fuel economy benefits. If the present cost of urea solution (branded as 'Adblue') and the typical 2009 fuel prices are used, the cost based fuel penalty is only ~ 2.5 %. Problems with urea SCR infrastructure still exist and debate about how the system should be implemented are still underway. In particular, there is worry that end users will deliberately disable the system to save further cost.

2.1.2 Lean NOx Traps (LNT)

The LNT system is a way of catalytically removing NOx from diesel exhaust using oxygen depleted exhaust gasses in a mechanism more similar to gasoline engines. The LNT catalyst is typically a ceramic substrate with wash coatings of alkali and transition metal oxides (and sometimes rare earth metal oxides). In a diesel engine, the high oxygen concentration and low CO levels block the chemical reduction of the NOx. The LNT system works by trapping the NOx as nitrates (NO_3) on the metal oxide catalyst surface during lean operation and reducing it during brief periods of rich engine operation. The storage of NOx only works within a narrow temperature range of typically 250 – 450 °C and this is conveniently the normal exhaust gas running temperature of some diesel engine applications.

The NOx trap regenerations take place for typically 5 seconds followed by 60 seconds of normal engine operation (Blakeman, 2003). During the regenerations, late post fuel injections are normally used to raise exhaust temperatures and deplete the exhaust gas oxygen. Some partially combusted products may pass out of the exhaust during regeneration, this is know as slip. Slip of NO, HC, particulates and CO present an emission legislation challenge, especially since the introduction of 'not to exceed' (NTE) legislation in the US in 2007. NTE (amongst other requirements) specifies that spikes of emitted levels of controlled substances may not exceed 150%

for more than 30 seconds (with some exceptions). The NO slip presents the largest problem with CO and HC emissions being removed by an additional oxidation catalyst. Particulate produced during rich combustion phase must be removed by a particulate filter and in most cases this limits the use of LNT technology to combined (NOx and PM) emission control implementations.

The LNT system has shown to be effective for removing up to 70% exhausted NOx with good aging performance (Tsumagari, 2006). Sensitivity to sulphur is a major design obstacle, however, and intermittent de-sulphation is required at least every 250 hours of operation for low sulphur fuel. This requires a hot reducing environment at around 600 °C for more than 5 minutes depending upon the catalyst. Thermal aging of DOCs and damage to DPFs is of concern during de-sulphation events. For fuel economy driven applications such as heavy duty trucks, the fuel economy reduction associated with LNTs may also be a factor. About 7% extra fuel is used to provide the rich combustion and de-sulphation events (Seher, 2003). Tsumagari (2006) used a dual bypassed filter arrangement to improve the fuel economy penalty to 1.35% at the expense of design complexity and expense.

In summary, LNT technology can achieve significant reductions in NOx levels when added to existing DPF implementations. The fuel economy penalty of typically 7% together with NO slip and sulphur intolerance make the LNT unattractive for heavy duty highway applications. LNT systems could help Light duty highway vehicles meet legislation and provide NOx treatment for locations without urea SCR infrastructure. For highway heavy duty diesel applications, the SCR is considered a better option.

2.2 Particulate After-treatment Methods

Diesel engines produce large volumes of particulate matter (PM) during combustion compared to their petrol fuelled equivalents. This section introduces the field of PM after-treatment and discusses the difficulties associated with each available technology.

PM reduction techniques invariably involve trapping the PM after its formation in cylinder. The trapped PM is mainly carbon (Neeft, 1995) and may be oxidised to CO_2 before being emitted with the rest of the exhaust. PM does not burn easily in exhaust conditions despite the heat released during its oxidation, often the exhaust temperatures must be increased to allow sustained soot burning. Most particulate after-treatment systems try to achieve complete oxidation of the PM to ensure the system requires little or no maintenance. There are many ways to oxidise the trapped PM, these can be divided into two categories known here as 'passive oxidation' and 'powered (active) oxidation'.

2.2.1 Novel PM Trapping Strategies

Some research has explored filter-less methods of PM trapping, they have all proved unsuitable for vehicle operation but will be mentioned here to illustrate the difficulties of PM after-treatment. Some work has gone into the development of an electrostatic precipitator for diesel exhaust particulates. The research by Farzaneh (1994) and Ciach (1996) has shown that effective removal of the particulates requires a large precipitator comparable in size to the engine in order to produce residence times required for high collection efficiencies. Furthermore, the systems developed consumed excessive amounts of electrical power which make them unsuitable for most vehicles. The failure to produce a viable after-treatment solution may be attributed to the high flow rates and small particle sizes. Electrostatic precipitators are more suitable to applications such as power stations where the particles are larger, relatively slow, there are no major size restraints and there is ample electrical power available. Kogelschatz (2004) describes such a system as used commonly for coal power stations, in these optimal conditions the collection efficiency was 99.9% by mass. The electrostatic precipitator method is widely used in vehicle tunnels to filter some of the agglomerated diesel PM from the air.

Methods such as cyclones have also been researched (Crane, 2000). The gas flow is rapidly swirled in cyclonic separators so that the particles within the gas experience a centripetal force and move to the outside of the rotating gas. The outer layer of gas containing the particulates may be 'skimmed off' and filtered or the cyclone used to

deposit the PM in a suitable collector. Cyclonic removal of particles is difficult with diesel exhausts due to the small size of the particles, although effective removal of large particles is possible. Crane showed that pre-agglomeration of the particles allowed approximately 60% mass reduction using a multi-cyclone system. As injection technology improves, the particulates produced by modern diesel engines are smaller and hence more difficult to remove by electrostatic precipitators and cyclones. If a successful on-the-fly agglomeration method is developed then electrostatic precipitators and cyclones may become a feasible alternative to DPFs. Present technology makes these methods of PM removal unattractive when compared to existing methods such as WFFs.

2.2.2 Passive PM Reduction

Catalytic methods of PM control are possible, these methods invariably use a filter (normally a WFF) to trap the particulates where they can be oxidised. The passive oxidation of PM is slow under the normal running conditions found in a typical diesel engine and is not self sustaining. To achieve steady un-catalysed burning of the trapped PM with oxygen, a temperature of more than 550 °C is required, known as the light-off temperature. The oxygen needed to oxidise the PM is always present with diesel engines due to the lean combustion. The temperature is normally the limiting factor for PM oxidation, typical diesel engine applications only produce the necessary regeneration temperatures intermittently and for this reason a catalyst that can reduce the light-off temperature is desirable.

One of the disadvantages of all passive filter regeneration systems is the uncontrolled levels of trapped PM. PM can build up during prolonged low engine load operation reaching several grams per litre of filter volume. If the exhaust temperature is then raised above the light-off temperature, a thermal run-away effect can occur. The heat release of the soot quickly raises the filter temperature and can cause thermal damage to occur. The filters used with this type of regeneration strategy must be able to withstand these high temperatures and thermal gradients, they are usually made from silicon carbide, an expensive filter material. The maximum safe PM loading for cordierite WFFs is 4 $g.litre^{-1}$ with mullite reaching 8 $g.litre^{-1}$ and silicon

carbide at 10-15 g.litre^{-1} (Johnson, 2006). Uncontrolled filter regenerations can be avoided by ensuring the soot loading does not exceed these levels, this requires a soot loading sensor which adds significant cost and is often inaccurate. Upon reaching the threshold, the engine must be immediately operated at high load to regenerate a portion of the trapped PM and this is not considered acceptable for many applications.

The two most common PM catalyst reduction techniques are fuel doping to reduce the light-off temperature and NO_2 based soot oxidation. The former is currently implemented using the rare earth metal cerium within a fuel additive. The cerium particles become incorporated in the PM and lower its light-off temperature. The lowered light-off temperature encourages passive PM oxidation at normal engine loads. The risk of uncontrolled regenerations is also higher, however, and a silicon carbide filter is normally used.

The trapped PM can also be oxidised at lower temperatures using NO_2 which is a normal diesel exhaust component. This mechanism is exploited by a family of passive regeneration systems using variations of the same basic mechanism. These systems use an oxidation catalyst with precious metal doping to convert NO to NO_2 in the exhaust flow. The NO_2 reacts with trapped soot in a DPF to form nitrogen and carbon dioxide. If the concentrations of NO_2 are approximately 16 times (by mass) the PM concentrations then a balance occurs between soot oxidation rates and PM production rates. This prevents PM build up in the filter at the expense of increased NO_2 production, sulphur sensitivity and high catalyst cost.

An oxidation catalyst may be used to reduce the PM emission without the possibility of uncontrolled regenerations. Modest PM mass reductions are possible since it oxidises hydrocarbons, found both in the particulates and as part of the exhaust gases (as well as CO and NO). By oxidising some of the organic fraction of the particulates, the total mass of PM in the exhaust is reduced. The main problem with oxidation catalysts used for PM control is the presence of sulphur in the fuel. The oxidation catalyst oxidised the engine out SO_2 into sulphate particles which contribute to the total PM mass. In fact, the total PM mass output can be more after the

oxidation catalyst than before it for normal 350 ppm sulphur fuel. Under normal operation the use of an oxidation catalyst can only be successful for PM reduction when used with low sulphur fuels.

2.2.3 Active PM Reduction

There are many types of active regeneration system, they invariably use either electricity or fuel to provide the energy needed to oxidise the PM that is trapped on a filter surface. The obvious disadvantage is the requirement of energy input which leads to a fuel economy penalty. This penalty is one of the main measures when comparing active regeneration systems and is usually expressed as a percentage increase in fuel consumption.

Systems that heat the trapped PM whilst in the exhaust flow have the disadvantage of the heat lost to the exhaust stream. It can be shown that the power requirement will be more than 18 kW to keep the exhaust temperature above light-off during mid load operation for a typical 100 kW heavy duty diesel engine (220 $kg.h^{-1}$, 250 °C). Fortunately, the regeneration of the particulate filter (DPF) does not need to be continuous. The filter is normally allowed to load with PM until the filter PM loading reaches a certain value, then the heating device is switched on and the filter temperature quickly rises up to light-off (Zelenka *et al*, 2002). The heating cycle finishes when the filter is regenerated and the heating device can be turned off until the next regeneration event.

The heating device can be an electrical heating element before (Zikoridse, 2000) or even within the filter (the Rypos Inc. system), with the electrical power being supplied from the engines alternator. This type of system often needs an oversized alternator to handle the high peak powers required to regenerate a DPF. Some powered systems have been developed to electrically heat the PM directly. This can involve a variety of methods and has the advantage of being able to operate more efficiently than heating the whole filter by reducing some of the heat losses. One method for achieving this type of regeneration is to remove the PM from a filter before oxidising it with a low power heater (Takesa *et al*, 1991), heating losses are substantially

reduced. Other methods have used magnetrons to heat the PM using microwaves (Garner, 1989).

The obvious method of heating the filter would be to use the diesel fuel itself and many systems do this. The fuel can be injected in cylinder during the exhaust stroke of the engine (late post injection) or inside the exhaust pipe before the filter. Fuel burning systems can use an oxidation catalyst to oxidise the fuel or use a flame burner system. In all cases, the chemical energy is released from the fuel and used to heat the filter to above light-off. This type of system still suffers problems from filter melting when uncontrolled regenerations occur, a soot loading sensor is normally used (often just the filter back-pressure). To control the regeneration more effectively, an exhaust bypass can be used to control the air flow through the filter, this gives direct control of the oxidation rate of the PM as well as reducing heat losses to the exhaust. By-passing is unpopular because it requires exhaust valves that are expensive, bulky and often unreliable. Emission legislation being introduced in the US (2007) calls for an absolute limit on the levels of emissions. If the exhaust is by-passed and left unfiltered, even for a short duration, it is likely to fail the emission tests. For this reason, any future bypassed system will effectively require two filters in parallel thus increasing the cost substantially.

2.3 Diesel Particulate Filter Regeneration

This section discusses the prior art of fuel burning, electrical and catalysed systems for DPF regeneration as summarised by the previous section.

2.3.1 Fuel Burning Systems

Fuel powered systems use diesel fuel to raise the exhaust temperatures above light-off so that the trapped PM oxidises and the filter regenerates. This is most efficient when the filter is loaded just below the safe regeneration limit since more of the input energy is used to heat the PM and due to the extra heat contribution from the burning PM. Zelenka *et al* (2002) developed a full-flow burner system that was successfully fitted to a road vehicle with only an estimated 2% fuel consumption penalty. His success was attributed to a complex computer controlled strategy that

used a large matrix of pressure and temperature sensors as well as data from the engine control unit (ECU). This type of implementation is prone to failure in durability tests due to the necessity to calibrate the control strategy and sensors which may fail or drift out of calibration over time. The durability test requirements for emission legislation are increasing, since 2004 in Europe the PM regeneration systems for passenger cars are required to operate for 100,000 km.

A similarly complex system was developed by Park (1996) that used a by-passed exhaust and a variable air flow strategy that eliminated transient temperature spikes. Fuel burner systems have been developed for many years and their implementation is now routine, some use a flame to oxidise the fuel whereas the majority use an oxidation catalyst to reduce HC slip. It is likely that tomorrow's fuel burner systems will require a large number of sensors and ECU integration.

Oxidation catalysts present a good alternative to fuel burner systems, fuel is released up-stream of the catalyst and is oxidised on its surfaces raising the exhaust temperature. More complete combustion of the fuel is possible thus producing lower HC emissions whilst liberating the same, or more, heat output. In addition, the DOC can contribute to NO_2 production which reduces the build up of soot in the filter. The system may regenerate passively for much of the drive cycle and only need occasional active regeneration. Singh (2006) developed such a system and showed that an active regeneration event was only needed after 7 hours of low load operation due to the additional passive regeneration. A study by Doumeki (2006) studied the oxidation catalyst and showed that excellent durability was possible despite the sustained and frequent high temperatures. The oxidation catalyst active regeneration system is therefore likely to be used in place of the burner in most applications. The additional passive regeneration means that the frequency of regeneration events can be lower and hence the fuel penalty is reduced. The additional cost of an oxidation catalyst is high and may outweigh the advantages in cost sensitive applications. In addition, the oxidation catalyst only begins to work after its light-off temperature is reached which can introduce some complications for a few low load applications.

2.3.2 Catalysed Systems

I. Cerium Fuel Additives

A WFF can passively regenerate if the exhaust temperature is higher than the light-off temperature, this can be reduced using cerium based fuel born catalysts. The fuel additives leave an ash by-product that gradually blocks the filter until it needs to be mechanically removed, the health implications of the ash are not yet fully understood. Blanchard (2003) demonstrated a highly optimised system with a 150,000 km service interval. In typical systems, the cerium additive is mixed with the fuel and is burned by conventional combustion. The result is a mixture of exhaust gases, particulates and sub-micron cerium containing particles. The particulates and cerium particles are trapped together inside the DPF. The cerium particles trap oxygen to form cerium oxide (CeO_2) which is made available to the surrounding PM by their catalytic action allowing the PM to oxidise at a lower temperature. The cerium continues to make oxygen available to the burning PM until it is deactivated by sulphur dioxide (SO_2). The temperature required for sustained oxidation of the PM was found to be 307°C by Jean *et al* (2005) in a controlled experiment; temperatures as low as 310°C are recorded for on vehicle tests. The action of the cerium additive was found to have negligible effect on the activation energy of the oxidation reactions it was catalysing by Jung *et al* (2004). In fact, Jung showed that the oxidation of PM was already metal catalysed by metal particles originating from the lubrication oil and engine wear. The lower temperature oxidation of the PM was attributed to an increase in the number of catalysed sites. Figures for the cost of the cerium fuel additives results in a fuel economy penalty, based on 2009 fuel prices, of about 1-2% (www.dieselnet.com, 2009). The cerium fuel additive system is presently being fitted to some passenger cars. The main disadvantages are sulphur sensitivity, infrastructure requirements (to supply the catalyst and dispose of the ash) and the need to use silicon carbide filters for thermal integrity.

The cerium based PM emission control is best implemented in conjunction with other systems. Salvat (2000) showed that a silicon carbide filter and cerium fuel additive combined with a DOC provided reliable performance at all engine conditions by using a late post injection strategy. The additional heating from the fuel allowed regeneration of the filter safely in circumstances where the filter approached the

maximum permissible loading. Similar systems using cheaper cordierite filters may soon be in use on passenger cars.

II. Continuously Regenerating Traps (CRT)

A catalyst can be used to produce NO_2 upstream allowing low temperature PM oxidation, this approach was patented by Johnson Matthey plc in 1990 and has been in regular implementation throughout the last two decades. The filter is regenerated under cooler exhaust temperatures than passive regeneration (250 – 350 °C) which allows many applications to operate without any additional heat input. The presence of an oxidation catalyst also promotes the oxidation of HC and CO but leads to sulphate problems. The balance point is where the rate of soot oxidation equals the engine soot output, this occurs at an NO_2 to PM mass ratio of at least 8:1. Much research has been developed to access the suitability of the CRT for different applications. A suggested minimum NOx to PM ratio of 16:1 is suggested by Blakeman (2003). Emission legislation reductions for NOx make CRT operation more difficult but continued research in the field has maintained its popularity and applicability. The greatest hurdle for CRT technology is that if the balance point is not maintained an uncontrolled regeneration can damage the filter. This could occur as a result of continued low load operation or DOC poisoning from high sulphur fuel.

Van Poppel *et al* (2004) evaluated the suitability of the CRT system for use on a city bus. They used low sulphur fuel (< 50 ppm) to avoid damaging the oxidation catalyst and to ensure that sulphate derived particulates were low. The study was aimed at estimating the suitability of this technology for city busses. They found that the system was successful in removing over 90% of the exhausted PM and in reducing the CO and HC emissions. The system was still effective after a year of continuous service. The study included measuring the exhaust temperature and NOx to PM ratio over a typical cycle. They found that the exhaust temperature was above 250 °C for at least 70% of the time and that the NOx/PM ratio was above 15 for 70% of the time. The maker of the CRT system (Eminox / Johnson Matthey plc) recommended that the NOx/PM ratio be at least 15 and that the exhaust temperature be at least 250 °C for 10% of the time. The results are therefore unsurprising since the CRT system

used was clearly suitable for the application and the CRT operating conditions were met.

Another method of catalysing filter regeneration is to use a catalysed diesel particulate filter (CDPF). The principle of operation is similar to the traditional to the CRT except the DOC function is incorporated into the filter as a catalyst wash coat. Allanson (2002) compared the performance of various DOC, DPF and CDPF combinations. The results showed a significant improvement over the CRT if a CDPF replaced the DPF. However, the CDPF had poor performance on its own. A system investigated by Setiabudi *et al* (2003) used a silicon carbide (SiC) foam coated in a platinum catalyst. The oxidation of PM by NO_2 was shown to produce NO, this was available for re-oxidation to NO_2 inside the foam giving the NOx a catalyst like activity. The filtration efficiency was reported as 40 – 70% for the foam. The main problems with this idea are the occurrence of extra NO_2 in the exhaust (i.e. NO_2 slip), poor filtration compared to the WFF and the use of expensive catalyst materials. Johnson Matthey plc have now exploited the benefits of using a catalysed trap with their catalysed continuously regenerating trap system (CCRT). Significant wash coat improvements have been reported as late as 2005 for the next generation CDPF filters and some car manufacturers are testing passenger car deployment (Pfeifer, 2005). The CCRT is basically the same as the CRT but with the addition of catalyst in the wall flow filter as well as the upstream DOC, it will continue to meet emission legislation for many applications.

2.3.3 Electrical Thermal Regeneration Systems

The temperature of the PM is the main consideration when developing a thermal regeneration system since un-catalysed light-off temperatures are typically 550-600 °C. Direct heating of the PM, the filter or the exhaust gas has been achieved electrically and has led to the development of several electrically regenerating systems. It is inefficient to heat the whole filter during normal exhaust flow conditions due to the heat lost to exhaust. To improve efficiency, systems that heat the whole filter often do so under reduced or controlled flow rates (i.e. 'by-passing'). By-passing the filter has two requirements which are unfavourable; Firstly the by-pass system

needs valves that are capable of high temperature operation, these tend to be bulky, expensive and in some cases unreliable. The second is the need for an additional filter as the by-passed flow will need to also be filtered due to the implementation of the 'Not To Exceed' (NTE) legislation limits. Some electrical systems can avoid by-passing by allowing the filter to load with PM and regenerating it quickly with intense heat similar to the way many fuel powered systems work. The major disadvantage is the high peak power that needs to be delivered which most normal vehicle electrical systems can not provide. This mode of electrical regeneration is restricted to diesel fuelled generators which have ample electrical power. Electrical heating methods usually involve resistive heater elements which can be placed before the filter to heat the gasses flowing through it or on the surface of the filter to try to ignite the trapped PM and encourage it to burn unassisted.

An upstream heater was proposed by Zikoridse (2000) that increased the operating range of a more conventional catalytic fuel additive strategy. The system used a wall flow filter coupled with a cerium based fuel additive that reduced the light-off temperature of the soot to 300 – 400 °C. The extra 100 – 200 °C temperature rise needed during low load operation was supplied by an electrical heating element placed in front of the filter. Since the desired temperature rise was relatively small, the instantaneous input power to the heater was about 2 kW. This corresponds to approximately 200 A from the vehicle battery which is equivalent to a large diesel engine starter motor. The heating duration was 2 minutes for every 2 hours of engine use and was found to keep the filter clean during a prolonged vehicle test on a light duty delivery vehicle. Ordinarily the exhaust temperatures for this vehicle were too low to use the cerium fuel additive alone, hence this technology can be used to effectively extend the operating range of the cerium fuel additive technology.

Some work has been carried out to develop a combined heater-filter that can self regenerate using electrical power. Rypos Inc. is one of the companies that developed a working and marketable system that has been extensively tested. The filter material is a type of nickel foam which is resistively heated using an electric current. Rapid regeneration is possible although several kW of peak electrical power are required. Electrical filter regeneration like this is ideal for electric diesel generators since they

are capable of supplying many kilowatts of power. It is unlikely that this type of filter and regeneration strategy could be applicable to vehicle use without a by-pass to lower the peak electrical power requirement.

A novel strategy of removing the soot from the filter before burning it electrically was proposed by Takesa *et al* (1991). The system used a specially designed filter, similar to a conventional wall flow filter that was cleaned using jets of compressed air. The PM was collected and burned separately to the filter and exhaust flow. The idea of removing the PM in this way has many advantages. For example, the filter does not experience high thermal transients, heat losses to the exhaust are low and ash is not deposited in the filter walls. The system required many valves controlling gas flows, a compressor and a compressed air storage tank. The prototype system had a high back-pressure and the exhaust by-pass valves were found to be unreliable. Overall, although the reverse flow concept has advantages, the implementation of this technology requires more development.

Systems have been developed that use microwaves to heat up the PM inside the particulate filter to regenerate it (Garner and Dent, 1989 and 1990). This strategy has several advantages over other methods of filter regeneration. The microwave energy is not absorbed by conventional ceramic filter materials or the surrounding exhaust system allowing direct coupling of electrical energy into the PM layer. The system can have no moving parts and can be powered by the vehicles electrical system. The microwave energy can be generated by a low cost conventional magnetron. Unfortunately, heat loss to the exhaust gases as the filter temperature was increased proved too high and light-off temperatures were not achievable under full flow. Ning *et al* (1999) implemented a highly controlled microwave regeneration system taking the advice from previous research. The test setup both bypassed the exhaust flow and regulated the air flow to the regenerating filter. The result was a bulky system that required careful control and could not filter the exhaust stream for the entire regeneration event. Peak electrical power consumption was around 1 kW which can be supplied by most large vehicle electrical supplies. It is unlikely that a microwave regeneration strategy will be produced commercially, despite on going research in this field.

2.4 Summary of Regeneration Technologies

Of the available systems, the highest performance regeneration strategies were too complex, expensive or bulky to be used for vehicle applications. Most systems also experienced difficulties during certain operating conditions. This section summarises the advantages and disadvantages of the after-treatment systems previously discussed and their likely applications.

For light and heavy duty diesel applications prior to 2011, the CRT and CCRT technology will effectively meet emission legislation in most applications. Late post injection and separate fuel sprays can be used where the operating conditions of the engine are likely to be unfavourable for CRT operation. From 2004, the light duty diesel sector has benefited from the low cost of LNT implementation in combination with a DOC and DPF, the integration of LNT de-sulphation with DPF regeneration could be exploited for some designs to reduce the fuel penalty. The LNT fuel inefficiency makes its integration into the heavy duty on-highway sector unlikely. These trucks will have the greatest benefit from urea SCR which has a growing support and infrastructure. Passenger car after-treatment will benefit most from a DOC coupled with a silicon carbide WFF. The addition of a cerium fuel catalyst could be used to improve the low load operation of these systems. The use of late post injection becomes possible as common rail injection systems become increasingly common. A late post injection strategy will effectively remove the risk of system failure due to uncontrolled regeneration.

The applications requiring only PM after-treatment will be best served by a DOC and DPF with late post injection, fuel spray or engine throttling. The HC slip created by the DPF regenerations presents problems due to NTE legislation and the US will probably be forced to use additional downstream catalysts. A few niche applications will see novel after-treatment technology such as the Rypos Inc. regeneration system which is ideally suited to electrical power generation applications. Other electrical systems are unlikely to become established mainly due to the low cost of the resistively heated metal foam filters. There is an opportunity for continuous electrical

_____

regeneration technologies that have low average alternator current demands. Takesa's (1991) reverse flow regeneration system could be feasible if a more compact design could be developed and the compressor removed. A summary of the after-treatment systems for both NOx and PM that are likely to occupy the market in the near future is shown in Table 2.1.

Technology	Advantages	Disadvantages
Urea SCR (+ DOC)	Low fuel penalty Excellent NOx removal Low cost	Sulphur sensitivity Requires infrastructure Not possible at low temperature
LNT	Moderate NOx removal Low cost	Sulphur sensitivity Poor fuel economy Needs advanced combustion control
CRT	Durable/ proven method Excellent PM reduction	Sulphur sensitive High initial cost Narrow operating range High NOx output
CCRT	Excellent PM reduction Improved operating range Reduced NOx output	Sulphur sensitive High initial cost Moderate NOx slip Possible uncontrolled regenerations
Cerium + DOC + DPF	Excellent PM reduction Proven durability Low sulphur sensitivity	High initial cost Possible uncontrolled regenerations Infrastructure required
Fuel Burner + DPF	Excellent PM removal Low sulphur sensitivity Low temperature operation	HC slip necessitates DOC Intolerant of some operating conditions Poor fuel economy
Throttle + DPF	Low cost No sulphur sensitivity	HC slip requires DOC Advanced control required Possible higher engine wear
Fuel oxidising DOC + DPF	Tested technology CRT like behaviour Low fuel penalty	Sulphur sensitive High initial cost Poor low temp performance

Table 2.1. Summary of diesel emission control methods

In summary, there is no single regeneration system that can yet be used for all applications. The constraints of exhaust temperature, composition, fuel economy and

initial cost will determine the system chosen for each application. An ideal regeneration system would be one that has the following features:

    i.   Low initial cost

    ii.   Low maintenance

    iii.   Low sensitivity to fuel properties

    iv.   No sensitivity to engine operation (load and speed)

    v.   Low additional emissions

    vi.   Low impact on fuel economy

    vii.   Suitable for any engine (with scaling)

So far there is no technology that can achieve all these goals. This research investigates the novel 'Autoselective' DPF regeneration method that can be used to overcome some of the difficulties encountered with the alternative systems described.

2.5 Plasma Regeneration of DPF

Autoselective plasma regeneration is a novel method of burning the soot trapped by a DPF using a glow discharge plasma. The key advantages of Autoselective regeneration are insensitivity to exhaust conditions, no sulphur sensitivity, no infrastructure requirement and low maintenance. Autoselective regeneration uses a continuous regeneration strategy (continuous low electrical power consumption), the glow discharge automatically commutes to the heavily loaded filter sections due to the higher conductivity of the PM compared to the filter material. The conversion of electrical energy to heat at the particulate layer surface results in high PM temperatures without high filter temperatures resulting in rapid oxidation rates and low power consumption. Unlike a flame burner where oxygen is removed from the gas as it is heated, atmospheric plasma heats and chemically activates the gas so that PM oxidation is further enhanced. The electrical power requirements of the system are comparable to the vehicle lighting system making it relatively easy to fit to a vehicle and retrofitting the system does not require any modifications such as engine tuning or fuel changes. The technology uses the well developed wall flow filter

technology offering 99% filtration efficiencies. Autoselective regeneration has shown a tolerance for changes in engine operating conditions in terms of exhaust gas composition, temperature and flow rate (Proctor, 2007).

Autoselective regeneration uses a low power glow discharge between metal electrodes with current of the order of 10 mA. The discharge is non-equilibrium which describes the property of different ion and electron temperatures. This property is a result of the strong electric fields within the plasma and the higher mobility of electrons compared to ions. The electron temperature is sufficient to provide the energy required for the production of reactive gas species such as O^- radicals, NOx and Ozone (O_3). The reactive species have been shown to allow lower temperature oxidation of PM. The bulk of the electrical power consumption is released as heat of which some occurs at the carbon to gas interface. The discharge is observed to rapidly oxidise the soot in this region.

The filter material may experience cracking and melting due to the high temperatures present within the plasma column and at the gas to PM interface. It is important not to damage the filter material when regenerating it since this will render the regeneration system ineffective. A cooling time was introduced early in the development of this technology during which the discharge current is interrupted to allow cooling of the filter (Proctor, 2007). By varying the duration that the discharge remains on and the duration of the rest time (typically 40 ms on and 50 ms off), it is possible to keep the peak temperatures below the melting temperature threshold of the particulate filter. These times will be known as the on- and off-times in subsequent chapters. The use of on- and off-times has a the further benefit of increasing the discharge mobility. The natural mobility of the continuous discharge is low since the hot plasma column makes a low resistance path for the discharge current which extinguishes during the off-time. When the discharge is turned on again, the conductive plasma path no longer exists and the discharge initiates at the easiest breakdown path which is normally the area of highest filter loading. This is an important process because the increased mobility ensures discharge is regenerating only the parts of the filter with the highest loading.

2.6 Concluding Remarks

This chapter has introduced the various diesel after-treatment solutions that have been previously developed. The literature review shows that all the available technology has significant limitations which ultimately make each technology suitable for only a proportion of applications. The Autoselective regeneration system has many advantages as shown by Proctor (2007). The insensitivity to engine operation conditions could enable production of a DPF regeneration system that can be scaled for all diesel engine applications. There is also a significant possibility of making a retrofit technology if the power consumption can be kept at a level comparable to a vehicular lighting system.

The remainder of this thesis describes the original research of the Autoselective regeneration system. Chapter 3 summarises the available power source options for the glow discharge and Chapter 4 investigates how the discharge can be optimised to offer better regeneration performance.

3. Electronic Plasma Power Supplies

This chapter discusses the challenges of sustaining electrical discharges and the resulting power supply complexities. The final part of this chapter details the design of some of the power supplies developed for the research.

3.1 Plasma Production and Maintenance

Plasma is a gaseous state of matter containing free charge carriers of dissociated electrons and ions making it electrically conductive. Plasma can exist under virtually all gas conditions in terms of composition, pressure and temperature making its properties extremely variable. This research concentrates on glow-like discharges at around atmospheric like conditions and up to moderately high temperatures (< 5000 K). A diagram showing how these discharges relate to other common forms of plasma is shown in Figure 3.1 (Roth, 1995).
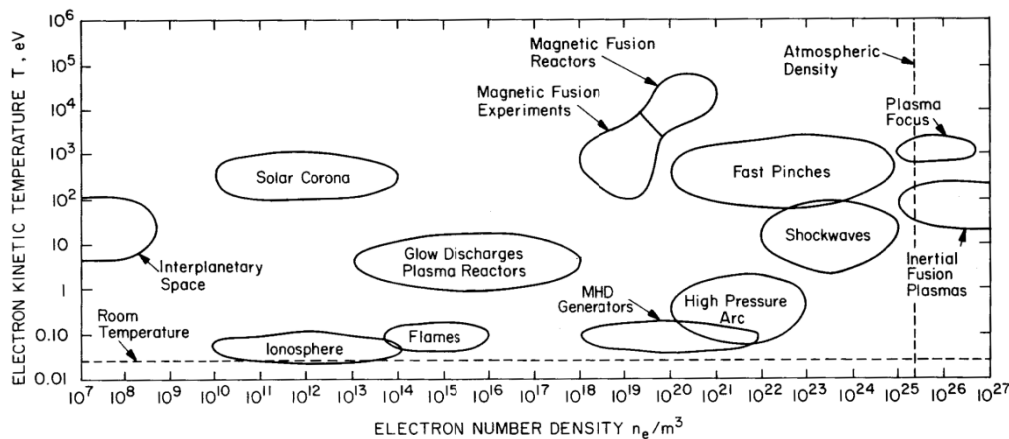
Figure 3.1 Plasma characterisation, adapted from Roth (1995)

Plasma is usually produced by supplying sufficient energy to the molecules and atoms of a gas to cause electron emission producing a positive ion and free electron. For this research, ionisation energy was supplied conveniently using electrodes and an applied voltage and current. Once the gas has become ionised, there is an attraction between the electrons and ions. Recombination of the electrons and ions

leads to energy release as heat, chemical changes and photon emission. The recombination rate increases with pressure since there are more collisions between electrons and ions, under atmospheric conditions the recombination time constant is of the order of 100 µs (Roth, 1995). Energy needs to be supplied continuously by the power source to keep the rate of ionisation equal to the rate of recombination, otherwise the plasma will eventually fully recombine to a non-conductive gas state.

3.1.1 Electric Breakdown

The power supply must be capable of supplying the ionisation energy to start the discharge, often know as ignition. When using static electrodes, ignition is nearly always initiated by applying a high voltage. When the voltage is sufficient, the insulating properties of the gas are overcome and a conductive channel forms leading to a spark. The voltage at which this occurs is called the breakdown voltage. The value of the breakdown can be approximated for air gaps of several millimetres using Paschen's law (Paschen, 1889) described by

$$V = \frac{a(pd)}{\ln(pd) + b}$$

Equation 3.1

were V is the breakdown voltage, p is the pressure, d is the electrode separation and the two constants a and b are determined by gas composition. For air at STP (IUPAC), a breakdown voltage of $\approx$ 3 kV.mm^{-1} is typical. The breakdown between the electrodes is known as an avalanche (Roth, 1995) because of the way the number of charge carrying electrons increases rapidly with distance from the cathode. The electric field at breakdown is sufficient to accelerate a free electron within the gap to a sufficient energy to cause an ionisation event releasing a second free electron. The initial source of the first electron is from either background ionisation, radiation or from photo-electric emission from the electrodes. Irrespective of the source of the electron, the ionisation event it causes results in a second electron being released and both experience an accelerative force in the electric field. The two electrons accelerate and cause further ionisations giving rise to additional electrons and this process continues giving rise to large numbers of dissociated electrons. The resulting positive ions accelerate towards and collide with the cathode causing additional

electrons to be released and a highly conductive channel is eventually formed between the electrodes. The charge built up on the electrode capacitance discharges rapidly into the channel forming a narrow arc discharge known as a spark.

3.1.2 Spark to Stable Discharge Transition

Immediately following the breakdown is the transition period. If the current is allowed to fall to zero, the ions and electrons in the gap recombine and the spark extinguishes. If the power supply can maintain a current between the electrodes that is sufficient to prevent extinguishing then a discharge is formed. The level of current delivered determines the discharge regime as shown in Figure 3.2 (Roth, 1995). If the current is within the glow discharge range ($\sim 10^{-3}$ to 10^{-1} A in air) then a glow discharge will form.

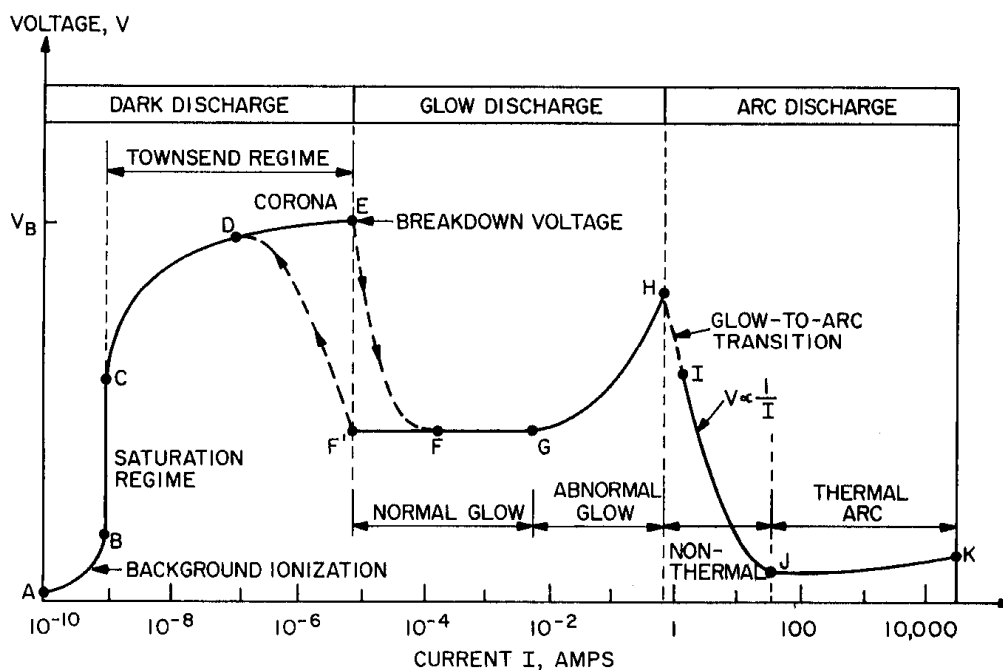**Figure 3.2** Current and voltage relationship of a typical plasma showing modes of operation (Roth, 1995)

The breakdown to glow transition was found to be a difficult process to achieve electrically. The electrode capacitance shunts the current away from the discharge (Hu, 2001) which leads to instability of the discharge current. Gas flow and adjacent matter remove charge carriers from the plasma encouraging it to extinguish

completely. The discharge will extinguish completely if it does not undergo the transition within the time it takes for the ions and electrons to recombine which is at approximately 1 ms for air at 1 atm and 300 K.

3.1.3 Sustained Glow Discharges

After the discharge transition has occurred, the plasma exhibits a negative resistance characteristic about its operating point (Herrick, 1980). Increases in discharge steady-state current result in a decrease in steady-state discharge voltage. This occurs because increases in current add energy to the discharge which increases the electron concentration and hence conductivity.

The increase in numbers of electrons results from the change of the recombination to ionisation ratio. This ratio determines the number of electrons and ions there are available for conduction. The discharge voltage is a measure of how difficult it is to transfer charge through the discharge so as more charge carrying electrons become available, the voltage drops. The recombination rate of electrons and ions has a time constant of the order of 100 µs for air (1 atm, 300 K, 15 mA glow discharge) such that the plasma can not react instantly to changes in current. The measured voltage and current waveforms for a 26 kHz discharge (atmospheric conditions, 3.5mm electrode spacing, steel electrodes, inductively stabilised) is shown in Figure 3.3, at this frequency the discharge behaves resistively i.e. the current and voltage waveforms are in phase.
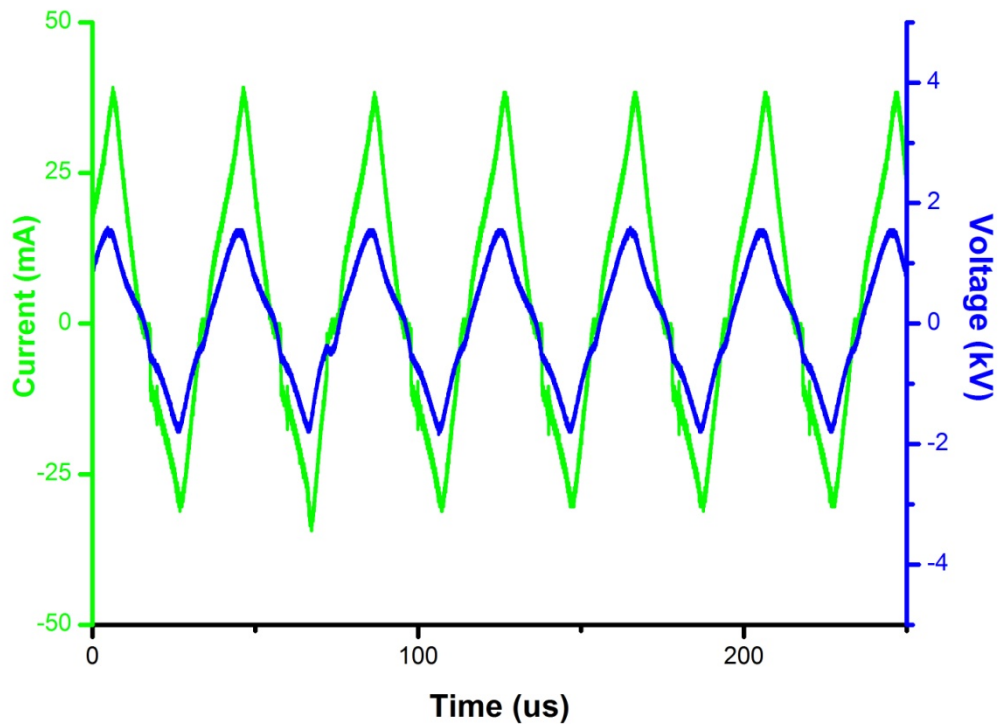
Figure 3.3 Example of discharge current and voltage at 26 kHz

At lower frequencies, the discharge exhibits negative resistance characteristics since the recombination time constant is faster than the changing discharge current. Figure 3.4 shows measured glow discharge waveforms at 50 Hz where the voltage decreases as the current increases. The voltage transients at the beginning of each half cycle are a result of the discharge extinguishing during the current zero crossing; each half cycle begins with a breakdown event.
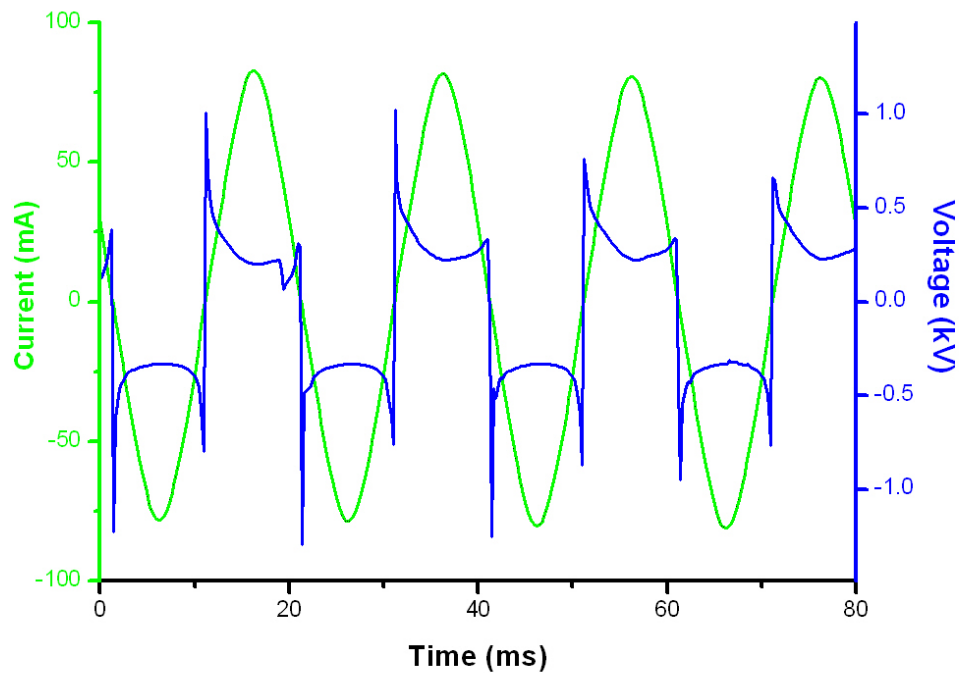
Figure 3.4 Example of discharge current and voltage at 50 Hz

The steady-state negative resistance characteristic can be plotted for a given electrode separation and environmental conditions, Figure 3.5 shows the measured characteristics for a 3.5 mm discharge in air. This curve describes the steady-state voltage of the discharge after the initial transient, the characteristic can be used to model the discharge behaviour as discussed later in Section 3.2.
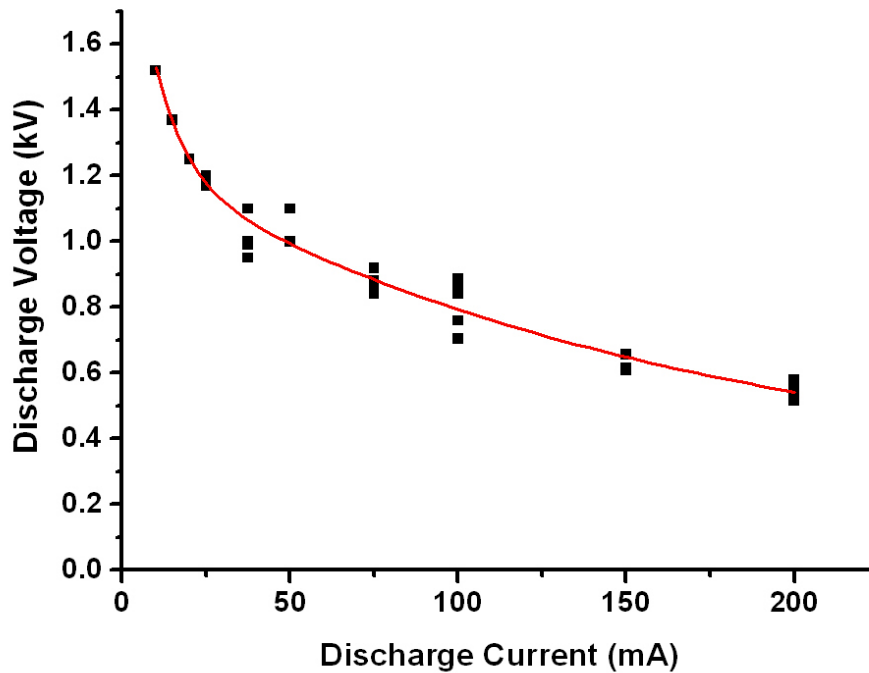
Figure 3.5 Steady-state peak discharge voltage versus rms current for atmospheric glow discharge over 3.5 mm electrode spacing

A step decrease in current will result in an initial decrease in voltage before rising to a higher value, the opposite is true for step increases in current. The 26 kHz discharge measured waveforms showing a step decrease are shown in Figure 3.6, the voltage can initially be seen to follow the discharge current before gradually increasing over the next few cycles (each complete cycle is 40 µs).
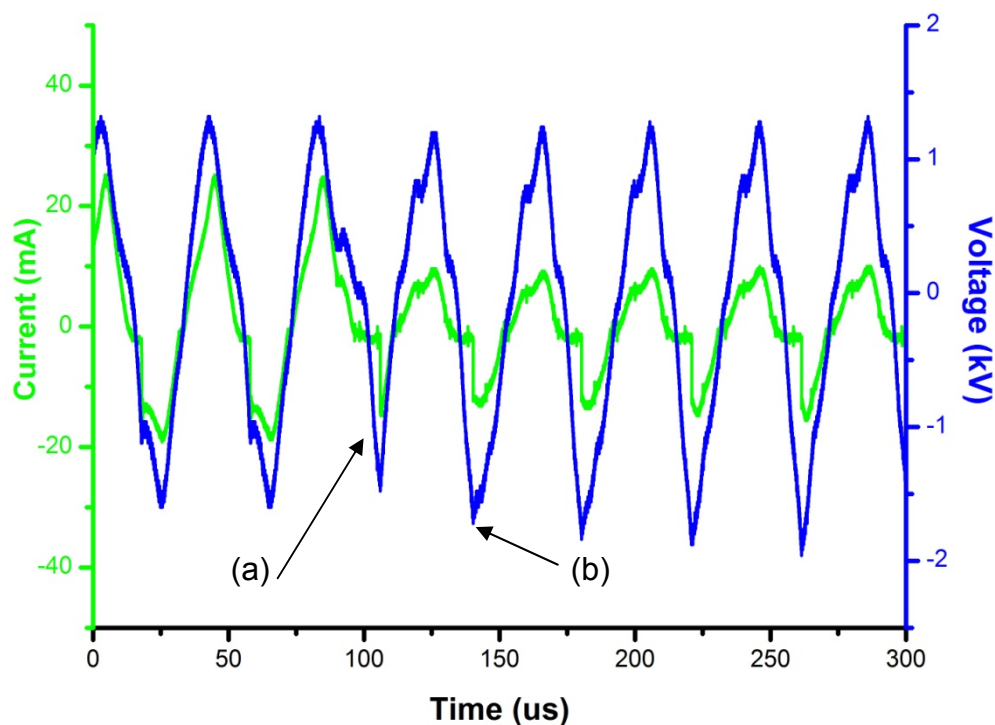
Figure 3.6 Discharge current step decrease transient. Drop in discharge current (a) results in an immediate drop in discharge voltage. The discharge then begins to increase (b) to the new higher steady-state value.

3.1.4 Electronic and Electrical Power Supplies

There are several power supply topologies used to sustain electrical discharges at steady-state, these will be discussed here. The discharge is usually between metal electrodes connected to the power supply. The supply needs to be designed to:

    i.   Achieve breakdown of the electrode gap

    ii.   Limit and regulate the current during the transition phase

    iii.   Sustain a steady current level during steady-state operation

Breakdown is achieved by applying a potential greater than the breakdown voltage to the electrodes (Paschen, 1889). For atmospheric plasma supplies, the breakdown voltage is often supplied by the action of a high voltage step up transformer capable of operating for sustained periods above the breakdown voltage.

During the initial transition period after breakdown, a highly conductive channel exists between the electrodes (Roth, 1995). This is an effective short circuit (zero resistance load) which could damage a power supply without a current limit. In most power supply topologies the current limiting is designed to accommodate this condition and the output can be shorted for short durations.

Sustaining the discharge after breakdown is difficult because the negative resistance characteristic of the discharge causes voltage control strategies to be unstable (Ben-Yaakov, 2001). The conventional method of sustaining a discharge is to place a larger dominant impedance in series with it, this may be inductance, capacitance or resistance. The power supply is designed to drive the dominant impedance which provides current regulation in the discharge; i.e. if an inductor with an impedance 3 times that of the discharge (R_p) is used in series (a typical value chosen), then a change in plasma voltage of +/- 100% yields a change in current of -12% and +5% respectively. The most important effect of the series impedance is that the negative resistance characteristic of the discharge is cancelled out which allows simple voltage control.

3.2 Series Impedance Stabilisation

The use of a series impedance is often the most convenient way to stabilise a discharge. There are a few applications were other stabilisation techniques can be used, these will be covered in subsequent sections. The series impedance in most applications is an inductor for reason detailed in the proceeding section.

3.2.1 Series Inductance

An ideal inductor has zero resistance and no magnetic losses, this is not the case in reality and both resistive heating and core losses (due to eddy currents in the magnetic path) lead to power dissipation. The size of an inductor is a function of its power dissipation assuming simple wound construction and reasonable limits on operating temperature (limited by a combination of the Curie temperature and insulation melting point). The size of an inductor is therefore a function of the losses

which can be simplified a sum of the real power and the product of the reactive power and loss factor shown in Equation 3.3.

$$P_{dissipation} = I_{rms}^2 \cdot R_{windings} + I_{rms} \cdot V_{rms} \cdot K_{loss}$$

Equation 3.2

where I and V represent the operating conditions of the inductor, R and K are the winding resistance and loss factor respectively. To make the inductor as small as possible, the wire gauge, core material and insulation need to be chosen carefully.

The exact dimensions of the component used are determined by the construction. Since the loss factor is a function of frequency, there are many differences between high frequency and low frequency inductors. The reactive power must be kept low to limit the size and losses of the power supply. The minimum inductor required that will enable voltage control of the plasma can be shown to be (see appendix III for details)

$$X_L \geq \sqrt{Rp \cdot Rn}$$
$$X_L = 2 \cdot \pi \cdot f \cdot L$$

Equation 3.3

where X_L is the reactance of the inductor, R_p and R_n are the plasma positive and negative impedances respectively, f is the frequency of operation and L is the inductance in Henries. In practice, a larger inductor is always used to guarantee stability. The concept of R_p and R_n are discussed later in section 3.3.

The size of the inductor will also be affected by the breakdown voltage required. Experience has shown that above approximately 1000 V, special winding techniques are required to insulate the inductor so that a breakdown does not occur between the windings. For voltages above 6 kV an insulating potting material is usually needed to prevent corona (i.e. parasitic electrical breakdown) leading to increased inductor size. The Autoselective power supply must supply voltages up to 30 kV requiring substantial insulation.

Inductor stabilised supplies have the advantage that they have an increasing impedance with frequency as shown in Equation 3.3. For this reason inductively stabilised plasma power supplies can use a square wave since the majority of the power will be at the low frequency harmonics. This enables the use of simple hard switching electronic power supplies.

For inductively stabilised power supplies, ignition can be carried out using the inductor itself; thus removing the need for other components. This can be achieved by resonance or by transformer action.

3.2.2 Series Capacitance

Capacitive stabilisation uses a series capacitor to limit the current through a discharge. The main advantages of capacitive stabilisation are higher power density for the stabilising element and ease of parallel combination. The higher power density results because capacitors can withstand far higher power throughput for a given volume.

Although inductors can be placed in parallel, experience has shown that they can not share the same magnetic paths and hence dense arrays are not possible. Capacitors can be placed in dense arrays and as distributed networks making them ideal for large volume plasma reactors. A special case known as a dielectric barrier discharge can be produced across a surface with distributed capacitance (Roth, 1995), this is shown in Figure 3.7. The dielectric in this case is a glass sheet, one electrode is a copper foil sheet behind the glass, the plasma spreads across the glass surface from the upper copper electrode (a two pence coin has been used for scale purposes). The barrier discharges are normally used where large plasma volumes are needed.

Figure 3.7 A dielectric barrier discharge, the dielectric is a glass sheet between the coin and copper foil ground plane

Capacitive stabilisation has two main disadvantages, one is that capacitive stabilised discharges are not useable with capacitive loads, a detailed example is given below. The second is that the impedance decreases with frequency which causes significant power to be drawn at harmonics of the drive frequency. This requires the power supply to be specially designed to drive a capacitive load, such supplies invariably use a large inductor to cancel some of the load characteristics of the capacitance which usually overcomes the power density advantages.

Capacitive stabilisation of the electrodes used for the Autoselective system is impractical at moderate frequencies (>10 kHz) due to the voltages required. This can be illustrated using the following example. A reasonable limit on maximum voltage is chosen at 50 kV for the example. The electrode capacitance is chosen to be 50 pF and the discharge is operating at 15 mA with a sustaining voltage of 2 kV and a breakdown voltage of 10 kV. These are realistic conditions for the Autoselective system when using inserted electrodes. The equivalent circuit is shown in Figure 3.8 where C_s is the stabilising capacitance, C_e is the electrode capacitance and R_e is the effective discharge resistance.
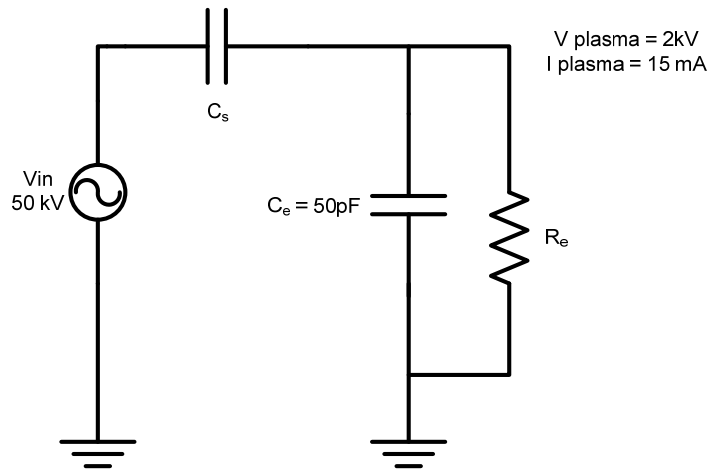
Figure 3.8 Capacitive stabilisation equivalent circuit

Using the equivalent circuit and known parameters (15 mA, 2 kV rms)

$$R_e = \frac{V_{plasma}}{I_{plasma}} \approx 133 \, k\Omega$$

Equation 3.4

The value for C_s can be calculated by solving the equivalent circuit. It can be shown that (see Appendix III for details)

$$C_S = \frac{1}{\omega} \left(\frac{1 + (\omega C_e R_e)^2}{\left|\frac{V}{I}\right|^2 - R_e^2} \right)$$

Equation 3.6

where V is the supply voltage amplitude, ω is the angular frequency and I is the load current flowing in R_e.

The breakdown voltage, V_{br}, is the voltage that is applied to the electrodes before the discharge has started and is simply.

$$V_{br} = V_{in} \frac{C_s}{C_s + C_e}$$

Equation 3.7

Figure 3.9 plots the above relationship showing the window of operation possible for capacitive stabilisation with respect to frequency. The window upper limit is the

highest frequency at which breakdown is possible (>10 kV), the lower limit is typically 1 kHz for air (Roth, 1995) set by the discharge extinguishing time constant. If the operating frequency is below 1 kHz the discharge will become discontinuous and stabilisation will not be possible. A narrow range of 1 kHz to 4 kHz is therefore possible.
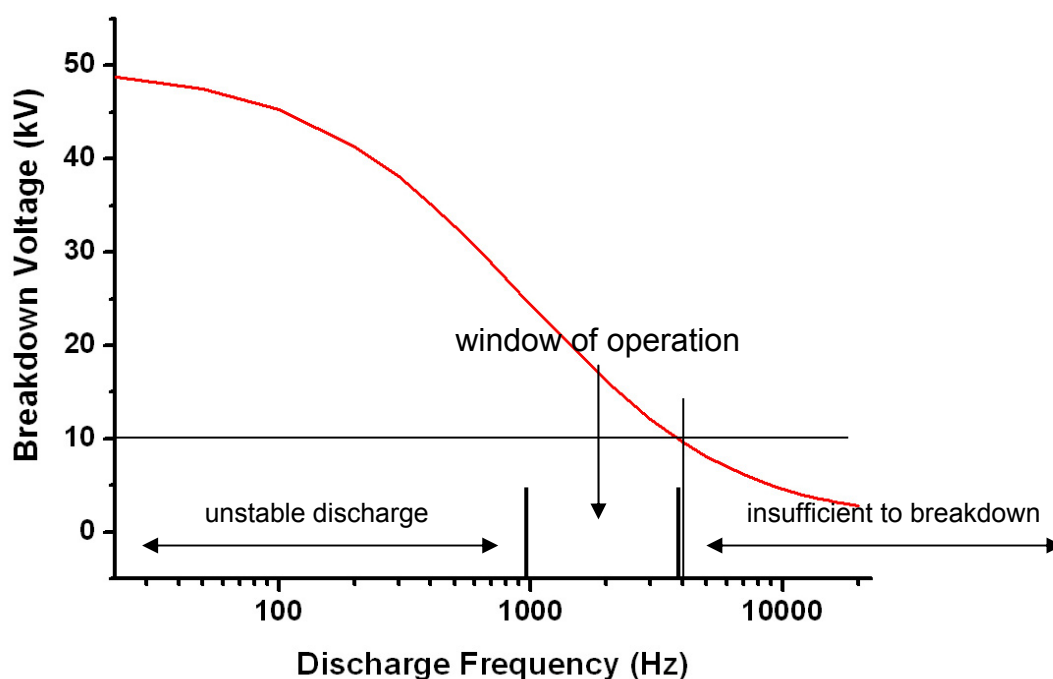
Figure 3.9 Available breakdown voltage versus frequency

In practice, it is difficult to create a sinusoidal voltage of 50 kV at frequencies less than 10 kHz without using a large transformer. Large transformers detract from the high power density advantage of capacitors. Capacitive stabilisation is therefore not attractive at low frequencies (<10 kHz) and is restricted to applications with either low size constraints or low electrode capacitance.

3.2.3 Other Stabilisation Techniques

In some cases other stabilisation strategies are used, this section briefly describes the main types and explains why they are unsuitable for Autoselective regeneration. The remaining power supply types can be divided into the three groups of series resistance, virtual impedance and energy limited.

Series resistance is similar to capacitive or inductive stabilisation in that series impedance is used to cancel out the undesirable negative discharge impedance. In the case of resistive stabilisation the losses are high since the current and voltage are in phase. For this reason, resistive stabilisation is only used when the power losses are either very small or the heating energy is useful to another process. The resistive impedance must be equal or greater than the plasma negative resistance which makes resistive stabilisation less than 50% efficient in most cases.

Virtual impedances are a relatively new method for controlling discharges. Theory suggests that the control loop can be designed to respond fast enough to emulate a series stabilisation network. In practice, the discharge parameters need to be well defined and constant to allow this type of control. Discharge lamps can be controlled using a virtual impedance as shown by Ben-Yaakov (2001).

It is also possible to control discharge power using an energy limited method. The control is achieved by limiting the current in an electronic converter or by applying controlled bursts of energy. Stability is achieved by preventing the discharge characteristics altering the controlled parameter (current or power). There are many possible configurations, one example is a capacitor discharge pulsed power supply. For this type of power supply a capacitor is charged to a specified voltage which is then discharged into the plasma. The power (P) is controlled by either the discharge rate (f) or the charging voltage (V) given by

$$P = f \cdot E$$

where

$$E = \frac{1}{2}CV^2$$
<div align="right">Equation 3.8</div>

where E is the stored energy and C is the capacitance. The main disadvantages of this method are the non-sinusoidal current waveforms, higher component stresses and large energy storage components. This type of power supply is not suitable for Autoselective regeneration because the non-sinusoidal current waveforms reduce the filtration efficiency of the WFF as detailed in Chapters 5 and 7.

3.3 Power Supply Control Theory

This section discusses how a power supply can be developed to control an electric discharge. Load characterisation is needed to build any power supply, the following section analyses the discharge load.

3.3.1 Discharge Load Modelling

The negative dynamic resistance (R_n) characteristics for the Autoselective discharge can be found from the from the derivative of the voltage (V_{rms}) and current (I_{rms}) relationship (Figure 3.5) which is approximated by (using an exponential curve fit)

$$V = a + b \cdot e^{-k \cdot I}$$
<div align="right">Equation 3.9</div>

where a, b and c are arbitrary constants measured from the results

$$a = 278$$
$$b = 403$$
$$k = 44.4$$

These figures are only valid between 10 mA and 30 mA discharge current, 3.5 mm electrode spacing and a 26 kHz discharge. The derivative of this is therefore

$$R_n = \frac{dV}{dI} = -b \cdot k \cdot e^{-k \cdot I}$$
<div align="right">Equation 3.10</div>

This expression describes the effective steady-state value of the negative dynamic resistance after the discharge has stabilised. The high frequency discharge impedance, or positive resistance (R_p), can be approximated from the same characteristic since the voltage and current both zero cross at the same time and are in phase above approximately 10 kHz (Roth, 1995). The transient resistance line is therefore the derivative of a line passing through the origin to the steady-state operating point i.e.

$$R_p = \frac{(a + b \cdot e^{-k \cdot I})}{I}$$
<div align="right">Equation 3.11</div>

where I is the discharge current. The relationship is illustrated graphically in Figure 3.10.
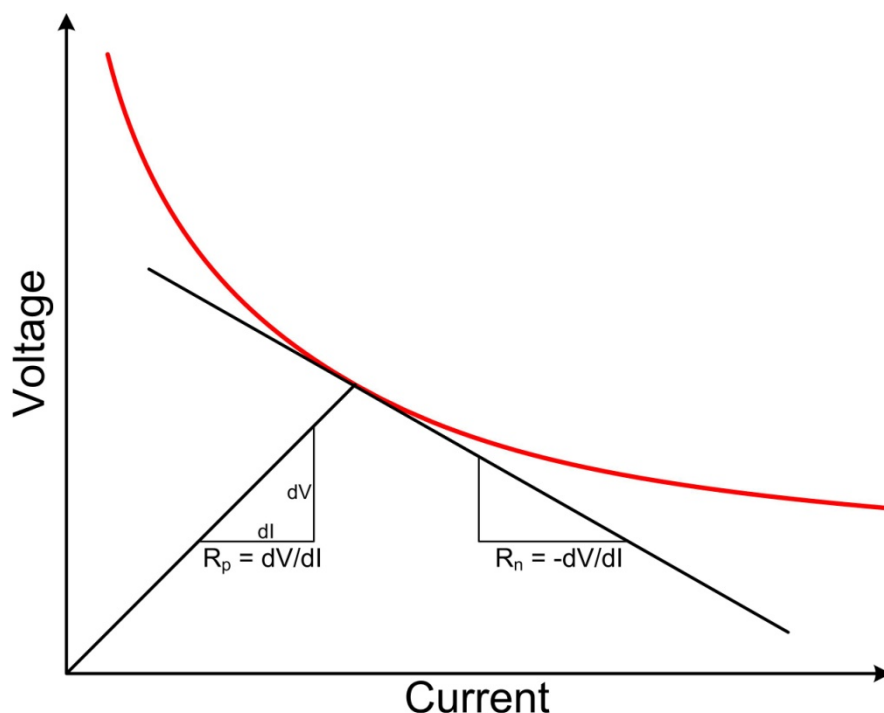

Figure 3.10 Resistance model of a discharge

The voltage-current relationship is described by the positive resistance R_p for deviations in discharge current that occur faster than the ionisation time constant. For slower deviations the discharge resistance follows the negative dynamic resistance R_n. The above analysis gives some insight into the way the discharge behaves as an electrical load but it can not provide any information about the response of the discharge at different frequencies. Frequency domain analysis of discharges was first described by Herrick (1980) and Laskowski (1981). A more thorough analysis is given by Deng (1995) who describes the complex impedance of a tube lamp. Although the literature focuses on the characterisation of discharge lamps, the same plasma physics and analysis can be applied to atmospheric discharges.

Figure 3.11 shows a possible discharge equivalent circuit (Deng, 2001) which has the response described by the relationship in Figure 3.10. The circuit has a steady-state (DC) resistance of R1 in parallel with R2 and at high frequency ($\omega \to \infty$) a resistance of R2, the inductance L models the frequency dependence due to the ionisation time constant. Z_s is the output impedance of the voltage supply which is used later in the

analysis. The circuit can be used to approximate the behaviour of the discharge if R1 is given a negative value. This model is most useful for small signal analysis for determining the stability of the discharge. In this case, R1, R2 and L take constant values.
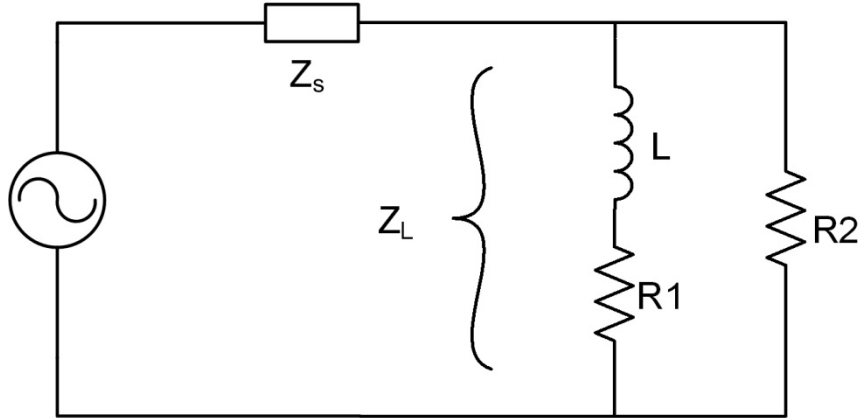
Figure 3.11 Equivalent discharge circuit

Using this as an approximation of the equivalent circuit, it can be shown that

$$R1 = \frac{R_p R_n}{R_p - R_n}$$

and

$$R2 = R_p \qquad \qquad \text{Equation 3.12}$$

where R_p is the positive resistance and R_n is the negative resistance as shown in Figure 3.10. This relationship yields a pole and a zero in the continuous (s) domain at

$$Zero = -\frac{R_p R_n}{L(R_p - R_n)}$$

$$Pole = -\frac{R_p(1 + R_n)}{L(R_p - R_n)} \qquad \qquad \text{Equation 3.13}$$

R_n is approximated by Equation 3.10 and R_p is approximated by Equation 3.11. By inspection, the dominant reciprocal term of the function for R_p (Equation 3.11) ensures that $R_p > R_n$. Since R_p - R_n is always positive, the zero is in the right hand

plane (RHP). The small signal discharge impedance can therefore be represented in the form

$$Z_L(s) = k\frac{s-a}{s+b}$$ Equation 3.14

were a and b represent the positive constants of the RHP zero and LHP pole respectively, k is an arbitrary constant and s is the Laplace operator. This is shown graphically in Figure 3.12.

This model has several simplifications that make it unsuitable for large signal analysis. Firstly, the model is only valid at the operating point during steady-state operation. The model breaks down at low currents due to extinguishing of the plasma. The model does not take into account the electrode voltage drops which add non linearity to the model. In practice, additional non-linearity is experienced from the discharge which does not behave exactly as a linear resistance. These limitations make the model unsuitable for transient analysis of the discharge, however, it is useful for determining the stability limits of a power supply using conventional control theory, this is detailed in the next section.
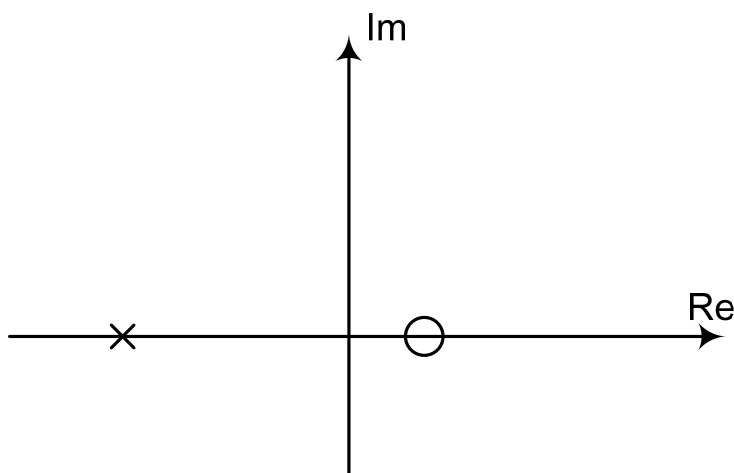

Figure 3.12 Discharge impedance representation and the complex plane

3.3.2 Control Theory Applied to Discharges

Conventional control theory can be used as a design tool when making power supplies for discharges. The large signal analysis is usually condensed into three regions:

     i.   Open circuit operation

     ii.   Short circuit operation

     iii.   Breakdown transient operation

This is because a large signal discharge model is difficult to simulate with normal techniques. The power supply must be capable of brief open circuit operation during the delay before breakdown. It must be able to provide sufficient breakdown voltages and successfully transition from breakdown to steady-state. The steady-state stability analysis can then be performed as follows.

Representing the discharge complex impedance in the form as shown in Equation 3.15

$$Z_L(s) = k\frac{s-a}{s+b}$$ Equation 3.15

shows that the impedance can not be directly driven by a voltage source since the resulting current will have an oscillatory RHP pole as shown by Equation 3.16.

$$\begin{aligned}I(s) \;&= \frac{V(s)}{Z_L(s)}\\&= \frac{V(s)\cdot(s+b)}{k\cdot(s-a)}\end{aligned}$$ Equation 3.16

If the circuit is represented as a voltage source with a series arbitrary impedance $Z_S(s)$, as shown in Figure 3.13, then the stability criteria can be found.
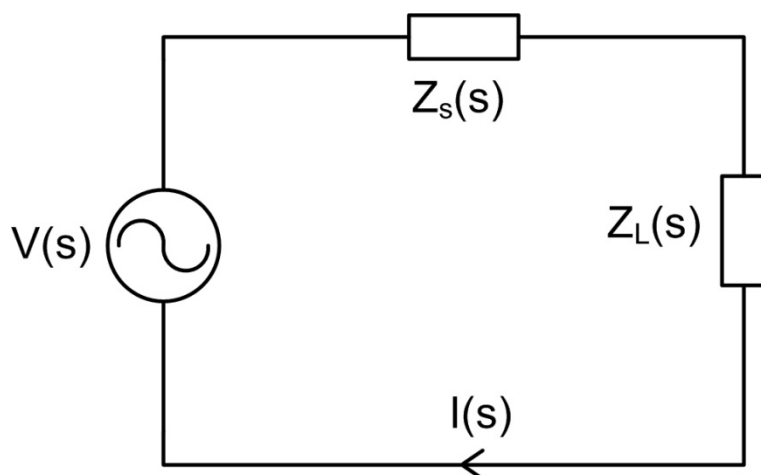
Figure 3.13 Circuit of discharge and source impedance

The circuit closed loop transfer function (CLTF) of the feedback system becomes

$$\text{CLTF} = \frac{V(s)}{Z_S(s)} \cdot \frac{1}{1 + \dfrac{Z_L(s)}{Z_S(s)}}$$

Equation 3.17

The characteristic equation (CE) of the system,

$$\text{CE} = 1 + \frac{Z_L(s)}{Z_S(s)}$$

Equation 3.18

determines the stability of the current I(s). Nyquist's stability theory states that the system will be unstable if the CE has any RHP poles i.e. the Nyquist plot encircles the point (-1,0). A sufficient, but not exclusive, condition for stability can therefore be expressed as (Deng, 2001)

$$\left| \frac{Z_L(j\omega)}{Z_S(j\omega)} \right| < 1$$

Equation 3.19

This shows that the stabilising impedance must be of greater magnitude than the lamp impedance at the operating point. This is a fundamental rule of discharge power supplies since failure to meet the criteria results in a power supply that can not maintain a stable discharge current. In practice, the entire range of output currents must be considered when designing the power supply since the magnitude of $|Z_L(s)|$

changes depending on the operating point. The design of a power supply for the Autoselective system is detailed in the next section.

3.4 Plasma Power Supply Design

Several power supplies were built during this research in order to test a variety of parameters such as frequency and current level. This section describes the development of the most successful power supply circuit, namely the voltage fed resonant transformer. The other power supplies developed for this research are detailed in the Appendix I.

3.4.1 Power Supply Types

The Autoselective technology was tested over a wide variety of conditions, the electrode array that performed best is used in this section here to compare different power supply types. The actual electrode array is detailed in Chapter 5.

The conditions for the comparison used a static electrode capacitance between 10 pF and 100 pF (dependant upon the soot loading). The break down voltage was approximately 20 kV - 30 kV. A current range of 10 mA to 30 mA was used, continuous current was a requirement. The latter effectively ruled out discharges below 1 kHz, no upper frequency limit was imposed although practical limits applied.

The capacitive stabilised type of power supply was immediately ruled out due to the high electrode capacitance and maximum voltage limit which closed the operating window as defined in Section 3.2.2. The energy limited (pulse) power supplies were ruled out by the need for continuous discharge currents. Pulsating currents reduced the filtration efficiency of the filter as detailed in Chapters 5 and 7. Virtual impedance power supplies were considered although stabilisation was not successful due to the changing discharge properties during the regeneration.

The most promising power supply type was inductive stabilisation which could be achieved in several ways, namely:
    i.   Voltage fed inductor
    ii.   Transformer fed inductor
    iii.   Combined transformer and inductor

The maximum discharge impedance was >100 kΩ, an inductor with reactance of the approximately of at least 150 kΩ would be required to ensure stability across the range of currents. A low operating frequency was considered to reduce the effect of electrode capacitance, in practice this led to difficulties with all the above topologies. An inductor wound for 1 kHz operation which required 30 kV of isolation was physically too large for the application. If the operating frequency was increased to 20 kHz, the inductor became smaller but the reactive power increased to 11 kvar at breakdown (30 kV, 20 kHz and 100 pF). Although 20 kHz was not the best choice from an efficiency perspective (high peak power), it ensured the electrical components were kept small and avoided the audible frequency range of humans (typical upper limit is 12 kHz to 18 kHz depending on age).

The voltage fed inductor circuit proved to be unfeasible since it required a supply capable of switching > 30 kV directly. This type of topology is only suited to low voltage applications such as fluorescent lamp ballasts (using current semiconductor technology).

The transformer driven inductor allowed operation from a low voltage switching supply but the parasitic capacitance of the transformer and inductor windings made the resulting output voltage much lower than the drive and led to interference between the stabilised outputs when multiple discharges were required.

The combined inductor and transformer was therefore the best topology for the application, the remaining difficulty was the large reactive power consumed by the parasitic capacitance during breakdown. This power could be supplied in two possible ways, either using an external pulsed power device or using the transformer itself. The latter was conveniently achieved by driving the high voltage transformer at its resonant frequency such that the breakdown voltage was developed over several cycles of oscillation. The peak reactive power was confined to the transformer secondary windings and electrode capacitance which greatly reduced the peak power demand on the electronic drive circuitry. This effect allowed breakdown to be

easily achieved providing the power supply was driven at its resonant frequency given by

$$f = \frac{1}{2 \cdot \pi \cdot \sqrt{L_L (C_p + C_e)}}$$

Equation 3.20

where L_L is the transformer leakage inductance, C_p is the parasitic capacitance of the transformer windings and C_e is the electrode capacitance. A model of the development of the voltage fed resonant transformer circuit was required to determine the effect of resonance on stability and current regulation. The design the electronic inverter and controller also required a model of the transient behaviour of the circuit. A transient model was derived from first principles as detailed in the next section.

3.4.2 Voltage Fed Resonant Transformer Analysis

A suitable high voltage 20 kHz transformer was sourced for the design (manufactured by 'Information Unlimited'). This research did not focus on further optimisation of the transformer itself but on the design of the control and drive electronics. The transformer parameters were measured and a circuit model was produced to enable the design of a suitable electronic drive.

A voltage fed half-bridge inverter was used to make the AC waveform for driving the transformer and shown in Figure 3.14.
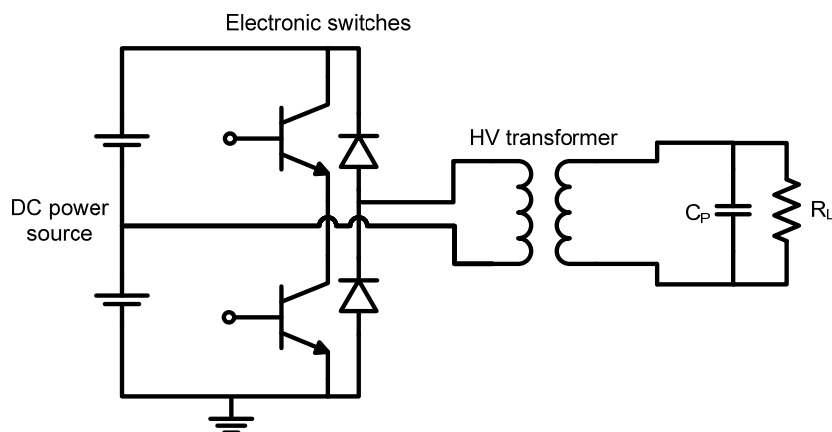

Figure 3.14 Voltage fed half-bridge and resonant transformer circuit

The leakage inductance of the transformer limited the discharge current and caused the output current waveform to be approximately triangular. The Fourier series of a triangle wave with an amplitude of 1 and period 2T can be shown to be (Weisstein, 2010)

$$f(x) = \frac{8}{\pi^2} \sum_{n=1,3,5...}^{\infty} \frac{(-1)^{(n-1)/2}}{n^2} \cdot \sin\left(\frac{n\pi x}{T}\right)$$

Equation 3.21

The total power, P, of the same triangle wave current applied to a resistor R is known to be

$$P = I^2R = \left(\frac{1}{\sqrt{3}}\right)^2 \cdot R$$

Equation 3.22

The power in the fundamental component of the series is therefore

$$P = I^2R$$
$$I = \left(\frac{1}{\sqrt{2}}\right) \cdot \left(\frac{8}{\pi^2}\right) \cdot \frac{-1^{(1-1)/2}}{1^2} = \frac{8}{\pi^2 \cdot \sqrt{2}}$$

Equation 3.23

It can be seen that the fundamental accounts for 98.6% of the power delivered to the load. This means that the half-bridge circuit can be approximated as sinusoidal voltage source which simplifies the analysis. The resulting model is shown in Figure 3.15.
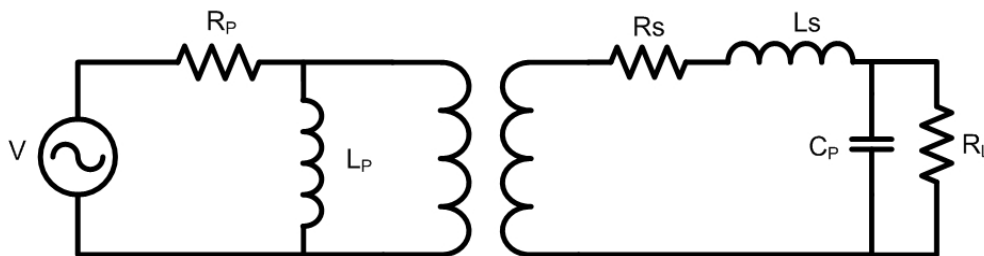

Figure 3.15 High voltage transformer model with sinusoidal source

The resistor R_p was measured to be less than 50 mΩ whereas the resistor R_s was 1800 Ω. R_p can be shown to consume only 4.4% of the total parasitic resistive losses assuming L_p is sufficiently large. The value of L_p was measured to be 6.3 mH resulting in an addition power dissipation of 1.9 mW in R_p. This allows the resistor to be excluded from the simulation without significant loss of accuracy, since L_p is then directly across the voltage source it can also be omitted. The voltage source can then be transformed across the transformer by multiplying by the turns ratio resulting in the circuit shown in Figure 3.16.
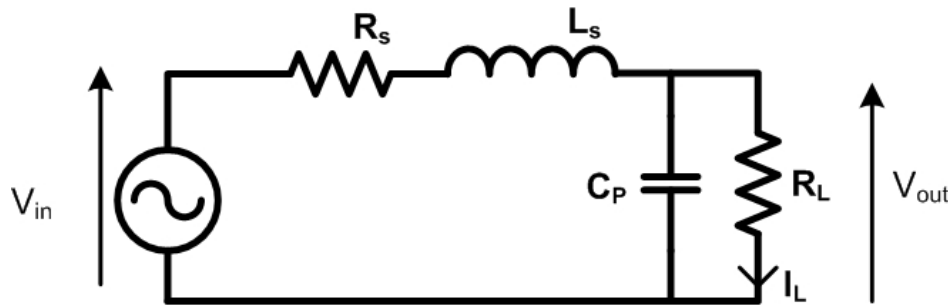
Figure 3.16 Voltage fed resonant transformer power supply equivalent circuit

The voltage transformation of the circuit is (derived using Thévenin from the complex impedances)

$$G(j\omega) = \frac{V_{out}}{V_{in}} = \frac{R_L}{R_L + (j\omega L_s + R_s) \cdot (1 + j\omega C_p R_L)}$$

Equation 3.24

The relationship of the supplied current to R_L is the current regulation ability of the circuit and is given by

$$I_L = \frac{V_{out}}{R_L} = \frac{V_{in}}{R_L + (j\omega L_s + R_s) \cdot (1 + j\omega C_p R_L)}$$

Equation 3.25

This relationship is shown in Figure 3.17 plotted with the frequency. The shaded green region shows a +/- 10% region around the 30 mA operating point, the current regulation is within 2% over the range of load resistance (0 Ω – 1 MΩ) if the frequency is exactly at the resonant frequency.
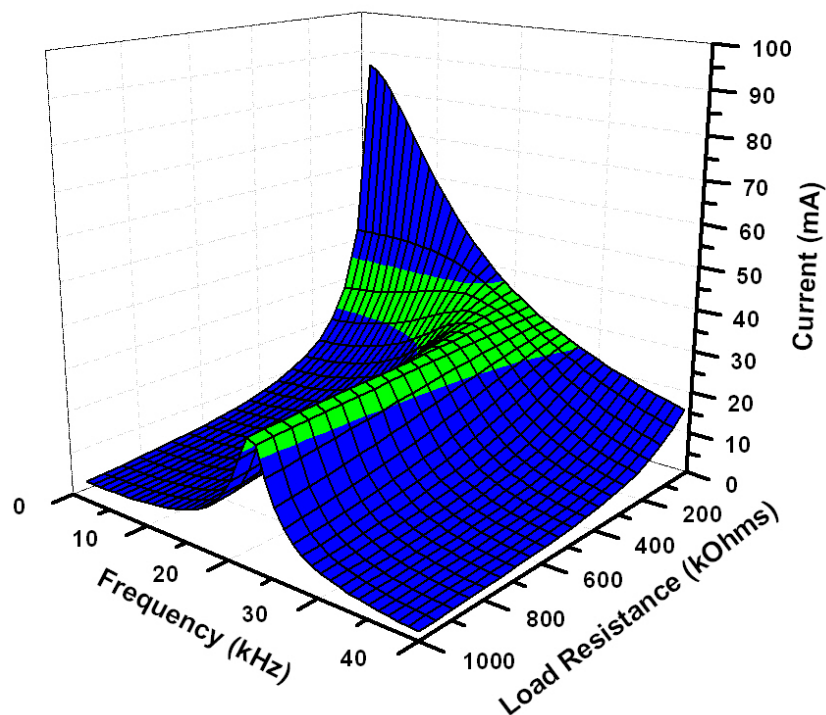
Figure 3.17 Current output versus frequency and load resistance

The voltage characteristic of the same circuit is shown in Figure 3.18. The breakdown requirement of 30 kV is easily achieved when operating at resonance. The plot also emphasises the importance of operation close to the resonant frequency at break down shown by the steeply sloping gradient corresponding to the load resistance of 1 MΩ, deviation from resonance by a small amount greatly reduces the available peak load voltage. After breakdown, the measured discharge impedance drops to approximately 130 kΩ and the frequency has a less pronounced effect on the output voltage (i.e. resonance is only needed for breakdown).
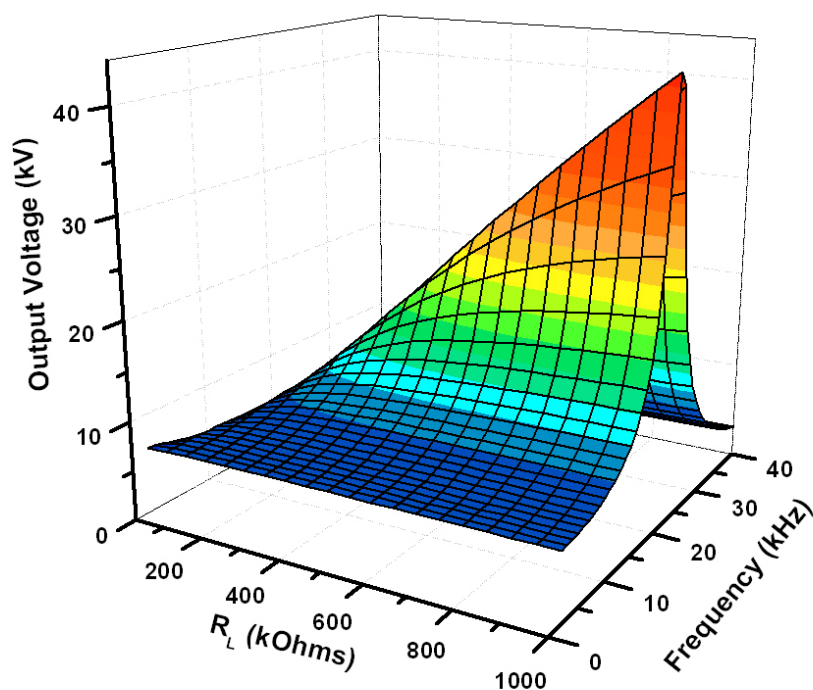
Figure 3.18 Output voltage versus load resistance and frequency

This section has shown the benefits of the voltage fed resonant transformer power supply with respect to peak power demand, complexity, current regulation and available breakdown voltage. The next section describes the design of an electronic power supply suitable for driving multiple resonant transformer outputs for powering Autoselective discharges whilst overcoming the difficulties of driving multiple transformers.

3.4.3 The Autoselective Compact Power Supply

A multiple output power supply was designed and built using the voltage fed resonant transformer topology described in the previous section, this section describes the power supply circuit and operation. The power supply was designed with 20 outputs for reasons detailed later in Chapters 5.

The 20 outputs were produced using an array of independent high voltage resonant transformers. This proved to be the smallest and most reliable method of implementing multiple inductively stabilised discharges. A modular construction was used to increase reliability. Multiple half-bridge inverters were chosen in combination

with a single controller, each of the ten half-bridge inverters was connected to two transformers.

The peak power requirements of the half-bridge sections was greater than 2 kW during the breakdown transient. The power supply was designed to operate from rectified mains (240 V AC rectifies to give a dc voltage peak of 339 V), a 2 kW peak demand corresponded to 5.9 A of DC current. In addition to this, the cycling resonant currents accounted for more than 10 kW of power (20 kHz, 100 pF, 30 kV) or approximately 30 A of inverter current. The resulting peak current if all 20 outputs were driven from a single half-bridge would have been over 600 A which is not easily achievable at rectified mains potentials. The modular construction allowed multiple smaller inverters to be used instead. A low cost IGBT (insulated gate bipolar transistor) was chosen for the half-bridge switching component because similarly rated MOSFETs (metal oxide semiconductor field effect transistors) were less robust.

The breakdown transient required that the power supplies were operated close to their resonant frequency at breakdown as highlighted by the previous section. However, all the transformers had slightly different resonant frequencies due to manufacturing tolerances. A frequency sweep was used to ensure each transformer operated at resonance long enough to achieve breakdown. Transient analysis was used to determine the time required at each frequency for breakdown to occur. After breakdown, the effect of the lowered discharge resistance resulted in a reduced sensitivity to frequency deviations such that the discharge did not extinguish as the frequency changed.

3.4.4 Transient Breakdown Analysis

To ensure that sufficient time was given at each frequency to allow for breakdown, a full analysis of the equivalent circuit was used in conjunction with measured values. The transient behaviour of the circuit in Figure 3.16 for a sinusoidal input voltage waveform ($V(t) = A \cdot \mathrm{Sin}\, \omega_0 t$) is shown in equation 3.26 (derivation in Appendix III).

$$V_{out}(t) = \frac{-\omega_o \cdot A}{2 \cdot \alpha} Cos(\omega_o t) + \frac{-\omega_o \cdot A}{2 \cdot \alpha} \cdot e^{-\alpha t} Cos(\omega_n t) + \frac{-\omega_o \cdot A}{2 \cdot \omega_n} \cdot e^{-\alpha t} Sin(\omega_n t)$$

Equation 3.26

where

$$\alpha = \frac{R_S}{2 \cdot L_S} \quad , \quad \omega_o = \frac{1}{\sqrt{L_S C_P}} \quad , \quad \omega_n = \sqrt{\omega_o^2 - \alpha^2}$$

Breakdown occurs once the voltage described by this increasing sinusoid exceeds the breakdown level. The sine term can be ignored because it has a coefficient several orders smaller than the dominant cosine terms thus allowing the breakdown criteria to be expressed as the inequality

$$1 - e^{-\left(\frac{R \cdot n \cdot \pi}{2 \cdot L_S \cdot \omega_0}\right)} > \frac{V_{bd}}{Q \cdot A}$$

where

$$Q = \frac{\omega_o \cdot L_s}{R_s}$$

Equation 3.27

in which n is a positive integer representing n number of half cycles of the sinusoidal waveform. The number of half cycles used must be an even number to avoid distortion of the transformer drive signal. The number of cycles used was higher than calculated to increase reliability. An example of the measured resonant breakdown transient is shown in Figure 3.19, the breakdown occured at 320 μs on the 7th cycle. The frequency sweep used 10 cycles per 1 kHz frequency step, this ensured proper breakdown for all resonant frequencies within the sweep range used (15 kHz to 26 kHz).
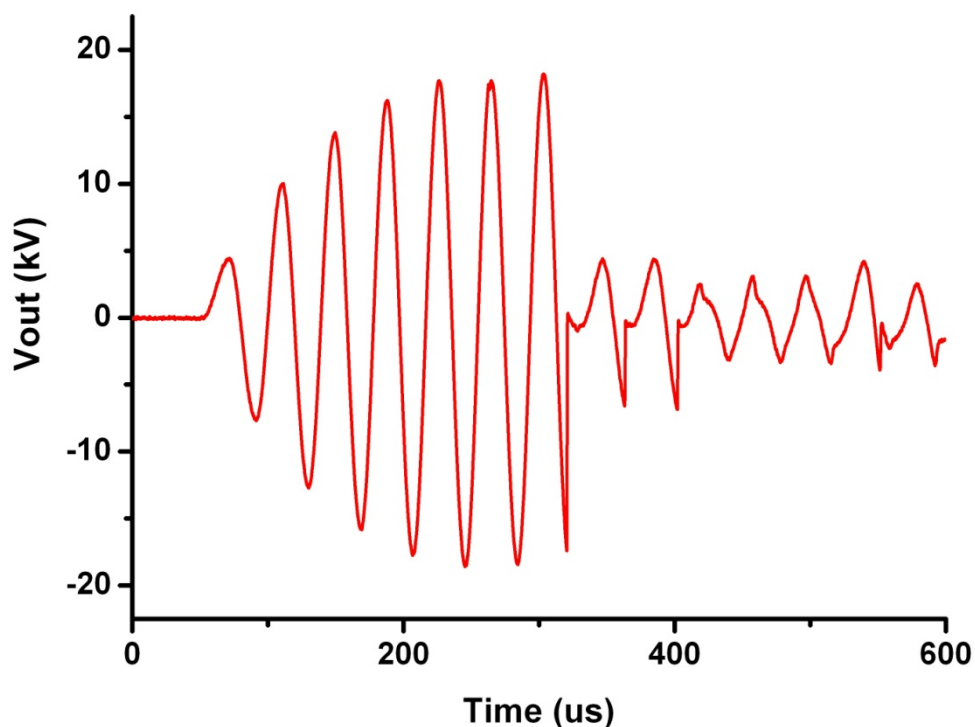
Figure 3.19 Measured breakdown transient showing resonance

3.4.5 Power Modulation

After breakdown occurs, the transformer drive amplitude has to be reduced to ensure filter damage did not occur from excessive heating by the discharge. If the half-bridge switching voltage was controlled directly, the rate of change of amplitude would be limited and waveform distortion may result. A direct control of the drive waveform was used instead similar to modern electronic induction motor drives. The half-bridge output was a high frequency carrier, pulse width modulated (PWM) with a low frequency drive waveform. The waveform was produced using a micro-controller which enabled synchronisation of the two frequencies, reducing waveform distortion due to beat frequencies. The transformer frequency characteristic was used as a low pass filter to remove the higher frequency components from the discharge current. A waveform of the transformer drive waveform and resulting discharge current is shown in Figure 3.20. The distortion of the discharge current has no measured effect on the discharge behaviour.
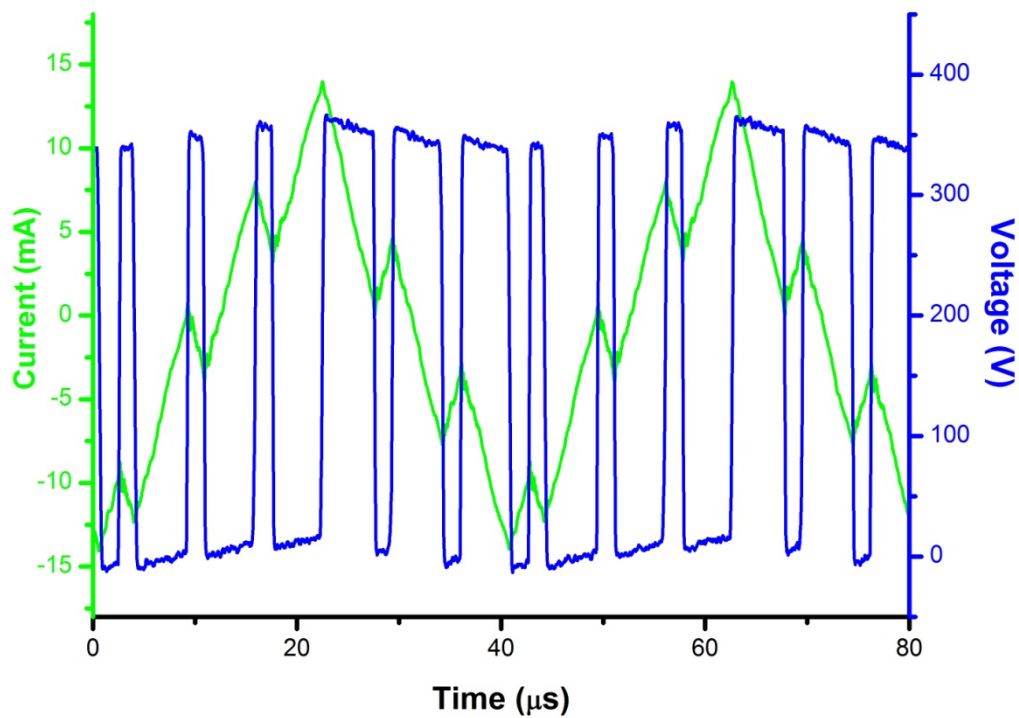
Figure 3.20 Graph of PWM voltage waveform at the half-bridge output (transformer input) and the resulting discharge current

3.4.6 Power Supply Schematic

The schematic of the multiple output power supply is shown in Figure 3.21 and a photo of the assembled power supply is shown in Figure 3.22. This section describes the functional blocks of the circuit.
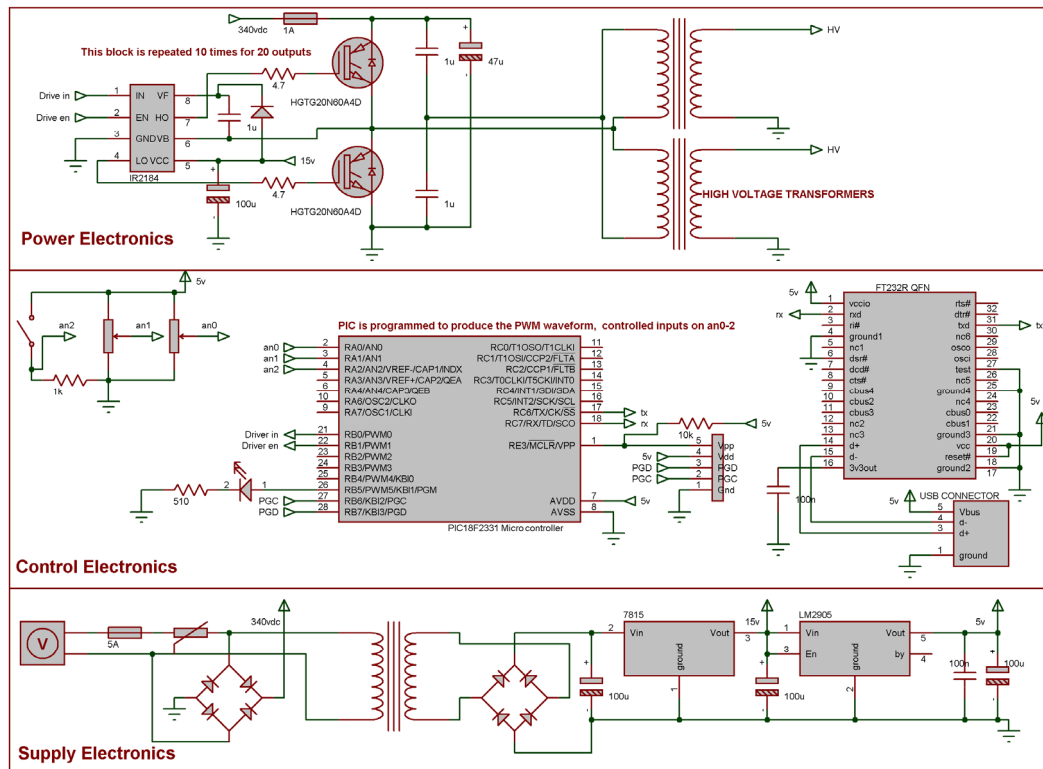
Figure 3.21 Simplified schematic of the PWM converter

Figure 3.22 Photograph of completed power supply

The power electronics comprises 10 half-bridge inverters using fast IGBTs as the electronic switches. They are switched on and off using a dedicated IGBT driver integrated circuit (IC) which converts the low voltage (5 V) signals from the

micro-controller into the levels required. Each inverter section has a smoothing capacitor which provides the instantaneous current pulses required by the circuit and reduces interference with other electrical devices. Each half-bridge drives a pair of high voltage transformers to produce two discharges. The signal wires of 5 half-bridges are connected together giving control of 10 discharges from a single signal bus. Separate buses for the half-bridge voltage and the gate drive supplies are used to minimise wiring effort.

The supply electronics are located on a separate printed circuit board (PCB) and provide the voltage levels required for supplying the half-bridges and the driver ICs. It contains two voltage regulator ICs to provide steady levels at 15 V and 5 V. Supply filtering by electrolytic capacitors is used to prevent the surges and high frequency currents produced by the power supply interfering with nearby electronics. The supply PCB also provides a support for the controller PCB and several connectors.

The power supply controller used an 8 bit microcontroller (PIC18F1330) which was chosen for its ability to operate at high frequency and for its advanced PWM module. The microcontroller code manipulated the module to produce the glitch-less switching waveforms required for correct power supply operation. Interface to the controller was made by the analogue to digital converter (ADC) and a communication module using the universal serial bus (USB). The ADC allowed analogue potentiometers on the front panel to change the operation on the power supply. The controller PCB was removable from its socket allowing remote connection to a PC for programming of the frequency sweep and power modulation parameters. Further details of the power supply are given in Appendix I.

3.5 Summary

In summary, electrical discharges are unconventional electrical loads that exhibit a negative dynamic resistance characteristic. The ion and electron recombination rate of the plasma leads to a frequency characteristic of the discharge impedance. When driven at moderate frequencies (>10 kHz) the discharge approximates a resistive load whereas at lower frequencies (<1 kHz) the negative dynamic resistance is

dominant. The small signal behaviour can be modelled as a RHP zero and LHP pole, this is useful for determining the conditions of stability when calculating stabilising impedances and control loops.

The electrode arrangement for the Autoselective system is highly capacitive which make inductive stabilisation the most suitable method of stabilisation. The voltage fed resonant transformer type power supply was shown to be the best suited for driving the electrodes. A multiple output supply was designed to use this type of circuit to produce 20 high voltage outputs. A single controller was used to provide the signals for 10 half-bridge inverters. The tolerance of the resonant frequencies was overcome using a frequency sweep.

The Autoselective system required fast control of the current amplitude which was provided using a PWM modulation scheme and high speed IGBT switches. The scheme allowed control of amplitude at a far higher rate than other topologies whilst reducing the size and complexity of the converter.

The next chapter investigates how varying the discharge properties affects the regeneration performance. The power supply described in the final section of this chapter is used for the later engine and flow-rig testing work detailed in Chapter 8.

4. Optimisation of the Autoselective Glow Discharge

This chapter describes the optimisation of the electrical discharges used for Autoselective regeneration. The regeneration system had previously only operated the Autoselective discharges over the range of frequencies between 10 kHz and 30 kHz and at current levels between 10 mA and 30 mA. This range is extended to determine the effect of frequency, current and crest factor on the regeneration performance.

4.1 Previous Work

In the early stages of the development of the Autoselective technology, different atmospheric pressure discharges were tested to determine their ability to oxidise soot (Proctor, 2007). The discharges tested were corona discharge, dielectric barrier discharge and glow discharge (see Table 4.1). The results showed that, although each discharge was able to oxidise diesel soot, the glow discharge oxidised the soot faster and with lower energy input. Regeneration rate and effectiveness were defined to make a numerical comparison of the regeneration performance. Regeneration rate is the mass of soot burned per second ($g.hr^{-1}$) and the effectiveness is the rate divided by the power input ($g.kW^{-1}.hr^{-1}$).
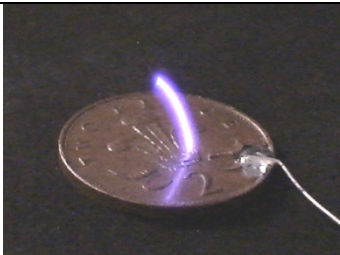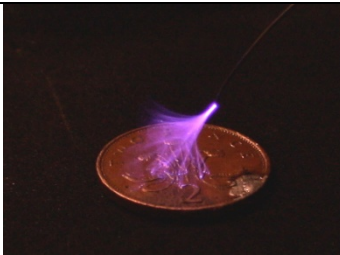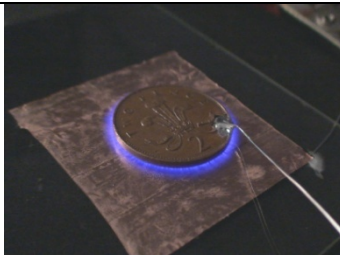
Glow Discharge	Corona Discharge	Dielectric Barrier
single current path	multiple current paths	multiple current paths
two discharge roots	one well defined root	no discharge roots
well defined discharge column	divergent discharge column	no visible discharge column

Table 4.1 Types of atmospheric discharges

Testing of the glow discharge proved its ability to function within the diesel engine exhaust environment of depleted oxygen, high humidity and gas temperatures from 100 to 800 °C (Proctor 2007). These tests also confirmed that the glow discharge was capable of regenerating PM under these conditions without producing significant levels of harmful by-products. A stable glow discharge can be sustained at all feasible frequencies from DC upwards and currents up to several hundred mA. However, it was not known how current and frequency would affect the regeneration process. This chapter summarises the original results obtained with currents up to 250 mA and frequencies up to 4 MHz.

Early work (Proctor, 2007) used a glow discharge within a cordierite wall flow filter between inserted wire electrodes. The discharge power supply normally used operated over a narrow range of frequencies between 10 kHz and 30 kHz. The power supply used a close coupled resonant transformer which is a conventional method of generating a stable glow discharge (see Appendix I for schematics). One characteristic of this power supply is that the actual frequency of operation is limited to a narrow range about the natural resonant frequency of the transformer, which means that this type of power supply can not produce a wide range of discharge frequencies. For this reason the effect of varying the frequency had only been investigated over a narrow range. Although optimisation was carried out with the available equipment, it was likely that a better operating point for the Autoselective discharge could be found. An understanding of how the variables such as frequency and current level affected the regeneration was needed to find the optimum operating point.

Amongst the many variables, there were three main factors:
  i.   Filter material
  ii. Electrode Geometry
  iii. Discharge current waveform

The main objectives of optimising these variables is to obtain a high regeneration rate for a low energy input whilst achieving uniform regeneration within the filter and avoiding damage to the materials used.

Filter damage depended on the discharge current and filter material amongst numerous other variables such as filter wall thickness, PM loading, air temperature and flow. The effects of discharge current on filter damage will be described in Chapter 5 and the damage mechanism is described in Chapter 6.

Regeneration distribution is also affected by the discharge current waveform. For clarity, this will also be examined in Chapter 5 to avoid creating any ambiguity in the conclusions made during this section of the research. This chapter only reports the discharge current waveforms effect on regeneration performance in terms of rate and effectiveness.

4.2 Early Flow-rig Testing

Testing of the Autoselective system had been carried out previously on exhaust simulation flow-rigs and on heavy duty diesel engines by Proctor *et al* (2007). This section summarises the results obtained during the flow-rig testing of the regeneration system using the original discharge power supply operating at 20 kHz and 15mA. The results obtained during flow-rig trials (Williams, 2007) often gave a good indication of what behaviour could be expected on engine tests especially in terms of filter damage and regeneration distribution. Figure 4.1 shows the flow-rig setup used to test WFFs. Air is blown through a by-pass, a heater and a filter. Accurate simulation of exhaust flow rates and temperatures is possible using this equipment. The flow-rig helped to demonstrate the range of operation of the regeneration system as well as accelerating the optimisation process.
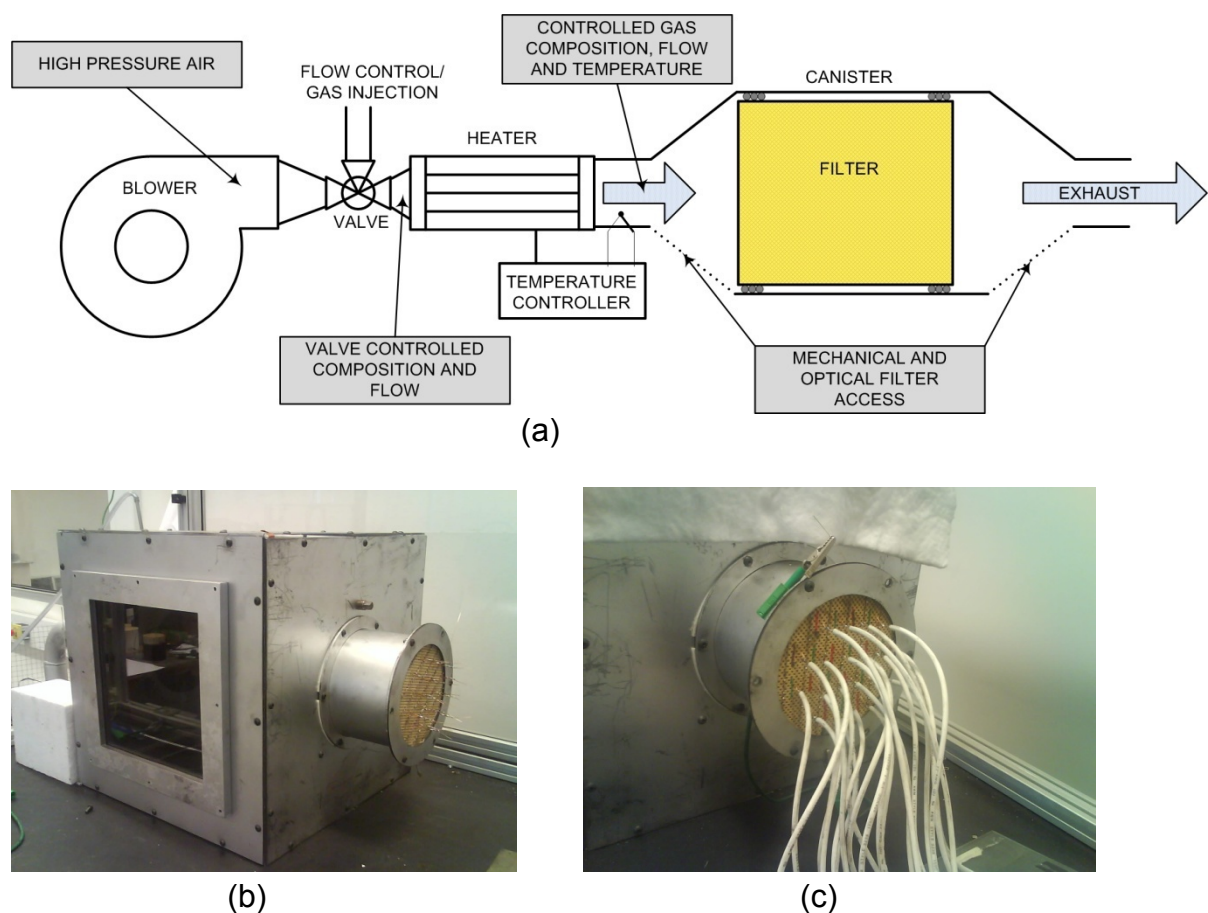
Figure 4.1 (a) Flow-rig schematic, (b) photograph of filter canister, (c) typical multiple electrode connections for a full filter test

One of the early difficulties encountered was discharge penetration depth when trying to achieve regeneration deep within the filter (Proctor, 2007). This led to the early adoption of inserted wire electrodes which are placed within the filter channels. The inserted wire electrode increased the electrode capacitance (by a factor of ~10) to 100 pF, this made breakdown difficult due to the reduced peak voltages (Williams, 2007). Driving a capacitance with a sinusoidal voltage waveform does not consume energy but it does require reactive power, this power must be delivered by the power supply which is often power limited due to the ratings of its components. The power supply must be capable of delivering the full reactive power demanded by the load even though this may be many times the real power required. By inserting electrodes, stresses were put on the power supply which was required to deliver the maximum reactive power given by:

$$P = \frac{V_B^{\;2}}{X_C} = V_B^2 \cdot 2\pi \cdot f \cdot C \qquad\qquad \text{Equation 4.1}$$

where P is the peak reactive power, V_B is the breakdown voltage, f is the frequency, X_C is the capacitive reactance and C is the electrode capacitance.

The results from the early flow-rig tests frequently showed filter damage, incomplete regeneration and non-uniform regeneration. Figure 4.2 shows the typical damage encountered; the images are of the sliced wall from a full filter (see Appendix II for details). The images show incomplete regeneration on the filter surface, the bottom image shows filter melting on a magnified section after the soot has been removed. Filter damage like this always occurred when current levels above 30 mA were used. A new power supply was needed that was capable of driving the inserted electrodes without causing filter damage and whilst maintaining regeneration performance. However, an understanding of how the frequency of the discharge affected the performance was required before designing a new power supply.
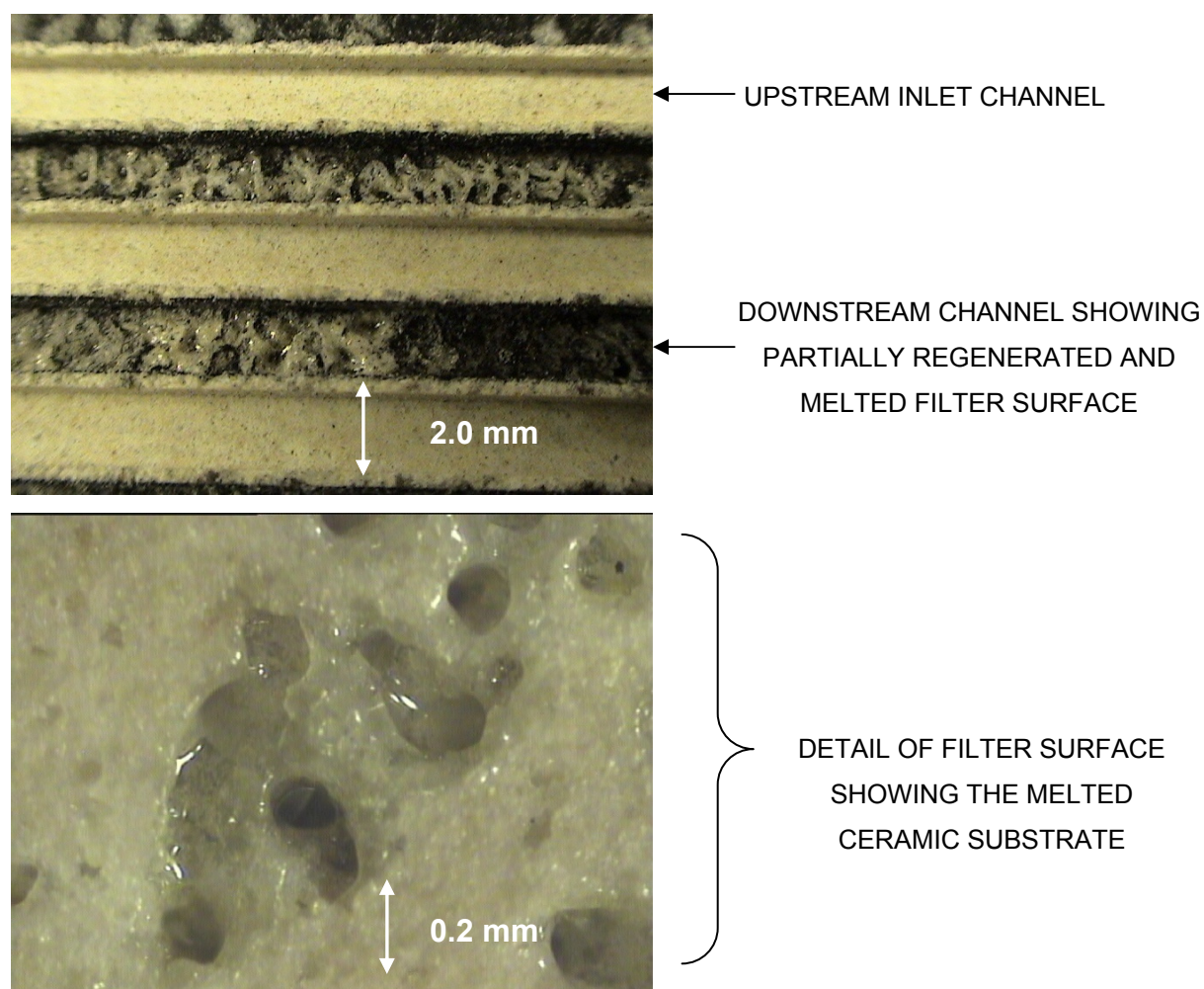
Figure 4.2 Partially regenerated and melted sections of a cordierite ceramic wall flow filter

4.3 Discharge Optimisation

Atmospheric discharge properties (for a constant geometry) are defined by their electrical current waveform which can be varied over a wide range of amplitudes and frequencies. The most thorough way to test all of the possible discharge operating conditions would be to set up a filter and regenerate it with a variety of different discharges. Pre- and post-weighing would enable the mass of PM regenerated to be determined and allow comparison of the different settings. However, this is not practical since it takes many hours to complete a basic test on a full filter and the mass loss may be influenced by other variables such as water adsorption. A repeatable test was needed to determine the regeneration performance of different

discharges. The test should measure the rate of oxidation of PM when operated at different conditions.

Diesel PM is not easily removed mechanically from a loaded DPF (Takesa *et al*, 1991) and this makes obtaining large quantities difficult. Carbon black was readily available as a test material and is produced in a diffusion flame similar to PM. Studies by Neeft (1995) and Clague *et al* (1999) have shown that its composition is similar to diesel particulate. The main difference between carbon back and PM is the chemical content adsorbed in the carbonaceous matter. PM may contain up to 50% by mass of organic substances as well as sulphates, metals and oxygen whereas carbon black is composed mainly of carbon. However, Clague showed that the structure of carbon black is identical to engine derived particulates in terms of structure and size of particles. Carbon black was therefore chosen as a substitute for engine derived PM in the tests reported here.

The tests were carried out without a filter since the effects of the filter substrate are not being investigated at this time. The experimental setup is shown in Figure 4.3. A copper crucible containing approximately 2 g of carbon black, compressed by approximately 150 kPa, was placed in a sample holder with a gap between the sample surface and a steel electrode. The gap was accurately controlled (to < 0.1 mm) using a threaded rod. The base of the crucible was connected to ground and the electrode to a discharge power supply. The following sub-section discusses the errors that were present using the described apparatus.
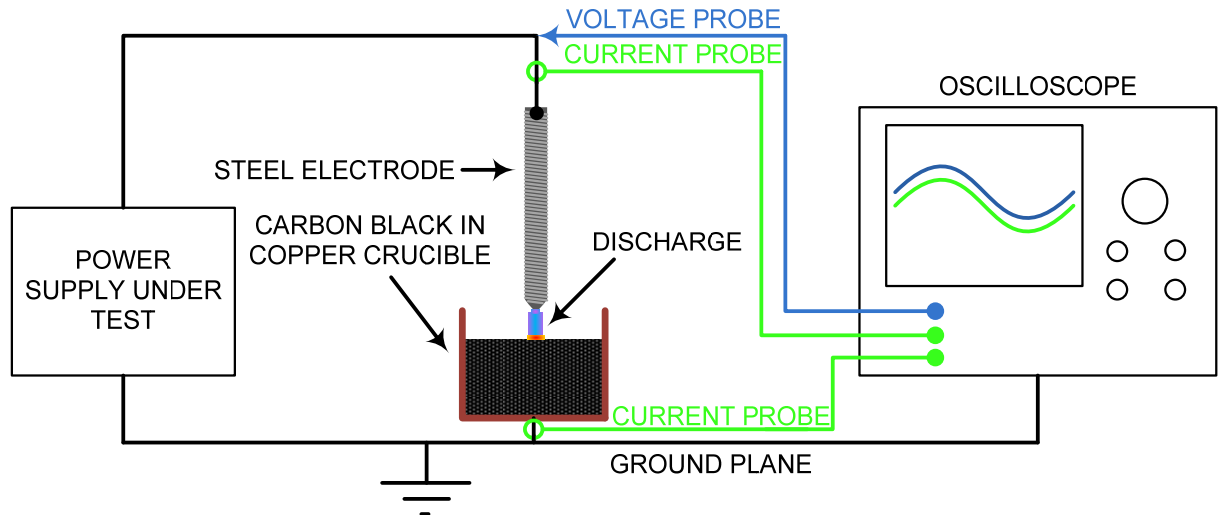
Figure 4.3 Experimental arrangement used to test the electrical discharge regeneration of carbon black

4.3.1 Electrical Measurement Errors

The plasma power and rms computations were performed by a Tektronics TDS5034B 3 GHz digital storage oscilloscope. The measured inputs were from a Tektronics P6015A 75 MHz 1000:1 high voltage probe and a Pearson 2877 200 MHz 1:1 current transformer. Where DC current measurements were necessary a high bandwidth current shunt was designed using modern RF impedance matching techniques, for alternating currents a 1 nF DC blocking capacitor was used. Figure 4.4 shows the current shunt, a bandwidth greater than 10 MHz was achieved.
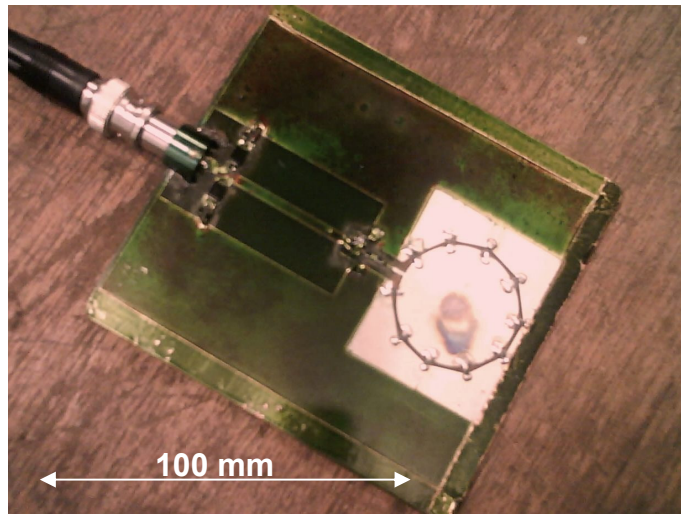
(a)
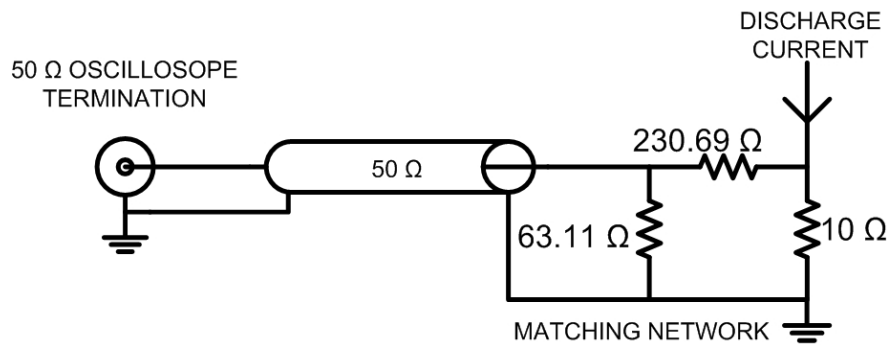
(b)

Figure 4.4 High bandwidth current shunt (a) used and circuit schematic (b)

The bandwidth of the measurement probes always exceeded the discharge frequency by at least one order which made the contributed error always less than 1%. The main instrumentation error was due to the delay of the scope when measuring 4 MHz frequency discharges. The effect of the delay, known as skew, is shown in Figure 4.5. The skew error was not a significant source of error for discharge frequencies less than 100 kHz.
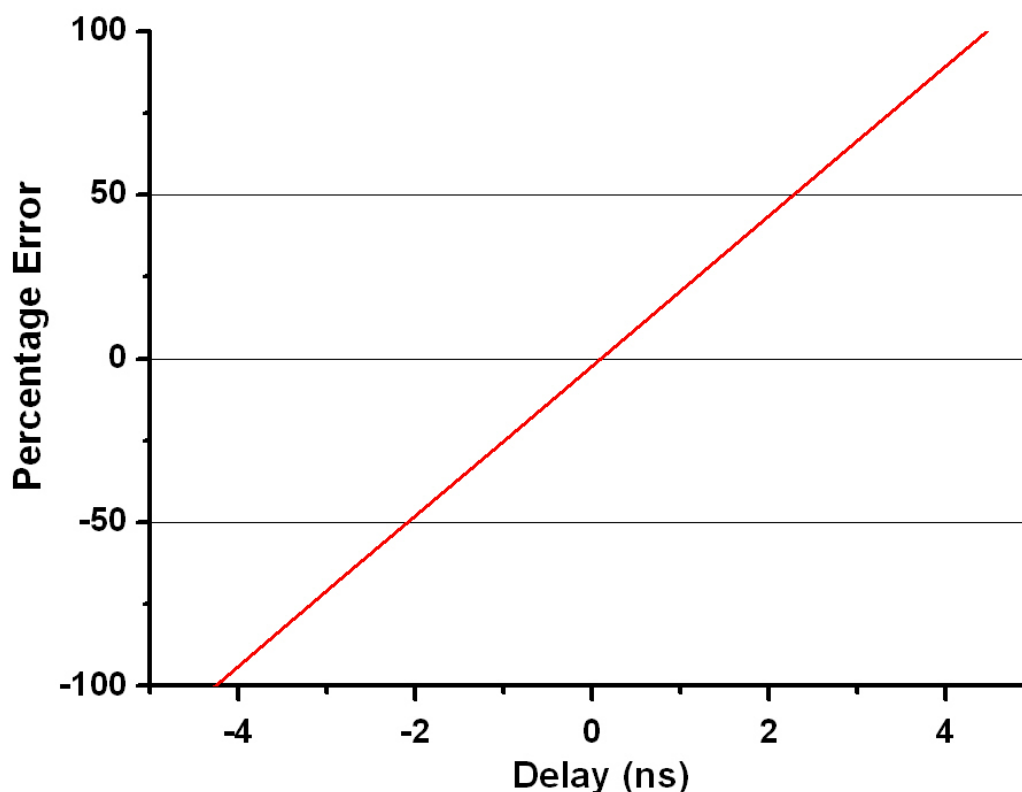
Figure 4.5 Calculated percentage error versus propagation delay between current and voltage probes

The resistance from the discharge root to the metal crucible was measured to be less than 1 Ω, the resulting power consumption was therefore insignificant (< 0.01% the discharge power) and was ignored. The rms current computation of the oscilloscope was used because the voltage and current are in phase for high frequency discharges making the rms current a good measure of the discharge power consumption. The digitising and calculation errors by the oscilloscope were not considered further because they were far less than the other measurement errors (< 0.1 %). The capacitance of the voltage probe caused capacitive current flow, the current probe was always located on the discharge side of the voltage probe to prevent this affecting the measured current. The capacitance of the wiring and electrode were compensated for frequencies above 100 kHz by subtracting the measured capacitive current from the discharge current. Finally, the noise introduced by the probes (measured with no discharge) introduced an error < 2% (typically 1%) of the measured value for each set of conditions used.

4.3.2 Mass Measurement Errors

The crucibles were weighed before and after-treatment by the discharge using a Kern ARJ 220 precision weighing machine offering a repeatable accuracy of 100 µg. Typical mass changes were of the order of 10 mg making the initial measurement error 1%. An experiment was conducted to find the contribution of moisture on the mass change. The total moisture content of 2 g of carbon black was found to be less than 0.5% of the typical measured mass change (10 mg). The crucibles were weighed three times before and after treatment by the discharge and at constant temperature (20°C) in order to reduce the measurement error. Additional mass measurement error could have resulted from loss of the carbon black from the crucible or objects falling into the crucibles therefore care was taken to prevent these producing spurious errors.

4.3.3 Other Systematic Errors

An initial test revealed that the soot oxidation rate was constant over the first 5 minutes, the test duration was set at 2 minutes. This was chosen based on the minimum mass loss required to produce accurate mass loss data. Time measurements were made using a stop watch, it was considered unnecessary to further improve the timing accuracy. The gap between the steel electrode and the crucible was made using an M4 threaded rod with 90° rotational markings. This provided precision positional accuracy using the thread pitch of 0.7 mm, a 3.5 mm gap was used based on the filter channel spacing (5 electrode rotations).

4.3.4 Summary of System Errors

The greatest sources of error were the electrical noise of the oscilloscope probes and the mass measurement uncertainty. The testing of the discharge was performed with the errors discussed in this section and the results from the tests are discussed in the next sections of this chapter.

4.4 Effects of Frequency and Current

Stable atmospheric discharges can be maintained between electrodes from DC to frequencies well into the GHz (10^9 Hz) range (Roth, 1995). Lower frequencies (<1 kHz) tend to produce discrete discharges beginning each time the discharge reaches the breakdown voltage and extinguishing each time the discharge current crosses zero (zero crossing). Higher frequencies produce continuous and uniform current waveforms since the plasma remains conductive during current zero crossings. The frequency at which discharges become continuous in still air is approximately 1 kHz. Power supplies were built to cover a range of frequencies up to 4 MHz to test the effects of frequency on regeneration performance. Table 4.2 summarises the ranges and topologies used and full details are given in Appendix I.

Frequency	Frequency Range	Transformer	Topology
DC	0 Hz	Medium frequency ferrite transformer	Current (flux) limited transformer and high voltage rectifier
Mains Frequency	50 Hz	Laminated iron transformer	'Neon sign' transformer
Low Frequency	100 Hz – 4 kHz	Laminated iron transformer	Capacitive stabilisation
Medium Frequency	4 kHz – 30 kHz	Ferrite transformer	Current (flux) limited transformer
High Frequency	30 kHz – 400 kHz	High Q Ferrite transformer	Current (flux) limited transformer
Radio Frequency	400 kHz – 4 MHz	Air core resonator	Class E tuned power supply
High Crest Factor	0 – 5 kHz	Laminated iron transformer	Pulse driven transformer

Table 4.2 Summary of the power supplies used for discharge testing

The regeneration rate determines the minimum number of discharges needed for the successful operation of the regeneration system. The tests used currents in the

10 mA to 250 mA range, however, currents above 30 mA were known to cause filter damage (Proctor, 2007) when used with cordierite WFFs. Current values from 10 mA to 30 mA are plotted in Figure 4.6 for a range of frequencies.
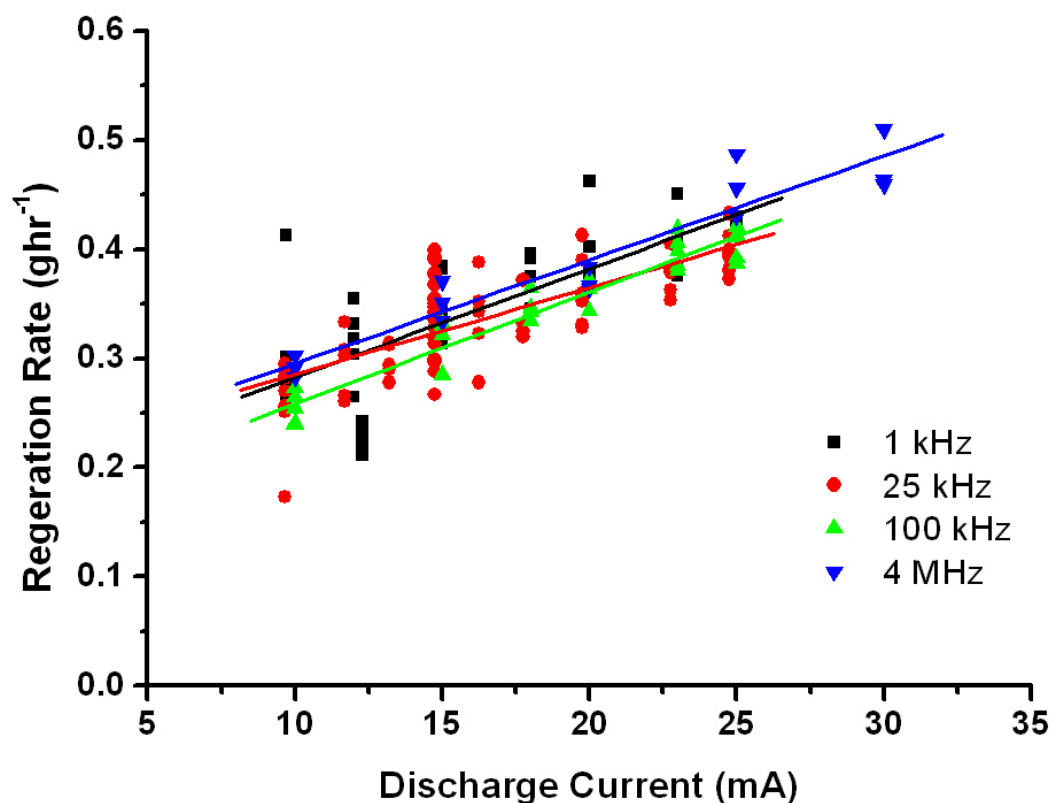
Figure 4.6 Variation of regeneration rate with current and frequency (linear fit)

The results show that there is no significant difference in regeneration rate for a given rms current over the range of frequencies 1 kHz to 4 MHz. This is useful from a design perspective since there are no restrictions on operating frequency with respect to regeneration performance. The results also show that regeneration rate increases with operating current. This could be attributed to the higher gas temperatures produced by increasing the current level. The rate of regeneration directly influences the number of discharges required and hence the complexity of the system. If a regeneration rate of 0.5 g.hr^{-1} is achieved, then a minimum of two discharges will be required for every gram per hour engine PM output in order to prevent PM build up. The minimum number of discharges is an important figure since

it is usually necessary to route a wire into DPF canister to carry the electrical current for each discharge. It is physically difficult to route more than a few tens of wires due to the thickness of the high voltage insulation.

A graph of the regeneration effectiveness is shown in Figure 4.7. The effectiveness of the regeneration system determines the minimum power requirements of the system for a given engine PM output. A target of 5 $g.hr^{-1}$ was used as a target PM regeneration rate for a heavy duty diesel application. This can be justified as follows: A typical 4.4 litre heavy duty diesel engine can be tuned to produce approximately 0.1 $g.kWhr^{-1}$ PM output whilst just meeting the NOx legislation limits pre 2005 (EURO III legislation). The PM production rate can be approximated as the engine duty cycle multiplied by the specific engine PM emission multiplied by the engine power. This gives 5 g/hr for a 100 kW engine at 50% duty with a specific PM emission of 0.1 $g.kWhr^{-1}$.

The energy consumption of the regeneration system is the PM production rate divided by the regeneration effectiveness. An effectiveness of 50 $g.kW^{-1}hr^{-1}$ yields a minimum energy requirement of 100 W at 5 $g.hr^{-1}$. Figure 4.7 shows that there is no significant difference in regeneration effectiveness at 4 MHz and 26 kHz discharge frequencies after taking into account the measurement error. The only observation that could be made is that lower frequencies may be more effective at oxidising the PM.
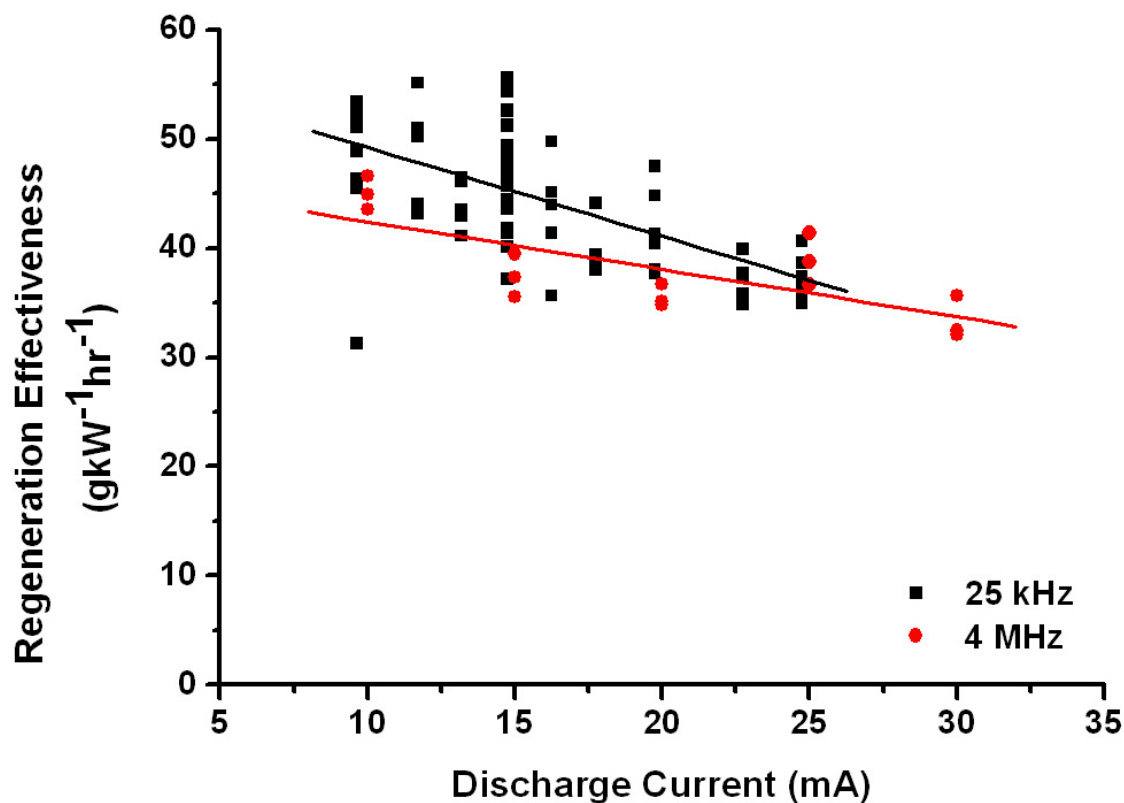
Figure 4.7 Variation in regeneration effectiveness with current at 26 kHz and 4 MHz (linear fit)

To obtain a better understanding of the effects of current, a wider range was tested up to 250 mA. These higher currents could not be used with cordierite wall flow filters because they are easily damaged by the higher temperatures. The extended results may prove useful if Autoselective technology is used with more thermally resistant filter materials. This data set contains a range of frequencies from 26 kHz to 100 kHz, however, the frequency is not plotted since it has already been shown to have little effect on the regeneration performance. Figure 4.8 shows the regeneration rate over this expanded range of currents. Figure 4.9 shows the regeneration effectiveness over the same range.
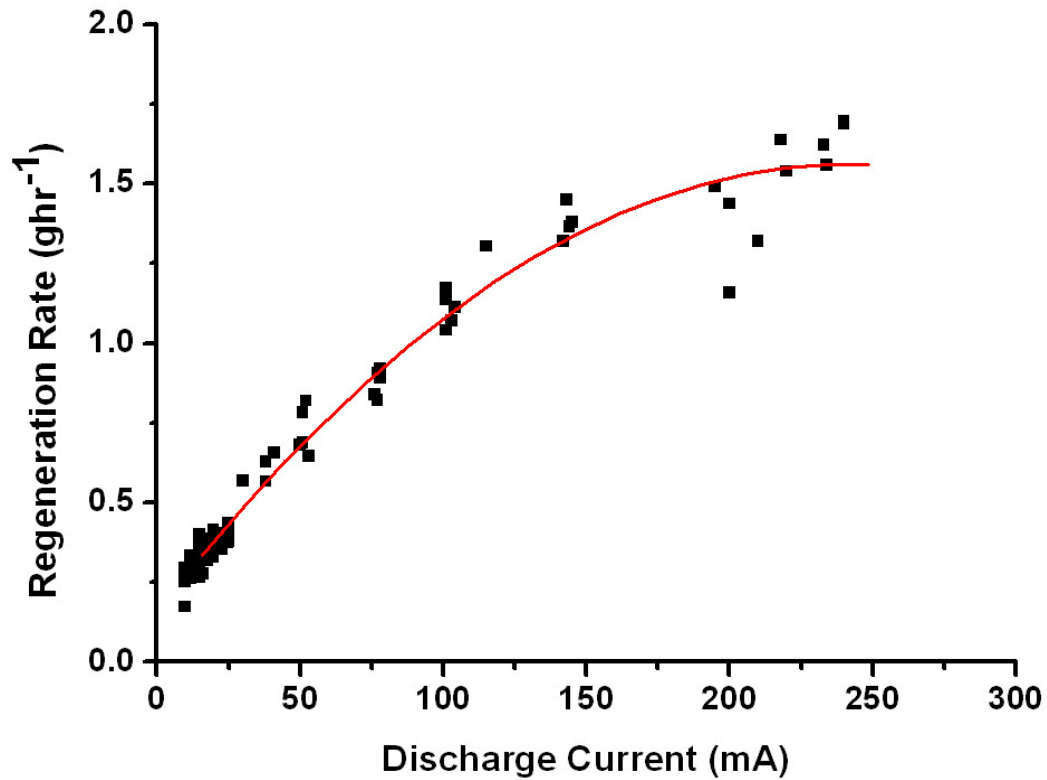
Figure 4.8 Variation in regeneration rate with current (2nd order polynomial fit)

Figure 4.9 Variation in regeneration effectiveness with current (2nd order polynomial fit)

The regeneration rate was found to increase with current so that fewer discharges would be needed to give regeneration at the engine PM output. However, the regeneration effectiveness (g.kW.h^{-1}) decreased indicating that more power would be required to regenerate the same PM output. Another effect of the increased current is that the filter may be damaged more easily due to the higher peak temperatures (Williams, 2007). This in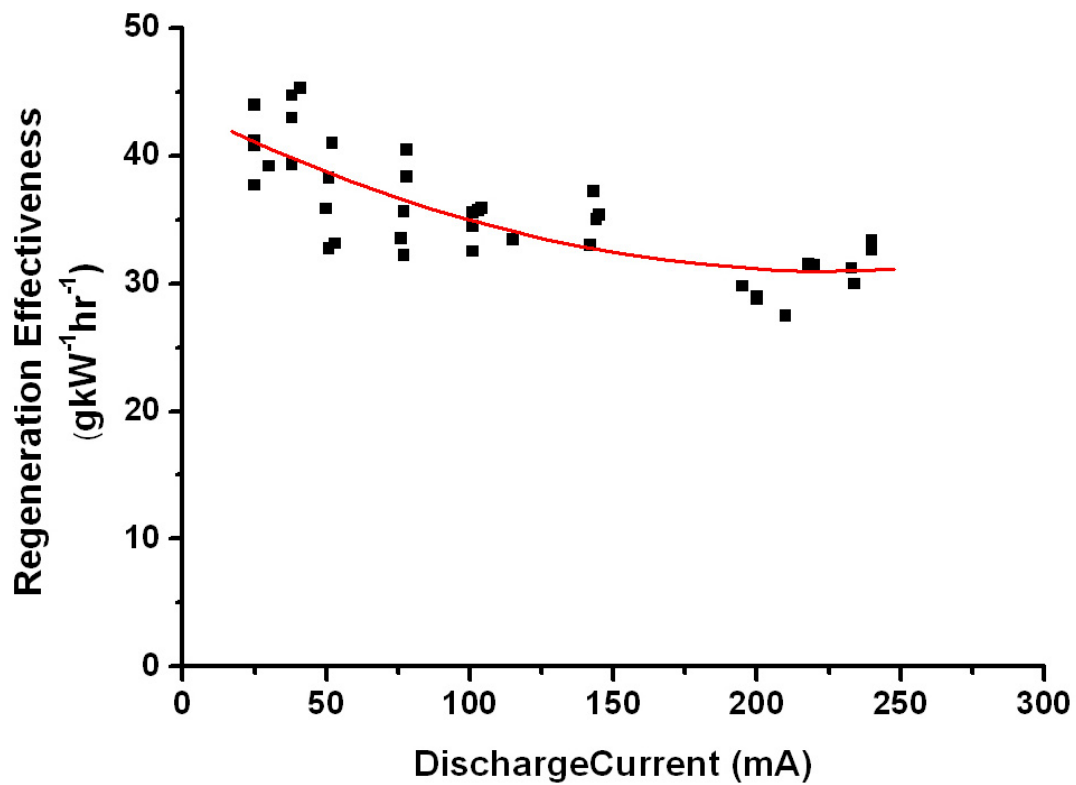dicates that there is a compromise between regeneration rate and system efficiency. An efficient system can be made using hundreds of low current discharges although this may increase system complexity. A system using fewer discharges may be possible at higher currents but this will have higher total energy consumption due to the loss in effectiveness.

In summary, it has been shown that frequency does not have a significant effect on Autoselective regeneration performance. This allows the choice of frequency to be based on other parameters such as power supply complexity and system cost. The regeneration rate was found to increase with current hence a higher discharge current is desirable to reduce the number of individual discharges required to keep up with the engine PM output. A system with fewer discharges is likely to be less complex and hence have lower production costs. The regeneration effectiveness was found to decrease with current which means more power would be required to operate the Autoselective system at higher currents. The increase in required power was approximately 50% for an increase in current of 10 to 250 mA.

4.5 Effects of Switching the Discharge

Initial results showed that 100 cpsi (cells per square inch) cordierite DPFs were easily damaged by atmospheric pressure glow discharges at 10 mA - 30 mA (Proctor, 2007). A more thorough analysis of this damage is detailed in Chapters 5 and 6. Damage was attributed to thermal effects from the discharge based on the melted appearance of the filter surface after prolonged exposure to a continuous discharge. It is possible to prevent the material melting by interrupting the discharge so that the filter material is given time to cool. This led to the use of accurately timed interruptions in the discharge as the primary method of damage avoidance. The

discharge was switched on and off over a period of 20 - 500 ms so that the filter peak temperatures stayed below the melting point of the filter material.

The interruption of the discharge also had the desirable property of increasing auto-selectivity. The increase in auto-selectivity was attributed to the breakdown event at the beginning of each on-time. Because the PM is conductive, it influences the electric field around the electrode causing the electric breakdown to take place in the region of highest filter loading. The resulting discharge will then burn the PM during the on-time. During the off-time the discharge extinguishes, leading to a repeat breakdown at the beginning of the next on-time. If the previous region had been cleared of PM, the breakdown would occur in a new region. In this way, the discharge spent more time in the heavily loaded sections of the filter which is one of the key desirable features of the Autoselective system.

A better understanding of the effect of on- and off-times on regeneration was needed to decide which combination would be most successful. An experiment was completed that tested a range of on- and off-times centred about the present best operating point. The range of 10 to 500 ms was tested and the results are seen in Figure 4.10. The duty-cycle referred to in the graph is the fraction of time the discharge is on.
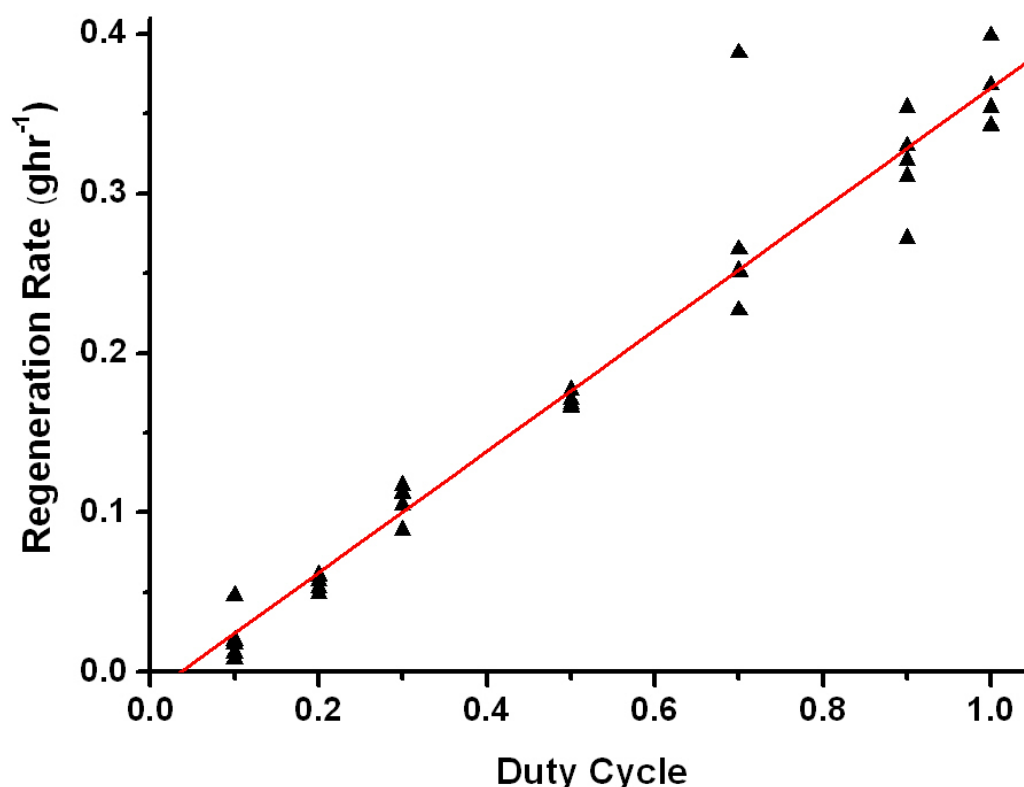
Figure 4.10 Variation in regeneration rate with duty cycle (ratio of on- and off-time) for fixed period of 100ms (linear fit)

The results show that the regeneration rate was closely proportional to the duty cycle. This means there is no significant PM oxidation during the off-time (for this period setting). This result also suggests that less than ~0.1 J of energy is required to begin oxidation of the PM based on the measured discharge power and x-axis intersect of the linear fit (and corresponding minimum on-time).

The results show that the regeneration system should use the highest possible duty cycle to increase regeneration rate. The results also suggests that the heating time of the PM is very short if the regeneration is to be attributed purely to the thermal effect of the discharge since oxidation begins within a few milliseconds. In order to try to quantify the lag between turning the discharge on and start of oxidation, a second test was completed where the period of the discharge on- and off-time was varied whilst keeping the duty cycle constant. If there was a delay of a few milliseconds

before soot oxidation began, then the discharge operated at 10 ms on and 10 ms off would regenerate significantly less than the 500 ms on 500 ms off case. The results for this test are shown in Figure 4.11. The period is defined as the sum of the on-time and the off-time.
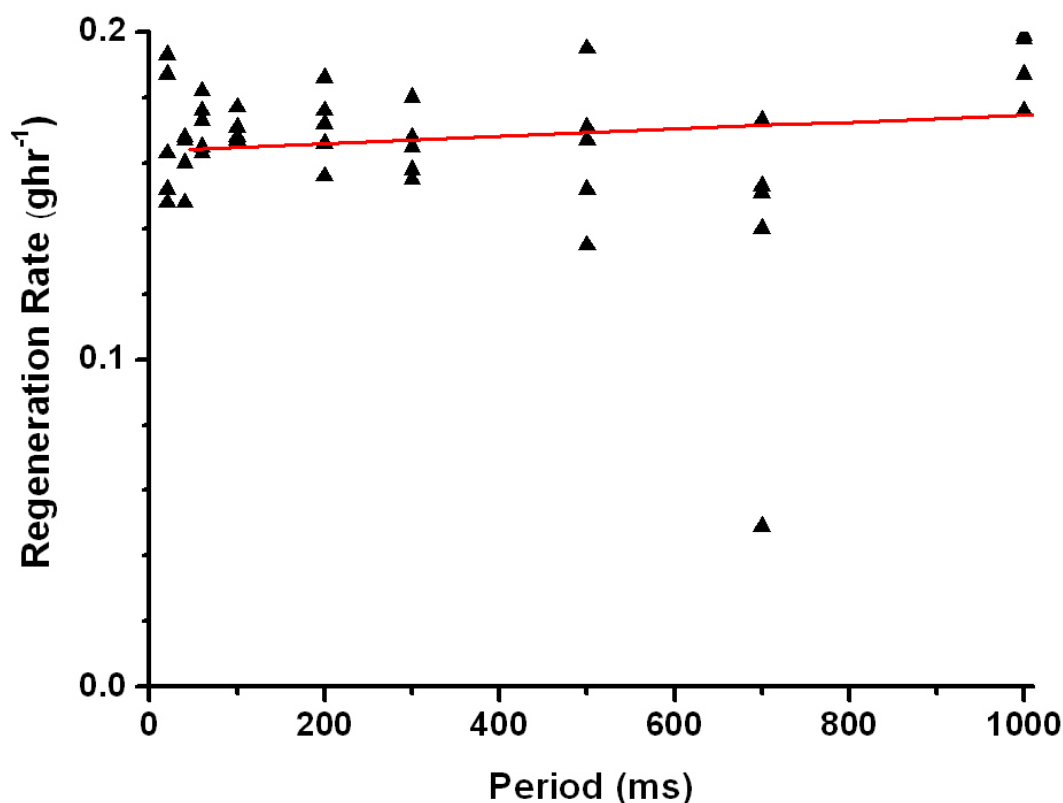
Figure 4.11 Variation in regeneration rate with period for a fixed duty cycle of 0.5 (linear fit)

The change in period had no significant effect on the rate of the regeneration. This could only be the case if the heating up and cooling down rate of the PM being regenerated was less than one millisecond. These results confirm that the regeneration of PM starts within a millisecond of breakdown and stops within a similar time upon discharge interruption.

It had been predicted that the heat release from the oxidising soot would make the cooling time constant much longer than the heating time constant which would have allowed shorter on-times to achieve higher regeneration rates than were measured. This was not observed in practice and is likely to be because the PM is not reactive

enough to cause significant sustained oxidation after the discharge is switched off. It can therefore be concluded that the regeneration rate and effectiveness can not be improved by switching the discharge. However, in a DPF there will be a different thermal time constant which may result in slightly improved results than those measured here, this is discussed in Chapter 5.

In conclusion, the duty cycle should always be maximised to maintain a high rate of regeneration. This is to reduce the number of discharges required to keep up with engine PM output and hence reduce system complexity and cost. The results show that the magnitude of the on- and off-times can be chosen based on the damage limit of the filter material. Observations of Autoselective behaviour suggest that off-times greater than around 1 ms (of the order of the plasma extinction time) are advantageous to ensure auto-selectivity. These findings facilitate choosing the operating point for the Autoselective discharge.

4.6 Effects of Current Waveform Shape

The shape of the discharge current waveform could be altered as well as the frequency. Previous work had always used sinusoidal and triangular waveforms (Proctos, 2007 and Williams, 2007), the effect of the waveform shape on regeneration performance is discussed in this section. Triangular and sine waveforms showed no appreciable difference in regeneration performance, however, other discharge waveforms may have an advantage and a test was performed to determine this. The accepted variables describing waveform shape are the crest factor and total harmonic distortion. The crest factor has been used for many years applied to the current waveforms in discharge lighting systems (for example fluorescent lights, see for example Osram's technical lamp specifications) and hence is more applicable to this discharge application:

$$CF = \frac{I^\wedge}{I_{rms}}$$
Equation 4.2

where CF is the crest factor, $I^\wedge$ is the peak current and I_{rms} is the rms current.

The crest factor is a measure of how spiked the current waveform is and has been found to be important in the discharge lighting industry when considering lamp life (Verderber, 1985). A new power supply was built that was able to achieve high crest factors using a pulse driven transformer. Crest factors between 1.4 and 14 were generated by varying the peak current and maintaining the RMS current by altering the pulse repetition rate. Measurements were taken for mass loss over the duration of the two minute test the same way as in previous tests. The results for the effect of crest factor on regeneration rate are plotted in Figure 4.12.
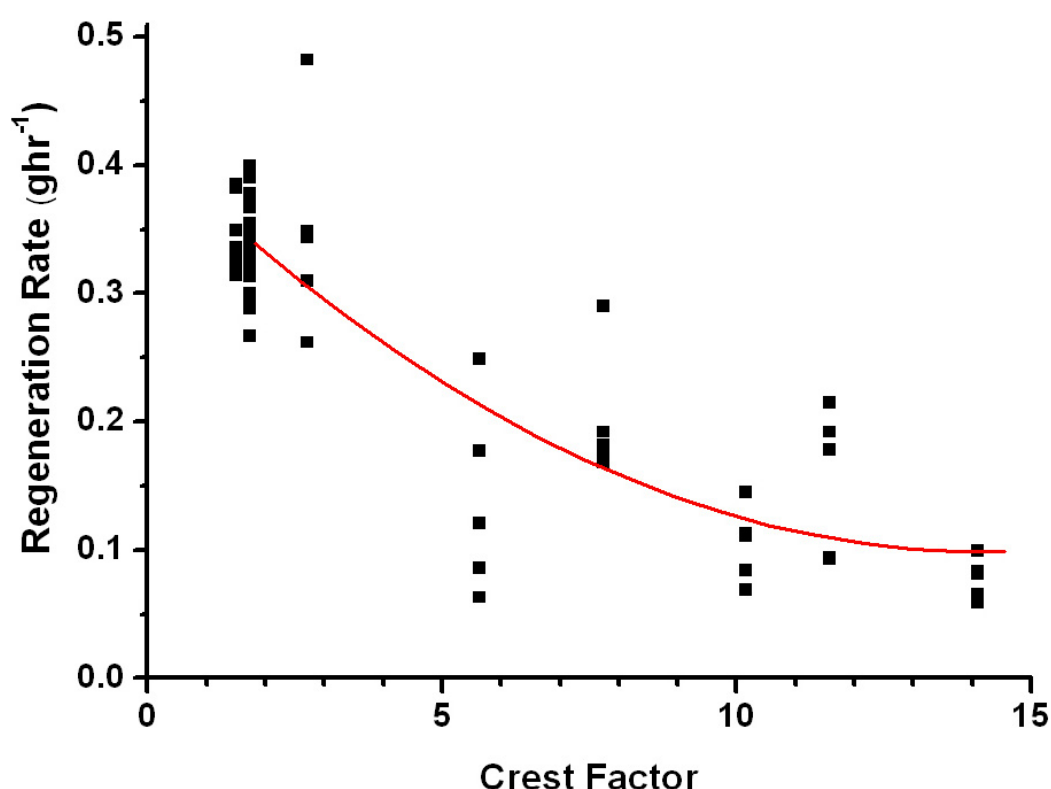
Figure 4.12 Variation in regeneration rate with Crest Factor for fixed RMS current of 15 mA rms.

The fluctuations in the measurements may be as a result of material lost from the samples during the testing. The high amplitude current waveforms used to generate the high crest factors caused small quantities of PM (~ 1 mg) to be expelled from the crucible. Despite the variations in the measurements, there is a clear negative trend to the results suggesting that high crest factors and hence spiked current waveforms are not beneficial to regeneration performance. The effectiveness and rate are nearly

constant at lower crest factors and the results show that crest factors between 1 and 3 will offer similar performance when used with the Autoselective system. This is an important factor for power supply design since crest factors below 1.4 are difficult to generate when powering atmospheric discharges and crest factors above 5 require oversized magnetic components. These results show that conventional power supply topologies are suitable for use with the Autoselective system and that more complex and expensive designs offer no advantages.

4.7 Conclusions

The frequency of the discharge current was shown not to be a factor in determining the regeneration performance. This allows the frequency to be chosen based on other factors such as electrical properties of the load. The use of inserted electrodes has produced difficulties when designing discharge power supplies due to the large capacitive component that they add to the load. Since the effect of this capacitance is inversely proportional to the frequency, it is easier to design a discharge power supply at a lower frequency and the research has shown that the lower frequencies will produce no regeneration performance reduction.

The work done investigating the effects of crest factor has facilitated the design of future discharge power supplies. Higher crest factors have higher instantaneous powers and therefore require different or more robust power supply techniques requiring bulky magnetic components scaled to accommodate the higher peak power. Conventional discharge power supply topologies provide crest factors between 1.4 and 3 which have been shown to be most effective for Autoselective regeneration. The suitability of conventional designs reduces the power supply size, complexity and cost.

The extensive results for the discharge current level enable predictions to be made of how regeneration performance will be affected. The results are also valuable for comparing the different on- and off-times selected for damage avoidance. Of particular interest is the compromise found between rate and effectiveness. The effectiveness and rate must be chosen to find an optimum operating point based on

filter damage, system complexity, system cost and power requirement. The results obtained allow comparison of different operating conditions.

The on- and off-times have been shown to rapidly switch the regeneration process on and off, and that there is no significant time delay between the switching of the discharge and the beginning or end of the regeneration. This means that the on- and off-times can be chosen purely to alleviate filter damage. This is important because it means that a materials durability under discharge conditions directly affects the regeneration rate associated with it. This knowledge will help to compare new materials to be used with Autoselective technology.

Overall, the discharge optimisation research has provided a deeper understanding about how the discharge current variables affect the regeneration performance. General conclusions can now be made regarding the current level and crest factor. A current of 10 mA to 15 mA with a crest factor less than 3 is required for an efficient system. The frequency of the discharge does not affect regeneration performance and can be chosen to facilitate power supply design. The on- and off-times should be chosen based on the damage threshold of the material which will determine the regeneration rate.

The next chapter looks at the effects of filter material and electrode geometry on regeneration performance. The relationship between the regeneration performance, the on- and off-times and the filter damage threshold will be explored in more depth. The effect of discharge frequency on the other system properties is also investigated.

5. In Filter Testing of Plasma Regeneration

This chapter describes the optimisation of the Autoselective regeneration process when applied to a 100 cpsi (cells per square inch) wall flow filter. Different electrode configurations, types and spacings were tested in conjunction with different discharge power supplies. The performance was measured in terms of regeneration distribution, number of required electrodes, effect on filtration and filter damage. Optimisation of the on- and off-times was carried out and a full filter flow-rig and engine test are described.

5.1 Regeneration Distribution

Previous work (Proctor, 2007 and Williams, 2007) had shown that the discharge could effectively regenerate parts of the filter, however, a full filter had not been regenerated at the start of this research. Incomplete regeneration distribution would allow parts of the filter to load with PM to high levels leading to uncontrolled regeneration and possible filter damage. Uniform regeneration of the entire filter volume was also required to keep the size of filter required for a given engine as small as possible.

Early work (Proctor, 2007) showed that it was difficult to oxidise all the PM present between the electrodes. The discharge often found pathways between the electrodes that it preferred irrespective of the PM loading. This lack of auto-selectivity was apparent in three modes: radially, axially and on an individual channel scale. Each of these problems was investigated and the results are presented in the following sub-sections.

5.1.1 Axial Partial Regeneration

Axial partial regeneration describes the case where regeneration does not occur evenly along the length of the channel. This was observed especially in the case of closely spaced electrodes. The electrodes used were bare copper wires located in the channels of the WFF. The discharge only regenerated regions close to the point

of breakdown, therefore, the preferentially regenerated regions must have presented easier breakdown locations. More importantly, when these regenerated regions were clean the discharge did not move to the regions of higher PM density so that auto-selectivity did not occur. The cause of this change in breakdown voltage was shown to be caused by variations in the electrode spacing occurring axially down the channel. This was due to the fact that the electrodes were not centralised in the channel. A test using wire electrodes and a section of wall flow filter showed that the regeneration occurred preferentially where the electrodes were closest as illustrated in Figure 5.1. This meant that axial partial regeneration would be improved using an electrode centralised within the channel that provided more constant electrode spacing.
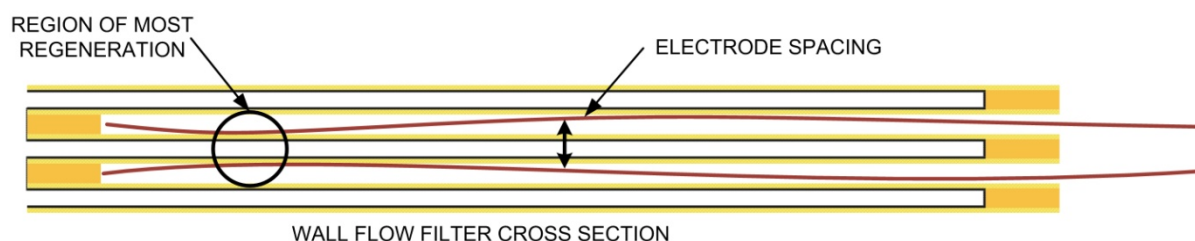

Figure 5.1 Inserted solid wire electrodes in a filter cross section showing the region of maximum regeneration at the closest electrode spacing

The most obvious method of reducing electrode spacing variation was to use a wire electrode of equal thickness to the channel. However, this would introduced problems with insertion since the thicker wire was found to damage the fragile walls of the filter. A thick wire electrode would also not allow flow to pass around it and a few hundred inserted electrodes would increase the filter back-pressure. A hollow braided electrode was tested and the electrode was centralised in the channel due to its shape. It had less effect on back-pressure because it was porous and it produced uniform axial regeneration. The braided electrode was difficult to insert and required careful placement using a piece of wire placed temporarily down its centre for support. A new spring electrode was therefore developed as illustrated in Figure 5.2. The spring electrode automatically centred itself to the channel when its diameter was close to the channel width (1.95 mm). The spring electrode was relatively stiff and easy to place in the channel as well as being a cheaper alternative to the braid.

Testing showed that if the pitch of the spring was low (<1 mm), it produced good regeneration distribution. The spring electrode was shown to be a good solution to solving axial partial regeneration and was adopted for future testing.
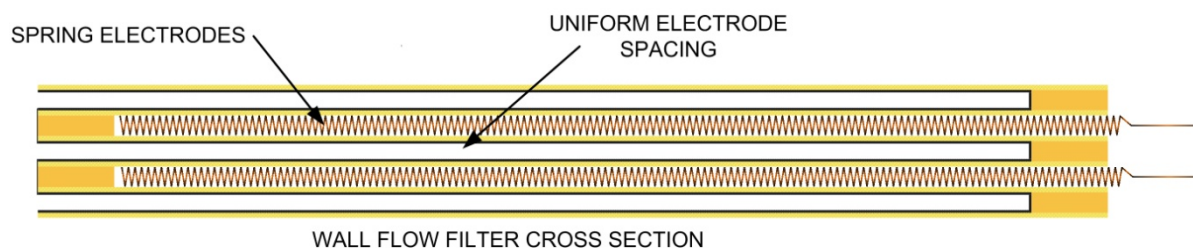

Figure 5.2 Diagram of spring electrodes showing more uniform electrode spacing

5.1.2 Radial Partial Regeneration

The regeneration is more complete closest to the electrodes when using inserted electrodes with a gap of more than one channel, radial partial regeneration is used to describe when regions are left un-regenerated by this effect. It is caused predominantly by the discharge current spreading out as it leaves the electrode and is caused by the parasitic resistance and capacitance of the filter and soot. The region close to the electrode always experiences a higher regeneration rate because the discharge current is not attenuated there.

Once the regeneration close to the electrodes is complete, the power supply must produce higher breakdown voltages as the gap between the PM and electrode increases. If the power supply can not produce the higher voltages then the regeneration stops, leaving large regions of un-regenerated filter. This cause of radial partial regeneration could be addressed in some cases by using higher voltage power supplies.

An experiments was conducted at 26 kHz using elevated voltages to enable breakdown under all conditions. The regeneration remained incomplete due to the discharge finding preferential paths through the filter even though they were free from PM. This cause of radial regeneration distribution was due to the electrode geometry and not the higher breakdown voltages. The cause was attributed to the electric field around the electrode at breakdown since the breakdown occurs along the region of

highest field strength. The regeneration was improved by using electrodes arrangements that kept the fields uniform, several configurations were tested with the best configurations are discussed in this chapter and Chapter 8.

The best electrode array tested was the checkerboard layout with its alternating ground and high voltage (HV) electrodes. This array placed every PM loaded channel between a HV and a ground electrode. The uniform electric fields and short electrode spacing led to no radial partial regeneration. The disadvantage was the large number of inserted electrodes required, approximately 600 for a 5.66" diameter 100 cpsi (cells per square inch) WFF. Testing consistently showed that the checkerboard electrode array gave better regeneration distribution than the linear array as illustrated by the flow maps of Figure 5.3. Flow mapping was carried out using a steady gas flow and a Pitot tube pressure measurement within each channel to measure the flow rate distribution (Proctor, 2007).
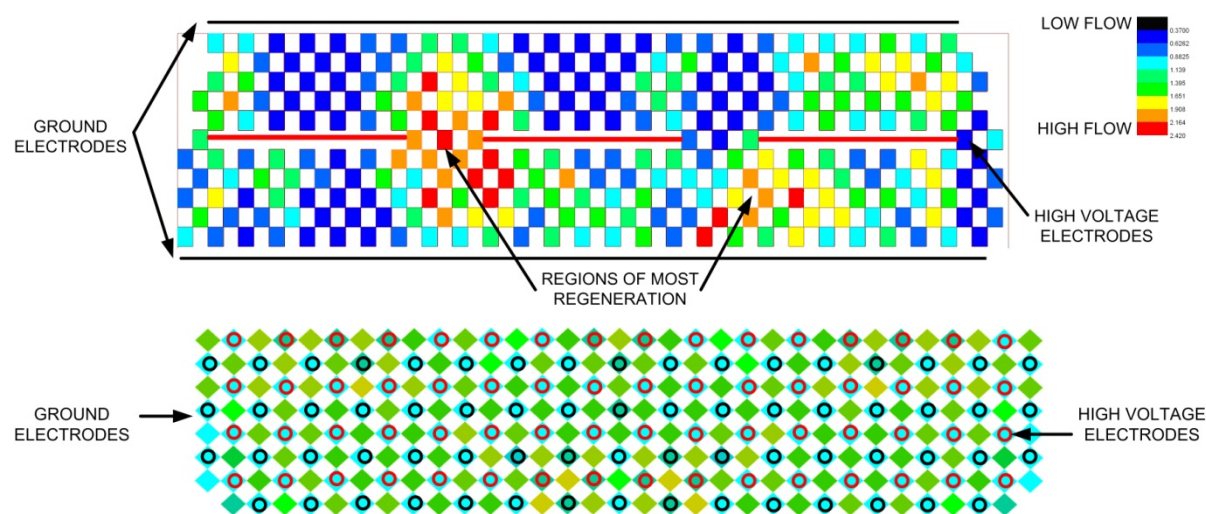

Figure 5.3 Flow maps of linear (top) and checkerboard (bottom) electrode arrangements

5.1.3 Per-channel Partial Regeneration

The discharge was observed to take preferred routes through the channels which left PM un-regenerated. If electrodes were placed on either side of a soot laden filter channel using uniform electrode spacing (i.e. the checkerboard electrode array), the

resulting discharges still left regions of the channel walls un-regenerated. The discharge was also observed to only cross diagonally between loaded channels for wider electrode spacings, leaving PM loaded regions un-regenerated. The patterns of PM left in the filter channel cross sections showed that the discharge sometimes did not auto-select all the soot in the channel. This was called 'per-channel' partial regeneration and is discussed in this sub-section.

The reason the discharge passed between the corners of the loaded channels can be explained by electrostatic theory since the electric field is strongest between the corners of adjacent loaded channels. This led to a preferred breakdown region in the corners leading to preferential regeneration in these regions and the process was termed the 'corner-effect'. Several electrode strategies were tried to alleviate this problem, the conclusion was that the discharge would always start at the corners of channels when the electrode geometry required it to cross between loaded channels. Once the corners were regenerated, the discharge was observed to regenerate the walls of the channels thus the corner-effect was not considered a major obstacle. The checkerboard array did not show the corner-effect since the discharge path was always across only one loaded channel.

The discharge left small regions of PM on the adjacent walls of the channel using the checkerboard electrode arrangement. Figure 5.4 shows a cross sectional diagram of a filter with inserted spring electrodes showing the remaining soot pattern which was termed the 'wall-effect'. Observations of the discharge showed that the discharge moved to the centre of the channel immediately after breakdown. This meant that the regions of PM left on the walls were never regenerated.
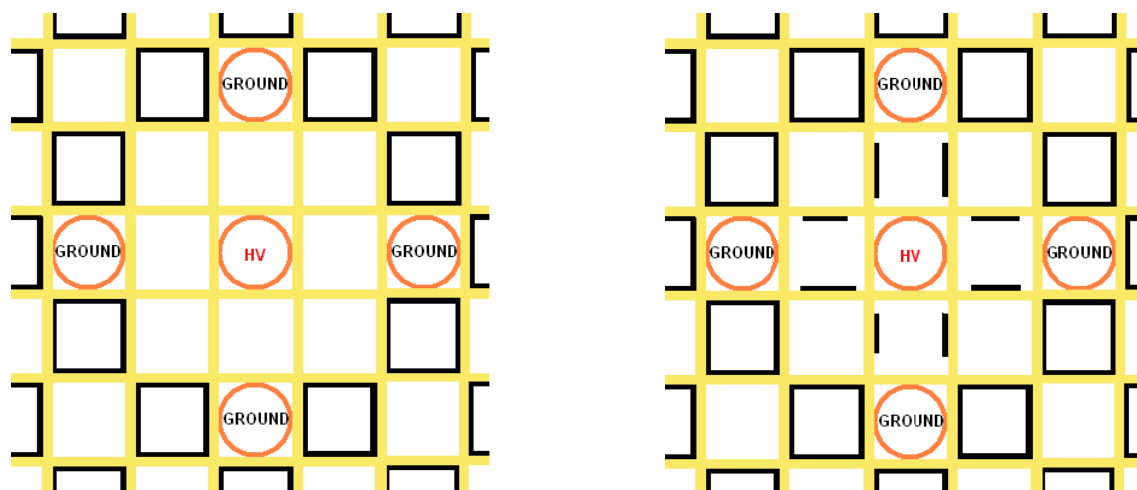
Figure 5.4 The ideal (left) and observed (right) regeneration patterns observed when using close electrode spacings, the 'wall-effect'

Another type of electrode (with an 'X' shaped cross section) was designed to increase the electric field in the un-regenerated regions and encourage better regeneration, shown in Figure 5.5. The 'X' shape was difficult to produce so a 'V' shape was used to test the concept.
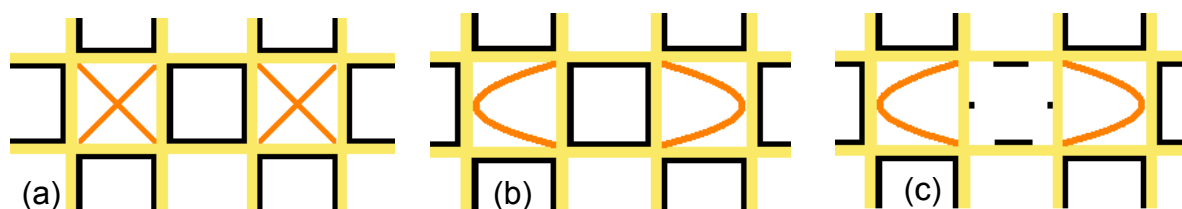
Figure 5.5 Cross type electrodes and their result on the wall-effect. (a) The cross electrode idea. (b) The 'V' electrodes used for the test. (c) The resulting regeneration pattern

The results showed very little improvements to the spring electrodes despite the discharge initiating along the PM on the filter wall. The reason for this lack of selectivity was attributed to the discharge preferring to travel through the air in the centre of the channel. The air needed to be made a more difficult path to make the discharge prefer to travel along the walls and soot. This was achieved by lowering the current which in turn lowered the ionisation level of the air and increased the discharge voltage. This had the effect of reducing the wall-effect and had the additional advantage of increasing the regeneration effectiveness (g.kWh^{-1}) as

_____

described in Chapter 4. The disadvantage of this solution was the loss of regeneration rate which led to the need for more discharges.

It was unclear at this stage whether the wall-effect would present a significant problem to the regeneration system. It was likely that as the regions of PM on the walls increased due to loading, the discharge would begin to clean them and an equilibrium would exist.

The wall-effect was further investigated using a flow-rig trial and a pre-loaded WFF. A simulated exhaust flow rate of 220 kg.hr^{-1} was made using a flow-rig (the heater capabilities were not used since the distribution was found to be unaffected by the gas temperature, the gas was around 70 °C), the filter was pre-loaded on an engine to 3.5 g.litre^{-1} and the electrodes were then inserted. The filter was sectioned after testing a range of settings and the channels adjacent to the electrodes were scanned into a computer for image processing. A scan of a typical wall affected channel wall is shown in Figure 5.6.

(a)

(b)
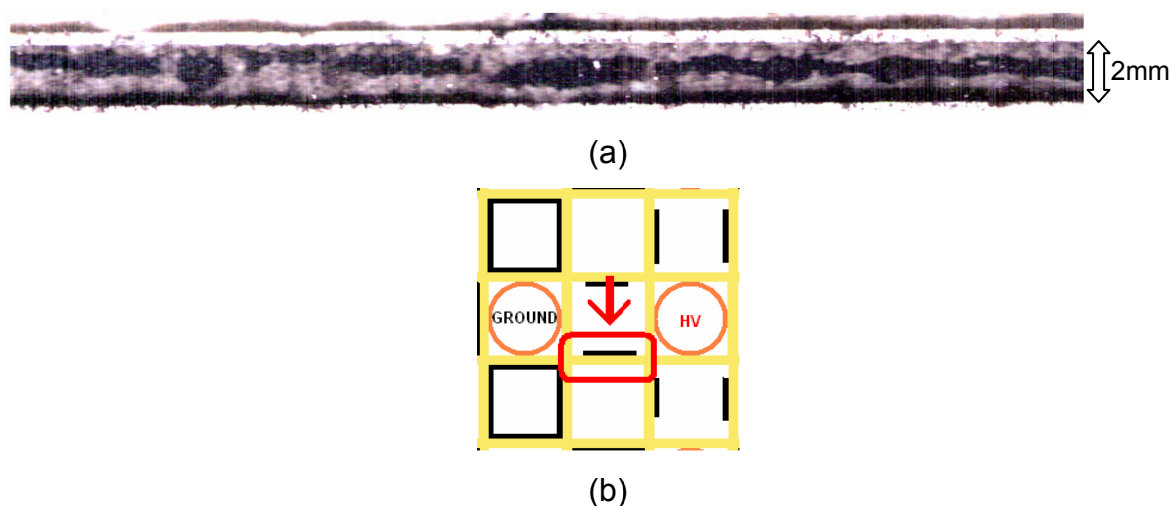
Figure 5.6 (a) The un-regenerated PM (black) left on the channel wall adjacent to the electrodes. (b) The filter cross section indicating (arrow and box) which channel wall is shown in the image and the viewing direction

The flow-rig was used to determine whether better distribution could be achieved using different currents or frequencies. The same power supplies described in Chapter 4 were used. Testing was performed at 300 kHz, 26 kHz and at DC. It was

hoped that a lower frequency (DC) would have a similar result to lowering the current on the wall-effect since both increase the discharge voltage due to the lower numbers of charge carriers. Lowering the current had already been observed to reduce the wall-effect and improve auto-selectivity. The results for different frequencies are shown in Figure 5.7, the results clearly show that the DC discharge made a significant improvement to the wall-effect whereas the high frequency discharge made it worse.

DC Discharge

These channels were almost completely regenerated

(a)

26 kHz Discharge

These channels showed significant evidence of the wall effect

(b)

300 kHz Discharge

These channels were nearly un-regenerated

⇕ 2mm

(c)

Figure 5.7 Wall-effect observed at different frequencies under flow conditions. (a) DC, (b) 26 kHz and (c) 300 kHz

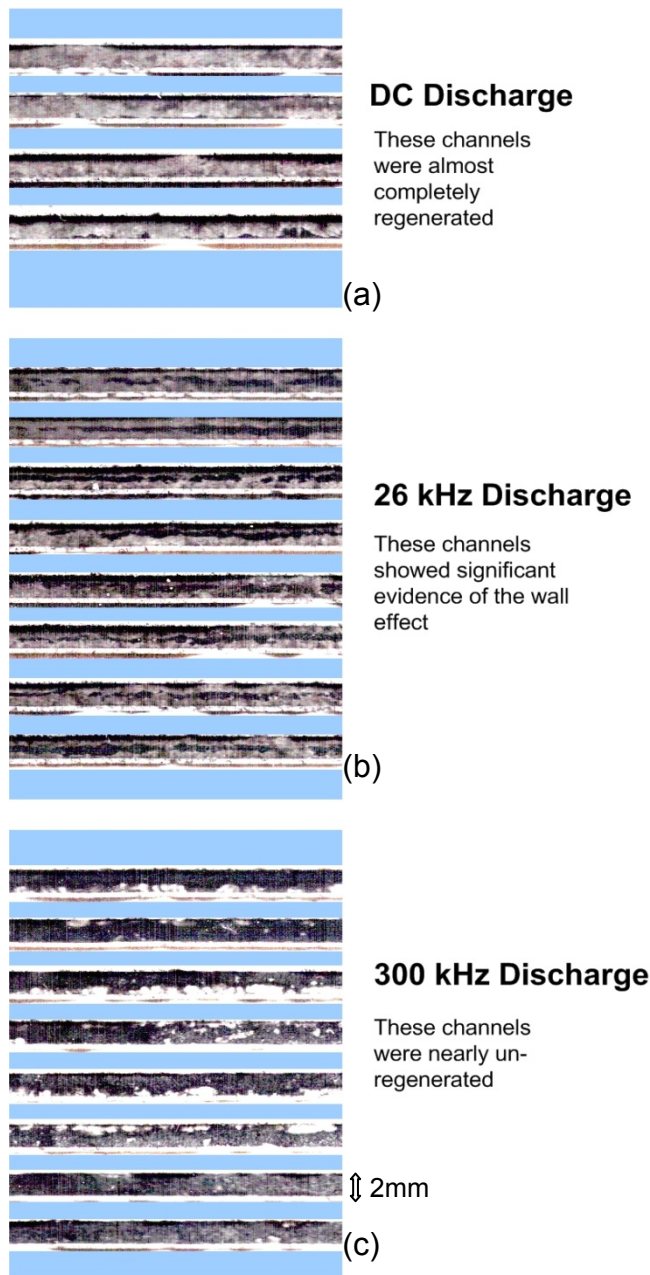The results of this regeneration distribution test suggest that a lower frequency would be advantageous to regeneration distribution when using closely spaced electrode arrays. However, results were also generated during this test that suggests the lower frequencies had an adverse effect on the amount of PM travelling through the filter and will be detailed in Section 5.3.

5.2 Regeneration Distribution Conclusions

The goal of this stage of the research was to find an electrode arrangement and power supply capable of regenerating an entire wall flow filter evenly and to determine the factors affecting regeneration distribution. Axial partial regeneration was overcome using the spring electrode. The radial partial regeneration problem and corner-effect were solved using the checkerboard electrode layout. The wall-effect was minimised using lower discharge currents and frequencies. The checkerboard electrode layout successfully achieved uniform regeneration of the whole filter, the number of spring electrodes required for a 5.66" diameter WFF was approximately 600.

5.3 Discharge Effects on the Filtration Process

Early observations of the Autoselective regeneration system indicated that there was a tendency for the downstream (clean side) walls of the WFF to become blackened due to deposited PM. No noticeable blackening was observed when the regeneration system was turned off indicating that the regeneration system was causing some PM to travel through the filter. Soot travelling through the filter indicates loss of filtration efficiency which is normally above 95% for a WFF. Future emission legislation is likely to be based on a particle count rather than a total PM output and this makes any loss in filtration efficiency a serious obstacle. Three modes in which the Autoselective system reduces the filtration efficiency have been identified, filter damage, blow-off and blow-through. These are now summarised in the following sub-sections.

5.3.1 Filter Damage

Filter damage is often observed when operating at high currents, with high duty cycles or with long on-times. Filter damage may be glassing, holing or a combination of the two. Glassing is the process where the filter material melts and the pores fuse to form a far denser ceramic with the appearance of glass. Holes are produced predominantly by the effect of excessive melting and the holes usually have a melted glass circumference up to 1 mm in diameter. When a hole is present in the wall of the filter, PM in the gas flow can escape directly through the hole without being trapped leading to a loss in filtration efficiency. Any level of filter damage is unacceptable since the accumulation of damage will either weaken the filter leading to fracturing or lower the filtration efficiency below practical limits.

5.3.2 Blow-off

It is possible for the discharge to remove the PM from the filter walls on the dirty side of the filter, this is known as blow-off. Blow-off mainly affects the caked layer of PM on the surface of the ceramic walls. The physical process by which the PM is re-entrained into the flow is investigated in Chapter 7. Although the dislodged PM is still on the upstream (dirty) side of the filter, the process of blow-off is still capable of reducing filtration efficiency since the dislodged PM must be re-trapped by the filter. A proportion of the all the dislodged PM passes through the walls because the WFF is not 100% efficient. If a large proportion of the trapped PM is repetitively dislodged, the result is a significant loss in filtration efficiency. Another potential problem encountered with blow-off is that the re-entrained particles may be broken up by the discharge forming smaller particles. Smaller particles are harder to trap and more likely to pass through the filter.

5.3.3 Blow-through

Blow-through is probably the most significant method by which the filtration efficiency of the WFF is reduced. Blow-through occurs when the fragile structure of the deep bed filtration layer is disturbed. The deep bed filtration layer occurs inside the ceramic wall and is formed when PM is trapped on the surfaces inside the porous ceramic. The dislodged particles move with the direction of the flow and are usually

immediately re-trapped by the filter. If particles are repetitively dislodged they are able to migrate through and escape from the deep bed layer into the downstream gas flow. It is therefore preferable for the regeneration system to not disturb this layer of filtration.

The regeneration distribution testing that investigated reducing the wall-effect also produced results that show how the filtration efficiency was affected by the discharge frequency. The results are shown in Figure 5.8. The sections of the filter were analysed for damage after the test was complete. Although some limited damage did exist, there were no holes in the ceramic wall. The blackening of the filter walls must therefore be attributed to a combination of blow-off and blow-through

Figure 5.8 Scan of filter sections showing channel blackening on the clean (downstream) part of the filter. Blackening increases gradually towards the downstream end of the channels. (a) is the result of a 300 kHz discharge, (b) results from 26 kHz and (c) from a DC discharge

The channel blackening is more pronounced in the downstream channels of the 26 kHz and DC (uni-polar) discharge tests. The difference in blackening shows that the filtration efficiency is being affected by the different discharge properties at each frequency. Lower frequency discharges repetitively breakdown the gas between the electrodes which creates a localised pulsating gas flow at the breakdown site due to

the rapidly expanding gasses. The electric field transients at break down are also responsible for additional forces on the particulates. Further investigation into the forces exerted on the PM has been carried out and will be discussed in a Chapter 7. The blow-off for the high frequency (300 kHz) discharge was less, most likely because it does not repetitively break down the gas between the electrodes.

In summary, it can be concluded that discharge frequency does have a significant effect on the filtration characteristics of the filter. Lower frequencies promote better regeneration distribution at the expense of a loss in filtration efficiency.

5.4 Effects of Electrode Geometries

A new close spaced electrode configuration had been shown to solve many of the regeneration distribution problems. It was not known how this new electrode array would impact the effectiveness ($g.kWh^{-1}$) and the regeneration rate ($g.h^{-1}$). This section describes the testing to assess the effects of varying the electrode spacing (gap) on regeneration performance.

The test used small sections of wall flow filter placed in the path of a 10 mA (rms) discharge with a low forced air flow (<1 $m.s^{-1}$). The sample was pre- and post-weighed. The power consumed by the discharge was measured using the oscilloscope. The average power was measured using an averaged sampling method over the one minute test.

The samples showed visible regeneration during the tests and minimal blow-off was observed hence the mass loss can be attributed to regenerated PM. The number of channels that the discharge had to traverse was varied to assess the effect on the regeneration performance. The filter used was a 100 cpsi (cells per square inch) cordierite wall flow filter loaded with 3 $g.litre^{-1}$ of diesel PM from a 4 cylinder 4.4 litre heavy duty diesel engine at mid load (1500 rpm, 150 Nm,). The apparatus shown in Figure 5.9 was used for the experiment.
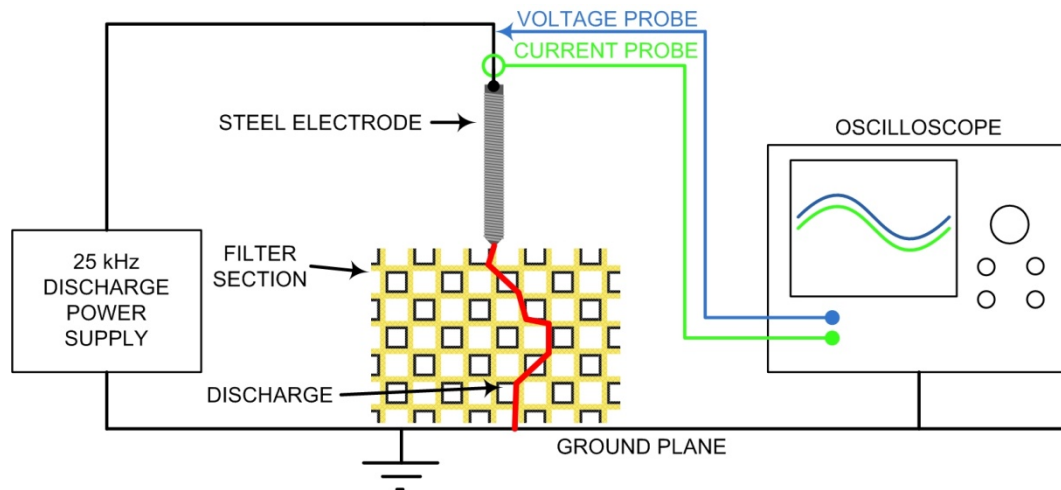
Figure 5.9 Apparatus for channel spacing tests

A fan consuming 0.5 W was used to force a steady low flow rate down each channel to ensure the regeneration had sufficient oxygen and to prevent excessive heat rise within the filter. The current transformer was a Pearson 200 MHz 1:1 current transducer and the voltage probe was a Tektronics 75 MHz 1000:1 high voltage probe. The signals were monitored on a Tektronics 3 GHz digital storage oscilloscope which was also used to calculate real-time power, rms current and average power. These results from this experiment are plotted in Figure 5.10 and 5.11, the channel spacing is a dimensionless integer variable describing the number of channels between the electrodes.

Figure 5.10 Regeneration rate versus channel spacing (linear fit)

Figure 5.11 Regeneration effectiveness versus channel spacing (linear fit)
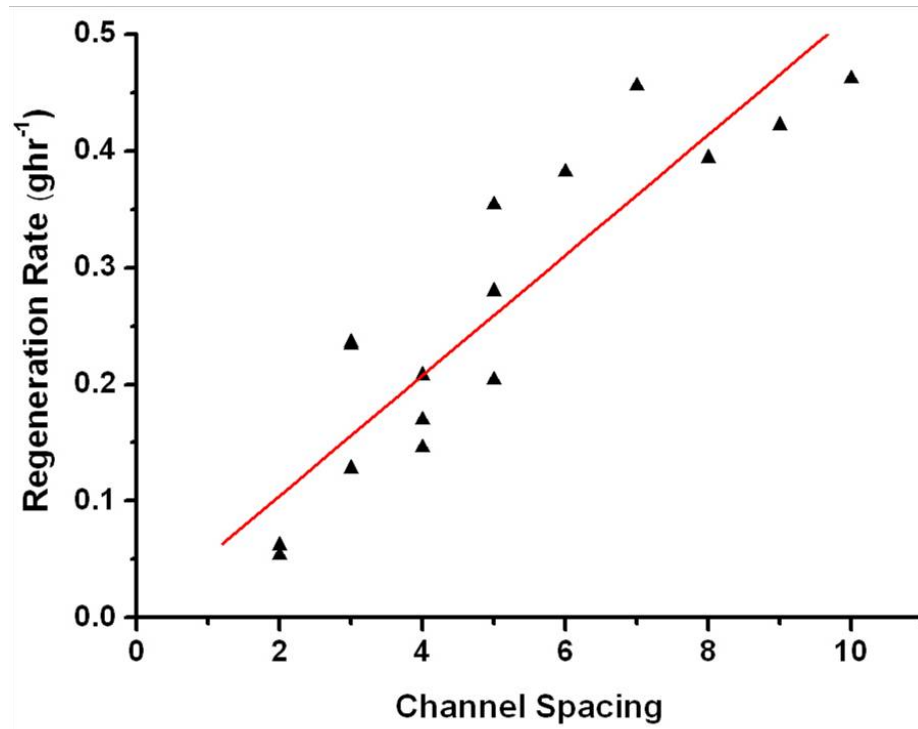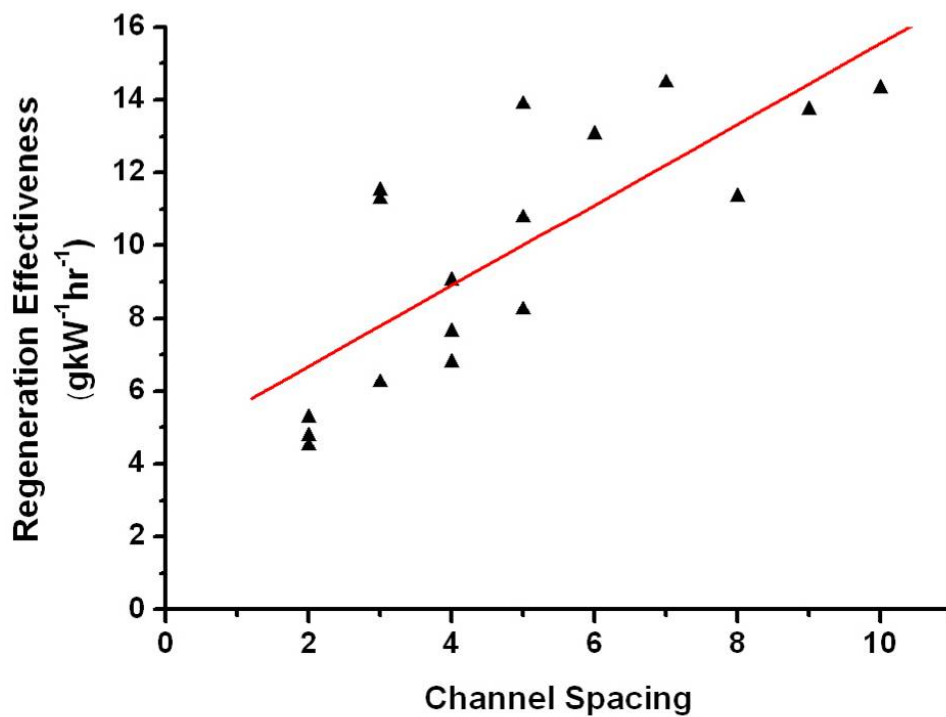
The results show an increase in both rate and effectiveness with channel spacing. This means that larger channel spacings are better for lowering system power and for

reducing the number of discharges required. The data was further analysed to represent the number of discharges and the minimum power input needed to meet a filter loading rate of 6 g.hr^{-1} (a typical value for 100 kW heavy duty diesel engine application with 2006 technology, EUROII engine at 50% load, 0.12 g.kWhr^{-1} specific PM production), see Figure 5.12.
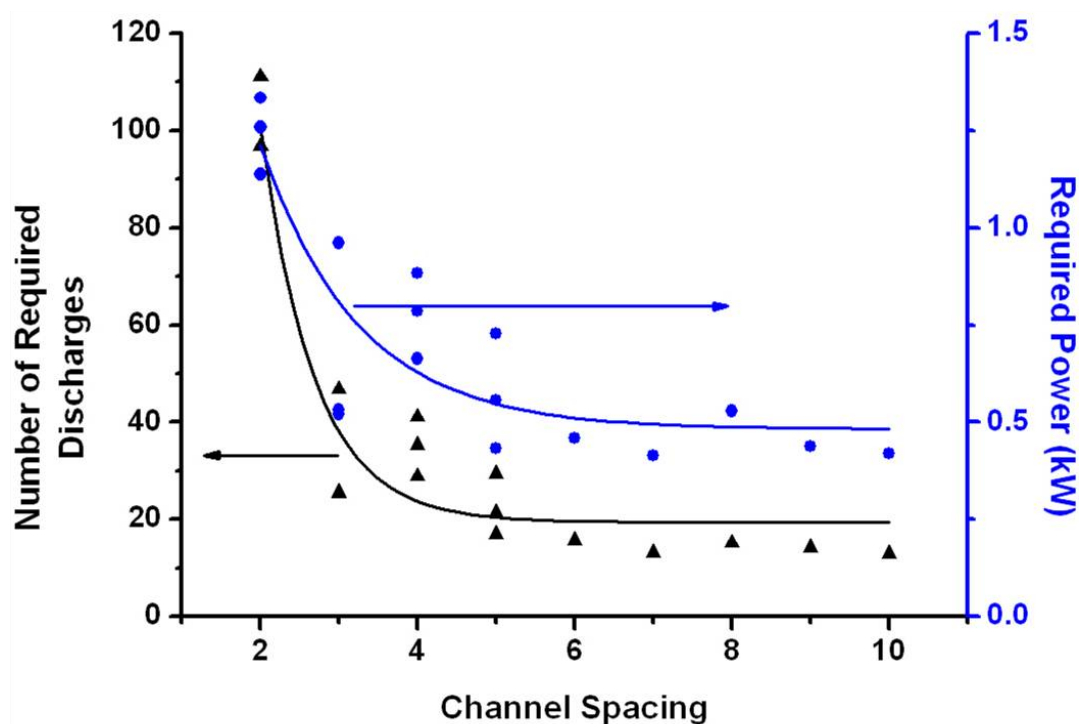
Figure 5.12 Number of electrodes and (discharge) input power versus channel spacing to achieve 6 g.hr^{-1}

The number of discharges does not include the effect of on- and off-times which will increase the number to approximately double due to the ~ 50% duty cycle limit.

In conclusion to this section, wide electrode spacings lower system complexity and power consumption. The regeneration distribution optimisation led to the adoption of the close-spaced checkerboard layout with an electrode spacing of 1. This section of the research suggests that the channel spacing should be 6 or more. An electrode array with this channel spacing would provide excellent regeneration performance if the regeneration distribution could be improved. Subsequent research was planned

to reduce the problem of poor regeneration distribution when using linear electrode geometries.

5.5 Filter Damage

One of the key control difficulties of the Autoselective process was due to the ability of the discharge to cause filter damage in a fraction of a second. This was due primarily to the rate at which heat was delivered to the PM and filter. Early work (Proctor, 2007) indicated that the discharge would melt the filter in still air with just 10 mA for 1 second. It is unacceptable for the filter to sustain any damage during normal operation since the accumulation of damage would lead to filter failure. The solution for preventing damage had previously been to modulate the discharge power i.e. to implement an on- and off-time. The filter is allowed to cool down sufficiently during the off-time to avoid melting. This has the added benefit of increasing discharge mobility by preventing the discharge becoming 'stuck' in one place. The auto-selection process was observed to occur only at breakdown and maintaining auto-selectivity required interrupting the discharge.

The fraction of time the discharge was on for (the duty cycle) needed to be as high as possible because useful regeneration only occurred whilst the discharge was operating. The results showed quickly that the duty cycle maximum may not necessarily coincide with the maximum on-time. A test setup was used in stationary air using a pin electrode and ground plane similar that used for the discharge optimisation tests. The clean filter to be tested was sectioned so that a single wall thickness sample was produced. A power supply was preset to give the current and on- and off-times under test. Each test subjected the sample to the discharge before checking for damage. If no damage occurred after a few seconds, the tests were repeated with successively longer durations up to 10 minutes in order to be sure that there was no cumulative damage. Further analysis of the undamaged samples was then performed using an optical microscope to check for microscopic changes to the structure. For each current, a maximum on-time was first found by using an off-time of several seconds (i.e. enough time for the filter to return to room temperature). The maximum duty cycle was then found by fixing the on-time and decreasing the off-time

from several seconds to a few tens of milliseconds until damage occurred. The minimum off-time for each fixed value of on-time was recorded. In this way, a safe operating region was defined for still air and a clean filter wall. These results were used to define a smaller region of interest for subsequent more detailed flow-rig tests.

Flow-rig testing was carried out under exhaust like conditions in terms of flow rate and temperature (220 kg.hr^{-1} and 200 °C). Since only the threshold of damage was of interest, a reduced experimental range was tested using a loaded filter (3.5 g.litre^{-1}). The results are shown in Figure 5.13. It was found that despite the higher gas temperatures, the flow-rig test sample was less easily damaged by the discharge. This is consistent with theory since the forced convective heat flux resulting from the much cooler flow-rig gas (200°C) was expected to be significant close to the melting point of cordierite material (~ 1450°C). The results from this experiment formed the basis for choosing on- and off-times for cordierite wall flow filters.
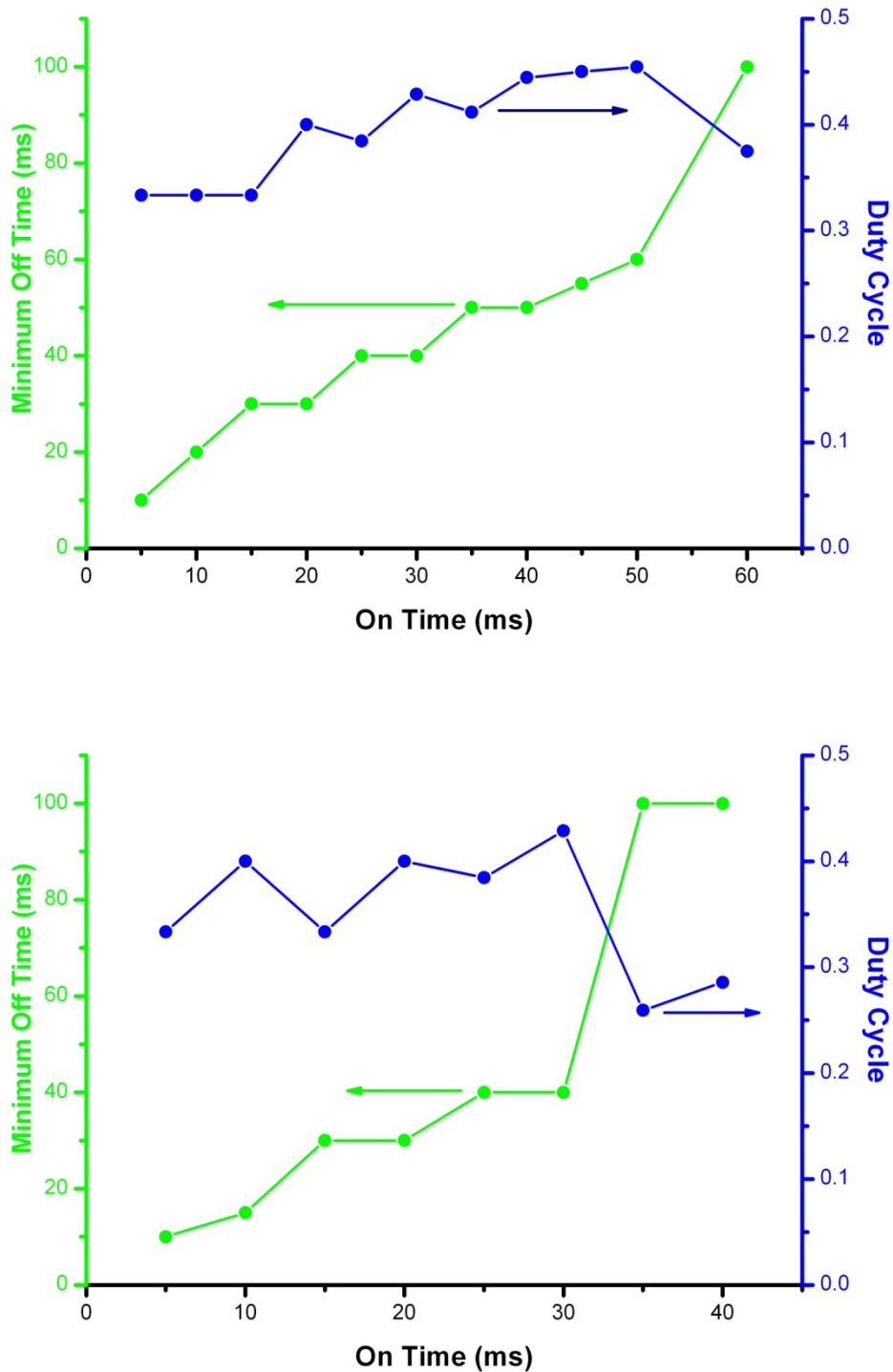
Figure 5.13 Damage threshold results for 100 cpsi (cells per square inch) cordierite WFF in a simulated exhaust flow. (Top) 10 mA current. (Bottom) 15 mA current

At 10 mA the highest duty cycle was achieved with 50 ms on and 60 ms off (duty cycle = 0.45). However, during one of the 50 ms on-time tests, slight surface glassing

damage was observed indicating that this setting was close to, but exceeding, the damage threshold. 40 ms on and 50 ms off was therefore the optimum, allowing a small safety margin and providing a duty cycle of 0.44.

At 15 mA, the highest duty cycle was 0.42 with 30 ms on and 40 ms off. The higher current would be expected to provide better regeneration rate (+7% higher calculated from previous results) making both set points very similar in terms of performance. The 10 mA case was considered a better setting because of the regeneration uniformity benefit from operation at lower currents.

5.6 Flow-rig Trials

Testing was carried out using a full filter and multiple electrodes to confirm the performance of the new settings before moving to on-engine tests. A standard 5.66" diameter cordierite wall flow filter was fitted to the flow-rig after being loaded with 3.5 g.litre^{-1} of PM and fitted with 600 inserted spring electrodes. The power supply was set to give the 40 ms on-time, 50 ms off-time and 10 mA rms current. The test required 300 discharges, however, only 30 power supply outputs were available. Therefore, the test was carried out in time segments of 15 minutes by moving the electrodes to different regions of the filter between tests; 9 individual tests were required to regenerate the whole filter in this manner. The back-pressure after each test was recorded and the result is shown in Figure 5.14.
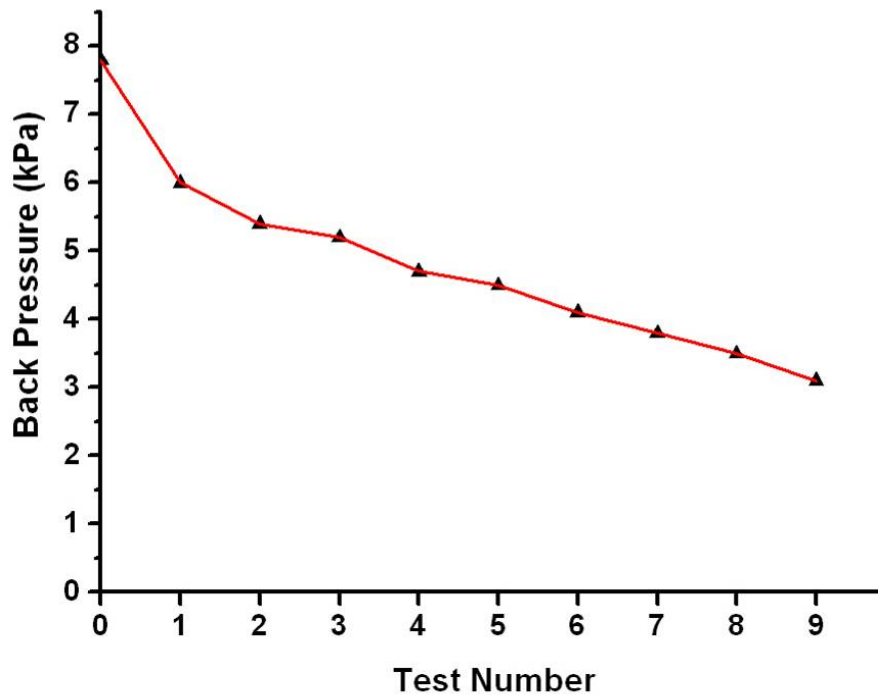
Figure 5.14 Backpressure after each test interval (220 kg.h^{-1}, 70 °C)

The back-pressure plot shows a steady rate of cleaning for the duration of the flow-rig test. The first segment of the test used the original settings (50 ms on, 50 ms off and 15 mA) from before the on- and off-time optimisation work in order to get a comparison. This test gave a larger back-pressure drop although filter damage was observed when the filter was sectioned. No damage was observed during the subsequent tests using the optimised settings. The filter was 'flow mapped' at the end of the test to confirm that the regeneration distribution was even. Flow mapping uses a steady gas flow and a Pitot tube pressure measurement from each channel to measure the flow rate distribution. The flow map is shown in Figure 5.15

_____

Figure 5.15 Flow map of half of the filter used in the flow-rig tests showing even regeneration of all channels

The flow map shows good regeneration distribution and a significant improvement to the flow rate in every channel containing an electrode. Sectioning confirmed that good axial regeneration distribution was also achieved. Partial regeneration did occur, ho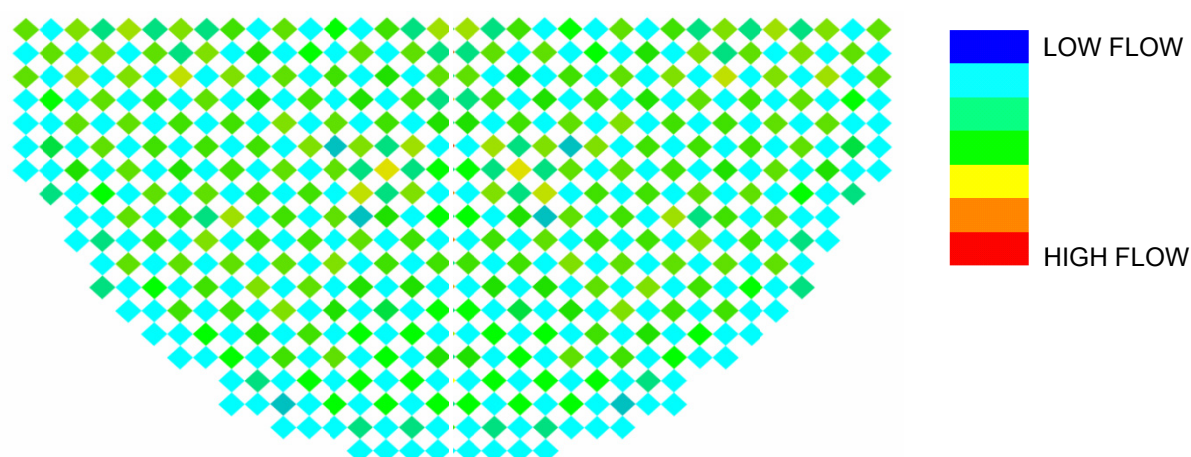wever, on a per-channel scale i.e. the wall-effect was observed in every regenerated channel. Previous distribution testing had shown that the wall-effect is a result of close electrode spacing due to the discharge preferring to pass through the air in the channel and not through the PM on the walls (Section 5.1.3).

5.7 On Engine Trials

The successful distribution obtained during the flow-rig trials was promising, testing began on engine. These tests provided the opportunity to see if the wall-effect would lead to eventual system failure since the engine test had a PM input during the test unlike the flow-rig. A smaller section of filter was to be used for the engine test to reduce the number of discharges required; approximately 100 discharges and associated high voltage feed-throughs were needed to regenerate an entire 5.66" diameter filter. To ensure that the engine could still operate at the correct speed and load, some of the exhaust flow was by-passed through an exhaust valve. The filter section was fitted with the electrodes and sealed inside the stainless steel housing with high temperature gas tight silicone sealant and fibre-glass lagging. The filter was loaded for an hour before the regeneration system was switched on. Initially there was no improvement in the rate of back-pressure increase so the power supply was

retuned. This resulted in the system back-pressure remaining constant for the rest of the test. When the system was switched off at the end of the tests, the back-pressure rose quickly indicating that the regeneration rate was equal to the engine soot output. Sections of the filter were checked for damage after the test confirming that the discharge operating conditions did not damage the filter. The test was considered to be successful and repeat tests gave similar results. The back-pressure and flow rate traces are shown in Figure 5.16.
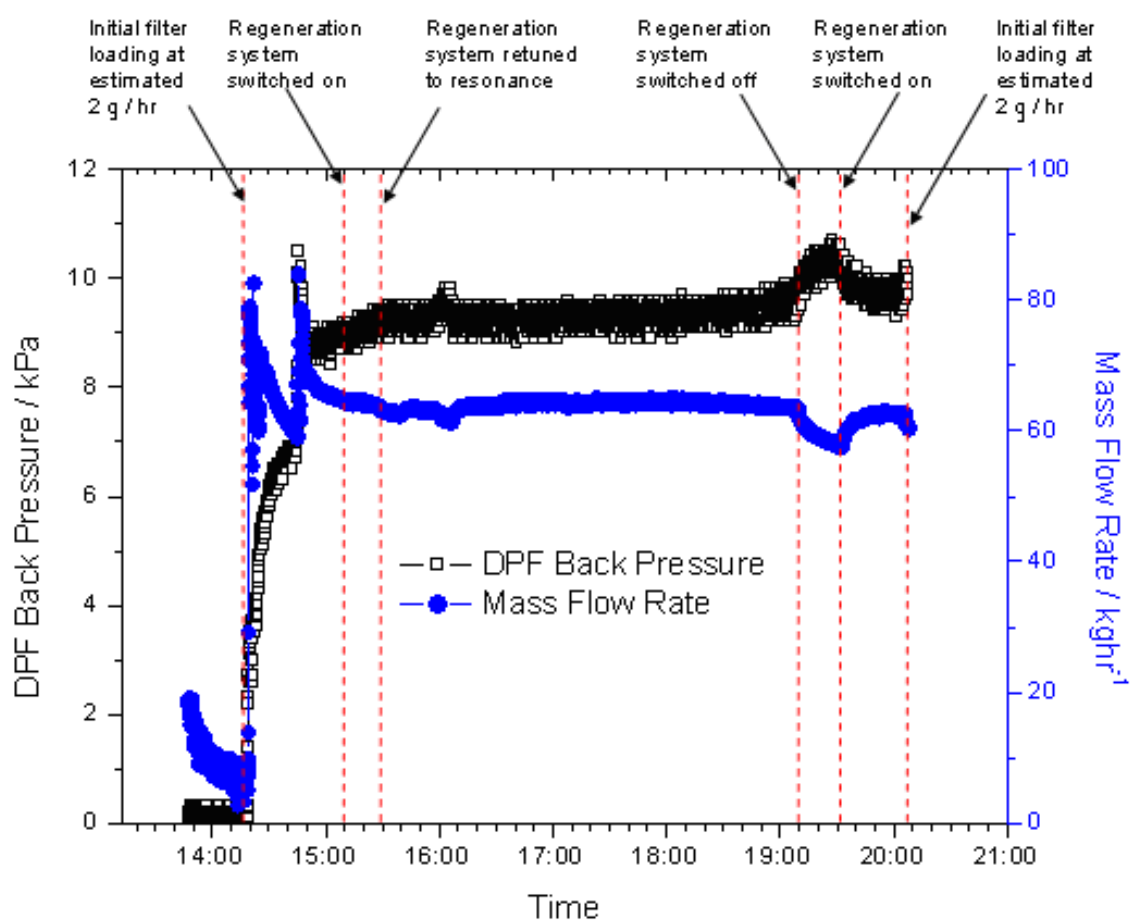
Figure 5.16 Back pressure and flow rate versus time for engine test

The system regeneration rate successfully met the engine soot output although several potential difficulties were identified with the system. One of the key observations was the change in resonant frequency during the initial loading of the filter. The resonant frequency was measured and set during the first part of the loading and was therefore suitable for a clean filter. After the filter was loaded with soot the capacitance of the electrodes increased due to the effect of adding

conductive material (PM) between the electrodes. This increase in capacitance decreases the resonant frequency of the transformers and hence de-tuned the power supply. The power supply was not in tune at the start of the test and this resulted in a short period of inactivity at the start of the test (between times 15:10 and 15:30 in Figure 5.16). This explains why the back-pressure did not begin to level out until the power supply was retuned. The effect of electrode capacitance is investigated more thoroughly in the next section.

Other disadvantages of the system include the difficulty of assembling the electrode arrangement and maintaining a separation between all the electrode wires (to prevent short circuits). The number of electrodes required for the checkerboard array makes all stages of assembly difficult and may have implications on filter durability. The number of HV wires from the power supplies was also a concern. Although the wires may only carry a few tens of milliamps, the insulation required for the high voltage is bulky. A full sized filter would require hundreds of bulky insulated wires and passing these into the exhaust can would be difficult. A simpler electrode arrangement using fewer HV wires would be easier to manufacture and cheaper. Testing has already shown that the checkerboard array has a low rate of regeneration and effectiveness (g.kWh^{-1}), its key advantage is its ability to clean the filter volume evenly. Wider spaced electrode geometries would give better performance and would be easier to assemble. For this reason, the research focussed on finding a more attractive implementation of Autoselective technology after this engine test.

5.8 Electrode Capacitance

The change in resonant frequency during engine testing of the regeneration system suggested that the capacitance of the electrode arrays changed with loading. This is probably due to the addition of PM between the electrodes which is partially conductive. The change in resonant frequency was responsible for the initial failure of the system to reduce the back-pressure. This is because the power supply topology used in the engine trial relied on resonance to achieve breakdown. A test was conducted to measure the effect of loading on filter capacitance. A single unit of the

checkerboard electrode array was used in conjunction with a capacitance meter; see Figure 5.17. The filter was loaded at a steady rate over three hours and the capacitance recorded at intervals.
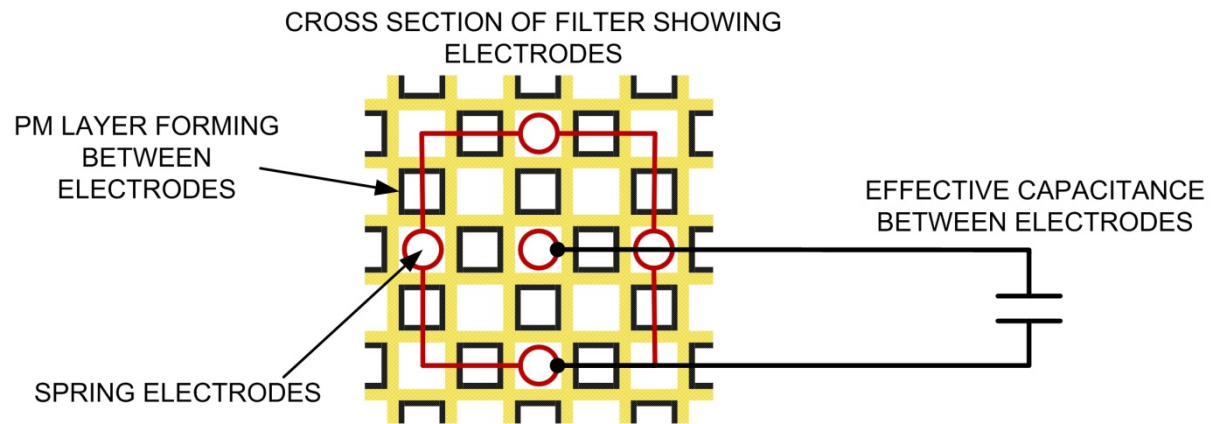
Figure 5.17 Experimental setup used for the capacitance versus loading test

The graph in Figure 5.18 shows the relation of estimated loading to electrode capacitance. The estimate of the filter loading assumed a steady loading rate throughout the test. This is not entirely true in practice, however, since the increasing filter back-pressure causes a slight increase in engine soot output. This means that early loading predictions are likely to overestimate the actual loading slightly.
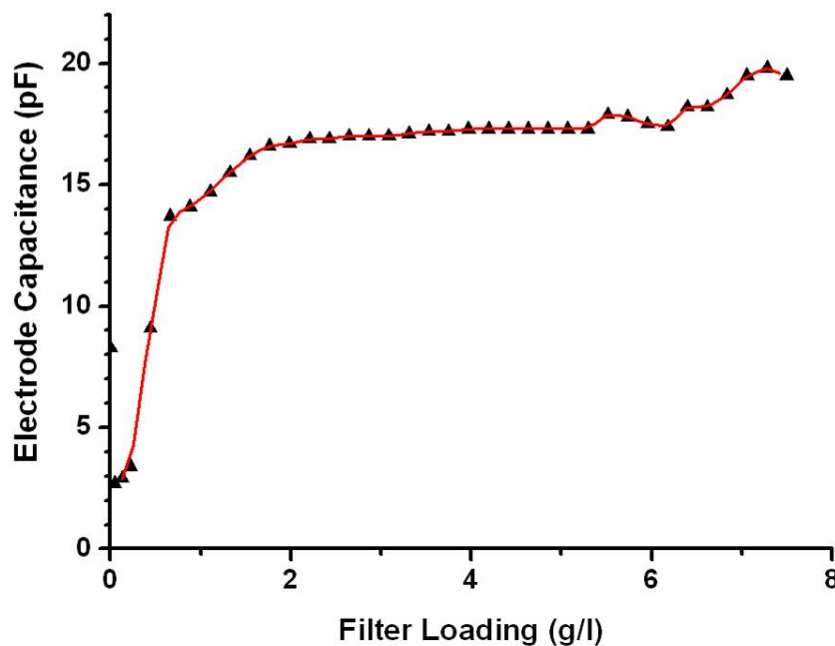
Figure 5.18 Electrode capacitance versus filter loading for a close spaced electrode array and a 5.66" diameter cordierite wall flow filter

The results show that there is an initial increase in capacitance as the filter loads. This initial increase then decays to a more gradual change in filter capacitance. The initial rapid change in filter capacitance is due to the deep bed filtration of the filter. It is known that the filter dielectric constant increases with the addition of soot to the porous ceramic walls (Moon *et al*, 1999). The soot deposited on the channel walls has an equally important effect since it forms a short path for charge transfer due to its relatively high conductivity. PM is deposited on the channel walls after the deep bed filtration layer forms and once a contiguous layer of PM exists on the walls the capacitance reaches a relatively steady value. Further increases in loading only increase the thickness and hence conductivity of the caked layer and have a low effect on capacitance. This means that after the initial change in resonant frequency, the power supplies are unlikely to be further affected by changes in loading. In conclusion, the effect of changes in capacitance will be most noticeable when a clean filter is loaded for the first time. A self tuning power supply would be useful to overcome this problem, although it may be possible to operate reliably without this feature.

5.9 Linear Electrode Optimisation

The main problem with the linear electrode arrangement was the poor regeneration distribution. In flow-rig trials, the conventional resonant power supply was used with the damage free settings found earlier in this part of the research and it was observed that no regeneration took place. The measurements taken concluded that the linear electrode breakdown voltage was higher than the maximum electrode voltage. If the power supply output was increased to compensate for this, the measured resulting current was above 15 mA and filter damage was observed. The problem was that the transformer drive level required for breakdown resulted in currents that caused immediate melting damage.

A power supply was designed that could alter the transformer drive level very rapidly. This was used to allow operation at two different amplitudes for breakdown and steady-state. The new power supply was called the 'transient power supply'. The

most reliable setting to cause breakdown was a 100 % transformer drive level and operation at 10 mA corresponded to ~30% amplitude drive. The breakdown transformer drive level needed to last at least 10 cycles at the resonant frequency (i.e. 0.5 ms at 20 kHz). The power supply was tested with these settings and damage free operation was found to be possible with channel spacings up to a maximum of 10 whilst still achieving the required breakdown voltage.

Although the power supply could break down 10 channels without causing damage, it was found to be difficult to achieve the breakdown to glow transition. The discharge was observed to immediately extinguish if the channel spacing was above 4. This would result in poor regeneration performance (< 0.1 $g.h^{-1}$) because the off-time was effectively increased. The channel spacing was reduced to 3 and a second breakdown amplitude pulse was added to the waveform after 20 ms to re-start the discharge if it had extinguished. More re-start pulses would have been possible although this would have resulted in significantly more blow-off and blow-through (this is detailed in Chapter 7). The research had shown that the electrode channel spacing needed to be 6 or more. The electrode spacing of 3 would be expected to produce approximately 50% the rate and effectiveness as a spacing of 6. However, the performance would still be around twice that of the checkerboard arrangement.

The new power supply also added the ability to change the frequency from cycle to cycle and this was used to implement a frequency sweep. The frequency sweep ensured that the transformer always operated at resonance for a short time (i.e. 10 cycles) such that breakdown occurred. After breakdown, the frequency of operation was not as important since the glow discharge over-damped the resonance of the transformers. Testing confirmed that a stable glow discharge could be sustained over a wide range of frequencies using the transient power supply.

Testing using a single electrode with the new power supply in a flow-rig revealed good regeneration distribution. The discharge was observed to start at the ends of the electrode row and gradually move towards the middle. This was in contrast to the measured and observed results from flow-rig and engine tests using the fixed amplitude power supply. It was concluded that some of the previously observed poor

regeneration distribution was as a result of the filter being damaged. Damaged parts of the filter encourage the discharge to continue to pass through them resulting in poor auto-selectivity. The distribution had been improved by alleviating filter damage using the new power supply and settings.

Testing multiple electrodes in the same arrangement led to the observation of inter-electrode discharges. The discharges between the high voltage electrodes would also be a likely source of poor auto-selectivity. The electrodes were moved apart until the inter-electrode discharges stopped. The electrodes were 10 channels apart which resulted in large areas remaining un-regenerated. To solve this issue, the high voltage electrode clusters were arranged into banks and powered separately so that adjacent electrode clusters were never powered simultaneously, this was known as phasing the high voltage electrodes. The result was that the high voltage electrodes could now be placed 5 channels apart which gave better regeneration distribution. The final combination of multiple wide spaced linear electrodes, phased electrode banks and the transient power supply were tested in the flow-rig to determine the final regeneration distribution. Figure 5.19 shows the flow map after this test compared to a previous linear electrode (Proctor, 2007) test, a significant improvement on regeneration distribution was observed.
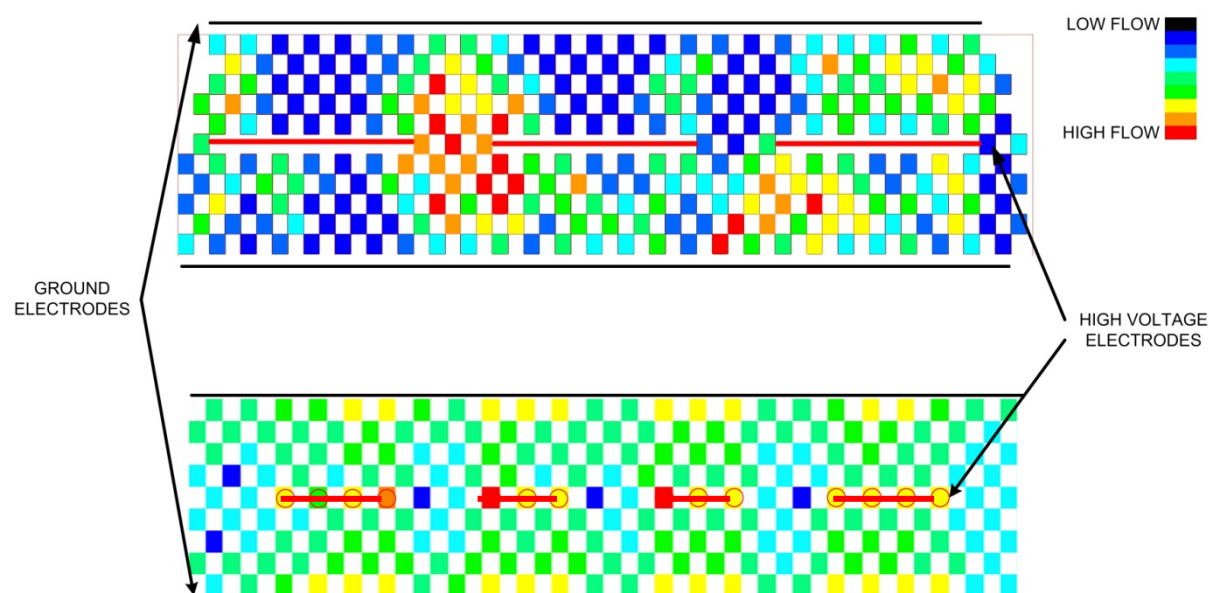

Figure 5.19 Linear electrode flow map comparison. (Top) Results from original power supply and simple modulation. (Bottom) New transient power supply and advanced modulation settings

The flow-rig results were promising and showed excellent regeneration distribution and uniformity. The regeneration performance and system complexity had also been significantly improved. A transient power supply with 20 high voltage outputs was constructed capable of regenerating a full filter and the new settings were moved to the engine test rig for on-engine testing. The final results and conclusions are detailed in Chapter 8.

5.10 Chapter Summary

In summary, the effect of current and frequency was tested on a 100 cpsi (cells per square inch) cordierite wall flow filter. A new electrode geometry was designed that allowed the full filter to be regenerated. A successful continuous regeneration was achieved and a steady back-pressure trace confirms that the system was able to keep up with the engine PM output. The system complexity was significantly increased in order to ensure that the whole filter was regenerated evenly.

The research then showed that performance could be enhanced by using wider electrode spacing which also reduced system complexity. In order to take advantage of this, the research continued with the aim of improving the linear electrode arrangement. The previous problems encountered were identified and solved. A combination of a novel power supply, phased high voltage electrodes and an optimised electrode arrangement led to a successful flow-rig test. A scaled up power supply was made to allow a full filter engine test. The new power supply used the newly developed transient amplitude control, frequency sweeping and two phase operation. The engine test is documented in Chapter 8.

It was shown that further research was needed to obtain a better understanding of the discharge regeneration and damage process. Knowledge of how the electrical power is delivered by the discharge could be used to reduce the risk of filter damage. Further work on how the filter was damaged by the discharge was carried out and is presented in the next chapter.

6. Discharge Energy Balance and Filter Damage

Autoselective regeneration was observed to cause filter damage if the discharge was operated continuously for more than 100 ms even at current levels as low as 10 mA. It was necessary to prevent filter damage since damage accumulation over time would result in poor particulate filtration and filter failure. A detailed understanding of the filter damage mechanism would be useful for predicting the effect of variables such as gas temperature, filter material, filter wall thickness and discharge current. This chapter describes the investigation of the discharge energy balance and the filter damage process. A simplified filter damage model is described and simulated using advanced software, model validation was carried out using damaged filter samples. The modelling aspect focuses on the energy balance of the discharge and the effect of changing the filter material. The next section characterises the types of filter damage.

6.1 Types of Filter Damage

There are several distinct damage types that are observed when sections of wall flow filter are looked at in detail. This section aims to categorise the observed damage to remove any ambiguity in the results presented later in this chapter. Figure 6.1 is a series of microscope images of the surfaces of filters; Figure 6.1 (c), (d) and (e) are of filter damage caused by the discharge and Figure 6.1 (a) and (b) are of undamaged filter.
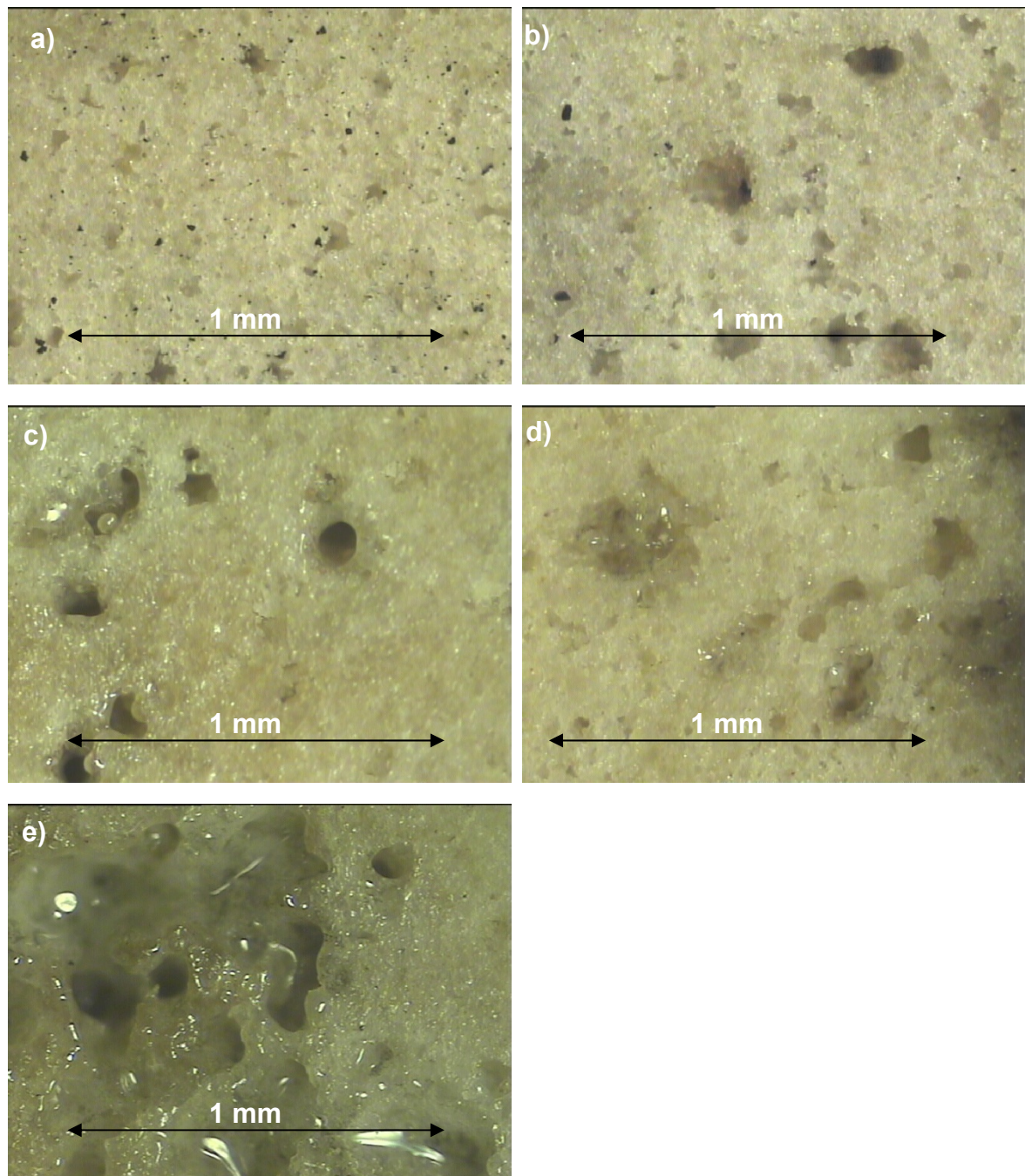
Figure 6.1 Types of filter damage

Figure 6.1 (a) shows a section of clean wall flow filter surface, the surface is porous with a highly disordered and random appearance. Figure 6.1 (b) is a naturally occurring oversized pore which intersects the filter surface creating the appearance of a hole. Observations show that occasionally areas of the WFFs have regions of higher average pore size, presumably from the manufacturing process. In some cases the pores may span the filter wall leading to a hole. This damage is was

termed 'ambient pitting' and 'ambient holes' and can be distinguished from discharge damage by the jagged edges to the holes. Ambient holes of around 150 μm were commonly observed in unused wall flow filters.

Figure 6.1 (c) shows pin hole damage caused by the discharge. This damage occurs when the discharge is operated at high currents well outside the operating area defined in Chapter 5. The occurrence of pin holes is normally associated with moderate to high flow rates (> 50 kg.hr^{-1} for a 5.66" diameter filter). A pin hole is characterised by a round hole through the filter wall encircled by a region of melted ceramic. During tests, it was observed that a pin hole could develop from an ambient hole whilst operating within the normal operating region. Once formed, these holes are indistinguishable from a pin hole formed by excessive heating by the discharge. In general, a pin hole surrounded by oversized pores is likely to have developed from ambient damage.

Figure 6.1 (d) shows surface pitting characterised by the areas of fused (melted) ceramic on the surface. This is a precursor to filter damage and does not alter the filter performance as measured during on-engine tests. Small regions of surface pitting have always been observed after Autoselective regeneration and are likely to be a result of weaknesses in the highly disordered filter surface. If the discharge power (or on-time) is increased further, the ceramic melts and fuses closing its porosity. This is known as glassing and can be severe as shown in Figure 6.1 (e). Glassing closes the pores of the filter increasing filter back-pressure and is usually accompanied by pin holes when flow is present.

6.2 The Need for a Heat Transfer Model

The process by which these types of filter damage occurred was not fully understood. Observations of discharge types, electrode root structures and damage modes have shown that the heat transfer from the discharge to the soot and ceramic is complex and transient. The use of on- and off-times to modulate the power input from the discharge has solved the problems of filter damage but also reduced the regeneration rate leading to the need for more discharges and electrodes. An

understanding of the way in which the filter is damaged may enable better regeneration performance which would allow the complexity of the system to be reduced. A clear understanding of the heat flows within the filter wall cross section will also help to predict the effect of filter parameters such as filter wall thickness and material. Future WFF materials could also be compared to cordierite without the need for lengthy tests.

6.3 Initial Modelling Considerations and Simplifications

The complexities of conventional discharge physics do not provide a useful platform for thermal analysis due to the way heat can be described in several ways such as 'rotational temperature' and 'electron temperature'. Simplifications could be made if the discharge could be treated as a simple Joule heat source.

Chapter 3 discusses the electrical properties of the discharge and has shown that, at the discharge frequency (~ 20 kHz), the discharge is a resistive electrical load. This makes the power consumption of the discharge equal to the product of the current and voltage. However, all possible routes of energy flux had to be considered before treating the discharge electrical power as a heat flux.

Nozaki (2001) showed the total electromagnetic radiation from the discharge column to be negligible since it accounts for less than 1% of the total energy flux emitted from the discharge (supported by visual observations, see Figure 6.2). Proctor (2007) showed that the composition of the gas leaving the discharge had low levels (several parts per million) of NO_x and ozone, the enthalpy change for the formation of these species is also negligible in these volumes. The electrical energy into the discharge is therefore an accurate measure of the heat released to the surrounding air. In the modelling described in this chapter, the air in the discharge column was treated as a resistor within which Joule heating occurred with an equal value to the electrical power consumption of the discharge.
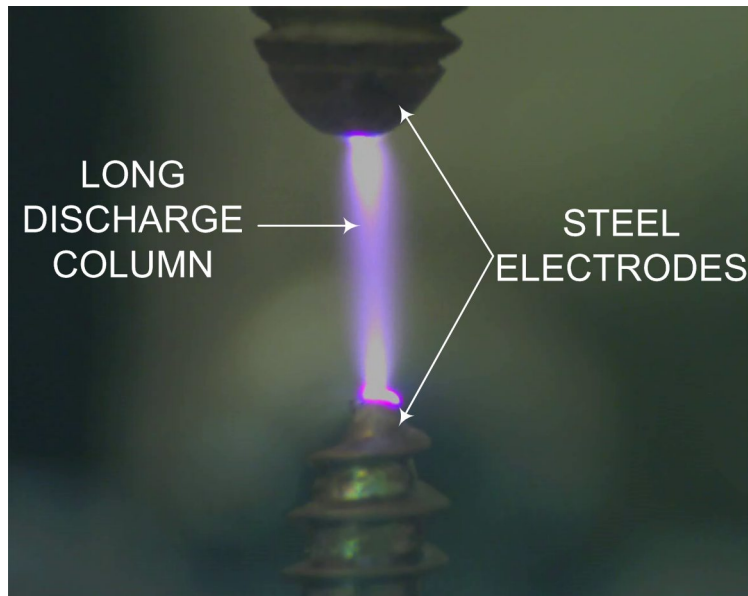
Figure 6.2 A 10 mA atmospheric glow discharge between steel electrodes consuming ~ 10 W of electrical power and producing little visible radiation

Further assumptions can be made if axial flows within and around the column are negligible. Without axial flow, the discharge can be modelled as a uniform resistor along which the heat release of each segment is equal to the product of the voltage across it and the current through it. A diagram of the heat flows within the discharge is shown in Figure 6.3; The effects of conduction at the electrode boundaries make the assumptions less valid due to the significant axial heat flow into the cooler electrodes in these regions, however, for a long discharge the assumptions are valid for regions far from the electrodes.

Figure 6.3 The heat flows from the glow discharge and electrical circuit
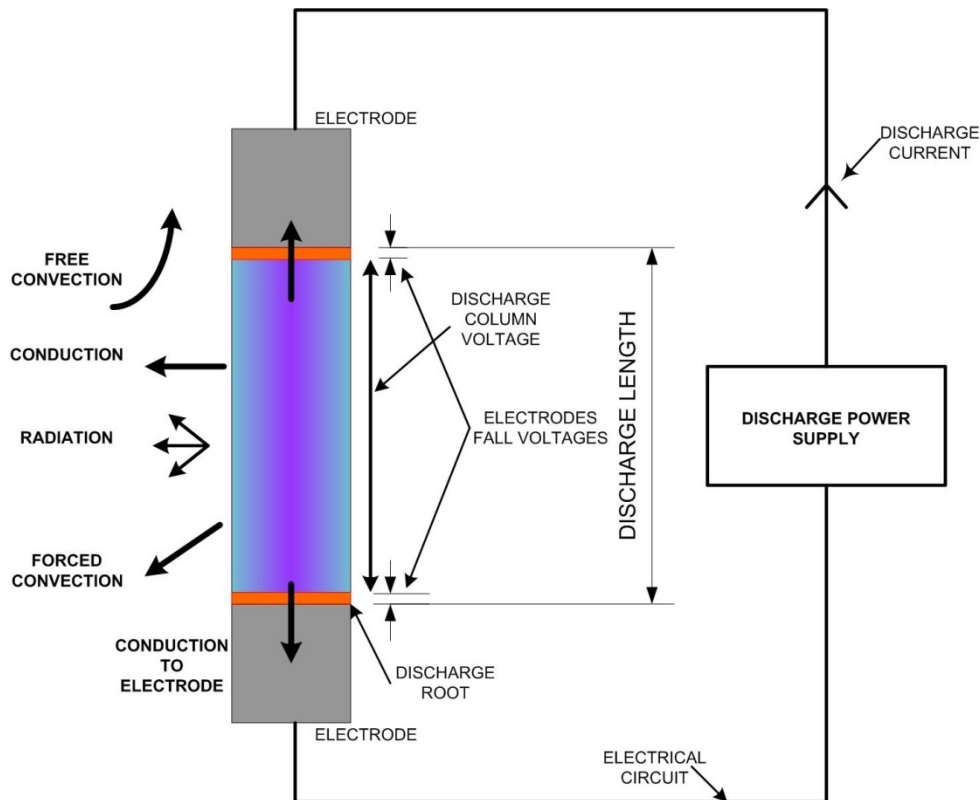
6.4 Electrode Root Considerations

The electrode roots are the regions where the energetic particles that carry the current in the discharge column are decelerated as they enter the electrode. Heat transfer takes place at the electrodes in different ways at the anode and cathode. Ion bombardment occurs mainly at the cathode and electron recombination at the anode. These collisions cause the electrical energy to be transferred to the electrode. In the case of ions that have collided with the cathode, their charge is equalised by electron transfer as they reach the electrode surface. This results in additional energy release from the ion as it returns to its ground state. At the anode, electrical energy is exchanged by electrons through collisions with the electrode surface. The electrode roots and their associated complexity are decoupled from the thermal model by placing the electrodes spatially distant from the test sample. Their contribution to the heating of the test sample is minimised, although the energy consumed by the electrode roots must be accounted for when determining the overall energy balance

of the model. This following section presents the way in which the electrode roots were accounted for in the model.

The electrode roots have several defined and well documented structures (Roth, 1995) which result from the behaviour of ions and electrons close to the electrode surfaces. At atmospheric pressure these structures become confined into a region less than 0.3 mm from the electrode surface with the remainder of the discharge being formed by the positive column structure. The discharge used in the model is alternating current which removes the asymmetry from the electrode root structures seen at DC, as illustrated in Figure 6.4 .
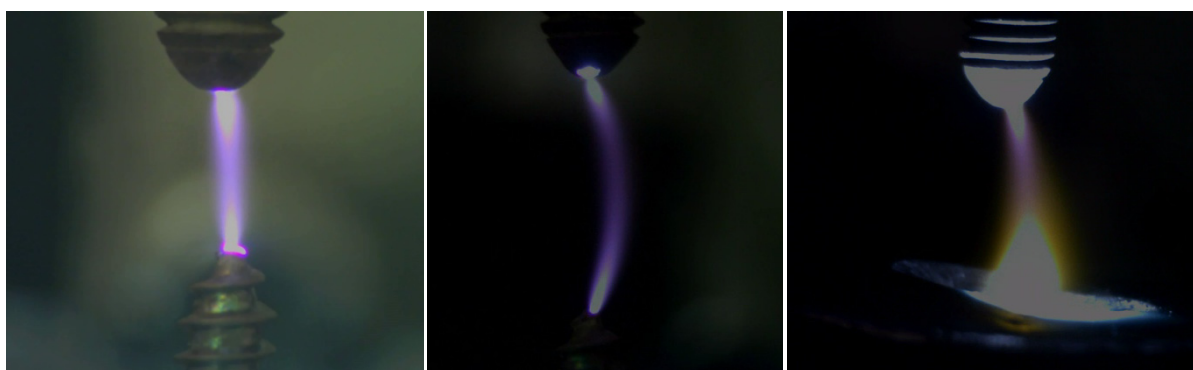

Figure 6.4 Glow discharge modes, *left to right:* 10 mA symmetrical AC, 10 mA DC, 10 mA AC discharging to a carbon black sample

The discharge was observed to form an electrode root on the surface of the particulate layer during regeneration. This root is more complex than the root formed on the metal electrodes since additional heat is released by the oxidising carbon. The electrode roots appearance is that of an intensely bright spot on the surface of the carbon as illustrated in Figure 6.4 (far right image). This suggests that the surface of the carbon is well above the threshold for thermionic electron emission of around 1000 K. The release of electrons from the carbon surface affects the discharge root energy balance and alters the electrode root structure. The thermionic electrode root on the PM surface behaves like an arc root structure leading to a wider discharge column. A hybrid discharge was observed, which has an arc discharge root on the particulate and a glow discharge root on the electrode. The unknown behaviour of this type of hybrid discharge made accurate modelling more challenging. A

steady-state condition energy balance was measured and is described in the following sections, however, the transient modelling of this system proved to be inaccurate due to the simplifications used. The reason for the inaccuracy was probably due to the large axial gas flow away from the oxidising PM.

6.4.1 Determining the Heat Output from the Discharge Root

The discharge roots are known to remain constant in size and structure as the discharge length changes. The roots have been observed to be approximately 0.1 mm to 0.25 mm in length. The discharge voltage increased linearly with length for long discharges and the electrode structures have a constant voltage irrespective of the length (for discharge lengths greater than the electrode root structures) known as the electrode fall voltage. It is possible to find the fall voltage by plotting the discharge voltage against the discharge length; extrapolating the relationship to give a 'zero length' value gives a good approximation of the electrode fall voltages and hence the power consumption at the electrodes. For discharges with different electrode materials and structures at each root, the fall voltage can be calculated using a reference electrode material for one electrode. This method was used to find the electrode fall voltages for a carbon black sample and a steel electrode, the results are shown in Figure 6.5 for different discharge currents.
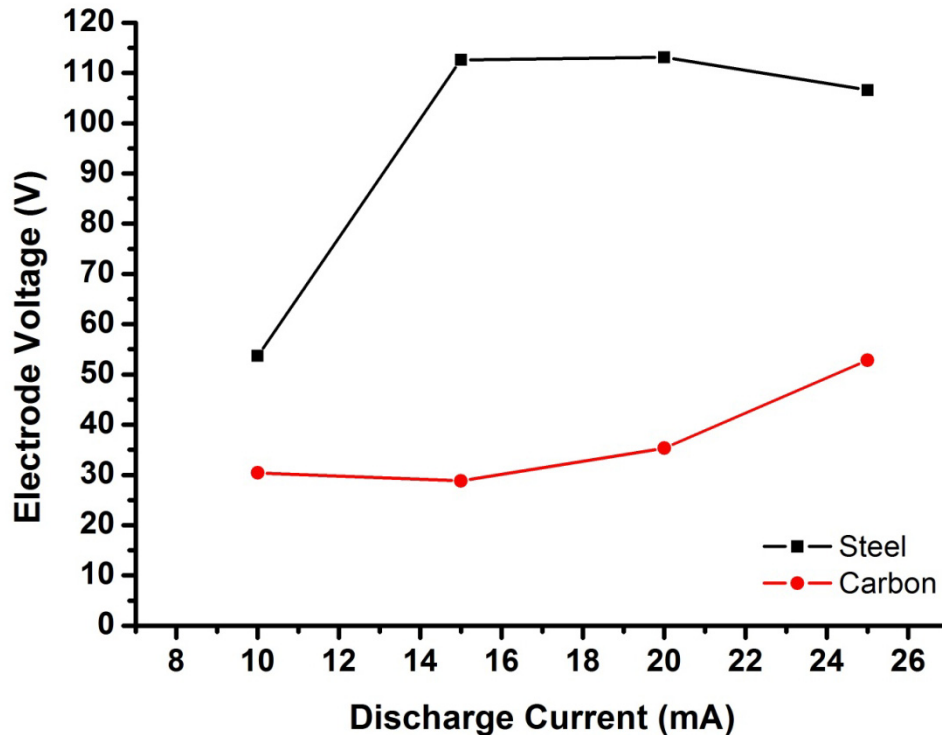
Figure 6.5 Graph of electrode fall voltage (rms) versus current

The results show that the carbon electrode root consumed significantly less power (~ 25 %) than the steel electrode. The heat output of the oxidising soot was calculated and compared to the electrode power consumption in the next section.

6.5 The Steady-State Energy Balance

This section describes a series of experiments designed to obtain data to allow a steady-state thermal model to be constructed. The electrode fall voltage is also included in the model to provide a far better understanding of the heat flows from the discharge during regeneration.

6.5.1 Determining the Heat Output from the Discharge Column

The discharge voltage was measured at different electrode spacings and currents. The change in discharge voltage allowed the power input per unit length to be calculated. The value remained constant to electrode separations of 0.7 mm

indicating that the 'long discharge' assumptions described in the previous section were valid. The experimental results are shown in Figure 6.6.
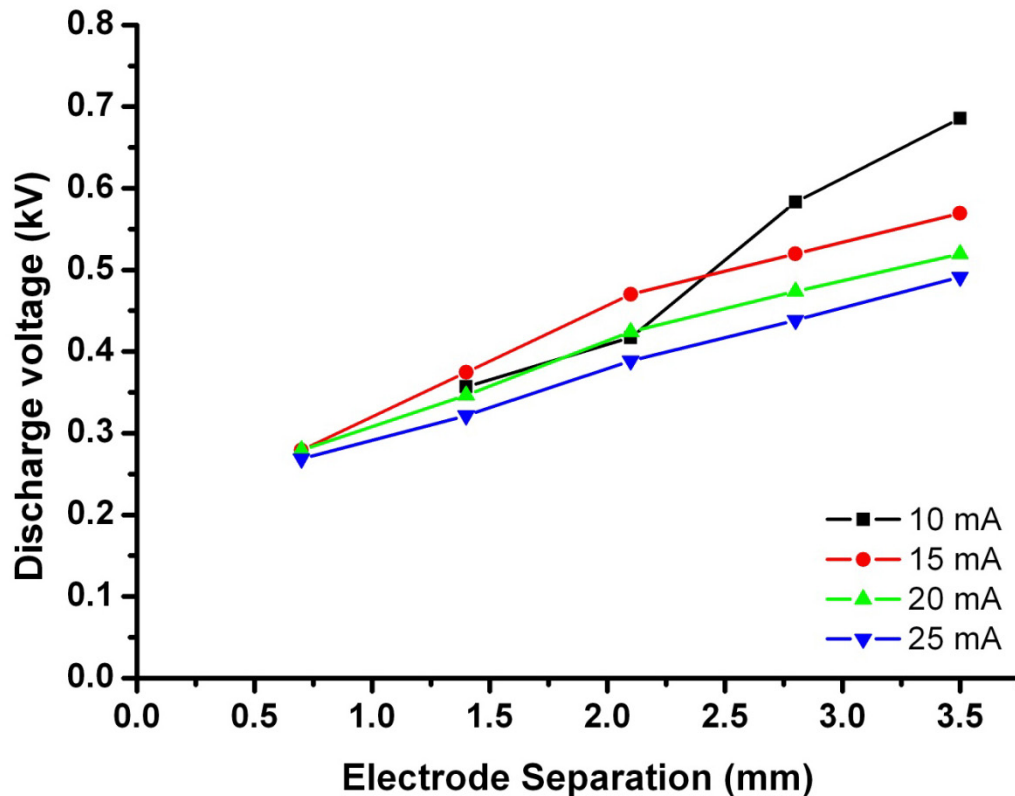
Figure 6.6 Graph of steady state discharge voltage (rms) versus length

6.5.2 Heat Generated by Soot Oxidation

The results obtained in Chapter 4 show the oxidation rate of the soot in grams per hour for a range of discharge currents. These results can be converted into the energy output from soot oxidation by choosing a suitable value for the heating value of PM and by making some assumptions. The main assumption is that the soot is fully oxidised and that no partially oxidised products are left. This was shown to be a reasonable assumption based on the work by Proctor (2007). The heating value of soot will be an approximation since the exact composition of the soot depends upon the operating point of the engine and the storage method of the collected soot. A heating value of 32.8 MJ.kg^{-1} was used for the calculations here after Law (2004). Table 6.1 shows a comparison of typical heating values for some substances.

Substance	Heating Value MJ.kg^{-1}
Diesel soot (Law, 2004)	32.8
Diesel	44.8
Carbon graphite	32.8
Coal (Anthracite)	29.6

Table 6.1 Heating value comparison

Figure 6.7 shows the value of heat output for a range of input currents as calculated from the heating value from the soot. A combined thermal energy balance model can now be constructed from the measured values for soot oxidation heat output, discharge column energy input and electrode fall voltage power consumption .
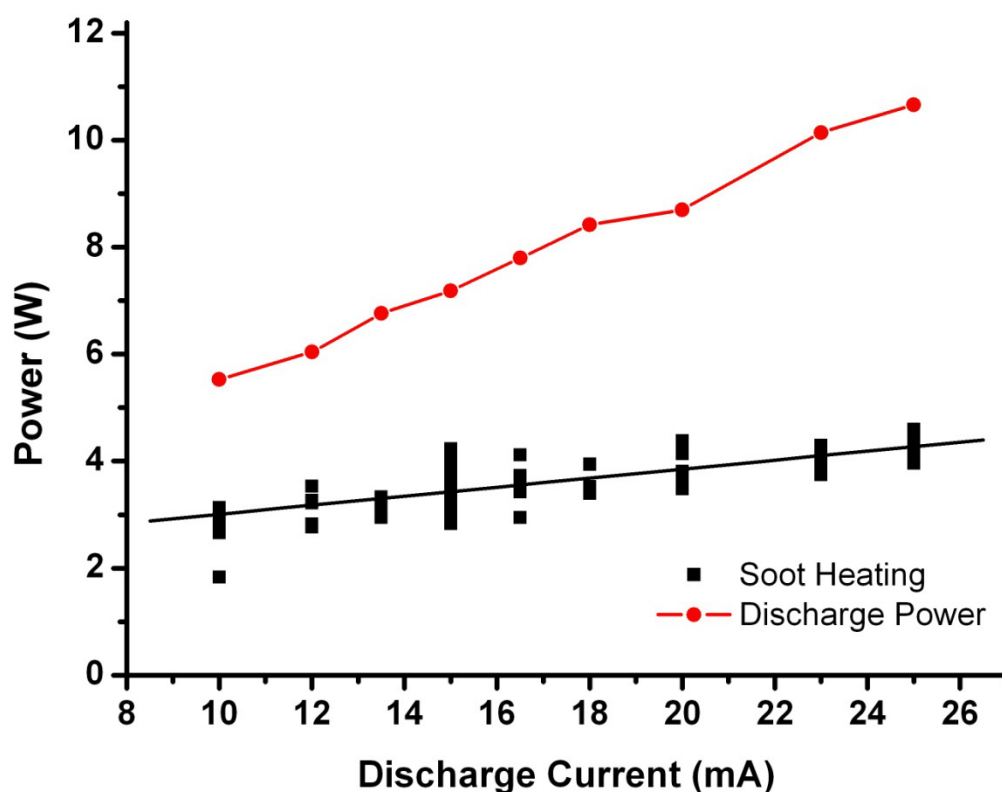

Figure 6.7 Graph of heat release from soot oxidation versus discharge current and power (using carbon black sample, electrode separation of 3.5 mm)

6.5.3 Steady-State Energy Balance of Regenerating PM

The steady-state energy balance of the discharge oxidising carbon black for a range of currents is shown in Figure 6.8. The results show that the discharge and electrode consumes more power as the discharge current increases. In contrast, the carbon black electrode consumes little of the electrical energy and the soot oxidation rate increases only slightly at elevated currents. The results agree with the data presented in Chapter 4 where the effectiveness ($g.kW.hr^{-1}$) was observed to decrease with increasing current.
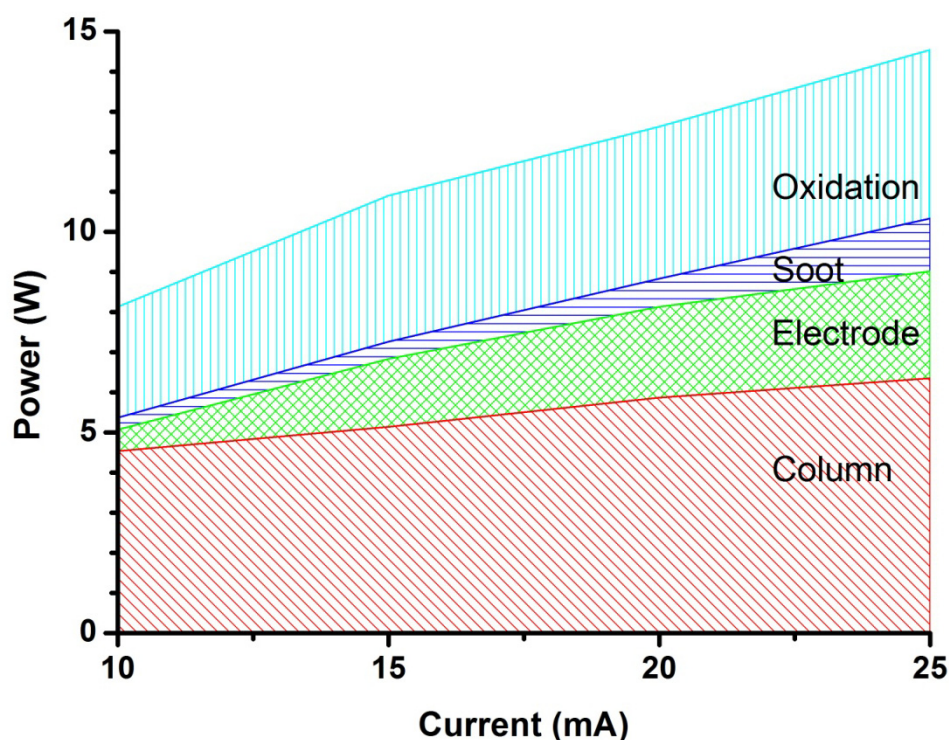
Figure 6.8 Graph of steady-state energy balance versus discharge current showing electrical demands of the discharge components and heat release from the oxidising PM

We can conclude that most of the electrical energy is used to heat the steel electrode and surrounding gas. The heat delivered to the electrode is certainly wasted and it is expected that significant improvements can be made by choosing electrodes with lower losses. The heating of the gas above the PM layer is likely to be essential for the regeneration process and can not strictly be counted as a loss. Of particular interest is the large difference between the PM oxidation heat output and the PM electrode root energy consumption (i.e. ~ 4 times the energy consumed by the

discharge root is released as heat output from the burning PM). This is likely to be responsible for the apparent high effectiveness with which the glow discharge oxidises soot.

6.6 Transient Heat Flows in the Filter Wall

The energy balance from the previous section is useful, however, it can not be used to model the transient heat delivered to the filter and the filter damage process. A transient analysis of the discharge power was carried out using the same equipment as the steady-state analysis and the digital oscilloscope was reconfigured to capture data over the 1 second tests within which time the filter was known to be damaged.

Because of the oscilloscope memory limitations the whole transient event could not be captured at sufficient resolution to guarantee that aliasing of the samples had not occurred. The oscilloscope was configured to sample at high resolution and multiply the voltage and current measures but only record a running total of the total energy delivered. This was later differentiated to give an accurate measure of the power input versus time. It should be noted that more information about the electrical load presented by the discharge during the damage process could have been useful for detecting the damage threshold and understanding the damage process. However, the current and voltage waveforms would have needed to be captured at a sample rate greater than ~ 10 times the discharge frequency for the whole 1 second test which was not possible using the available equipment. It would be expected that the discharge waveforms would have changed during the damage process and the electrical properties of the discharge through-filter section would have altered significantly as the filter melted.

The transient test was performed 10 times for each of the following cases:

I.   7 g.litre^{-1} loaded filter section
II. 3 g.litre^{-1} loaded filter section
III. Clean filter section
IV. No filter section (i.e. pin to pin discharge only)

The no-filter case was used to calculate the power consumed by the filter section by subtracting it from the other waveforms. A schematic of the test is shown in Figure 6.9.
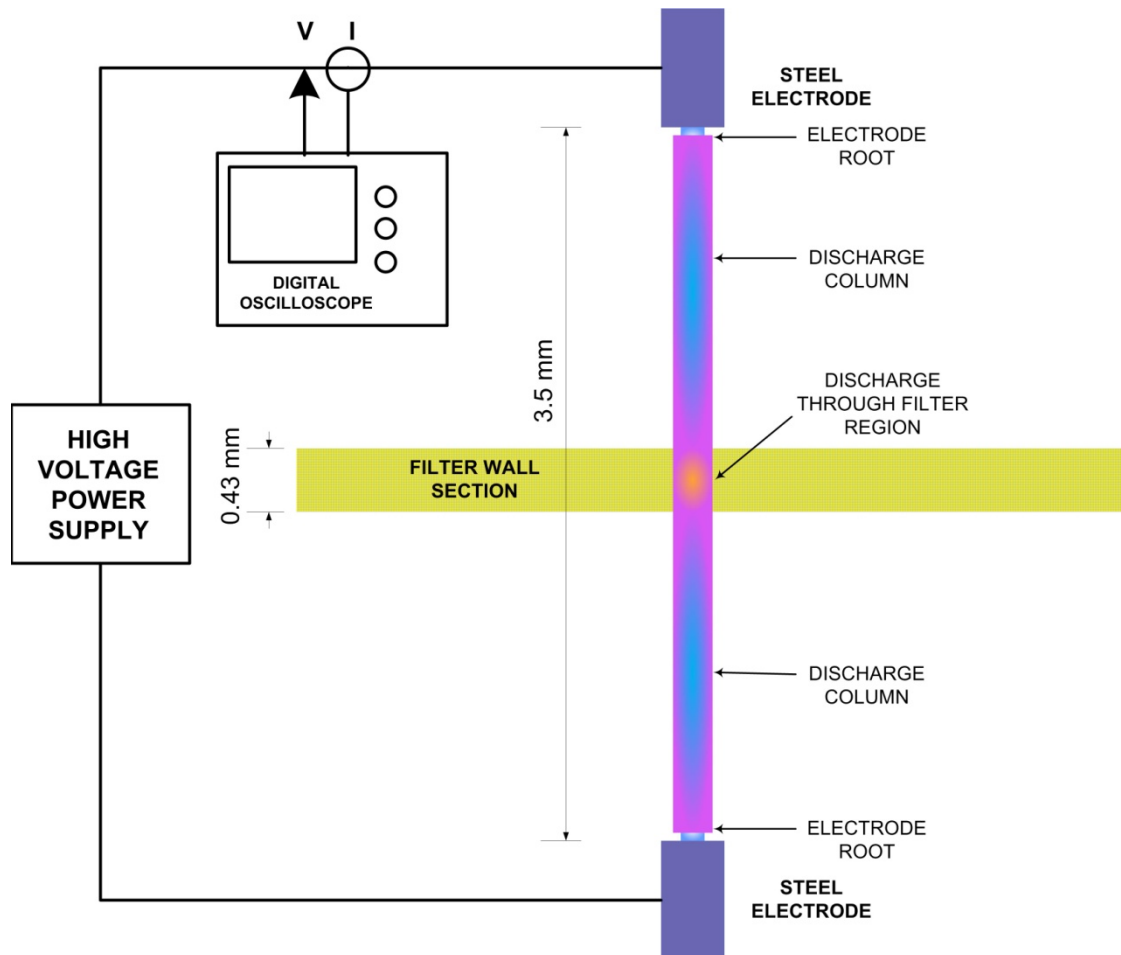
Figure 6.9 Transient analysis experimental setup

6.6.1 Transient Model Assumptions

The heat flows into the filter were calculated from the experimental data using several assumptions discussed in this section. The main simplification was that the discharge was a uniform heat source, i.e:

$$Q = Q_{total} \cdot \frac{dl}{l_{total}}$$

Equation 6.1

where Q is the heat produced by a short length, dl, of the discharge and Q_{total} and l_{total} are the total heat output and discharge length respectively. A further assumption was

that the total heating term was the product of the discharge column voltage and current product, i.e

$$Q = I \cdot (V_{dis} - V_{elect}) \cdot \frac{dl}{l_{total}}$$
Equation 6.2

where I is the discharge current, V_{dis} is the discharge voltage, V_{elec} is the combined electrode fall voltages. Equation 6.2 was used to calculate the heat flux level into the air above the filter in the subsequent model.

This relationship was also used to calculate the heat release within the through-filter section of the discharge as follows. The heat input of the length for the discharge corresponding to the filter thickness (0.43 mm) was subtracted from the difference between the transient power input results to obtain the heat flux released inside the 'through-filter' region of the discharge, i.e:

$$Q_{filter} = P_{filter} - P_{nofilter} - (P_{nofilter} \cdot \frac{l_{filter}}{l_{total}})$$
Equation 6.3

where Q_{filter} is the heat flux released inside the filter section, P_{filter} is the total power consumption of the discharge passing through the filter section, $P_{nofilter}$ is the total power consumption with the filter removed (no filter case) and l_{filter} is the filter thickness.

The Q_{filter} approximation in Equation 6.3 does not account for heat flux into the filter from the discharge above the filter. The actual heat flow into the through-filter region requires modelling and this is presented in section 6.7.

6.6.2 Transient Results

After processing the data from the oscilloscope, the transient discharge power (Q_{total}) could be plotted as shown in Figure 6.10. Anomalous results were observed for the PM loaded filter sections after calculating the heat flux into the through-filter region of the discharge as described in Section 6.6.1. The initial power consumption of the 3 g.litre^{-1} sample actually corresponds to zero or negative heat flux release in the filter. The power drop was more likely to be due to the lowering of the overall discharge column voltage due to oxidising PM entering the plasma above the filter

and increasing the conductivity of the whole column by thermionic electron emission. The loaded filter samples were not considered further because of the effects of the soot on the discharge and because the significant axial flow from the oxidation products makes the modelling approximations invalid; Subsequent modelling used only clean filter samples.
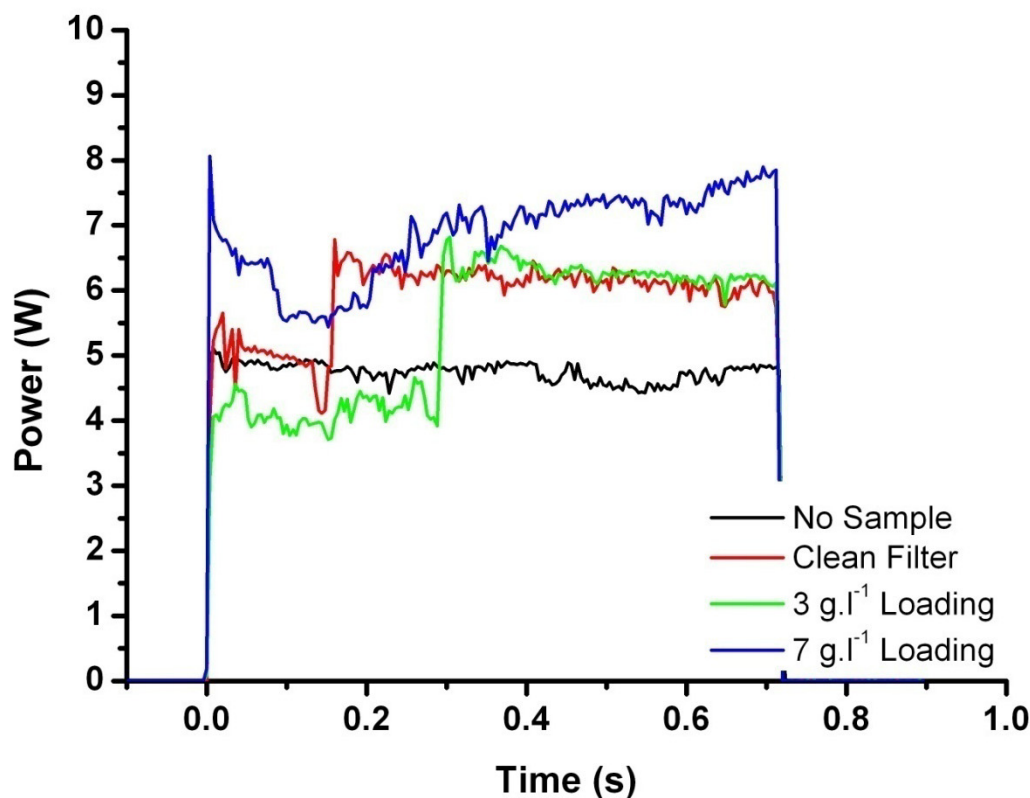
Figure 6.10 Typical power input versus time (after breakdown) for various filter samples at 10 mA

6.6.3 Summary

The transient energy consumption of the discharge was measured for several filter samples over a time period sufficient to result in filter damage. The heat flux into the regions of the discharge above, below and within the filter were calculated by making reasonable assumptions about the discharge structures. The heat flux values will be used in the next section to create a transient model of filter damage for the clean filter sample.

6.7 Transient Modelling of Filter Damage

This section uses the results collected in Section 6.6 to construct a filter damage model using a finite element analysis computer simulation (COMSOL Multi-physics 3.4). The model is based on the experimental setup used for the transient tests. Validation of the model used samples of filter damaged by the discharge over known time periods.

6.7.1 Damage Modelling Simplifications

This sub-section explains the simplifications and assumptions used to create the model. The modelling program, COMSOL 3.4, has a dedicated heat transfer problem solver taking into account a variety of conditions such as flow, conduction, convection and changes in density. The program has been used in the same way as described here to accurately model systems of extreme heat transients and thermal gradients whilst maintaining accurate predictions of gas flow and heat transfer. Bauchire (2009) used the same simulation modules to predict the density changes in a welding arc plasma showing its applicability to the extreme temperatures and thermal gradients present in the damage test. The limitation of the model used is encountered when the flow velocities approach a mach number of one (Alshayji, 2009) which was a condition that was not experienced during the simulations. The main sources of error in the modelling work are from the assumptions listed in this section and Section 6.6.

Free convective flow was not modelled for the model validation tests, this also added another axis of symmetry. Forced convection from the expanding air was still modelled, however, model predictions suggest it had little effect on the filter damage process. A simulation was performed to assess the effect of excluding free convection, this is covered later.

Radiation from the discharge column was shown by Nozaki (2001) to be < 1% of the electrical power consumption. However, the radiation from the through-filter section was likely to be responsible for a proportion of the heat transferred from the filter. If the region was assumed to be a black body radiation source at the filter melting point (and no heat was reflected or emitted back) then the radiated heat flux can be shown

to be ~0.4 W which is up to 50% of the calculated heat release in the filter. In reality, the radiated flux would be much lower, however, the over prediction of the melted region in the simulations presented later in this section could have resulted from the lack of radiation in the simulation. Future modelling would ideally include radiating flux to improve accuracy.

The discharge was modelled as explained in the previous sections, the main assumption being that the discharge was uniform over the length used. For a uniform column, the power per unit length can be calculated from the voltage and current product. This electrical power was shown to be used almost exclusively for heating the region of air within the discharge column (i.e. Joule heating). The full complexities of discharge analysis were not considered because they were not applicable to the melting process since no significant chemical reactions were occurring.

6.7.2 The Model Geometry

The three dimensional model geometry was made to be a close representation of the actual damage tests performed. Figure 6.11 (a) shows the three dimensional representation of the model used showing the electrodes, filter section and the discharge passing through the filter wall. The rotational symmetry resulted in a simple cross section and greatly reduced computation requirements. Another axis of symmetry was also gained by choosing not to model free convection. The resulting two dimensional model cross section is shown in Figure 6.11(b).
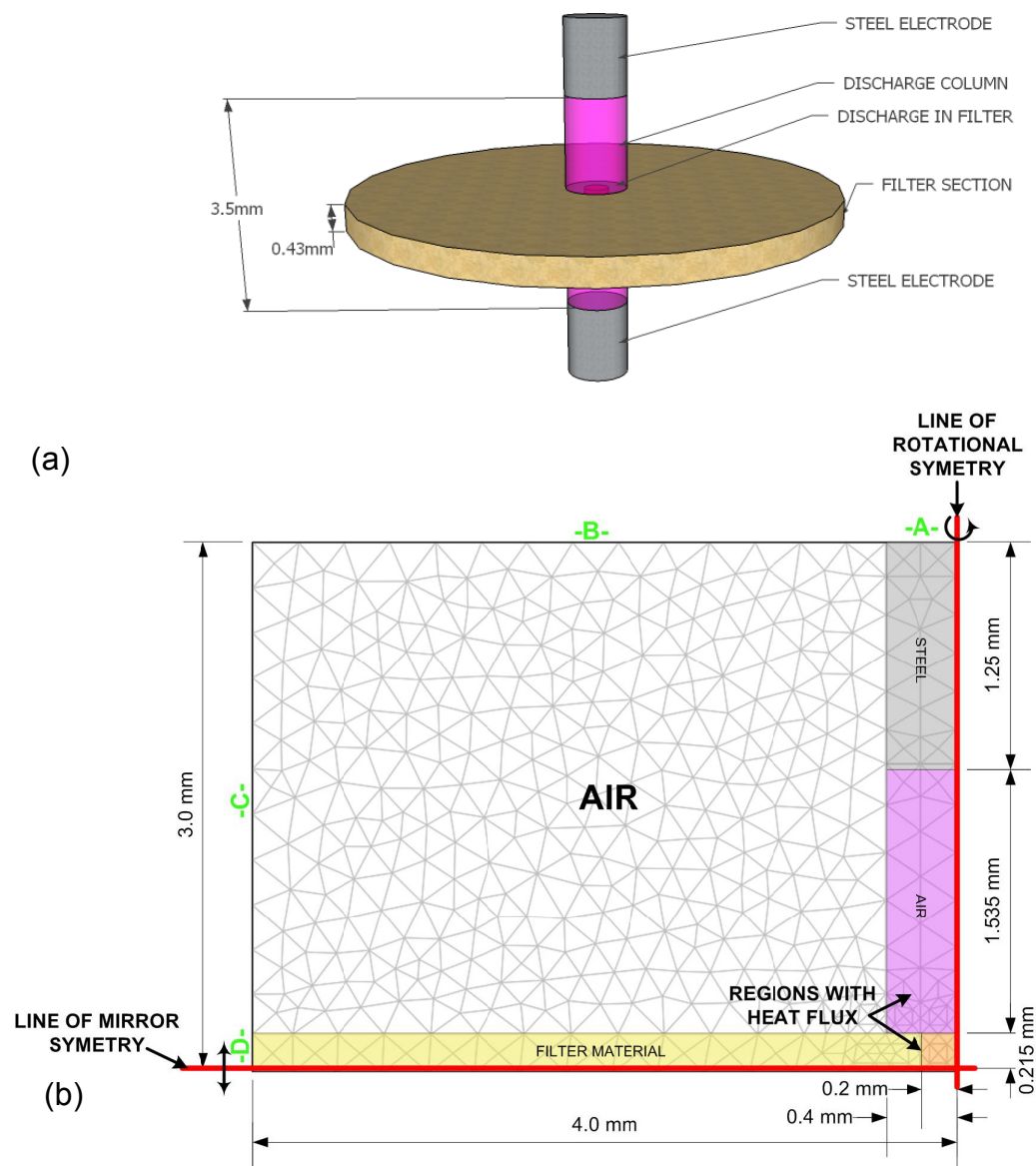
Figure 6.11 (a) Illustration of expanded model. (b) Model geometry used by the solver showing the finite element mesh used

The boundaries 'b' and 'c' of the model shown in Figure 6.11 were configured as open for the gas flow and as insulation for the heat flow (valid whilst the temperature gradient is low at the boundary). Boundaries 'a' and 'd' are solid for the gas flow and constant temperature for the heat flow. The materials were not allowed to change state in the model since only the threshold of damage was of interest and because the model would be invalid for predicting the melting behaviour of a porous ceramic. The diameter of the discharge was measured from its appearance and the through-filter section of the discharge was approximated from observations. The heat flux and

dimensions of these regions is discussed in section 6.7.5. The porous structure of the filter was not modelled due to the greatly increased complexity, however, the average pore size (17 - 30 μm) was significantly smaller than the discharge diameter (0.4 - 0.8 mm). The bulk thermal properties were used instead and this is detailed in section 6.7.4.

6.7.3 Free Convection Considerations

Initial simulations showed that including free convective flow in the model increased the computation time and had little effect on the model outcome over the first 500 ms. Figure 6.12 shows the model predictions for the temperature and flow profiles of the model with and without free convection after 0.5 seconds, the temperature profiles are very similar after this time. The white region of the temperature profile represents the proportion of the model > 1450 °C (i.e. the melting point of the filter).

Figure 6.12 Simulation temperature and flow predictions at 0.5 seconds with (right) and without (left) free convection

However, after 5 seconds the temperature profiles are markedly different which indicates that free convection must be included for simulations of more than ~ 1 second; see Figure 6.13. In addition, the high thermal gradient at the upper model boundary seen in Figure 6.13 (left) made the insulating boundary assumptions invalid.
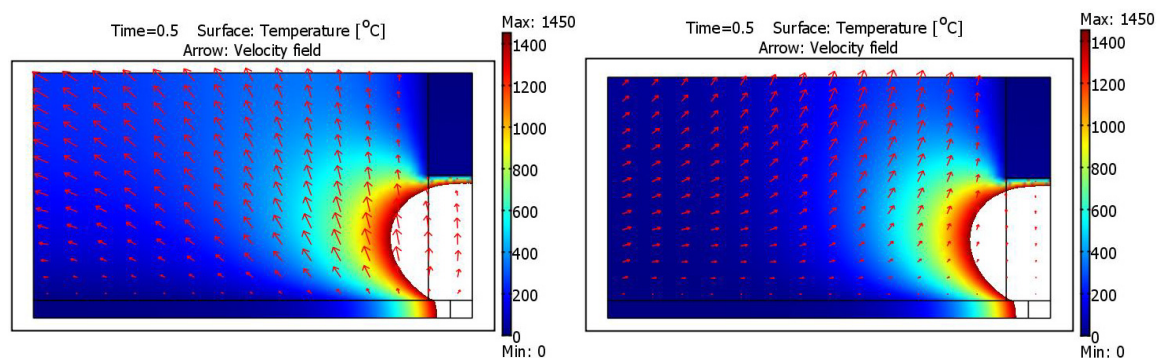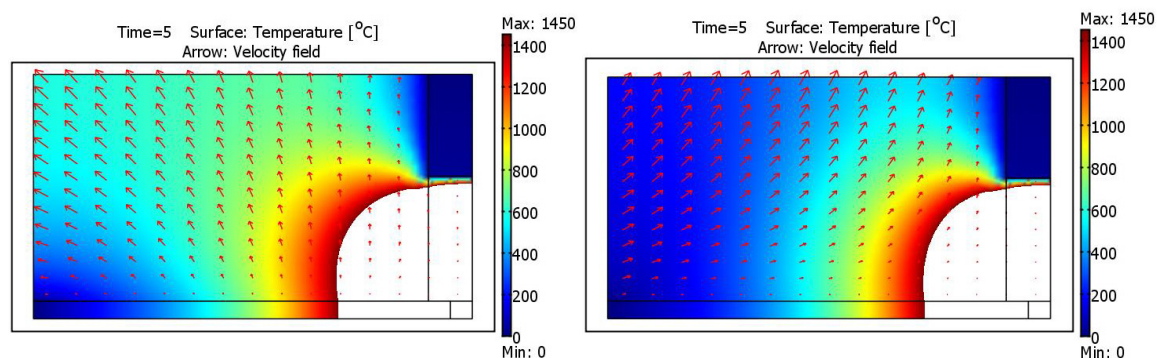
Figure 6.13 Simulation temperature and flow (arrows) predictions at 5 seconds with (right) and without (left) free convection

The time taken to reach the filter melting point changed by ~ 5 ms by excluding the free convective flux which was an acceptable loss of accuracy (~ 3% deviation) for the gains of simplicity and reduced simulation time. Experimental observations of the damaged samples used for the data collection showed that when the discharge crossed the filter vertically, the damage observed on each side was visually the same; i.e. the effect of convective flow from the discharge underneath the filter did not affect the actual damage process.

6.7.4 Model Material Property Inputs

The damage threshold was measured at the point the peak filter temperature reached the melting point of cordierite, taken to be 1450 °C (diesel.net, 2009). The thermal properties of the cordierite were calculated from the work by Leach (1992) and the electrode properties (steel) used values from the computer program library (FEMLAB 3.4), the values used are shown in Table 6.2. The model was solved using the Navier-Stokes equations (for the air flow) in conjunction with the general heat transfer equations. Solving the model took about 5 minutes using a 2 GHz Pentium IV processor PC.

Material	Thermal conductivity	Source	Heat capacity	Source	Porosity
Filter (cordierite)	0.54 $W.m^{-1}.K^{-1}$	Leach (1992)	1120 $J.kg^{-1}.K^{-1}$	Grigorio (1996)	42%
Electrode (steel)	80.4 $W.m^{-1}.K^{-1}$	Model library	450 $J.kg^{-1}.K^{-1}$	Model library	-
Air	Function of Temp	Model library	Function of Temp	Model library	-

Table 6.2 Model material properties

The initial conditions for the model materials and boundaries were fixed at standard temperature and pressure (IUPAC, 273.15 K, 100 kPa) and the gas flow velocities were all set to zero. The next section discusses how the heat input from the discharge was modelled.

6.7.5 Transient Heat Flux Inputs

The values for the heat fluxes were found from the transient and steady-state data as described in section 6.6. Figure 6.14 graphically shows the typical discharge power over a 1 second transient with the clean filter section (black trace) and without a filter section present (red trace). The difference between the two curves represents the additional electrical power consumption as a result of the filter section. A simplified heat flux profile was used rather than a single data set from one of the transient tests. The simplified heat flux levels were calculated from the approximation of the transient heat input data illustrated as the straight lines drawn on Figure 6.14. The change in heat input occurring at ~160 ms caused the adoption of two release values. The lower value was used for the first 160 ms and the higher for the remaining time.
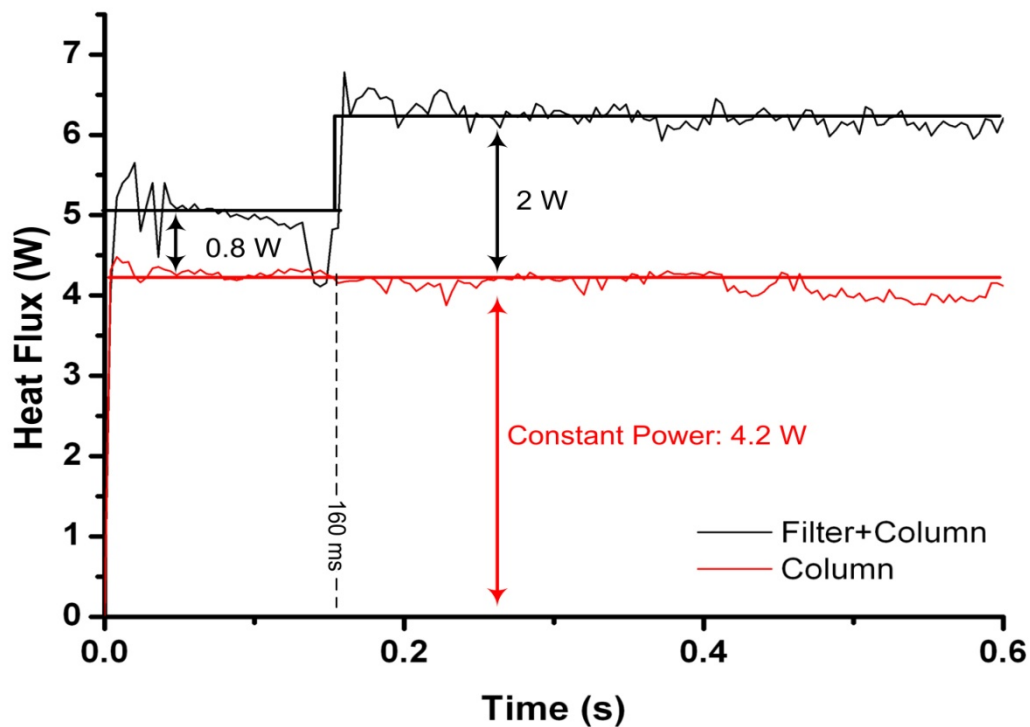
Figure 6.14 Graph of typical discharge power showing the approximations (bold lines) and the extra power consumption resulting from the filter section

The diameter of the discharge was approximated from measurements of the discharge appearance. Figure 6.15 shows images of the discharge at the interface with the filter surface. The gap used in the experiments was smaller than shown which kept the discharge straight as it passed through the filter. The heat flux calculations would have been less accurate had the discharge been curved.
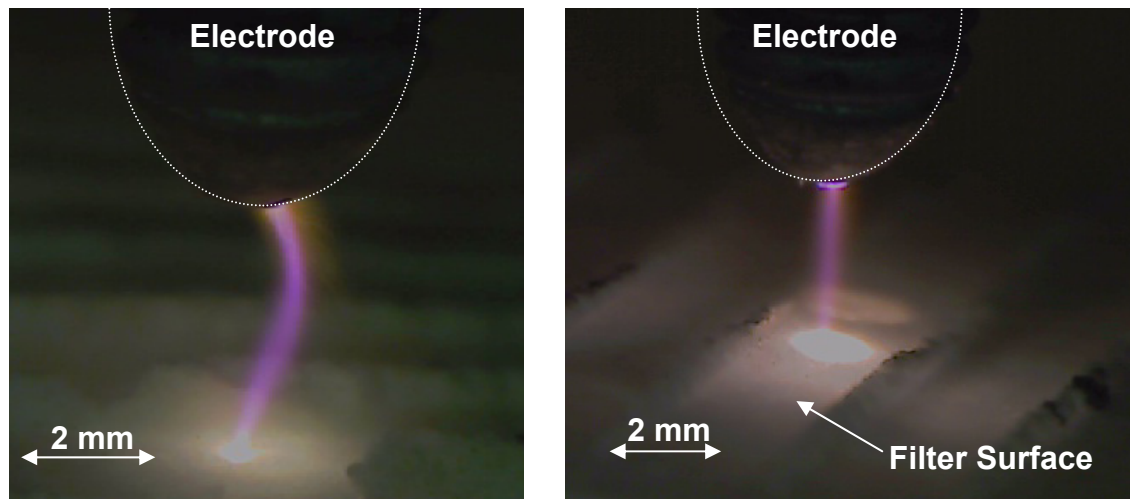
Figure 6.15 Discharge at the interface with the filter surface showing the column constriction

The through-filter region was set to half the diameter of the discharge to approximate the observed reduction in diameter. The heat flux per unit volume was then calculated as described in Section 6.6 based on the calculated volumes of each section and the results are shown in Table 6.3.

Region	Input Heat Flux ($W.m^{-3}$)
Discharge column (constant)	2.72×10^9
Through-filter ($0 \leq t < 160$ ms)	1.48×10^{10}
Through-filter ($t \geq 160$ ms)	3.70×10^{10}

Table 6.3 Heat flux in to the discharge regions

Heat flux from the electrode root was not included in the model because the electrodes were sufficiently remote to prevent heat transfer from the electrode root to the filter section. The electrode was included in the model to more accurately model the expanding discharge column. The electrode temperature did not increase more than a few degrees above the ambient temperature during the 1 second tests.

6.7.6 Model Validation Using Observed Damage

Model validation was performed by comparing the model predictions to the observed damage on samples of cordierite filter. The onset of damage was most important for the validation, however, the model was allowed to continue the simulation until 500 ms to compare the damage radius to the model predictions as well. An image sequence of the model predictions and the measured damage for the test sample is shown in Figure 6.15.
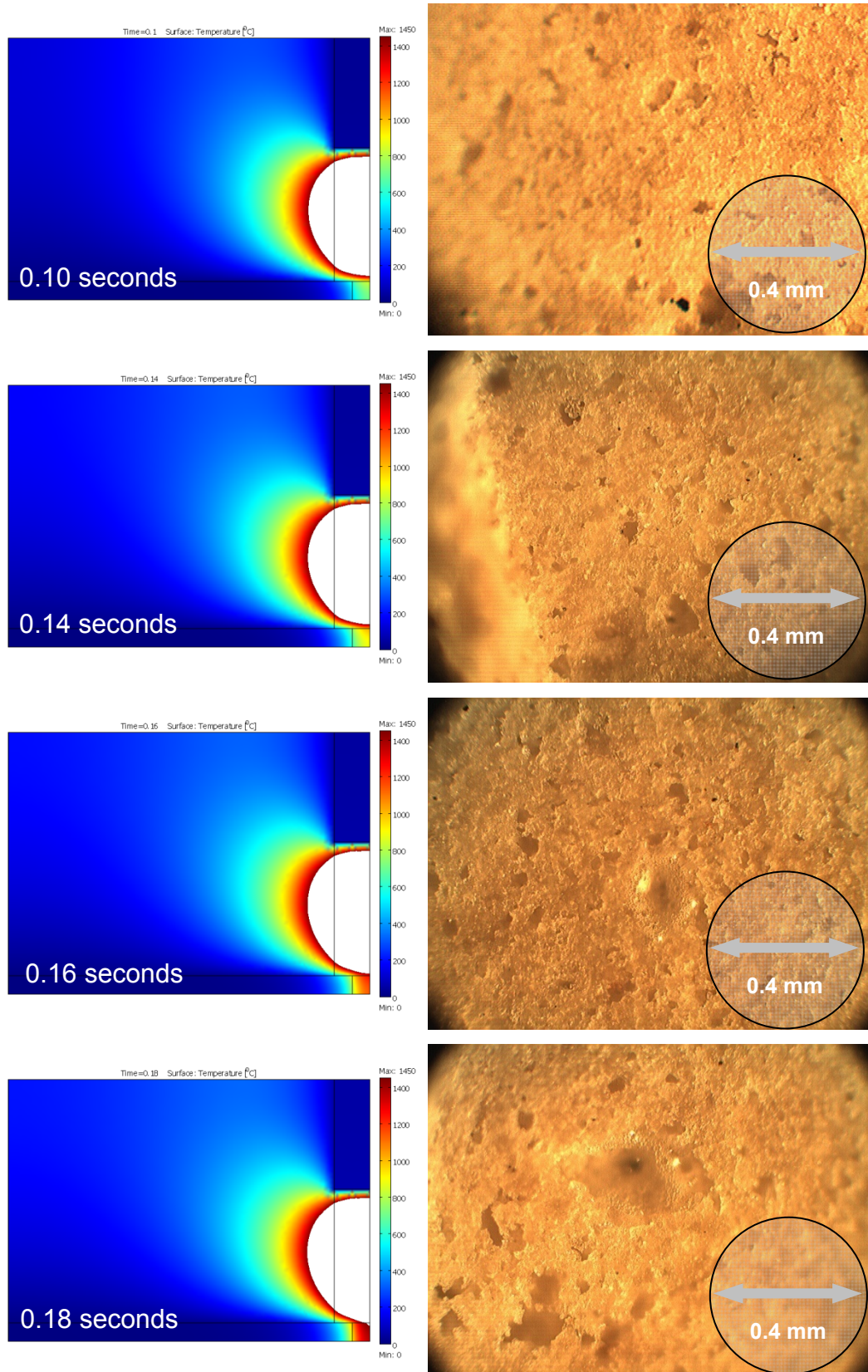
Figure 6.15 Comparison of model to measured damage results
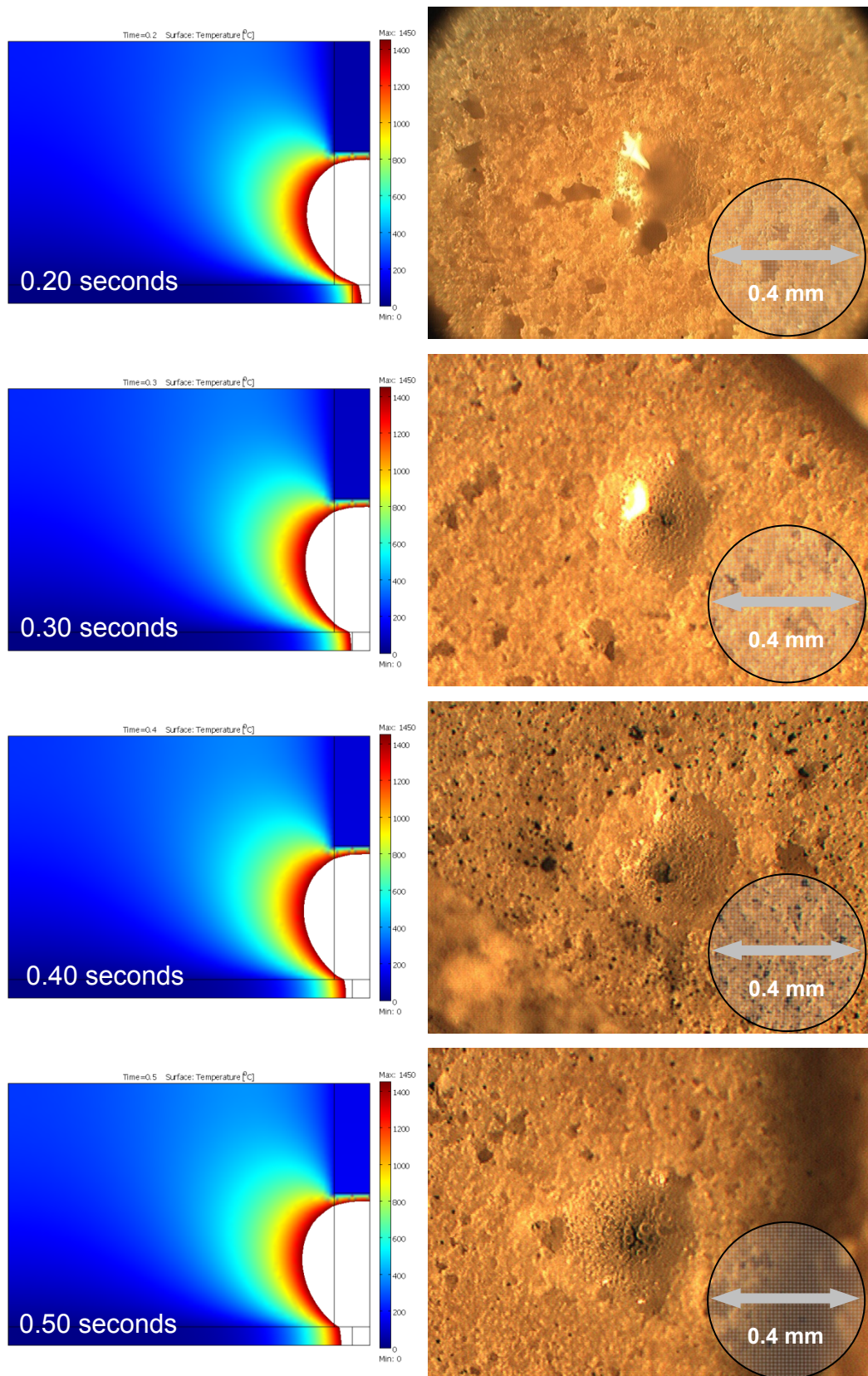
Figure 6.16 (continued) Comparison of model to measured damage results

The damage threshold was taken to be the time when part of the filter reached the material melting point of 1450 °C (diesel.net, 2009). This occurred first at the point corresponding with the surface of the filter in the centre of the discharge, a graph of this temperature is shown in Figure 6.16.
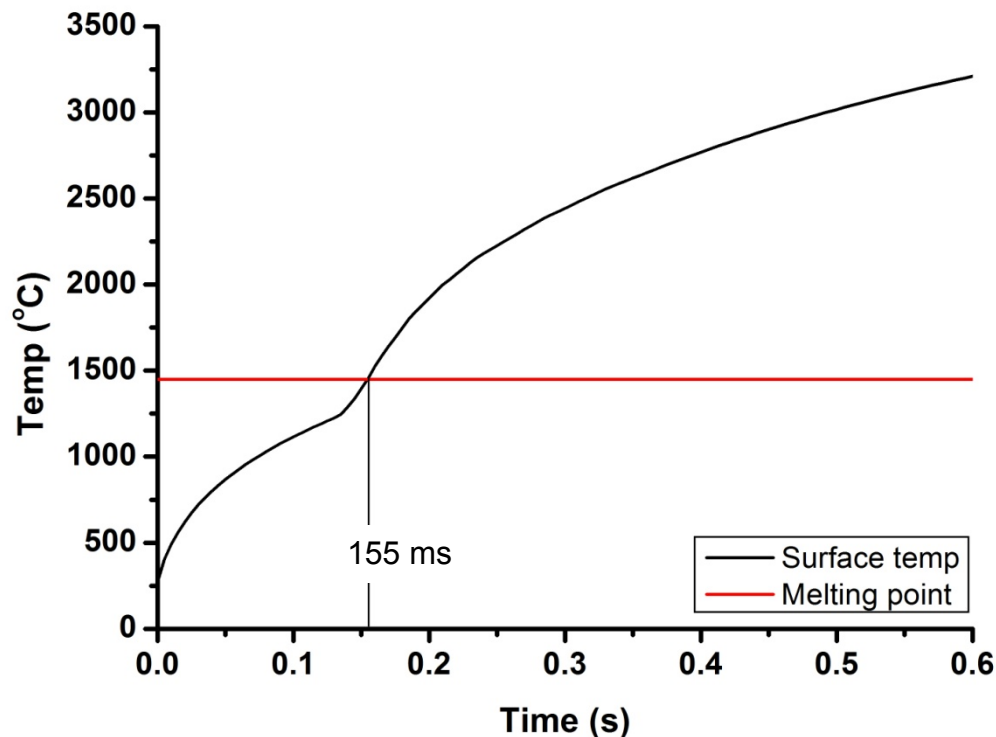
Figure 6.17 Graph of peak surface temperature versus time showing melting threshold (1450 °C)

The predicted melting threshold or damage threshold in this case is a good indication of the observed results (damage was observed to occur in the sample between 140 ms and 160 ms). However, the model over estimates the radius of the melted region after 200 ms and this could be due to the effects of free convection, radiation or enthalpy (ΔH_{fus}) because the model does not take into account changes of state. The model validation shows that approximations of the damage threshold can be made without the need for more complex models. The model can be applied to other materials from their physical characteristics to determine the durability of these materials to discharge damage.

6.8 Application of the Model

This section uses the model to examine the main contributor to filter damage and to estimate the performance of other potential filter materials.

6.8.1 Filter Damage Energy Balance

The model was changed to alter the heat distribution in order to consider the main contributors to filter damage. This information would be useful for understanding how the discharge damaged the filter. Four cases were considered:

    i.   No heat flux in the filter, normal discharge heat flux

    ii.   Normal heat flux in the filter, no discharge heat flux

    iii.   All discharge heat flux delivered to the discharge

    iv.   All discharge heat flux delivered to the filter

The predicted temperature profiles of the peak filter temperatures are plotted in Figure 6.17. The heat flux in the filter was fixed to the lower of the heat flux values used for the validation (25.5×10^9 W.m^{-3}), this is because the observed change in heat flux at ~155 ms was probably due to the filter surface melting and hence would make the comparison less valid.
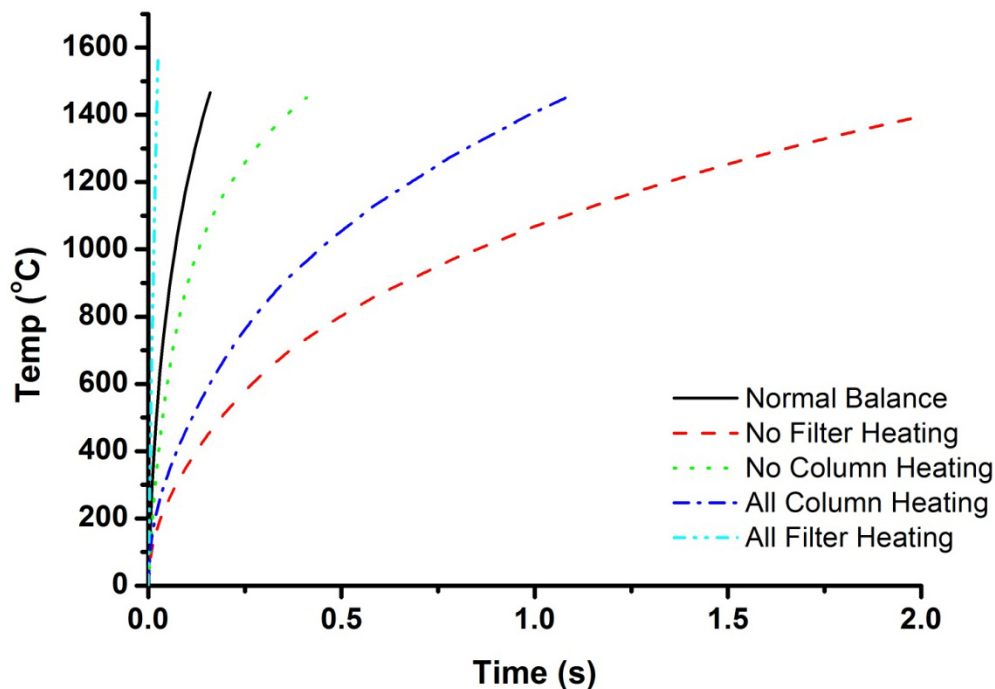

Figure 6.18 Graph of peak filter temperature for different heat flux configurations

The model predicts that the heat flux from the discharge passing through the filter is most significant to the filter damage process. Removing the heat flux from this region resulted in no predicted filter melting for a 2 second simulation despite 4000 K gas temperatures above the filter surface. This result agrees with the observations made during testing when the discharge was observed to take a path along the filter surface instead of through it. Novel filter geometries could be employed to take advantage of this effect resulting in a more robust regeneration system without the need for more expensive filter materials.

6.8.2 Comparison of Other Filter Materials

The main aim of the transient model was to determine whether other filter materials would be more robust to damage from the discharge, this sub-section discusses the available filter materials and the model predictions. As future materials become available, the model could be used as a starting point for determining the suitability of the material for Autoselective regeneration. The material properties considered are shown in Table 6.4 based on a 42% porous crystalline structure (i.e. identical to the cordierite wall flow filter substrate). The modelling assumed identical wall thickness to the cordierite sample and the same initial conditions as used in the validation. The change in discharge power during the validation (at ~ 150 ms) was likely due to the change in material state, therefore, the power into the filter region was kept constant at the lower value (25.5×10^9 W.m^{-3}).

Material	Thermal Conductivity	Specific Heat Capacity	Melting Point
	W.m^{-1}.K^{-1}	J.kg^{-1}.K^{-1}	°C
Cordierite	0.54	1120	1650
Alumina	11.4	640	2054
Zircon	1.39	312	2400
Silicon Carbide	27.4	18.1	2730
Mullite	1.24	468	1850
Nickel	29.6	260	1453

Table 6.4 Material properties used for the modelling tests

A plot of the peak material temperatures predicted by the model is shown in Figure 6.18 in which the lines are terminated at the material melting point to aid comparison.
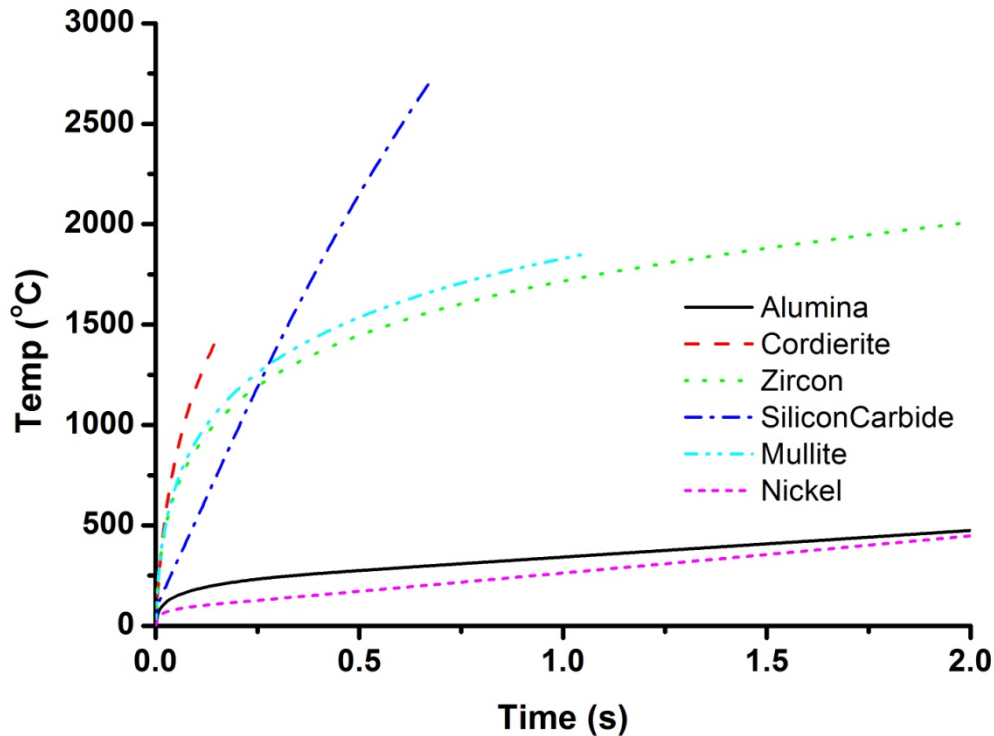
Figure 6.19 Graph showing predicted surface temperatures for each material. The end of each line represents damage threshold (melting point)

The model predicts that similar performance to cordierite can be achieved by mullite and zircon without the melting point limitation imposed by cordierite. It would take more than 2 seconds for a zircon ceramic filter to be damaged in this configuration. The higher thermal conductivity of the filter materials nickel and alumina ensured they were far from their melting points by the end of the simulation. However, this is not an indication of their suitability since the low temperatures predicted by the model indicate that there would be poor soot regeneration especially for the deep bed filtered layer. Silicon carbide has a low specific heat capacity resulting in a rapid heating by the discharge. However, this property left it vulnerable to thermal damage despite its high melting point.

In the comparison we assumed the heat flux into the filter sample would be the same for each material, in reality this is not likely. The electrically conductive nickel filter would have a discharge root on the surface (delivering more power than was included in the model) and the discharge would not be inclined to pass through the filter as predicted. The same could be true for the silicon carbide which can be electrically conductive if certain impurities are present. The predictions for the mullite, alumina and zircon are reasonable for comparative purposes. The zircon performed the best since it quickly achieved a temperature capable of rapidly oxidizing the soot whilst keeping below its melting point. However, due to the high cost of zircon, mullite would be a better alternative for a DPF material and it is recommended for future research for filter materials used with Autoselective regeneration.

6.9 Chapter Conclusions

The types of filter damage were characterised and the ambiguity about ambient damage was removed. The energy balance of the Autoselective discharge was calculated and shown to change with current. The results supported the work from Chapter 4 showing that the lower currents offered higher regeneration effectiveness. The energy balance shows that for a metal to PM discharge, significant improvements can be made by changing the metal electrode material. In the case of a PM to PM discharge, the rate of oxidation will be expected to double due to the presence of two soot burning sites. This type of discharge occurs when the discharge becomes segmented by the regions of conductive PM as it passes between inserted electrodes in the filter. For the PM to PM discharge, the effectiveness is expected to more than double due to the absence of the metal electrode loss. This explains the results shown in Chapter 5 where extending the channel spacing made a significant improvement to the measured effectiveness.

The transient modelling of the discharge was based on the assumption that it behaved like a uniform cylindrical 'gaseous resistor'. This assumption was shown to be invalid when there was PM on the filter surface and as a result the modelling concentrated on the clean filter damage threshold. Several assumptions were made to reduce the computation time of the model including symmetry boundaries,

insulating boundaries, no radiation and no free convection. A series of tests provided data about the melting damage observed for different discharge exposure times. The 10 mA condition was investigated for the validation and the visual appearance of the filter damage was in good agreement with the simulation. The discharge heat flux was divided into two regions and the region inside the filter was shown to be the most important factor when determining the damage threshold. The heat flux levels were held constant whilst comparing several other known DPF materials.

The simulation of different materials showed that zircon and mullite made good candidates for future testing but high conductivity ceramics may suffer poor depth bed regeneration. The rapid heating of cordierite suggested that, although vulnerable to damage, it had the lowest required energy input to begin regenerating. As more computing power becomes available, a revised model incorporating filter channels and gas flow could be developed that could be used to determine the optimum on- and off-times for a filter.

7. Analysis of Particulate Re-entrainment

It was observed that the use of low frequency (<1 kHz) and DC discharges caused significant blackening of the down-stream (clean side) channels during flow-rig experiments. In this chapter, the mechanism by which particulates were able to pass through the filter is investigated. A novel reverse flow regeneration method, based on the findings is also proposed.

7.1 Forces on the Trapped Particulate

Initial observations suggested that the blackening of the down-stream channels was caused by particulate passing directly through the filter walls. Further investigation showed that this was not as a result of filter damage. The particulate was either passing directly through the filter walls or the discharge was dislodging trapped particulate. Down-stream blackening was also observed in a flow-rig without particulate in the airflow and this could only be caused by the latter. Dislodged particulates would re-enter the gas flow moving further into the filter matrix before being re-trapped. If this process was repeated, particulate would eventually begin to pass through the filter resulting in a loss of filtration efficiency and downstream blackening.

The particulate adheres to the filter surface of the filter in three ways as summarised in Figure 7.1. The most significant of these is the intermolecular force caused by the uneven distribution of electron density on the molecular surface. This results in electrostatic attraction (i.e. Van der Waals forces). Mechanical forces can also account for some of the adhesion forces holding the particulates within the filter matrix although these are more likely to apply to large agglomerates of a comparable size to the filter pores. The chemical bonding of the particulates with the ceramic is unlikely due to the low reactivity of the filter surface. Chemical interaction between particulates is much more likely due to the presence of hydrocarbon compounds and reactive inorganic compounds. Once the particulate has reached a sufficient concentration within the filter, coagulation leads to the production of a caked layer on

the upstream side of the filter wall. The caked surface is supported by the forces holding the particulates together. It was noted that on occasions the caked layer could be separated from the ceramic surface as a solid layer.
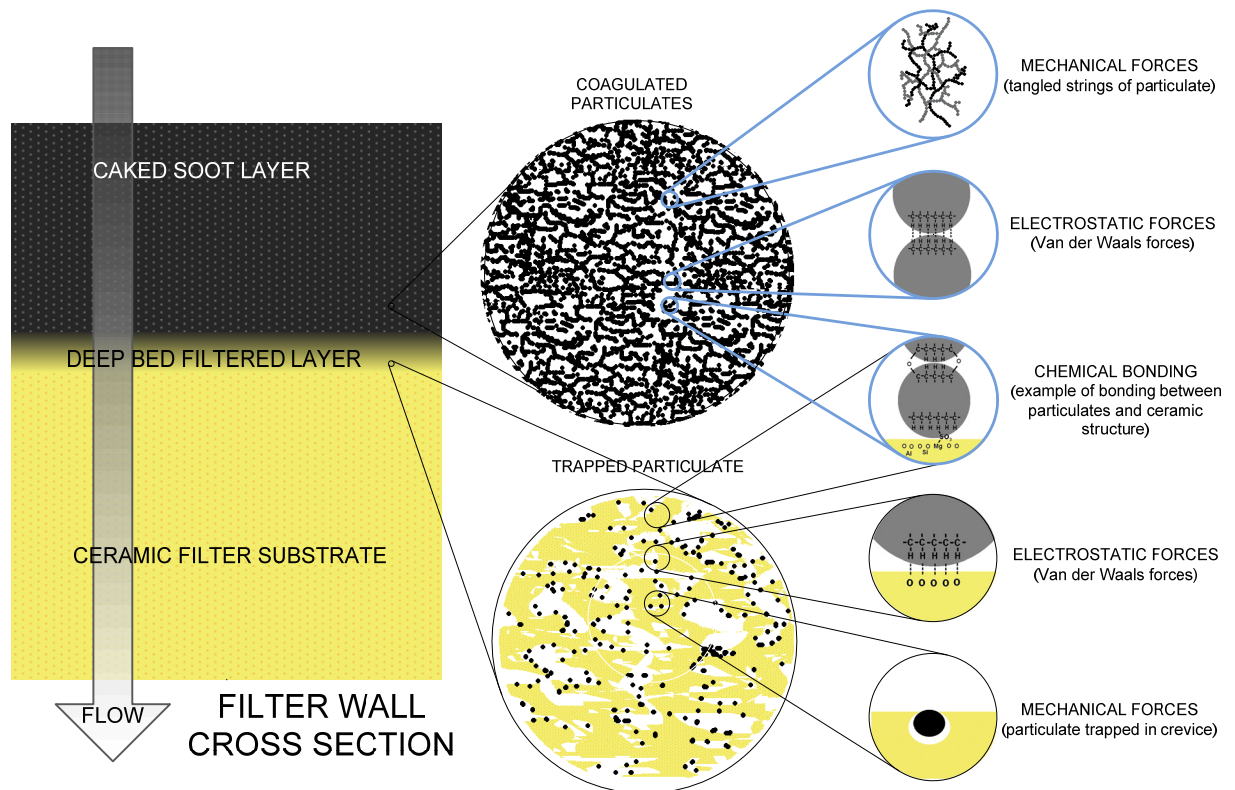
Figure 7.1 Structure of the filter layers and forces retaining particulates

The blackening of the downstream channels of the filter could only be attributed to particulates passing through the filter walls. If particles are dislodged from their resting position, the flow would move them further into the filter before they were once again removed from the flow. Under the influence of successive dislodgement and retention, there would be a drift of particulates through the filter leading to an apparent reduction of filtration efficiency. This diffusion of the particulates through the filter could be caused by disturbing either the caked layer of PM or the deep bed filtered layer.

The force that dislodged the particles needed to be investigated in order to take measures to preserve the wall flow filter efficiency. Initially, it was thought that the re-

entrainment of particulates was due to electrostatic interaction between the particulates and the pre-breakdown electric field. Just before the discharge is initiated between the electrodes, the electric field is at its highest amplitude, the breakdown voltage. The pre-breakdown electric field would cause the PM to experience the highest amplitude electrostatic force which may be responsible for soot re-entrainment.

7.2 Identification of the Re-entrainment Mechanism

For electrostatic forces to affect a particle, it must be charged as shown in Figure 7.2 where F is the force exerted on the object with charge Q in an electric field of strength E.

$$F = QE$$
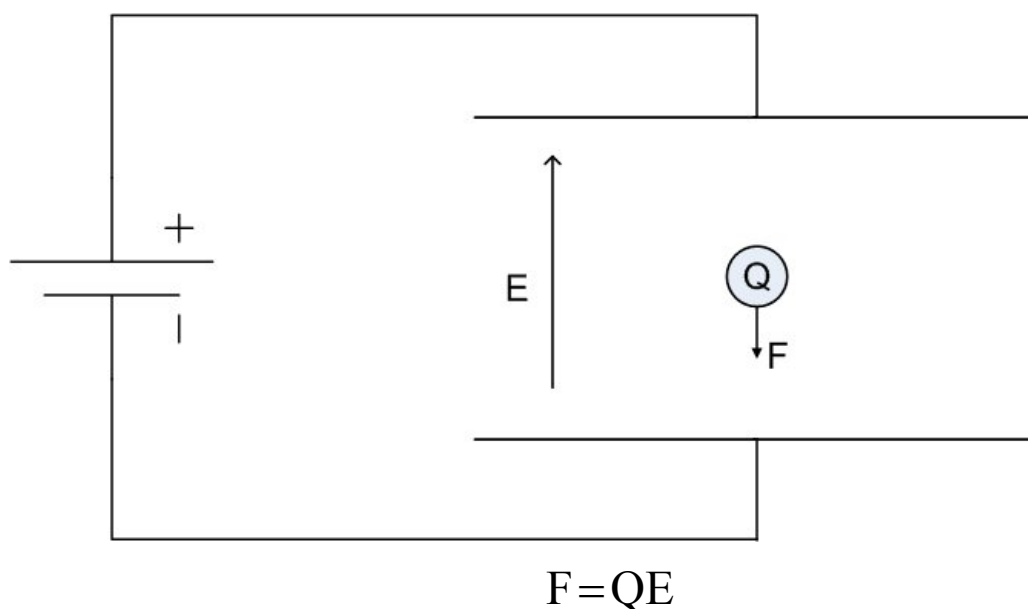
Figure 7.2 Electrostatic forces on a charged particle

Diesel particulate is conductive due to the carbon composition and conductive objects cannot hold charge unless they are insulated from grounded objects. The particles in the depth bed layer are often insulated from the rest of the grounded caked layer, these particles may experience forces if they are charged. The work by Wright (2003) suggests that in optimum conditions the particles are unable to accumulate more than a few electrons of free charge. The force on a particle can be calculated if some assumptions are made. For example, consider the case of a 10 nm diameter particle, assuming a charge of 3.2×10^{-19} C (i.e. two electrons), that is

trapped between the grounded soot layer and an electrode one channel width away (2.86 mm) with an electrode breakdown voltage of 3 kV. The force is 3.36 $\times 10^{-13}$ N which when converted into a pressure, assuming a 10 nm diameter area of interaction, is 4.3 kPa. This is comparable to the back-pressure values of the filter and probably not sufficient to remove the particle from the surface. The free acceleration of the particle once dislodged, assuming a density similar to solid graphite, is 3.1 $\times 10^8$ m.s^{-2} which is large. Any free charged particulate would be expected to interact with this field.

An experiment was used to test the interaction of free particulates within an electric field. Two parallel plate conductors were arranged with a spacing of 10 mm and 10 kV was applied across them. The test arrangement is shown in Figure 7.3. The particulate was placed on the lower plate and were retained there by gravity. When a DC voltage was applied, the particulates were influenced by the electric field and organised themselves such as to close the gap between the electrodes by forming a conductive bridge between them. When a 20 kHz 10 kV AC voltage was applied, the particulates were also influenced by the fields and were observed to form a diffuse cloud of particles within the electrode gap. This suggests that the particulates had a low enough inertia to exchange energy with the high frequency voltage waveform and experienced an oscillatory force proportional to the applied voltage. This experiment confirmed that the particulates were influenced by electrostatic forces when free to move.
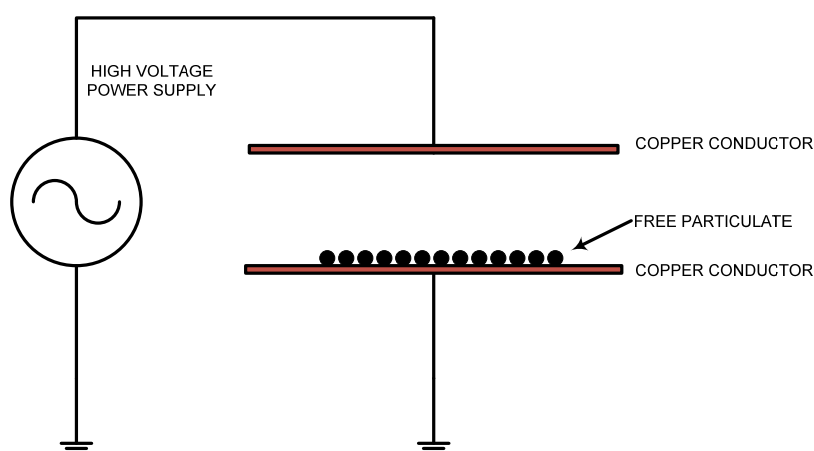

Figure 7.3 Test to observe particulate behaviour in electric fields

The test was repeated using a soot laden wall flow filter and a flow-rig to test the ability of electric fields to cause particulate re-entrainment into the air flow. The electric field was applied to the electrodes for fifteen minutes and no downstream blackening was observed after sectioning the filter. The applied voltage was just below breakdown (2 kV) to ensure there was no actual electric discharge. The lack of blackening of the down stream channels showed that the discharge was important to the re-entrainment mechanism. Initial thoughts were that the fast changing transient fields produced at breakdown may be important. Figure 7.4 shows the normal resonant breakdown transient of the power supplies used, the breakdown transient results in a high dV/dt transient on the electrode which translates to a rapid change in electrostatic force.

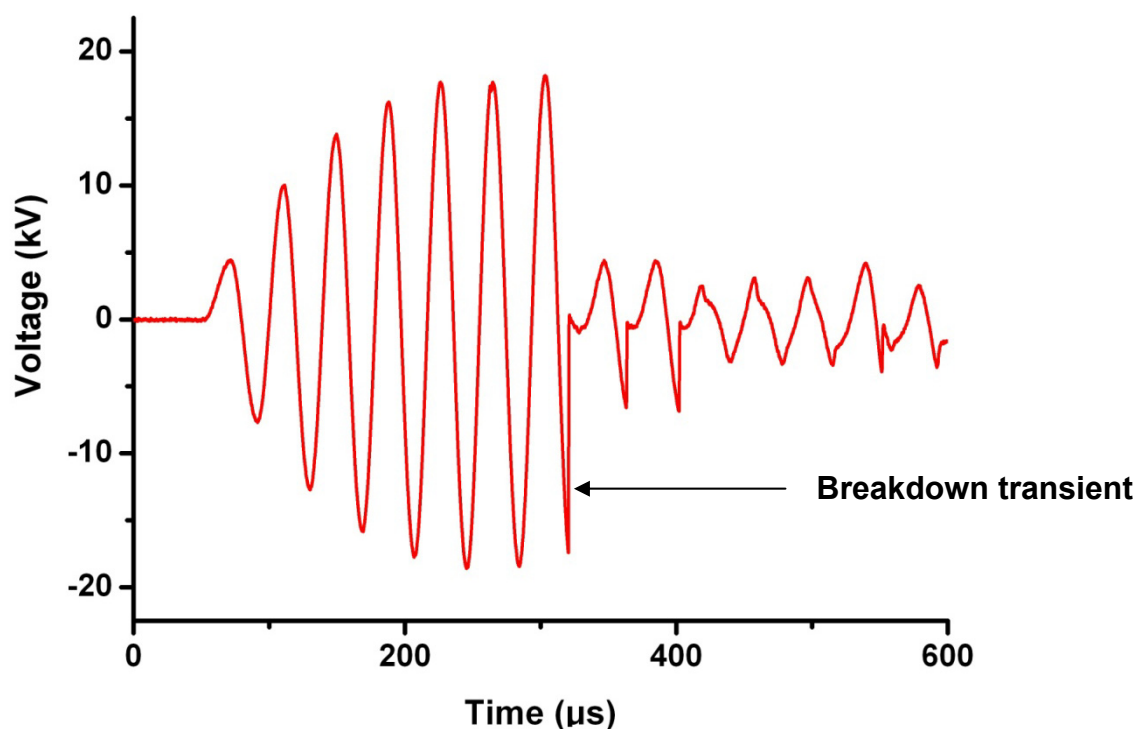**Figure 7.4** Normal breakdown transient for Autoselective power supply showing voltage transient

A test was used to determine whether the rapidly changing field may be responsible for soot re-entrainment. The test placed a loaded filter sample in the apparatus described in Figure 7.5. The resonant power supply was used with the primary voltage set to produce a breakdown after resonating for approximately 1 ms. The

power supply had a variable on-time allowing the resonant waveform to be interrupted before a breakdown occurred. The test used a repetition rate of 1 Hz such that Autoselective regeneration was almost negligible due to the low duty cycles. The results showed that no soot was dislodged unless a discharge was initiated supporting the previous flow-rig observations. Some soot was dislodged if the on-time was extended to allow breakdown to occur (on-time > 1 ms). After breakdown the discharge was continuous for the remainder of the on-time. Further increases in on-time resulted in no increase in dislodged soot. It can be therefore concluded that the PM is removed from the filter surface during the breakdown transient.
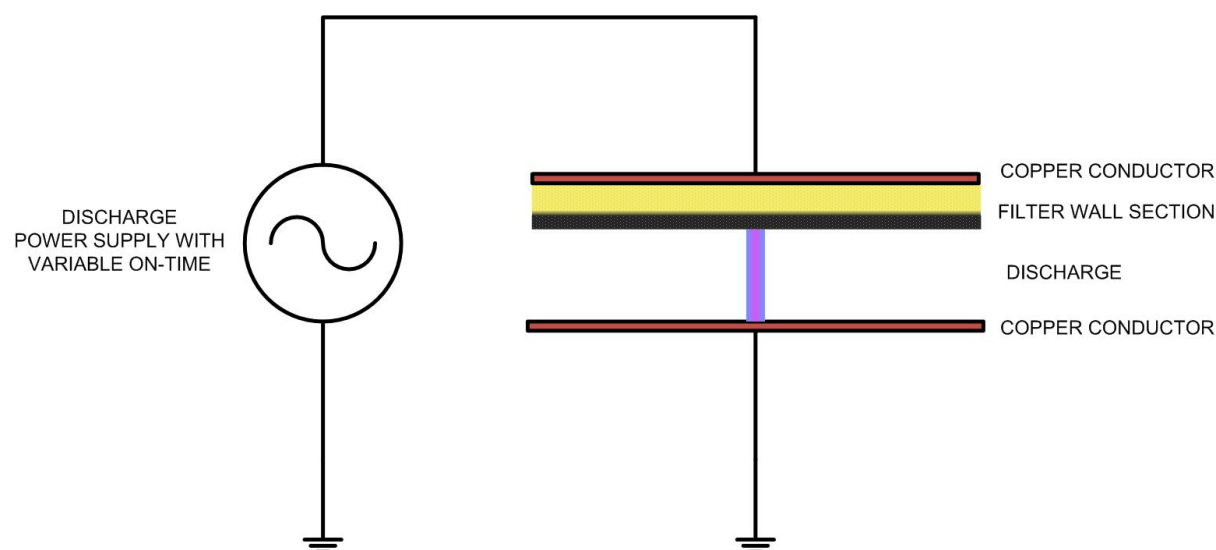
Figure 7.5 Testing of the Autoselective discharge for particulate removal

An experiment was designed to separate the effect of the electric field transient from the actual discharge so that they could be investigated separately. Figure 7.6 shows the test arrangement which used a spark gap to discharge the electric field applied across a filter section. The discharge was prevented from occurring at the filter surface using a glass insulator sheet. The voltage waveform, and hence electric field, applied to the sample was almost identical to the previous test including the high dV/dt transient at breakdown. It was observed that the electric field transient was incapable of removing the trapped PM. During the experiment, however, it was also observed that loose particulate not attached to the filter was affected by the electric field as previously tested. This experiment confirmed that the electrostatic effect was not responsible for dislodging the particles although free particulate is affected by the electric field. This sequence of tests together show that the PM is dislodged from the

filter by the electric discharge initiated during breakdown and no soot is removed by the steady state (i.e. 10 mA) discharge current.
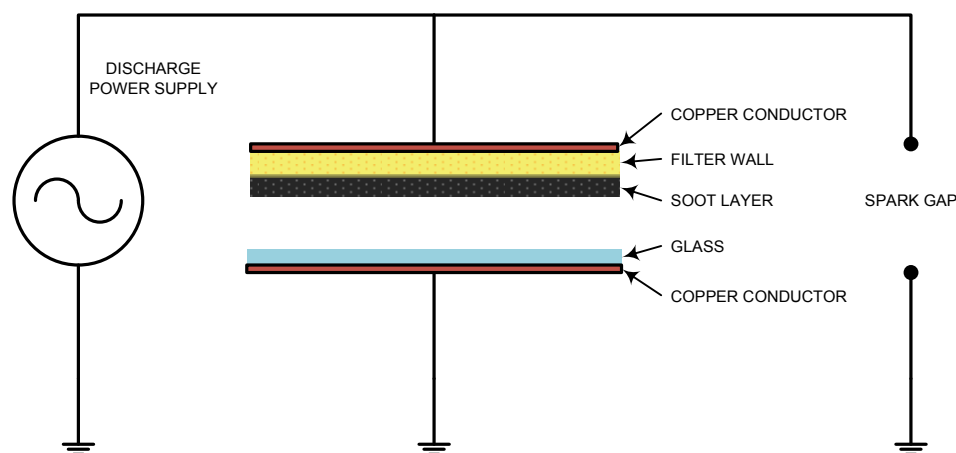

Figure 7.6 Experimental layout of transient electric field test

In conclusion, the downstream filter blackening was caused by trapped particulate travelling through the filter due to a combination of flow and forces dislodging the particles from the filter walls. The experiments described show that the particles within the filter experience a force due to the electrostatic fields between the electrodes. However, these forces are insufficient to break the adhesive forces binding them to the filter. Particles not bound to the filter (including in the gas flow) will experience oscillatory movement due to the AC electric fields, especially during transients. These may be partly responsible for some of the diffusion of soot through the filter. However, the main reason for the soot re-entrainment was the force created by the discharge at the instant of breakdown. This is investigated in the next section.

7.3 Electro-Acoustic Forces

When the electric field between two conductors exceeds the dielectric breakdown threshold of the gap between them, a spark occurs and current flows to reduce the electric field. A spark is a discontinuous narrow column of plasma with a high current density. The plasma produced is in the thermal arc mode and is highly conductive (~ 5 Ω, Boynton, 1904). The high current (> 10 Amps) through the arc is sufficient to rapidly heat the gas producing an acoustic pressure wave as the gas expands. This process can be observed naturally in the form of thunder and on a smaller scale as the popping sound heard when insulating fabrics such as polyesters are rubbed

together. It is probable that these electro-acoustic forces are responsible for soot removal from the filter surface.

7.3.1 Analysis of the Electro-Acoustic Force

At breakdown, a streamer discharge crosses the gap between the electrodes and the charge equalises across the gap forming a spark. The spark discharge plasma is in the arc state and is many thousands of degrees K. The arc channel widens and the discharge extinguishes unless the current is held above zero. The widening of the channel is the factor determining the velocity of the pressure pulse (Braginskii, 1958) and this is determined by the heat generated and the thermal conductivity of the gas. The visible light and other electromagnetic radiation from the arc is less than 1% of the energy delivered to the discharge (Uman, 1968). The majority of the energy delivered is used to form the acoustic pressure wave with the remaining energy being left as heat. The voltage and current waveforms of the spark show very rapid energy transfer. Rise times of approximately 20 ns are common for the Autoselective system.

An experiment was designed with a pin and plane electrode geometry between which a section of filter could be placed and a spark initiated. Previous experiments had isolated the actual breakdown event as the cause of soot removal. A power supply was designed to produce only the breakdown transient (without the subsequent glow discharge) with variable current amplitude and duration. Figure 7.7 shows the power supply circuits and Figure 7.8 shows the parameters of the spark discharge current waveform.
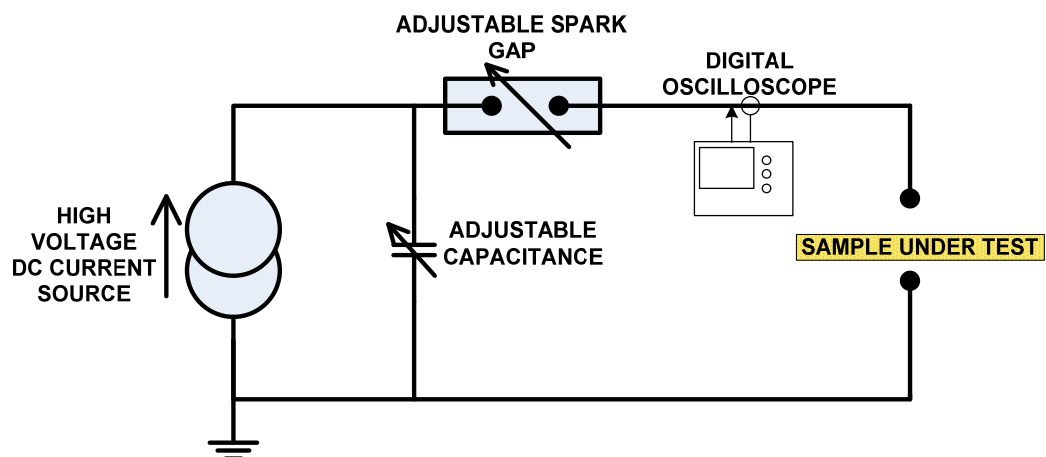
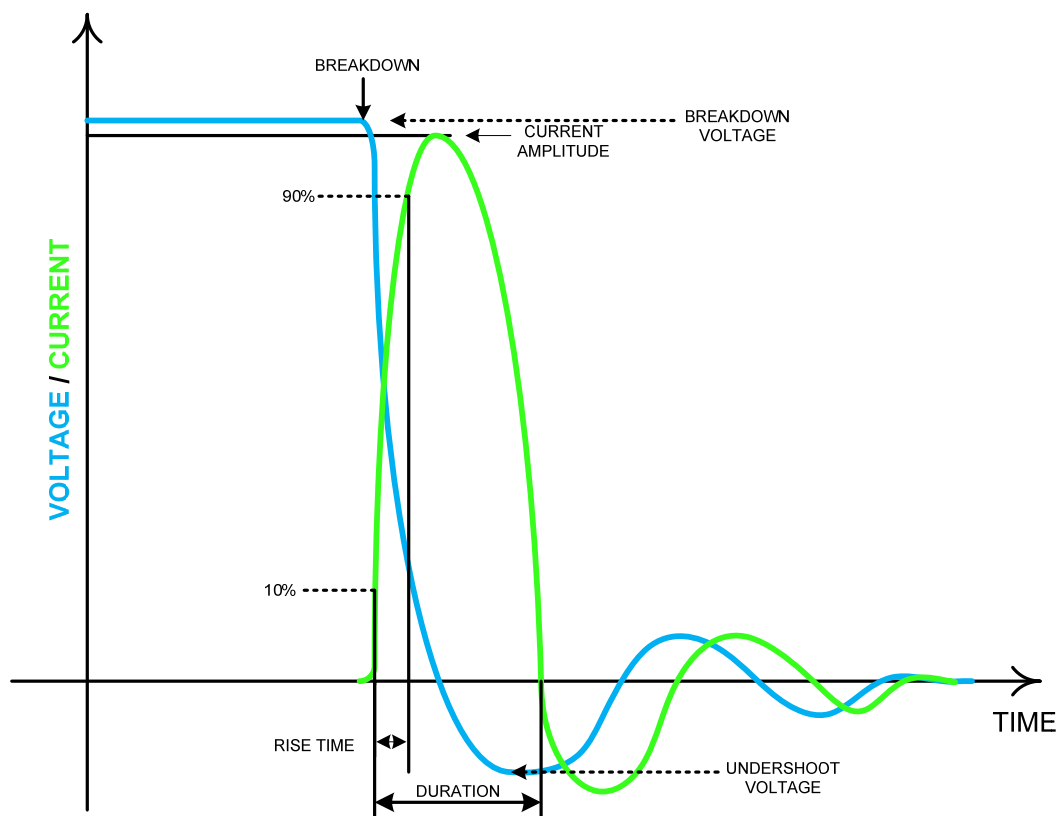**Figure 7.7** Variable DC pulse power supply

Figure 7.8 Graph of spark parameters

Figure 7.8 shows several parameters that can be used to analyse the spark and the energy delivery. The energy in the circuit before the spark forms is the energy in the capacitor and after the spark channel forms the residual energy can be approximated

by the undershoot. The energy delivered during the current pulse is therefore given by

$$E = \frac{C}{2} \cdot \left(V_{bd} - V_{us}\right)^2$$

Equation 7.1

where V_{bd} and V_{us} are the breakdown and undershoot voltages respectively and C is the capacitance. The rise time of the current pulse is normally 20 ns - 100 ns (depending upon the inductances of the wires) which is only enough time for a sonic pressure front to move 7 µm - 33 µm. The discharge must expand supersonically to reach the observed diameter of 200 µm - 500 µm. Khachalov (2007) demonstrated wave front velocities of 1500 m.s^{-1} which is in close agreement to those approximated here (~ 2000 m.s^{-1}). The energy release can analysed in the same way as Amer (2008) analysed laser induced dielectric breakdowns. In this case, the calculations by Zel'dovich (1966) can be applied using the assumption that the wave front radial position r at time t is

$$r = \varepsilon_0 \left(\frac{E}{P_o}\right)^{1/5} \cdot t^{2/5}$$

Equation 7.2

Where P_0 and ε_0 are the pressure and compensation factor respectively and E is the energy release. Taking ε_o to be unity (after Amer, 2008) the radius of the supersonic shock wave can be approximated from the energy released as represented from the voltages and capacitance value, assuming no residual heating of the gas. For a 500 pF capacitor, 25 kV breakdown voltage and a 5 kV undershoot the shock radius is 5.2 mm after 6.4 µs. The actual values used have many assumptions and are probably not accurate, but it is interesting to note that the radius of soot removal is of similar order to the shock wave radius prediction.

7.3.2 Testing of the Pulsed Discharge

The first variable tested was the amplitude of the current pulse, the peak current was measured using a 20 MHz bandwidth 10:1 'Pearson 411' current probe. Increased current amplitude produced noticeably louder sparks and dislodged large pieces of agglomerated soot from the caked layer on the filter surface. This was the expected

outcome because more energy was being delivered to the discharge at higher currents. The amplitude was increased gradually from 50 A to approximately 1000 A at which point pieces of ceramic filter > 1 mm across were broken from the sample by the discharge leaving holes in the filter. This experiment confirmed that there was ample energy available during a spark of only a few tens of amps to break the adhesion forces between the soot and filter and even enough to cause damage to the ceramic filter wall at higher current levels.

In another test, a series resistor was used to limit the amplitude and rise time of the current pulse. Rise times within the range of 10 ns to 10 us were possible, longer rise times dislodged significantly less soot from the filter. The capacitor size was varied within the range of 1 nF to 10 µF so that the pulses had durations of up to 100 us. At this duration and at a current of just 3 amps (rms), melting damage was seen on the surface of the ceramic and no soot was dislodged. The damage is shown in Figure 7.9 where there is also significant discolouration of the filter caused by the sputtered metal electrode surface. Sputtering is the evaporation of electrode material occurring when there is a high discharge current and low electrode temperature. This experiment showed that the rate of energy input into the filter was a factor in determining soot ablation.
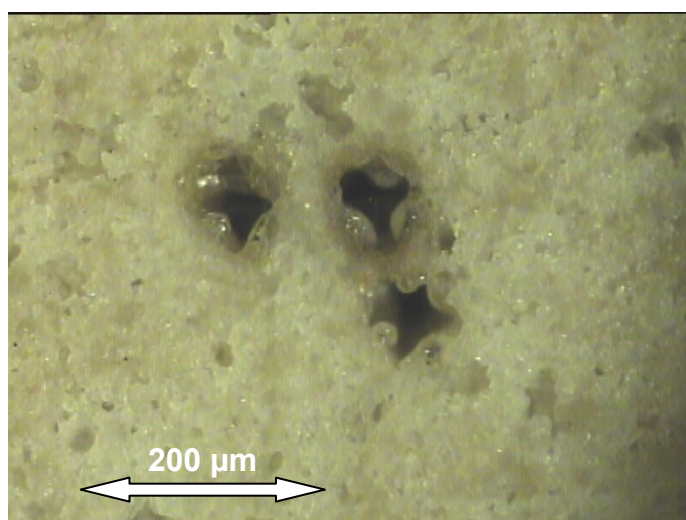

Figure 7.9 Damage from long duration current pulses, 100 µs with 3 A

Previous experiments showed that high peak currents dislodged larger volumes of soot per pulse. A range of different capacitors (25 pF to 100 µF) were tested with the resistance and inductance of the circuit minimised to shorten the current rise time. Increasing the capacitor increased the rise time but led to more soot being dislodged suggesting that peak power input was of more importance. The filter was inspected visually for damage (after 100 pulses) and the largest capacitor not causing visible damage was 500 pF. This corresponded to 1.5 MW of peak power and a current of 150 A - 200 A when a break down occurred at 25 kV. The results show that energy delivery within the first part of the pulse was critical; if the pulse was stretched over several microseconds then the filter is heated but no soot removal occurs. This is consistent with the theory shock wave formation since the peak overpressure, which controls the shock radius, is a function of energy delivery time (Crocker, 1998).

In summary, the force responsible for breaking the bonds holding the soot to the ceramic was identified as an electro-acoustic force. An experiment was conducted using an intense discharge adjacent to a section of PM loaded filter wall. The experiment illustrated in Figure 7.10 was used to determine whether the acoustic force travelling through the air was the source of the soot removal. An intense arc discharge of more that 2 kA and peak power of 10 MW was initiated just beneath (but not through) a section of loaded filter so that only the acoustic pressure wave interacted with the soot layer. No soot removal was observed despite the intense energy release. The test was repeated with the discharge initiated through the filter wall and a radius of 12 mm of soot was removed. From this experiment it can be concluded that the acoustic pressure wave travelling through the air was not capable of removing soot from the filter on its own.
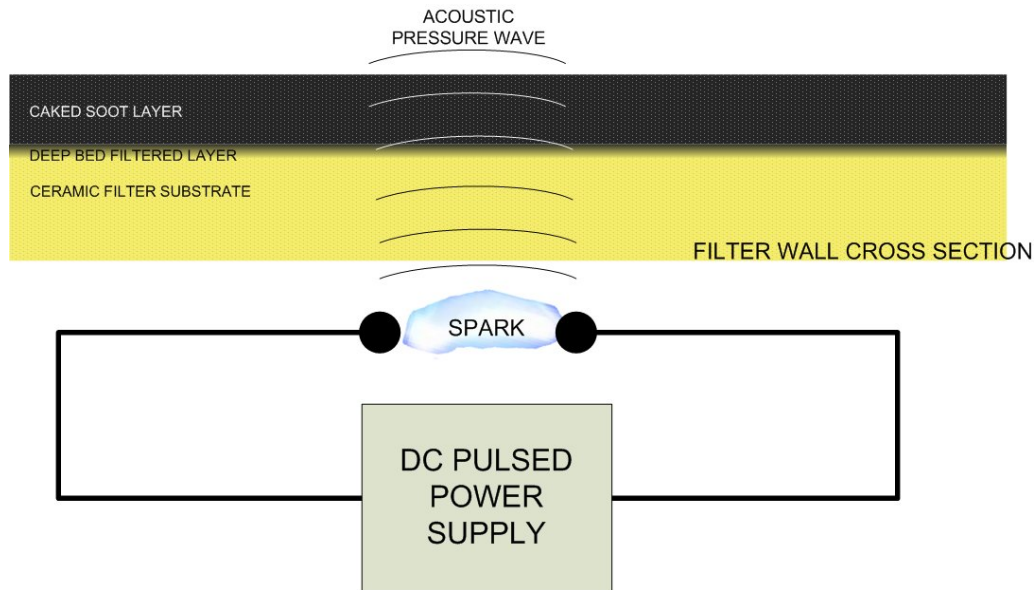
Figure 7.10 Adjacent discharge force test

In the case of the discharge travelling through the filter wall, the main differences are that the pressure wave can propagate within the ceramic matrix expanding the air between the soot layer and the ceramic surface. It is likely that the expanding gas caused by the discharge also travels through the pores of the filter wall and breaks the bonds holding the soot to the surface. The soot can then be removed by both the acoustic wave travelling through the air and by the electric field. Figure 7.11 summarises the forces removing the soot.
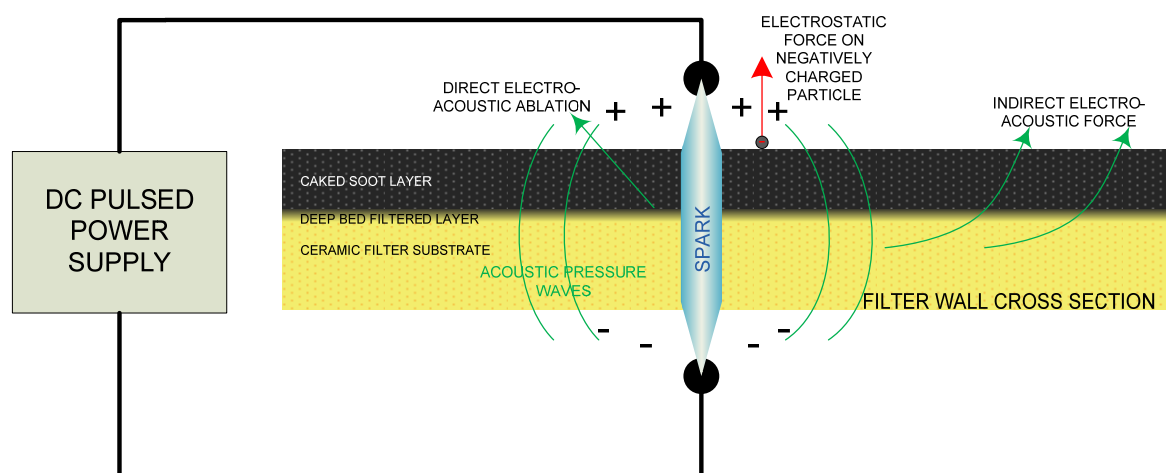
Figure 7.11 Summary of forces removing soot

7.3.3 Summary

The force that is responsible for the removal of the soot from the surface and causing particulate re-entrainment is from the acoustic pressure wave created by the spark discharge occurring at breakdown. The electric field between the electrodes has also been shown to be capable of accelerating free soot particles and hence may facilitate the diffusion of the soot through the filter. The electric field alone was not responsible for breaking the bonds between the soot and the ceramic.

A resistor can be used on the output of the Autoselective power supply to limit the pulse amplitude and hence peak power at breakdown, this was shown to be an effective way to prevent disruption of the particulate layer. In the case of some electrode arrangements, however, the addition of resistance to the power supply output may not be effective since much of the resonant capacitance occurs on the electrode; in this case, the resistance would create over damping of the resonant waveform leading to electrical breakdown difficulties. The power supply would also become less efficient since the discharge current would flow through the resistor. The best solution for resistance addition would be to use an electrode with a distributed resistance which may prove to be costly for production. For this reason a compromise must be made between resistor size and required breakdown voltage, a smaller resistor will have less effect on resonance but will not limit the current and peak power as effectively.

7.4 Potential Use of Electro-Acoustic Particle Re-Entrainment

The initial experimentation was aimed at reducing particulate re-entrainment to prevent downstream blackening when using the Autoselective regeneration system. This section investigates exploiting the re-entrainment mechanism by reversing the flow in the filter and increasing the breakdown transient. This encourages the removal of the soot from the filter and hence regenerates it.

A high energy discharge has been shown to effectively remove the soot from the walls of the cordierite wall flow filter without damaging it. Other regeneration strategies have attempted to do this with the aim of cleaning the filter (e.g. Takesa *et*

al, 1991). This type of regeneration system normally uses a high pressure reverse air flow to carry the soot back out of the filter into a storage vessel. The engine must normally be stopped for reverse flow to be possible, which means the high pressure air must be stored on vehicle. The main difficulty in implementing reverse flow regeneration systems is that the soot is bound to the filter by strong forces that are not easily overcome. The electric discharge has been shown to effectively remove soot from the filter with high power low energy pulses.

Experiments were used to test the ability of the pulsed discharge to remove soot from within a filter. A section of wall flow was used with the end plugs removed to allow gas flow, one of the tests is shown in Figure 7.12 (a). A schematic view of the tests is shown in Figure 7.12 (b). A low flow rate was produced with a 12 W blower facing the rear of the filter. Different numbers of electrodes and orientations were used during the tests to compare the factors of regeneration distribution, rate and volume cleaned.
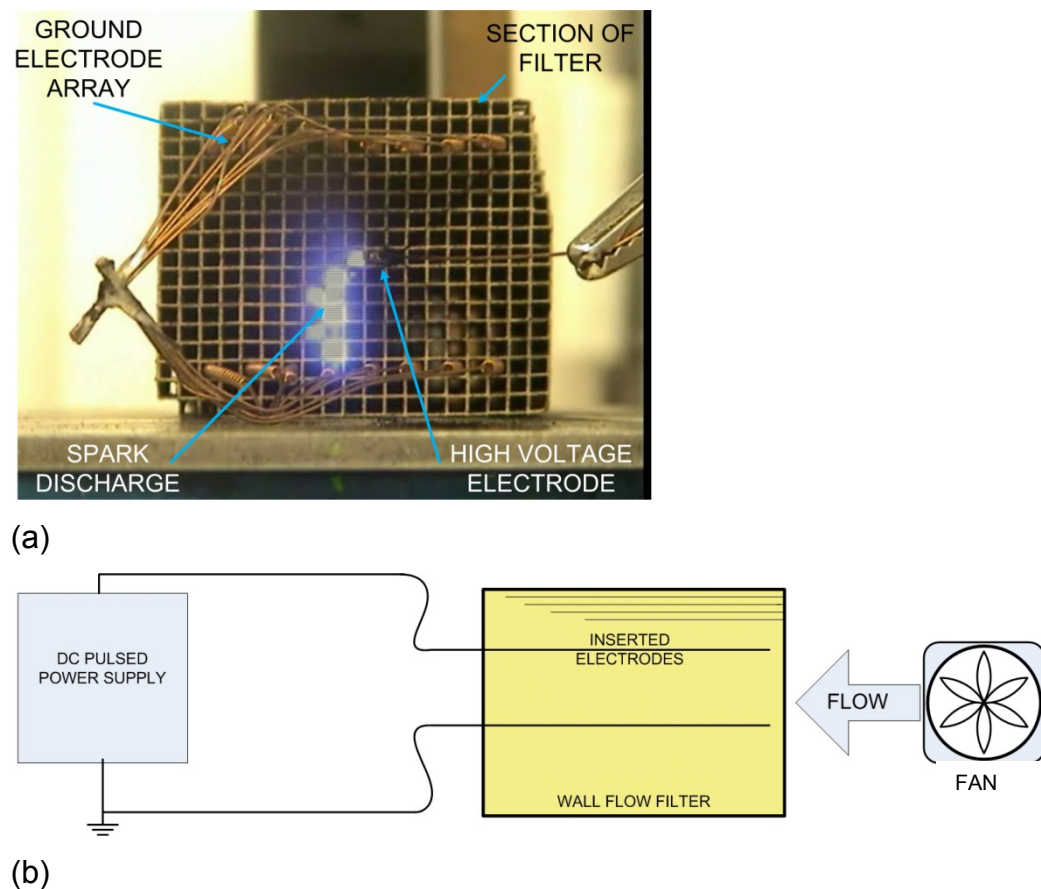

(a)

(b)

Figure 7.12 (a) Regeneration testing of the electro-acoustic effect. (b) Schematic of the regeneration testing

During the tests, small micro-discharges were observed between the electrodes due to parasitic current paths. The power supply could not provide a voltage high enough to achieve breakdown unless this current was reduced. The spark gap was used to act as a controlled switch that could be set to switch the power supply and capacitor to the electrodes at a preset voltage. The spark gap allowed the power supply to store energy on the capacitor without the influence of the leakage currents. When the capacitor voltage reached the spark gap breakdown voltage, the spark gap broke down and applied the voltage to the electrodes. Reliable breakdown was achieved by setting the breakdown voltage of the spark gap to above the breakdown voltage between the electrodes. Soot was removed by the resulting spark and this was carried out of the filter by the air flow.

The sparks were observed to automatically move to the regions of high soot loading similar to the Autoselective system and this was a useful property that could significantly reduce system complexity. In each test regeneration was allowed to continue until the discharge became 'stuck' in one place, then the regeneration distribution was observed. The regenerated areas were almost completely free from the caked soot layer although the deep bed filtered layer was still visible. Figure 7.13 is a photograph of the surface of the filter walls which shows that the area between the electrodes was uniformly regenerated in some cases. Pre- and post-weighing was used to show that the effectiveness and rate of the regeneration was more than 400 $gkW^{-1}hr^{-1}$ and 7 $g^{-1}hr$ respectively (about one order of magnitude better than the Autoselective system).
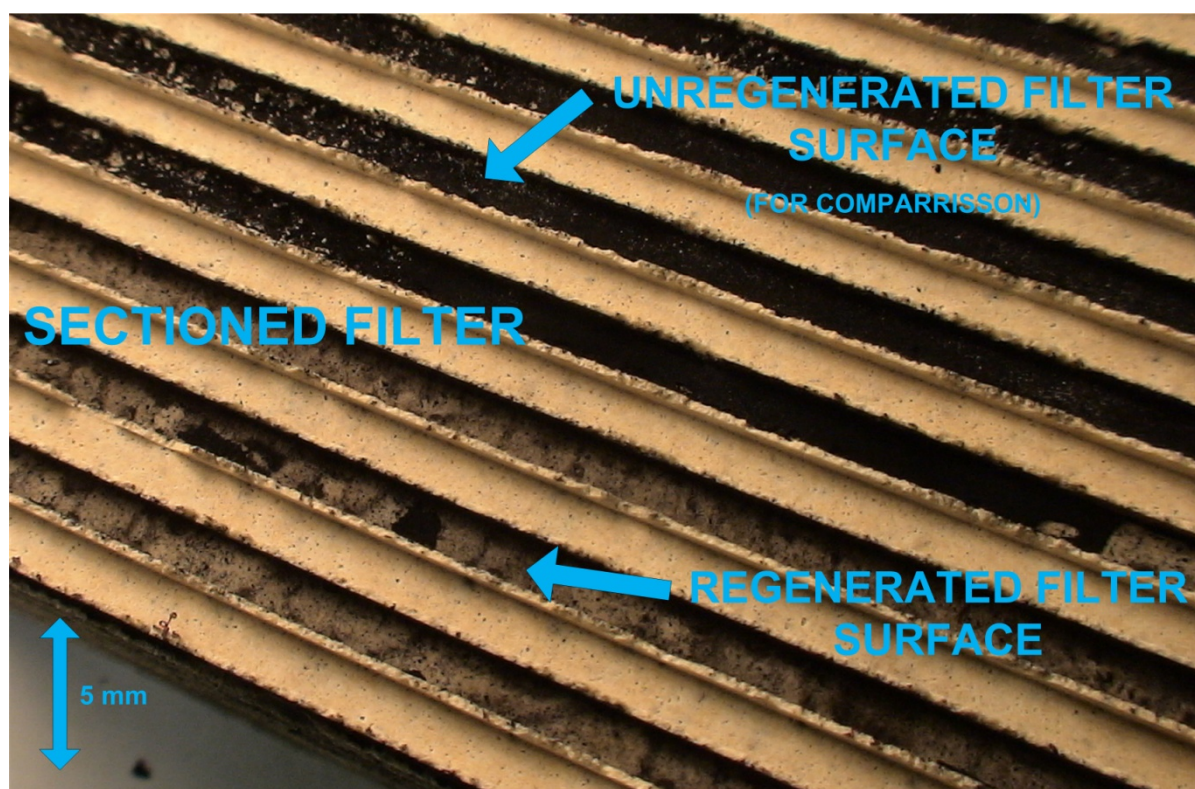
Figure 7.13 Regenerated surface on a filter section after the test

If these figures ware scaled for a system with 10 discharges fitted to a typical 4.4 litre heavy duty diesel engine, the resulting average power consumption would be 10 W. A filter loaded to 4 g.litre^{-1} could be regenerated in less than 4 minutes. It should be noted here that these figures were produced by an un-optimised power supply and it is likely that performance could be further improved. The conclusion of this set of tests was that the electro-acoustic effect could be used to enable an effective reverse flow regeneration system.

7.5 Non-Thermal Electro-Acoustic Regeneration Advantages

The electro-acoustic pulses produced by a high power discharge through a wall flow filter wall have been shown to be a potentially useful regeneration method. This novel method of removing the soot from a filter has a number of advantages which will be discussed in this section. This new regeneration strategy was called 'non-thermal electro-acoustic regeneration' or NEAR.

A key difference of NEAR to other types of regeneration strategy is that it requires reverse flow. In vehicle systems, this may be achieved by stopping the engine and reversing the flow using a blower. In many applications it is not practical to stop the engine, in these cases the reverse flow can be provided using exhaust valves and a second filter.

There are several advantages associated with the NEAR method, many of these are a result of the lower temperatures used compared to thermal regeneration. Thermal regeneration puts stresses on the wall flow filter which has led to the development of expensive thermally resistant filter materials. Thermal regeneration also requires a high power input due to the high soot oxidation temperature (> 550 °C) and low exhaust temperatures (~ 250 °C). In addition, because the soot is not burned by the NEAR regeneration system as it is removed, it does not contribute to the engine's CO_2 output, reducing engine emissions (albeit by ~ 0.1%).

In wall flow filter applications using thermal regeneration, the service interval of the filter is limited by the build up of ash within the filter and can range from 50,000 km to 300,000 km depending on the vehicle and engine duty (Johnson, 2006). Ash arises from the combustion of metals present in the fuel and engine oil and as a result of engine wear (Kittleson, 1998). The metals produce oxides and sulphates that gradually block the channels of the filter and increase the back-pressure of the system. Removal of the ash from the filter can not be achieved by heating and it usually requires filter removal to enable cleaning (e.g. using an FSX Equipment Inc. pneumatic DPF cleaning system). The ash particles are part of the particulates and removed from the filter with the soot using NEAR which alleviates the ash build up problem.

Finally, the values measured for regeneration performance are significantly higher than those for Autoselective regeneration and most other regeneration systems. An implementation of the NEAR system using a non-bypassed filter is illustrated schematically in Figure 7.14.
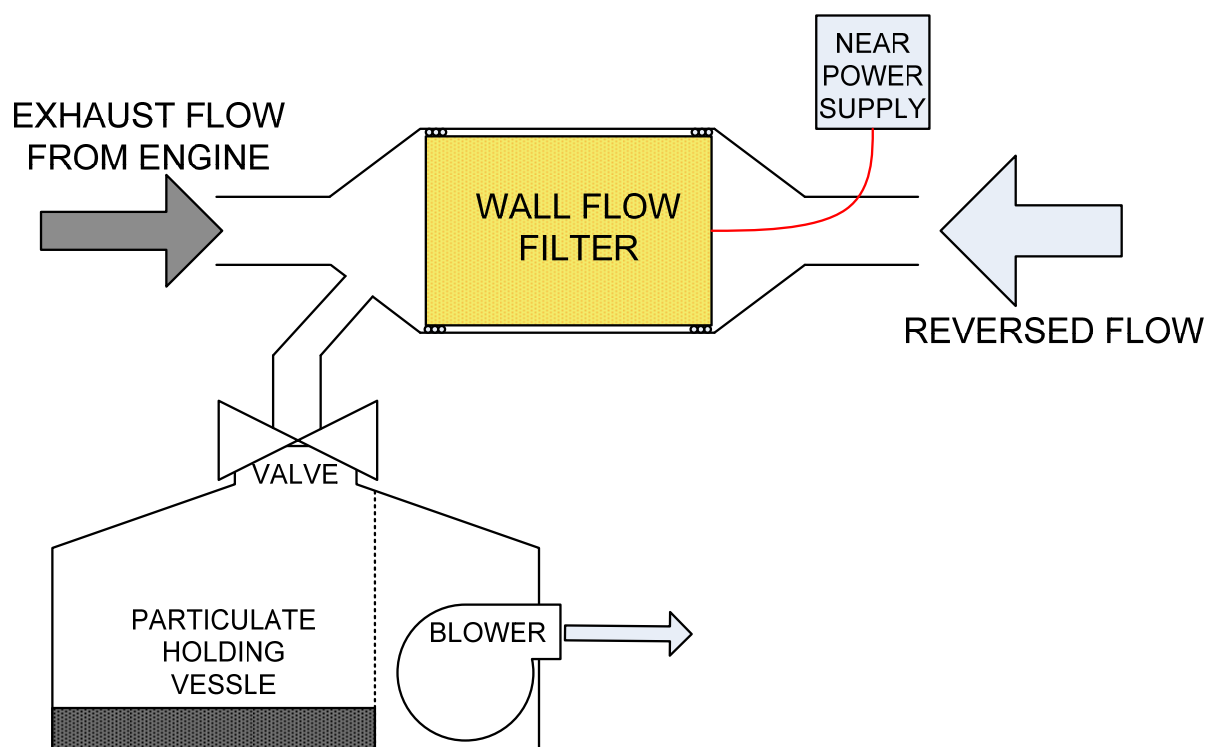
Figure 7.14 One implementation of the NEAR approach

7.6 NEAR Full Filter Flow-rig Testing

A full filter test was carried out on the flow-rig using a pre-loaded filter. The soot that was removed from the filter was trapped in a second clean filter placed downstream, Figure 7.15 shows the arrangement. The test used the same DC power supply as the other tests with an energy storage capacitance of 660 pF. The electrodes were arranged in a hexagonal configuration with the high voltage and ground electrodes 8 channel widths apart. There were 15 high voltage electrodes but only one power supply so the test was segmented into 15 short tests. This segmented test was equivalent to a single short test since the air flow alone would not remove the soot from the un-regenerating regions of the filter. Each of the test segments lasted 3 minutes during which time the power supply consumed 16 W from the mains (measured by a ProElec PL09564 power analyser). After the test was completed the filters were weighed to determine the soot removal, the back-pressure of the regenerated filter was also measured. The NEAR system removed 5.25 g of soot and reduced the filter back-pressure by 86% during the test. If 15 power supplies had

been used, the test duration would have been 3 minutes and the power consumption would have been 240 W.
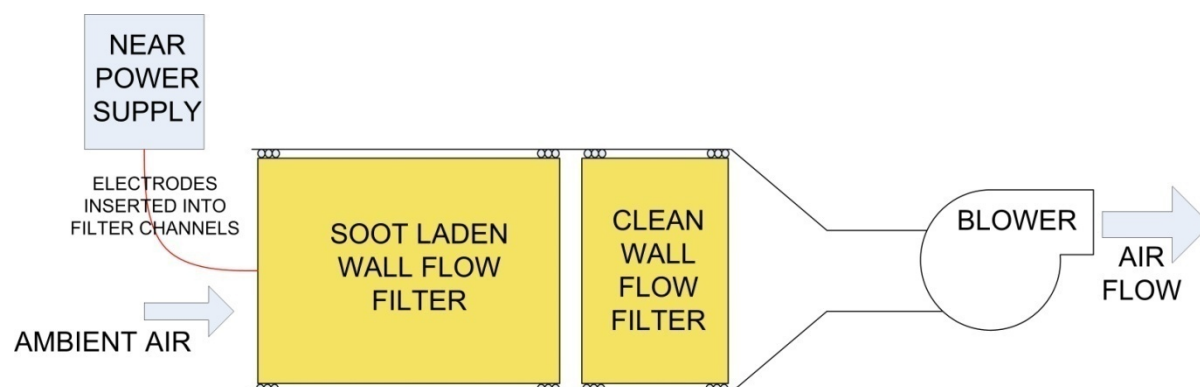
Figure 7.15 NEAR full filter demonstration test

After sectioning the filter the filter surface was inspected for damage and regeneration distribution. Most of the filter between the electrodes had no caked layer of soot, however, the areas between the ground electrodes and close to the end plugs still showed significant amounts of PM. There was small amounts of filter damage observed in the form of some pin holes ~100 µm across, the small diameter of which would be unlikely to reduce the filtration performance of the filter. Figure 7.16 shows an example of the damage observed which is likely to have developed from an existing oversized pore. The pin hole can be distinguished from other forms of ambient damage by the melted edges.
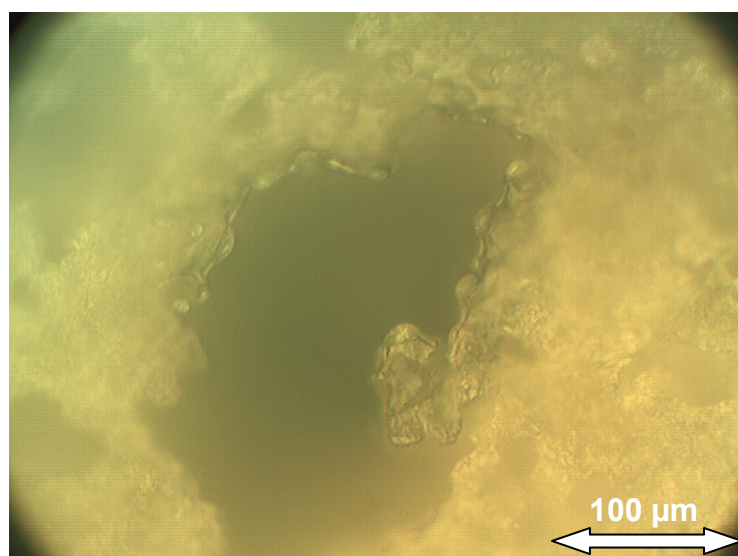
Figure 7.16 Damage observed to the filter surface during the flow-rig NEAR test

This test shows that the NEAR regeneration system can achieve excellent regeneration performance. This experiment used settings that were not optimised and a power supply which was designed for reliability rather than efficiency. It is likely that significant improvements can be made to all aspects of the NEAR system especially in terms of effectiveness, rate and power supply size.

7.7 Chapter Conclusions

The cause of particulate re-entrainment is predominantly due to the forces created by expanding gas within the filter walls caused by the rapid heating of the air by the discharge. This process is known as an electro-acoustic effect. There are also electrostatic forces created by the interaction of electric fields with the particulates. These are not sufficient to break the adhesive forces holding the particulates to the filter. Electrostatic forces may be part responsible for the diffusion of particulates through the filter by applying oscillatory forces on the free particulates inside the filter wall. The movement of the soot through the filter wall is strongly affected by the air flow direction.

Electro-acoustic forces can be used to deliberately dislodge soot from the filter walls so that it can be carried out of the filter by a reverse air flow. A system was proposed that used a DC power supply to remove soot from a filter with a small number of inserted wire electrodes and testing on a flow-rig showed better performance than the Autoselective system. The main obstacle for the implementation of the NEAR system is the need to reverse the flow through the filter during regeneration. Certain diesel engine applications may be able to use an 'end of shift' regeneration system that purges the filters at intervals with the engine stopped. For these applications, benefits such as low power and no ash accumulation can be realised. For other applications, a dual filter bypassed exhaust system could be used.

8. Flow-rig and Engine Testing

Much of this research concentrated on producing a PM after-treatment solution for a heavy duty diesel engine. Flow-rig and on-engine tests were used throughout the project to test the developments made. This chapter describes the development of a working prototype regeneration system using the Autoselective technology. The proceeding sections discuss the flow-rig and on-engine testing and the contribution they had to the research. The key findings resulting from each test are also described.

8.1 Initial Linear Electrode Trial

Early in the development of the Autoselective regeneration system, a full filter on engine test using a linear electrode array was performed to determine the current system performance. The test used the fixed voltage power supply and the newly designed frequency sweep device which ensured all the transformers operated at resonance for part of the time. An on- and off-time of 45 ms and 55 ms was used respectively in conjunction with a power supply (i.e. Variac) voltage of 180 V. The test used 10 feed-throughs made from silicone high voltage cable and a borosilicate glass plate, a photograph of the arrangement is shown in Figure 8.1.

High voltage feed-through arrangement

Exhaust system access to filter
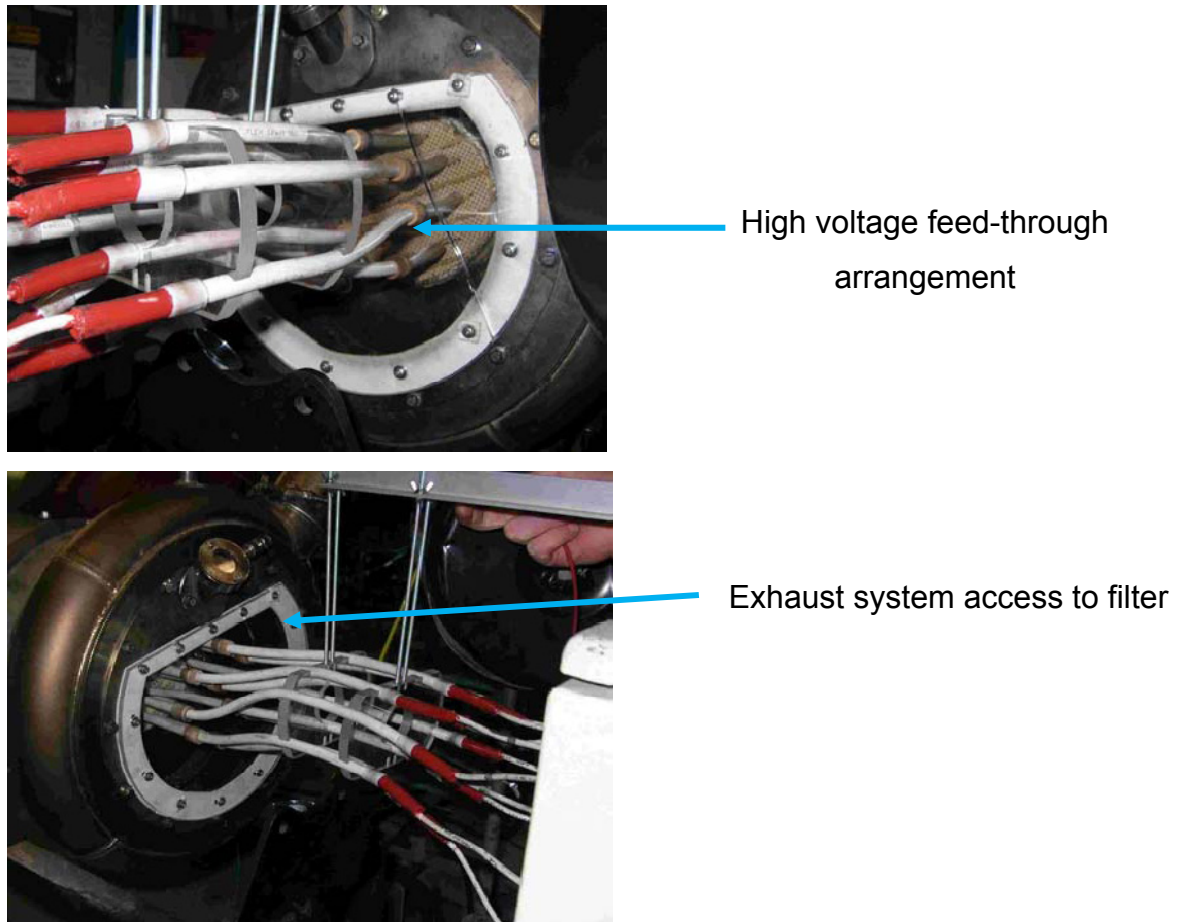
Figure 8.1 Feed through assembly

The test began with a filter PM loading phase lasting for 200 minutes followed by a regeneration phase of 120 minutes. This was then repeated for 30 minutes and 43 minutes respectively before the regeneration system was switched off. A graph of the back-pressure versus time is shown in Figure 8.2. The success criteria was to produce a constant or falling back-pressure whilst the regeneration system was switched on indicating a regeneration rate that matched or exceeded the engine PM production rate.
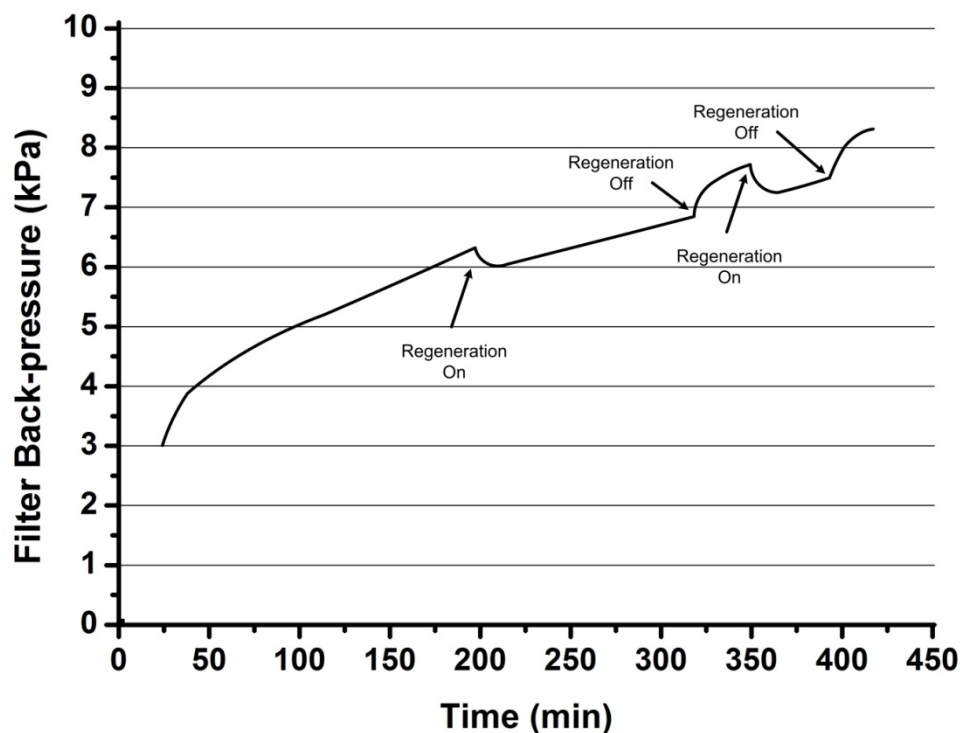
Figure 8.2 Back pressure versus time for the linear electrode test

The results showed that a reduction in back-pressure occurred during the 15 minutes after the regeneration system was switched on during each regeneration phase. The increasing back-pressure after 15 minutes confirmed that the regeneration rate had fallen below the engine PM production rate. There was a reduction in the rate of back-pressure increase during the regeneration phases as shown by the difference in gradient of the back-pressure curves at 250 minutes and 150 minutes. The back-pressure characteristic could be explained if small sections of the filter were being cleaned very rapidly and kept clean while the system was on. These sections could be modelled as a separate regenerating filter in parallel to a non regenerating filter. The filter that was not being regenerated would gradually fill up with soot leading to the overall increasing back-pressure observed. If this model is used, the regenerating part of the filter is only 5% of the total filter volume indicating poor regeneration distribution.

The filter used for the test was sectioned and unfortunately excessive glassing filter damage was observed around the high voltage electrodes. Flow mapping of the filter

indicated that the discharge had become fixed along particular routes thus explaining the poor regeneration distribution. This was a side effect of filter damage since the damaged hot regions remained conductive whilst the discharge was switched off. This encouraged the discharge to re-ignite at the site of damage reducing auto-selectivity. After this engine test, the research concentrated on finding new ways of improving the distribution of the regeneration whilst avoiding filter damage.

## 8.2 Subsequent Research Findings

8.2.1 Electrode Findings

Early research had identified the need to place the electrodes within the filter volume by inserting from the down-stream side to avoid the parasitic losses of the caked soot layer (Proctor, 2007). The parasitic losses made controlling the Autoselective discharge difficult. Electrodes that were placed down-stream of the filter did not come into contact with the caked soot layer and were able to produce an Autoselective discharge.

The electrode shape and position were found to be critical for correct Autoselective operation, this part of the research is described in more depth in Chapter 5. The electrode material was not found to be important and copper was used for the majority of tests due to its ease of soldering. The distance between the electrode and the channel wall was found to affect axial discharge distribution especially for electrode arrays with short electrode spacing. This was expected since electrical breakdown between conductors is more likely to occur where they are closest because of the higher electric field. The solution was to centre the electrodes in the channel thus providing an even spacing around them. In practice this was most easily achieved by using a spring electrode with an outer diameter equal to the channel width. Spring electrodes were used for 100 cpsi (cells per square inch) wall flow filters to make regular contact with the channel wall and provide even axial distribution.

The electrode positions of the ground and high voltage (HV) electrodes within the filter had an effect on the radial regeneration distribution. Increasing the channel

spacing between the ground and HV electrodes led to better regeneration rate and effectiveness but also to higher electrode voltages and poor regeneration distribution. Two basic types of electrode geometries were identified, namely the 'hexagonal' arrangement and the 'linear' arrangement. Linear electrodes, as used in the previous engine test, provided more even voltage distribution leading to more complete regeneration of regions between the electrodes. Linear electrode configurations also required more electrodes and often showed filter damage due to adjacent electrodes discharging to each other. The hexagonal array (hex array) required fewer electrodes but had a decreasing discharge current with increasing radius from the high voltage electrode. This led to poorer regeneration distribution further from the central high voltage electrode. Reducing the electrode spacing to a single channel for either the hex array or the linear array produced the same pattern known as the checkerboard array, the electrode array types are illustrated in Figure 8.3. The checkerboard array used the maximum possible number of electrodes and had the lowest regeneration performance. The checkerboard array did, however, offer the lowest electrode voltages and best regeneration distribution.
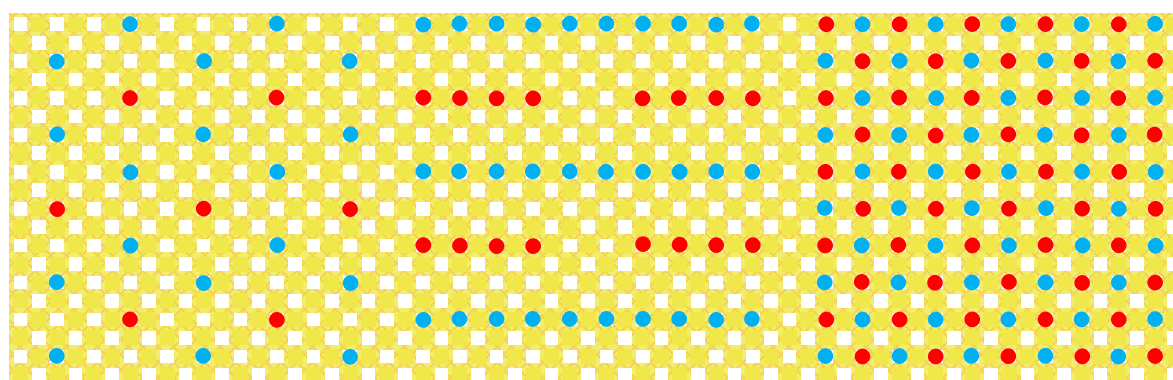
(a) Hexagonal   (b) Linear   (c) Checkerboard

Figure 8.3 Examples of the hex, linear and checkerboard electrode arrangements as observed from the downstream filter end. Red represents high voltage electrodes, blue represents grounded electrodes

The number of electrodes for the checkerboard array was considered to be of manufacturing significance. Electrode arrays consisting of hundreds of electrodes would be difficult to reliably and cheaply manufacture. A summary of how the electrode arrays affect system parameters is shown in Table 8.1.

	Hexagonal Array	Linear Array	Checkerboard Array
Number of Electrode Wires	100	200	600
Breakdown Voltage (kV)	20	15	2
Regeneration Distribution	Poor	Good	Excellent
Regeneration Performance	Good	Good	Poor

Table 8.1 Comparison of electrode geometries, all value approximate and dependant upon channel spacing used (based on 5.66" diameter 100 cpsi wall flow filter)

8.2.2 Discharge Considerations

The penetration of external discharges into the filter was found to be a function of voltage and frequency, high frequency (> 300 kHz) discharges could not penetrate the filter due to the losses caused by electrode capacitance as described in Chapter 3. However, low frequencies required larger magnetic components and made the system bulky. The frequency used for the previous linear electrode test was ~ 20 kHz and this was a good compromise between size and losses. The voltage required to achieve a discharge penetration sufficient to bridge the gap between the linear electrodes used for the previous engine test was ~ 15 kV. This was shown to be primarily dependant on the breakdown voltage between the electrodes and was a function of electrode spacing (Chapter 5).

8.2.3 Discharge Control Method

The Autoselective discharge current needed to be controlled accurately in order to prevent filter damage. This was a high priority of this research and several control methods were tested. After the first linear electrode engine test, a current of 10 mA was shown to be optimal (as discussed in Chapter 4). The high voltage transformer was used as the primary current regulation mechanism in the plasma power supplies

which was set by the drive voltage to the transformers. The drive frequency also needed to be close to resonance in order to achieve the voltages required for breakdown (as described in Chapter 3). When driving multiple transformers, the spread of individual resonances was too wide to use a single frequency drive. A frequency sweep proved an effective way of achieving breakdown across a bank of individually tuned sub-circuits.

The previously described linear electrode test used a fixed voltage half-bridge inverter that was switched on and off asynchronously using an external timer circuit. The problem with this type of power supply was that the transformer drive voltage was constant and could only be changed using the external variable AC power source (e.g. a Variac). The linear electrode array had a breakdown voltage (~ 15 kV) that required a 180 V amplitude transformer drive level, this resulted in a discharge current of ~ 30 mA which is well above the damage free operating range identified in Chapter 5. The checkerboard array had a lower breakdown voltage allowing the transformers to be operated at the drive level needed to regulate the discharge to 10 mA. The checkerboard array was subsequently investigated and the testing is described in the next section.

8.3 Full Filter Checkerboard Flow-rig Test

Flow mapping consistently revealed regeneration surrounding the high voltage electrodes. The checkerboard electrode array, shown for a full filter implementation in Figure 8.4, ensured every soot laden channel was adjacent to a high voltage electrode. It was expected that this electrode configuration would therefore provide 100% regeneration distribution. On- and off-time optimisation had shown that the best performance without filter damage was achieved with 40 ms on-time, 50 ms off-time and 10 mA of discharge current (details in Chapter 5).
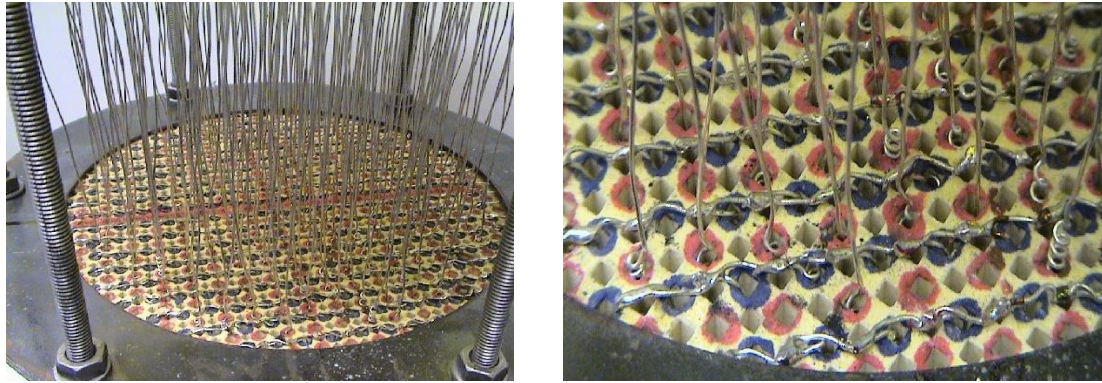
Figure 8.4 The checkerboard electrode geometry (coloured markings were to aid assembly)

The checkerboard array had the lowest breakdown voltage possible since the electrodes were as close as possible. The spring electrodes were used for this test to improve axial regeneration distribution. The total number of HV electrodes was higher than the number of available high voltage power supply outputs so the test was segmented and the powered electrodes were moved between segments. The back-pressure, see Figure 8.5, was measured during the test and the flow rate was kept at 220 kg.hr^{-1}, which was a level typically for the exhaust flow from a 4.4 litre heavy duty diesel engine.

Figure 8.5 Back pressure drop during checkerboard electrode testing

The back-pressure of the filter was reduced from 7.8 kPa to 3.2 kPa during the test. The drop in back-pressure corresponded to regeneration of approximately 53% of the filter. This was a significant improvement over the linear electrode array (5 %). The filter was sectioned and showed no melting damage and the regeneration was uniform throughou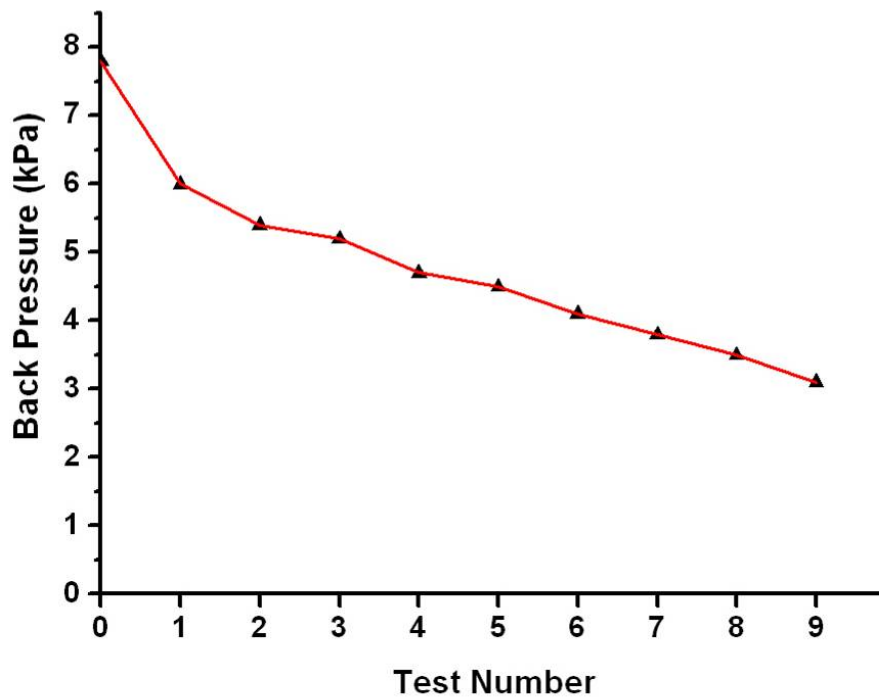t the filter volume. A per-channel regeneration distribution issue was observed which was called the 'wall-effect'. The wall-effect was characterised by the channel walls adjacent to the discharge path showing poor regeneration (see Chapter 5 for details). Tests showed this was because the discharge preferred to pass through the gas within the channel rather than through the soot layer. The wall-effect could be improved by using lower discharge currents, lower frequency discharges and higher flow rates. It was not known how the wall-effect would affect the regeneration system when operated on an engine. It was possible that the un-regenerated sections would gradually increase in loading until the discharge began to regenerate then, restoring auto-selectivity. An engine test of the checkerboard array was performed to answer this question.

8.4 On Engine Checkerboard Test

Following the successful flow-rig test, an engine test was planned using the same settings and electrode arrangement. A full filter test would have required a power supply with 75 high voltage outputs, however, in order to avoid building additional power supplies, the test used a third of a 5.66" diameter wall flow filter.

An exhaust by-pass rig was fitted to the engine to provide flow control through the filter section and was essential to ensure the engine could be operated under normal mid-load conditions. Two thirds of the exhaust flow was diverted around the filter using an exhaust valve. The filter was loaded with approximately 3.5 g.litre^{-1} of PM before starting the regeneration. The back-pressure dropped when the regeneration system was turned on and was kept stable (at constant flow) during the test indicating that the regeneration rate was equal to the soot input into the filter. The detailed back-pressure and flow rate for the test are shown in Figure 8.6.
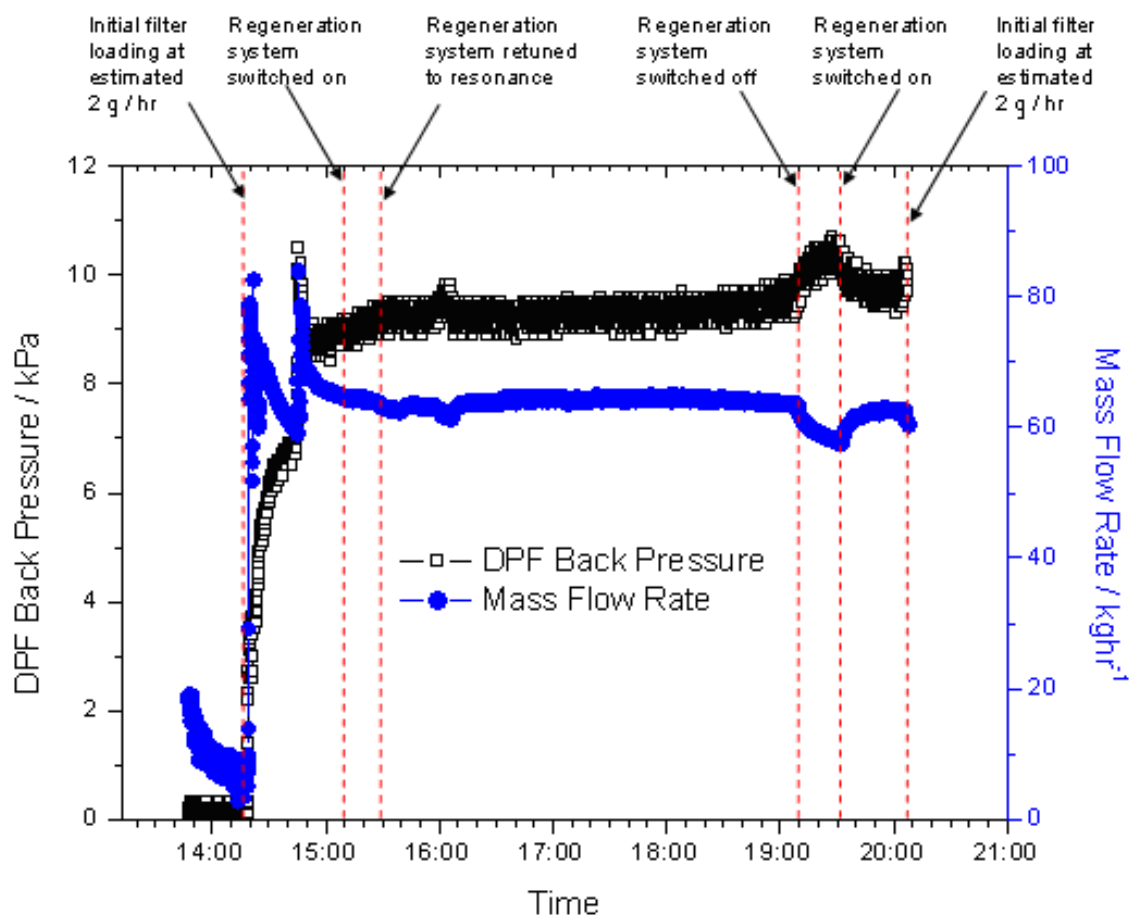
Figure 8.6 Back-pressure and flow rate during the checkerboard on engine test

This was a successful test since the Autoselective system had been shown to be capable of operating as a workable regeneration system. The wall-effect had not resulted in the failure of the system showing that it could reach a balance point. Sectioning of the filter showed a thickened soot layer on the affected walls, however, no channel had become completely blocked with PM.

The main concerns were the power consumption (> 2 kW for a full 5.66" diameter filter), the large number of inserted electrodes (approximately 600 for a full filter) and the number high voltage feed-throughs (approximately 75 for a full filter). The high voltage feed-through arrangement is shown in Figure 8.7. Three times the number of high voltage wires would have been required for a full filter test. In addition, the silicone insulation used for the engine tests would be unsuitable for the full exhaust temperature range of a diesel engine. If each feed-through was itself made from ceramic, like automotive spark plugs, the assembly would have been larger.
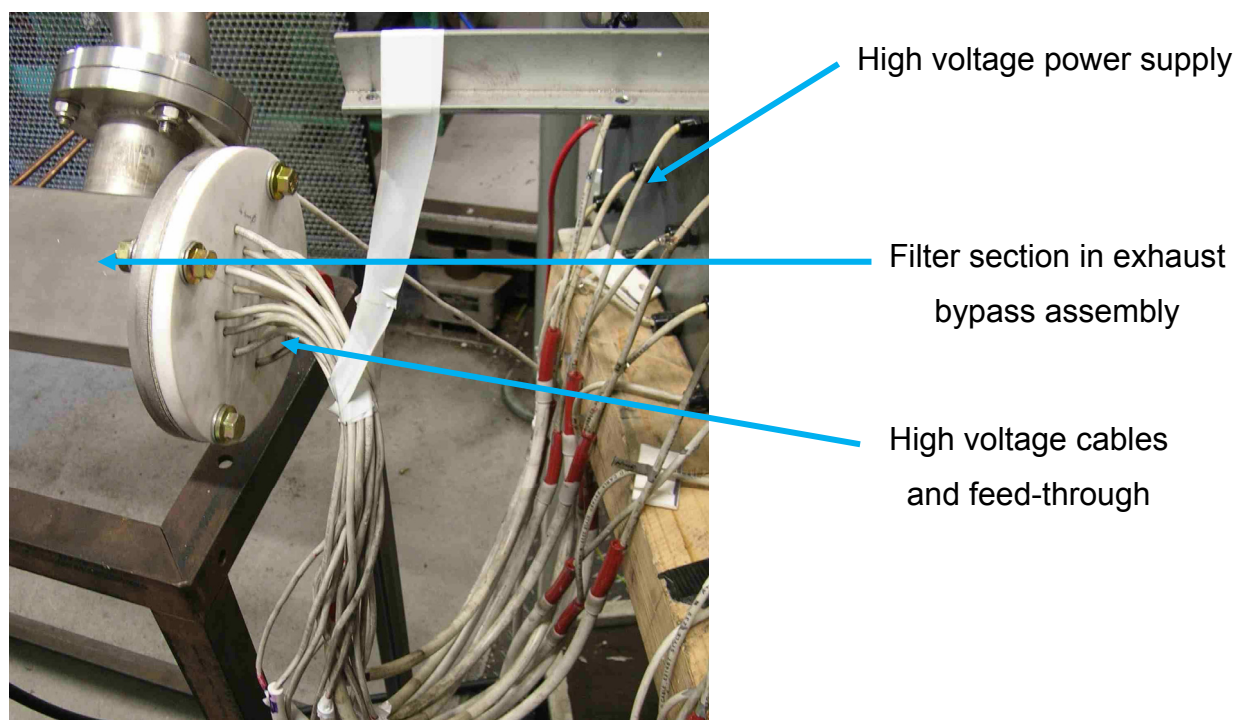
Figure 8.7 High voltage feed-through arrangement used for engine test

8.5 Subsequent Research Findings

One of the difficulties to implementing the Autoselective technology was making the whole system practical to be fitted to a production engine for use in a vehicle environment. The ultimate aim was to produce a system for a heavy duty diesel vehicle application. The main factors were reliability, efficiency, size and cost (including assembly complexity). The checkerboard tests showed that the Autoselective system could be made into a regeneration system for a heavy duty diesel application, however, the system was bulky and currently unsuitable for vehicle operation.

The cost of the research was not normally a factor in the decisions made. However, the cost of the final system was important and the main contributor to cost was system complexity. The connection between the high voltage power supply and the electrodes presented the main challenge. Historically high voltage insulation for automotive applications would be provided using a ceramic feed-through insulator not unlike a spark plug. This would provide a high temperature, high voltage,

mechanically strong and gas tight insulator to pass electrical power into the exhaust system. The potentially high costs associated with the electrical feed-through led to research into reducing the number of high voltage wires entering the exhaust system and DPF canister. A compromise between regeneration performance and electrical feed-through requirements was made with the final number of conductors reduced to 20. The electrode configurations were re-investigated in an attempt to reduce both the number of feed-throughs and the overall number of electrodes whilst maintaining the regeneration performance of the checkerboard array. The reason the previous linear electrode test failed was because of filter damage and poor distribution. A new power supply and phased electrode method was designed to overcome these problems.

8.5.1 Transient Power Supply

The damage occurred during the previous linear electrode tests (Section 8.1) because the discharge current was ~ 30 mA which was well outside the damage free operating region identified and discussed in Chapter 5. The current could not be reduced to 10 mA because the fixed transformer drive voltage would be insufficient to cause breakdown between the electrodes. A novel power supply, described in Chapter 3 and Appendix I, was used to allow transient control of the transformer drive voltage in addition to the frequency sweep and on- and off-times. This allowed the transformer drive to be increased for several milliseconds at the start of the on-time to allow breakdown. The transformer drive voltage was then reduced to allow operation at the correct current level.

Further testing revealed that at 10 mA the discharge could extinguish prematurely during the on-time thus lowering regeneration performance. This was addressed by using a second frequency sweep half way through the on-time which re-ignited any extinguished discharges. The final switching waveform had a sweep from 20 kHz to 10 kHz lasting 8 ms (at 170 V drive) followed by 14 ms of fixed frequency operation (20 V to 80 V drive; frequency dependant on electrode configuration) then another shorter sweep lasting 4 ms followed by 14 ms constant operation. This sequence was

repeated after a delay of 50 ms to produce a 40 and 50 ms on- and off-time respectively.

8.5.2 Phased Electrodes

Testing of the linear electrode arrays revealed that there were frequently discharges between the high voltage electrode rows. These discharges could potentially carry twice the discharge current and lead to filter damage. The adjacent electrode rows were phased so that they did not operate simultaneously. This prevented the discharges between the rows which provided better auto-selectivity, distribution and prevented damage.

The new transient power supply and optimised linear electrode array were tested in a flow-rig to compare the performance to the checkerboard array. The electrode spacing was increased until the power supply was unable to break down the gap at a ~ 10 channels. At this spacing the discharge did not fully undergo transition to the glow discharge state. The electrode spacing was reduced further until the correct Autoselective discharge was restored at ~ 3 channels. The high voltage (HV) electrode rows spacing was also reduced until optimal cleaning of the area between the HV rows was achieved. With the optimised linear array the system now required only 20 outputs for a full filter and ~ 30 % the total number of electrodes of the checkerboard array.

8.6 Flow-rig Linear Electrode Test

The optimised linear array was tested on a full filter flow-rig test using the transient power supply and the optimised settings discussed in the previous section. The electrodes were driven with frequency sweeps and a steady-state current of 10 mA with an on- and off-time of 40 ms and 50 ms respectively. Downstream open access, see Figure 8.8, was used to view the regenerating discharges and allow connection of the high voltage electrodes.

Filter protruding from flow-rig system

High voltage wires attached to inserted electrodes
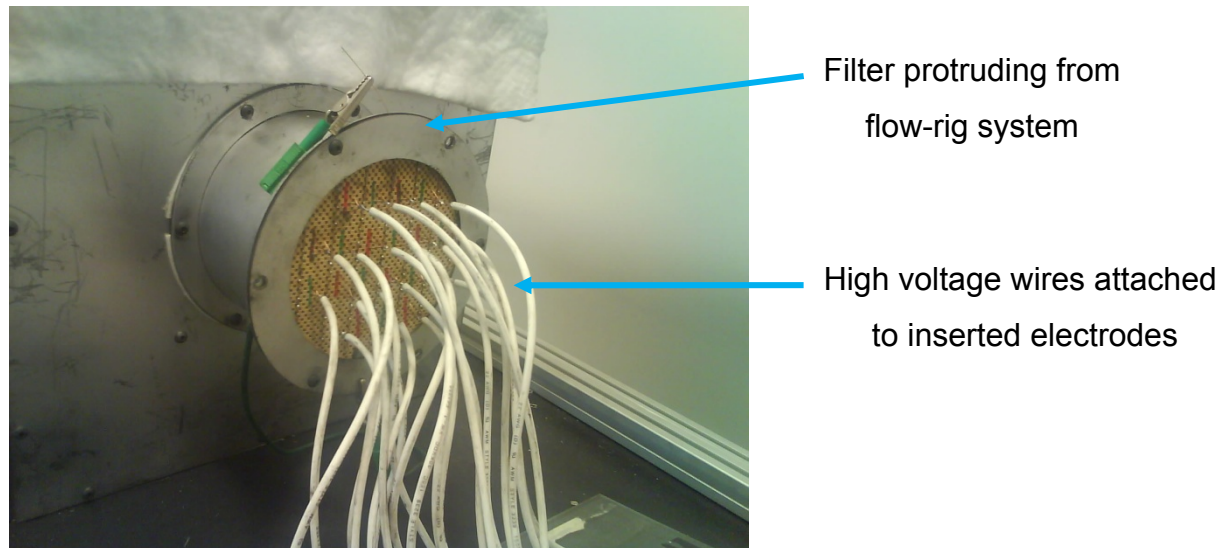
Figure 8.8 The flow-rig test downstream side showing high voltage wires and inserted electrodes

The tests showed that a regenerating discharge could be established between the electrodes under flow conditions. A flow-rig test using a pre-loaded filter was used to determine the performance of the wide spaced electrode arrangement under engine like conditions. The flow-rig emulated the typical exhaust temperature and flow rate of the diesel engine used for the on-engine testing. As shown in Figure 8.9, the back-pressure dropped when the regeneration system was switched on and continued to drop during the test. The filter was flow mapped after the test to determine regeneration distribution around the high voltage electrodes; see Figure 8.10.
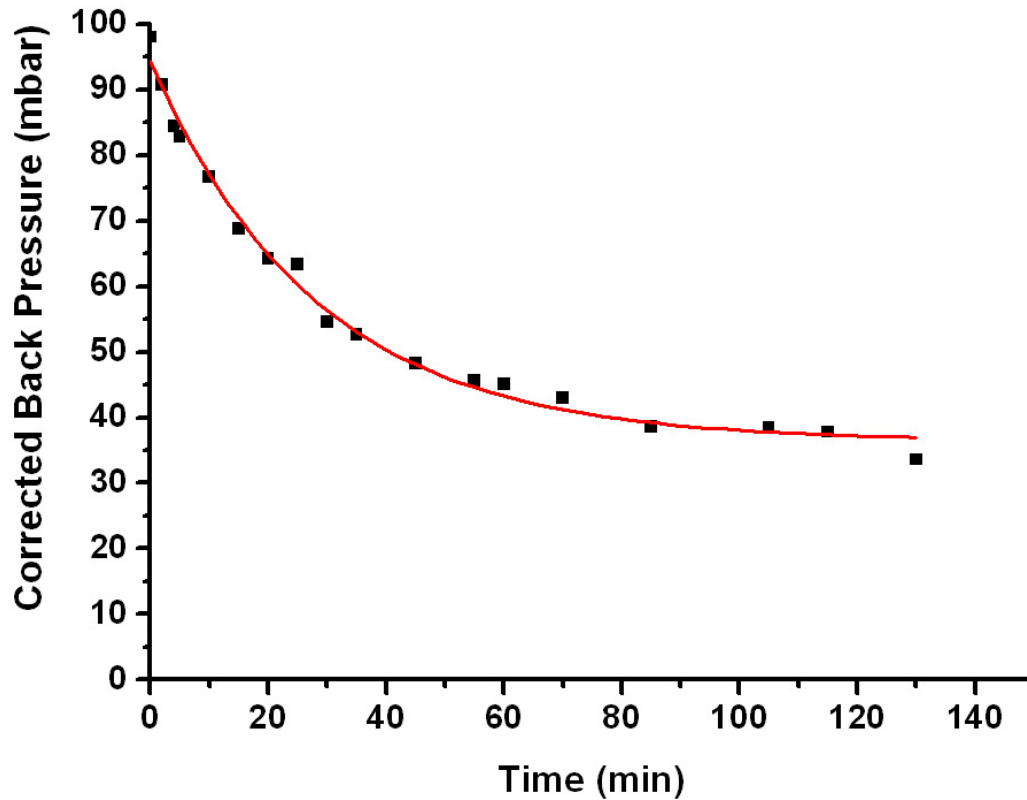
Figure 8.9 Back pressure plot of flow-rig test
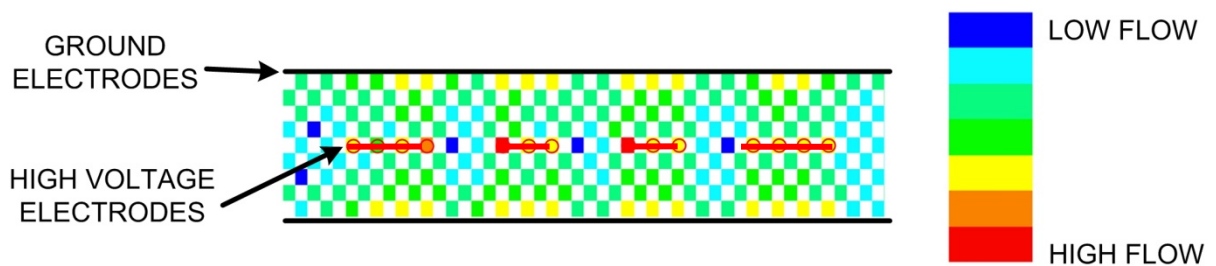
Figure 8.10 Flow map of the linear electrode arrangement

The filter showed no visible damage when sectioned after the test. Regeneration distribution was verified visually and using flow mapping. A back-pressure reduction of 66% was achieved during the 2 hour test. The new power supply and linear electrode array had improved regeneration performance to the checkerboard tests in terms of regeneration distribution, power consumption and simplicity. The new settings were ready to be tested on an engine.

8.7 On Engine Linear Electrode Tests

The wide spaced linear electrode test was repeated on a test bed engine. This engine test used identical power supply settings and electrode arrangements to the flow-rig test. The filter was loaded with soot with the electrodes inside the filter with the regeneration system switched off. The regeneration system was switched on after the filter reached a soot loading of approximately 3.5 g.litre^{-1}. The filter back-pressure was monitored to establish the performance of the regeneration system. The engine operating point was used to regulate the soot input into the filter and the flow rate. These were verified using a combination of manufacturer engine maps and exhaust sensors. The filter back-pressure for the first test is shown in Figure 8.11. The results show that the regeneration system did reduce the back-pressure initially and that the rate of back-pressure increase was also reduced during the whole test. This was accomplished with a total electrical power input of 520 W. Filter sectioning showed no filter damage or significant blow-through. However, the regeneration system performance decreased quickly within the first 30 minutes.
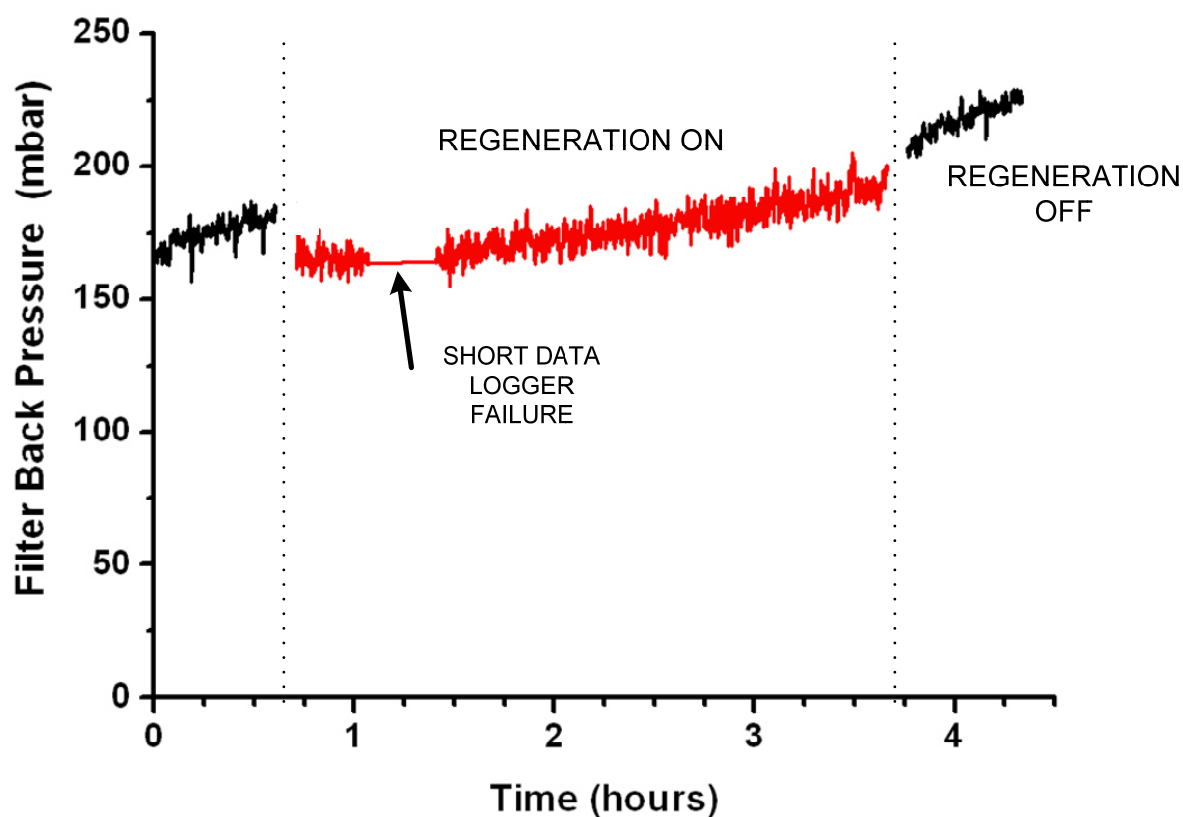

Figure 8.11 Filter back-pressure during test

It was suspected that the filter front face was becoming clogged with soot and allowing the discharge to occur outside the filter without regenerating. This observation had been made on other occasions when the front face became clogged with a continuous layer of soot effectively shorting it to the grounded filter canister. The external parasitic discharges shunt the main discharge current and prevent regeneration. An example of the previously observed parasitic discharge path is shown in Figure 8.12. This discharge path could be prevented by wiping the front face of the filter to remove the caked soot layer. The first test was repeated with the front face of the filter being wiped at 15 minute intervals. Although a temporary reduction in back-pressure was observed, the results showed that wiping the front face did not fully restore regeneration performance each time.
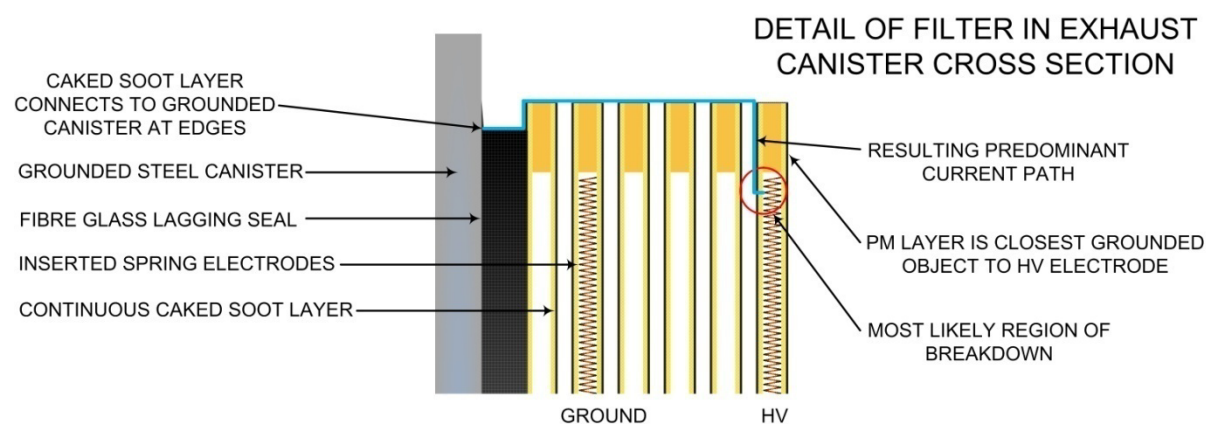
Figure 8.12 Path of observed parasitic discharges

The proposed parasitic discharge explanation did not fully explain the difference in results between the flow-rig and engine tests. In order to fully understand the differences, another test that allowed optical access of the regenerating discharge was undertaken. This test revealed that the discharge started normally when the system was switched on but quickly stopped after approximately 5 minutes. Stopping the engine quickly restored regeneration over a similar time scale. The engine test also revealed the existence of parasitic discharges on the front face of the filter as shown in Figure 8.12. The main differences between the flow-rig and engine trials were the gas composition, PM input and the front face soot layer. In the engine test, the front face soot layer was connected to ground by the continuous layer, but this is not true for the flow- rig since the layer is broken. In the engine test, the exhaust flow

also had a higher humidity, CO_2 content and particulate level. Further testing was carried out to determine the effect of the exhaust flow and particulate loading on the front face soot properties.

The results showed that the resistance of the soot layer decreased as the filter soot loading increased, as expected. The exhaust back-pressure is likely to have a similar effect since compressive forces on carbonaceous particulates are well known to cause drops in resistivity due to reorganisation; this effect was used extensively to produce the early 'carbon' microphones. The results also show that stopping the engine causes an increase in measured resistance which is reversed when the engine is re-started. This transient change in resistance occurred over the same timescale as the observed reduction in the number of regenerating discharges. Further measurements revealed that the change in resistance was strongly linked to the temperature of the soot. Increasing the temperature decreases the soot resistivity, shown in Figure 8.13, as observed by Williams (2007).
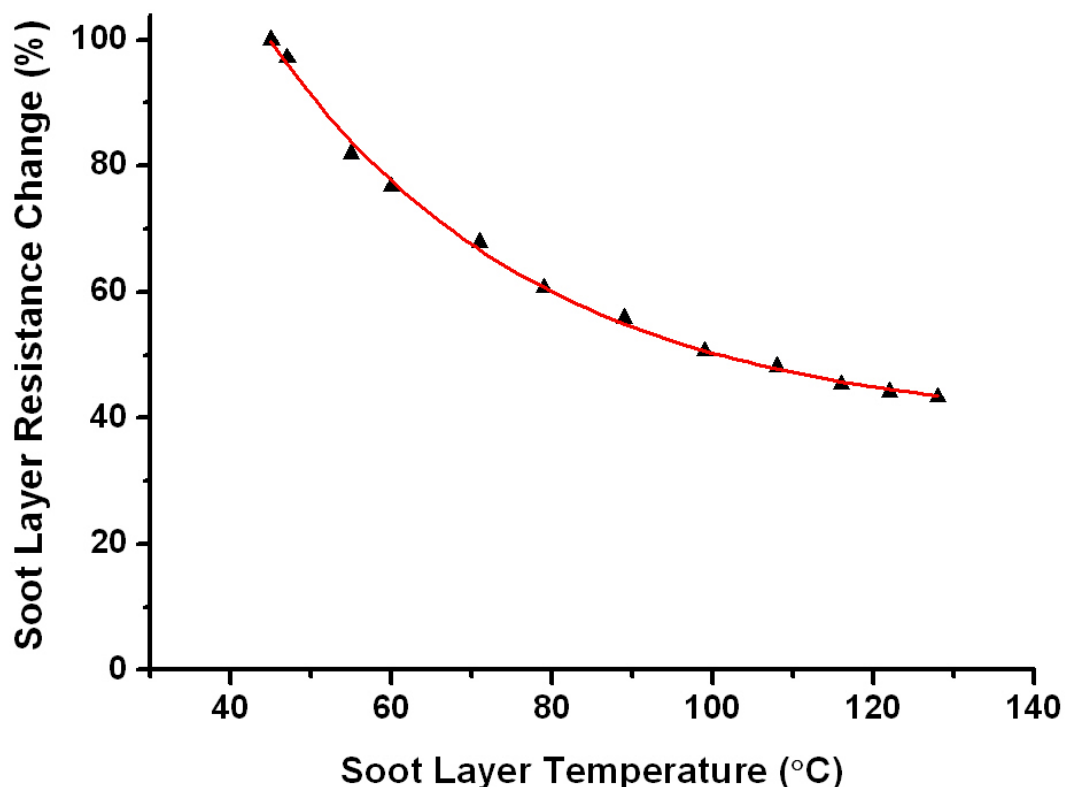
Figure 8.13 Change in soot resistance versus temperature

The drop in resistance of the soot layer caused the parasitic losses of the filter to increase, the parasitic components are illustrated in Figure 8.14. The resulting additional losses prevented discharges forming and shunted existing discharge current. This resulted in a reduction of the number of regenerating discharges.
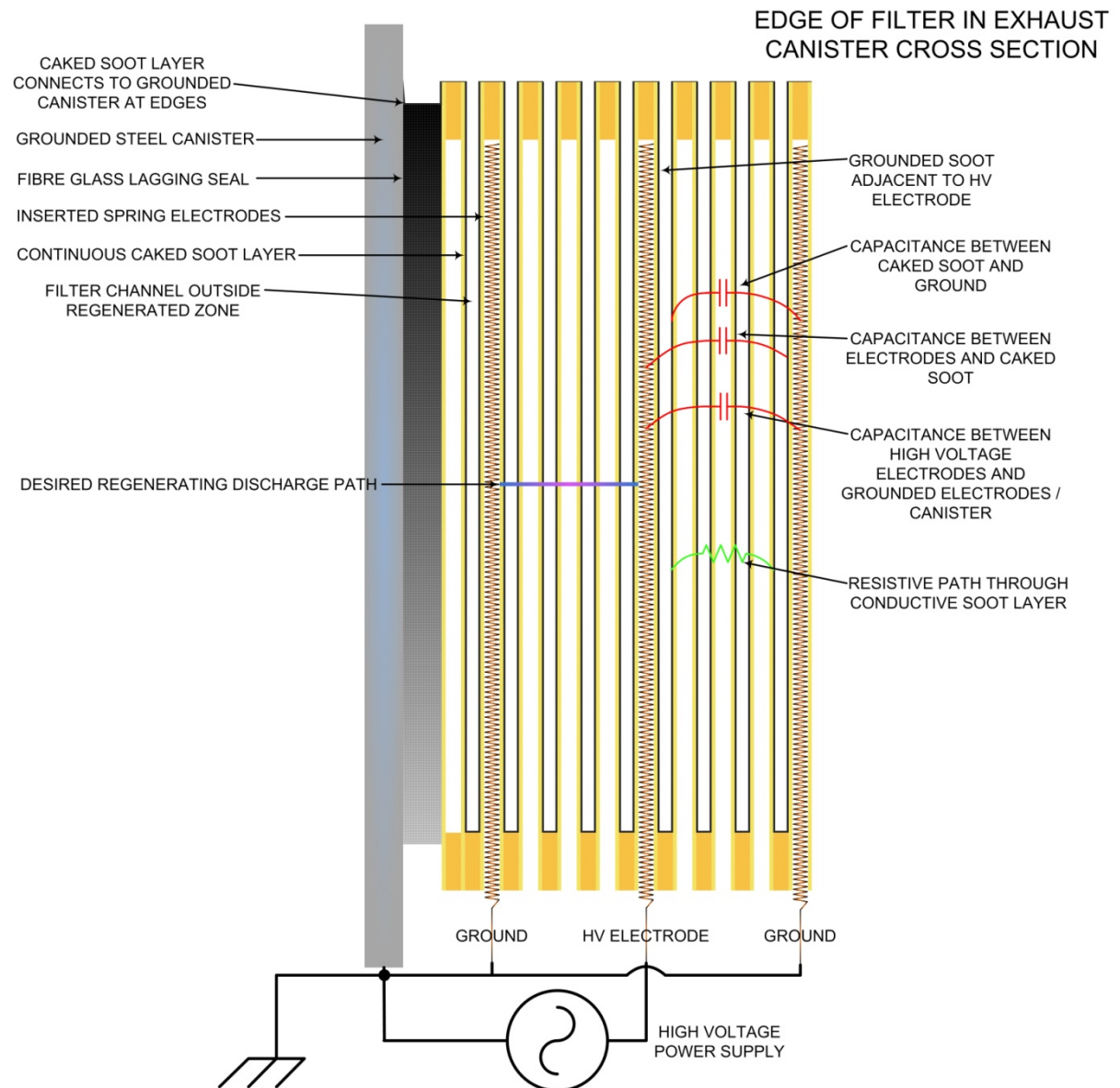
Figure 8.14 Schematic of the filter cross section with electrodes showing parasitic characteristics

Comparing the results of the flow-rig and engine trials show that the discharge was significantly affected by changes in soot layer characteristics. In the flow-rig, small discharges were observed on the front face of the filter during regeneration. In this

case, there were no particulates in the gas flow, which led to these regions becoming gradually regenerated resulting in improved regeneration performance. Figure 8.15 clearly shows the bright rings around the high voltage electrodes where soot has been removed. There was a distinct lack of such regeneration around the ground electrodes indicating that the parasitic discharges were not continuous. The discharges were a result of the peak instantaneous voltages on the high voltage electrodes which resulted in capacitive and resistive current flow through the soot layer. This also explains the importance of grounding the front face soot layer. If the front face is grounded, more current would be able to flow through this path resulting in greater losses. The engine test did not show evidence of these regenerated regions which indicates that the discharge was not able to regenerate the front face at the rate that it was loaded by new soot from the engine.
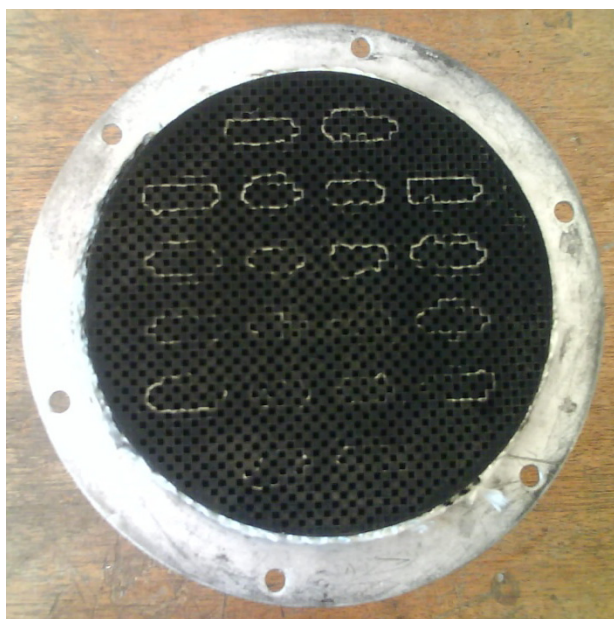
Figure 8.15 Front face of filter from the flow-rig test showing regenerated regions

The result of the combination of these factors was that the regeneration system was unable to maintain active regeneration throughout the engine tests. The parasitic losses prevented the power supply from achieving breakdown by reducing the peak output voltage. Increasing the output transformer drive level had previously been shown (Proctor, 2007) to cause damage. The only way to ensure breakdown would be to further reduce the electrode spacing resulting in a loss of regeneration performance and increased system complexity as explained in Chapter 5.

8.8 Summary of System Developments

This section summarises the developments made to aspects of the Autoselective system. The reasoning behind the decisions is also briefly summarised. A full explanation can be found in Chapters 3, 4, 5 and 7.

8.8.1 Electrode Type

Early testing used single copper wires as electrodes, although this resulted in preferential regions of regeneration. This was found to be caused by a combination of the variation in distances between the high voltage electrode, channel wall and the ground electrodes. The electrode spacing was made uniform and symmetrical to reduce preferential cleaning radial to the high voltage electrode. Further improvements were required, especially when using smaller electrode spacings. The electrodes needed to have a uniform even contact with the channel walls. A spring electrode was therefore chosen, as explained in Chapter 5, because it was readily available, easy to locate in the channel and did not block gas flow.

8.8.2 Electrode Geometry

Wide electrode spacing caused initial problems with filter damage and poor distribution. The checkerboard electrode array reduced the channel spacing to a single channel. Regeneration distribution was then uniform and damage could be alleviated using on- and off-times and low current levels. However, regeneration performance was reduced by the close electrode spacing. Results showed that a channel spacing of 6 would be most desirable, as described in more detail in Chapter 5.

8.8.3 Current Waveform

The results showed that a low discharge current level would result in better regeneration efficiency and distribution but lower regeneration rate. Discharges above 15 mA caused rapid filter melting damage as described in Chapter 5. Currents

< 5 mA were not possible for normal atmospheric glow discharges within the filter. A discharge current of 10 mA was therefore chosen for subsequent tests. Discharge frequency needed to be < 100 kHz to reduce the effect of capacitance but > 1 kHz to avoid excessive blow-through (detailed in Chapter 7). A discharge frequency of ~20 kHz was found to be convenient and effective. No advantages were found whilst testing different waveform shapes or frequencies.

The 10 mA discharge required a low transformer primary voltage level to sustain it (≈ 50 V). This amplitude did not provide sufficient secondary voltage to break down wide spaced electrodes. A new power supply which allowed transient control of the primary voltage level was built and details can be found in Chapter 3 and Appendix I. Higher amplitudes were used during the breakdown transient, this allowed a 10 mA discharge to be sustained between wide spaced electrodes.

8.8.4 On- and Off-times

The on- and off-times were chosen to avoid filter damage whilst maximising duty cycle to produce an adequate regeneration rate. A 10 mA discharge had a maximum duty cycle with about 40 ms on and 50 ms off and this research is detailed in Chapter 5.

8.8.5 Increasing Channel Spacing

The linear electrode array was re-tested with the new transient power supply set to 10 mA, 40 ms on and 50 ms off. The breakdown could be initiated over 10 channel spacings but the transition to glow discharge did not occur unless the channel spacing was < 6. The discharge was observed to extinguish prematurely during the on-time if there was flow through the channels. Additional higher power frequency swept breakdown pulses were added after 20 ms into the on-time which helped to re-ignite extinguished discharges. The channel spacing was reduced to further improve regeneration reliability resulting in approximately 50% less regeneration performance (as described in Chapter 5). A channel spacing of three channels produced favourable flow-rig testing. However, during engine trials the discharge failed to initiate correctly. This was primarily due to the grounded front face soot layer which

was continuously increasing in thickness. One possible solution would be to further reduce the electrode spacing to 2, this would result in a further reduction in regeneration performance between 20 and 50%.

8.9 Chapter 8 Conclusions

The Autoselective regeneration technology was tested over a range of potential settings and electrode arrangements. The final testing of the system used settings and hardware that were chosen based on several fundamental studies (as described in Chapters 3, 4, 5 and 7). A successful regeneration was achieved during an on-engine test using a close-spaced electrode array. This type of array had unfavourable drawbacks and was replaced with a wide spaced electrode array. The wide spaced array was successfully tested in a flow-rig environment but failed to perform on an engine. The reasons for the difference in performance show that closer electrode spacings are required. The resulting drawbacks of this would, at this stage in the development, make the system un-attractive for commercial on-vehicle heavy duty diesel applications. Improvements to the performance could be made using different filter materials. A detailed description of the recommended future research is given in Chapter 9.

9. Conclusions

This chapter presents the conclusions from the research towards the optimisation and implementation of the Autoselective regeneration method. The main conclusion of this thesis is that new filter materials and geometries need to be considered in order to make a system that can fully compete with existing diesel particulate filter regeneration technology.

9.1 Research Summary

The literature survey revealed that there was a need for low power electrical regeneration systems to compete with existing direct fuel powered and catalyst methods. A new concept of diesel particulate filter regeneration using atmospheric glow discharges was investigated called the Autoselective system. The system used a cordierite wall flow filter with inserted wire electrodes to produce electric discharges inside the filter volume. The discharge current waveform was studied to determine the effect on the regeneration performance. The types of electrodes and their placement within the filter were investigated. The effect of the discharge on filtration performance was studied and a new method of reverse flow regeneration was identified. The Autoselective electric discharge was analysed to find the energy balance as it regenerated the filter. Filter damage by the discharge was characterised and avoided using a novel power modulation strategy. The mechanism of filter damage was studied and a model was created and validated. The model allowed other filter materials to be compared without requiring test samples. The highly optimised system was used for flow-rig and engine testing using the test power supplies designed and built as part of the research. Successful filter regeneration was shown to be possible during engine operation.

9.2 Conclusions

This research investigated the Autoselective regeneration system for use with the cordierite wall flow filter. The key conclusions drawn from the research are as follows:

1. Using inserted electrodes with the wall flow filter results in electrode capacitances in excess of 10 pF per electrode. This relatively high capacitance complicates the power supply requirements due to the capacitive current flow.

2. High frequency operation (>100 kHz) was inefficient due to the electrode capacitance. Operation from 10 kHz to 30 kHz was best achieved using a resonant transformer. This resulted in a transformer for each high voltage output.

3. The resonant frequency of each transformer was different due to the component and system tolerances and because the electrode capacitances changed with filter loading. Electrical breakdown between the electrodes was achieved by operating close to resonance. Using a single frequency for all the transformers resulted in unreliable breakdown for those not close to their resonant frequency. Sweeping the frequency made it possible to operate with a single controller.

4. Certain electrode geometries required some high voltage electrodes to be un-powered while neighbouring electrodes were on. This required the use of phased electrodes. Two phases of electrodes were required to operate a linear electrode array.

5. Lower operating currents gave better distribution and effectiveness, 10 mA was chosen as the optimum as this was the lowest current that could produce a stable glow discharge within the filter. The power supply could not breakdown the gap between the electrodes at this current level so a high amplitude current pulse had to be superimposed on the current waveform to start the discharge. This was shown to be achievable using a novel pulse width modulation based transformer drive capable of fast transient current modulation.

6. Capacitive stabilisation of the discharges allowed multiple discharges to be powered from a single voltage source. A novel method of analysis showed that capacitive stabilisation was limited to the range 1 kHz to 4 kHz due to the electrode capacitance. In practice, the requirements for capacitive stabilisation made it an unattractive practical choice (voltages ≈ 50 kV were required).

7. The discharge current optimisation showed no clear optimum for regeneration performance in terms of frequency, crest factor or on- and off-times. A range of values was shown to be suitable and the operating point should be decided based on other factors such as power supply topology and filter damage thresholds.

8. The discharge current level was important in determining regeneration performance. Low currents had much higher regeneration effectiveness $(g.kW^{-1}.h^{-1})$ but lower regeneration rate $(g.h^{-1})$.

9. Power modulation can be used to prevent damage to the filter by the heat from the discharge. Turning the discharge on and off with accurate timing was shown to be a suitable modulation method. The regeneration rate was shown to be proportional to the duty cycle. A range of on- and off-times were tested with different current levels, the highest duty cycle for the 10 mA case was produced by 40 ms of on-time followed by 50 ms of off-time. This gave the highest damage-free performance possible for a cordierite filter of 100 cells per square inch.

10. The system could be operated with a close electrode spacing to give a high regeneration rate and uniform regeneration distribution. This implementation was demonstrated on a diesel engine and flow-rig trials with a constant back-pressure trace from the filter indicating continuous filter regeneration. This implementation required 600 electrodes and 60 power supply outputs making the implementation cumbersome and difficult to assemble. The close spaced electrode array gave poor regeneration effectiveness $(< 5 \ g.kW^{-1}.h^{-1})$.

11. The system was demonstrated on a flow-rig using a wide spaced and highly optimised linear array. Excellent performance in terms of regeneration rate, effectiveness and distribution was achieved with only 20 power supply outputs and 150 electrodes being required for a 5.66" diameter filter. This implementation, however, failed to give comparable results during engine testing due to the higher parasitic electrical losses experienced during engine tests.

12.   The electrode spacing was shown to be critical to both regeneration rate and effectiveness. Electrode spacings of at least 3 filter channels were shown to be needed to make a competitive system.

13.   The effect of the discharge on filtration efficiency was investigated. The breakdown transient was shown to be responsible for dislodging soot from the filter surfaces. This was shown to be due to the expanding gas caused by the rapid heating by the discharge at breakdown. The electrostatic forces were also shown to have secondary effects on the loosened particulate.

14.   Deliberately applied electrical breakdowns between inserted electrodes were shown to be a highly effective method for removing soot when used in conjunction with a reverse flow. The regeneration performance measured during basic tests was higher than the Autoselective system. A novel, low power regeneration method was therefore identified for use as an 'end of shift' or dual-filter regeneration system and this is the subject of on-going research.

15.   The Autoselective discharge was analysed to determine the energy balance. The results showed that little of the energy went to heating the soot and that the energy released by the soot was significant and comparable to the discharge electrical power. The results showed that performance enhancements could be made by using electrodes made with specialised materials or coatings to reduce the discharge energy consumption.

16.   The energy balance results, supported by the electrode spacing results, showed that the regeneration performance could be increased by at least a factor of two through segmenting the discharge as it traversed the electrode gap. This occurred naturally in loaded filters since the discharge path was broken up by the filter walls.

17.   Filter damage was classified into ambient and discharge derived damage, the latter was further sub-divided into surface pitting, glassing and pin-holing.

18.   A discharge model was developed using basic assumptions, the model can be used to compare filter materials for suitability. The initial modelling showed that mullite ceramic filters would be more suitable than cordierite. The model used transient power data from a transient damage test, the transient data for other materials can also be incorporated into the model to improve its accuracy.

9.3 Recommended Further Work

This section lists the potential research areas identified during this work. It is hoped that the work presented in this thesis might facilitate the future work in these areas.

a.   Investigation of the electro-acoustic reverse flow regeneration method. A new method of reverse flow filter regeneration was found whilst investigating particulate re-entrainment. This method was provisionally shown to exceed the performance of the Autoselective system. Further investigation is essential to confirm the initial findings and assess any opportunities for the new technology.

b.   Investigation of new filter materials for Autoselective regeneration. The modelling work suggests that cordierite is a poor material choice because of its susceptibility to filter damage. Other filter media are available and further investigation is needed to determine whether they can be used with the Autoselective system. The modelling work can be used to approximate the optimal on- and off-times used without the need for testing. More advanced filter materials could make the system work with larger channel spacings which would simplify the design and attractiveness of the regeneration system.

c.   Investigation of new filter geometries for Autoselective regeneration. The modelling and energy balance measurements showed that new filter designs could be used to prevent filter damage and increase performance without the need for more expensive materials. The damage modelling showed that the filter was much less susceptible to damage if the discharge did not pass through the filter wall. The energy balance showed that creating segmented discharge paths

increased regeneration performance. A more robust regeneration system could be made if a filter was designed such that the discharge path was broken up by air gaps with no current paths through the filter.

d. <u>Filter soot loading sensors</u>. The results obtained for the electrode capacitance versus loading show an increase in electrode capacitance with filter loading. This property indicates that the electrode could be used as a soot loading sensor. The sensor would be a low cost alternative to other technologies.

References

Agarwal A.K., Singh A.K., Sinha S. and Shukla M.K. (2004) Effects of ERG on the exhaust gas temperature and exhaust opacity in compression ignition engines. *Sadhana, Vol. 29, Part 3,* pp.275 – 284.

Amer E., Gren P. and Sjödhal M. (2008) Shock wave generation in laser ablation studied using pulsed digital holographic interferometry. *Journal of Physics D: Applied Physics, Vol. 41, 215502.*

Alshayji A. E. (2009) Mixing Layer Analysis in Variable Density Turbulent Flow. *Proceedings of the COMSOL Conference Boston, 2009.*

An H., Kilroy C. and McGinn P.J. (2005) An examination of microwave heating to enhance diesel soot combustion. *Thermochimica Acta 435,* pp 56 – 62.

Bauchire J., Bertrand E. Izarra C. (2009) Numerical Modelling of a Free-Burning Arc in Argon. A Tool for Understanding the Optical Mirage Effect in a TIG Welding Device. *Proceedings of the COMSOL Conference Milan*, 2009.

Baulig A., Sourdeval M., Meyer M., Marano F. and Baeza-Squiban A. (2003) Biological effects of atmospheric particles on human bronchial epithelial cells. Comparison with diesel exhaust particles. *Toxicology in Vitro, Vol. 17,* pp 567 – 573.

Bianchi D. (2005) Catalytic Oxidation of a Diesel Soot Formed in the Presence of a Cerium Additive. III Microkinetic-Assisted Method for the Improvement of the Ignition Temperature. *Energy & Fuels, Vol. 19,* pp 1453 – 1461.

Bosch Automotive Handbook (2004). Multiple Authors. Published by Robert Bosch GmbH. *ISBN 1-86058-474-8*.

Boynton W. P. (1904) The Conductivity of a Spark-Gap, *The American Physical Society.*

References

_____

Braginskii S.I. (1958) Theory of the development of a spark channel. *Soviet Physics Jetp, Vol. 34(7), No. 6,* pp 1068 – 1074.

Clague A.D.H., Donnet J.B., Wang T.K. and Peng J.M.C. (1999) A comparison of diesel engine soot with carbon black. *Carbon 37, 1553 – 1565.*

Conway R., Chatterjee S., Beavan A., Lavenius M., Viswanathan S. and Walker A. (2005) Combined SCR and DPF Technology for Heavy Duty Diesel Retrofit. *SAE Paper 2005-01-1862.*

Crane R.I. and Wisby P. (2000) Light-duty diesel exhaust after-treatment by multicyclone particulate separator with and oxidation catalyst. *Proc Instn Mech Engrs Vol 124, No.7, Part D*, p 741-749.

Deng E.E. (1996) Negative Incremental Impedance of Fluorescent Lamps. *PhD Thesis of California Institute of Technology.*

Dori R. and Kushner M.J. (2002) Repetitively pulsed plasma remediation of NOx in soot laden exhaust uing dielectric barrier discharges. *Journal of Physics D: Applied Physics, Vol. 35,* pp 2954 – 2968.

Doumeki R., Kodama K., Hiranuma S., Takeda Y. and Iwata T. (2006) Development of DPF Systems for Commercial Vehicles – Pre-Catalyst Supporting to Active Regeneration. *SAE Paper 2006-01-1529*.

Farnoud A., Huang C. and Armendariz A.J. (2008) Using electrostatic precipitation to control diesel exhaust particulate emissions. *12th U.S./North American Mine Ventilation Symposium 2008.* ISBN 978-0-61-20009-5.

Farzaneh M., Allaire M.A., Marceau K. and Lachlance P. (1994) Electrostatic capture and agglomeration of particulates emitted by diesel engines. *IEE 0-7803-1993-1/94*, pp 1534-1537.

Garcia E., Osendi M.I. and Miranzo P. (2002) Thermal diffusivity of porous cordierite ceramic burners. *Journal of Applied Physics, Vol. 92, No. 5,* pp. 2346 – 2349.

Garner C.P. and Dent J.C. (1989) Microwave Assisted Regeneration of Diesel Particulate Traps. *SAE Paper No. 890174.*

Garner C.P. and Dent J.C. (1990) Development of a Microwave Diesel Particulate Trap Regeneration System. *XXIII Fisita Congress, Torino, Italy, 905116.*

Green J.B., Story J.M. and Wagner R.M. (2001) Microwave-Regenerated Diesel Exhaust Particulate Filter. *Society of Automotive Engineers, Paper No. 2001-01-0903*.

Hammer T. (2002) Non-thermal plasma application to the abatement of noxious emissions in automotive exhaust gases. *Plasma Sources Science and Technology, Vol. 11, A196-A201*.

Haverlag M., Kraus A., Sormani J., Heuvelmans J., Green A., Kaldenhoven L. and Heijne G. (2002) High-frequency cold ignition of fluorescent lamps. *Journal of Physics D: Applied Physics, Vol. 35,* pp 1695 – 1701.

Heering W (1977) Simulation of the Dynamic Behaviour of High Pressure Discharge Lamps. *Applied Physics A: Materials Science & Processing, Vol.12, No 4,* pp 321 - 325.

Herrick P.R (1980) Mathematical Models for High-Intensity Discharge Lamps. *IEEE Transactions on Industry Applications, Vol. IA-16, No. 5* pp. 648 – 654.

Heywood J.B. (1988). "Internal Combustion Engine Fundamentals." McGraw-Hill Inc. *ISBN 0-07-100499-8, 1988.*

References

Hu Y (2001) Analysis and Design of High-Intensity-Discharge Lamp Ballast for Automotive Headlamp. *PhD Thesis of Virginia Polytechnic Institute and State University.*

Iranmanesh M., Subrahmanyam J.P., Babu M.K. **(2008)** Simultaneous reduction of Smoke and NOx emission of diesel and biodiesel fueled engines by using Diethyl Ether as supplementary oxygenated fuel. *15th ISME International Conference on New Horizons of Mechanical Engineering, 18-20, pp270 – 279, ISBN: 8188901342.*

Jacobs T., Chatterjee S., Conway R. and Walker A. (2006) Development of Partial Filter Technology for HDD Retrofit. *SAE Paper 2006-01-0213.*

Johnson T.V. (2006) Emission Control in Review. *SAE Technical paper series 2006-01-0030* .

Jung H., Kittelson D.B. and Zachariah M.R. (2005) The influence of a cerium additive on ultrafine diesel particulate emissions and kinetics of oxidation. *Combustion and Flame, Vol. 142, pp. 276 – 288.*

Kagawa J. (2002) Health effects of diesel exhaust emissions – a mixture of air pollutants of worldwide concern. *Toxicology 181 -182, pp 349 – 353.*

Kandylas I.P. and Koltsakis G.C. (2002) Simulation of continuously regenerating diesel particulate filters in transient driving cycles. *Proc. Instn. Mech. Engrs. Vol. 216 Part D:J Automotive Engineering, pp 591 – 606.*

Kelly, D.W., Reddoch T.W. and Kelly-Wintenberg K. (2003) Reducing Soot Emissions from Diesel Engines Using One Atmosphere Uniform Glow Discharge Plasma. *SAE Paper 2003-01-1183.*

Kitamura T., Ito T., Senda J. and Fujimoto H. (2001) Potentiality of Oxygenated Fuels on Soot-Free Diesel Combustion. *Proceedings of Busan Engine International Symposium Dec 12-14 2001 p.155.*

References
_____

Kittelson D.B (1998) Engines and nanoparticles: a review. *Elsevier Science Journal of Aerosol Science Volume 29, Issues 5-6, 1 June 1998, Pages 575-588.*

Kittelson D.B., Watts W.F. and Johnson J.P. (2002) Diesel Aerosol Sampling Methodology-CRC E-43 Final Report. *Coordinating Research Council, Alpharetta, GA.*

Kittelson D.B. (2008) Physics of solid particles emitted by IC-engines. *Course on Ultrafine Diesel Particles and Retrofit Technologies for Diesel Engines, Nov 12th 2008.*

Kogelschatz U. (2004) Atmospheric-pressure plasma technology. *Plasma Physics and Controlled Fusion, Vol. 46, pp B63 – B75.*

Kolke R., Schrewe K., Steigert S., Fahrseugtechnik H.J.S *(editors)* **(2004)** Particluate Emission Filters and their Contribution to Diesel Emission Control. *Article for the AVL Particulate Symposium, 3rd International Exhaust Gas and particulate Emissions Forum, CD Proceedings, pp 244-257.*

Koltsakis G.C. and Stamatelos A.M. (1996) Modeling Thermal Regeneratioin of Wall-Flow Diesel Particulate Traps. *Reactors, Kinetics and Catalysis, American Institute of Chemical Engineers Journal, Vol. 42, No. 6, pp 1662 – 1672.*

Koltsakis G.C., Katsaounis D.K and Samaras Z.C. (2006) Filtration and Regeneration Performance of a Catalyzed Metal Foam Particulate Filter. *SAE Paper 2006-01-1524.*

Koltsakis G.C., Konstantinou A., Haralampous O.A. and Samara Z.C. (2006) Measurement and Intra-Layer Modeling of Soot Density and Permeability in Wall-flow Filters. *SAE Paper 2006-01-0261.*

Konstandopoulos A.G and Kostoglou M. (1999) Periodically Reversed Flow Regeneration of Diesel Particulate Traps. *Society of Automotive Engineering, Paper No. 1999-01-0469.*

Kook S., Bae C., Miles P.C., Choi D. and Pickett L.M. (2005) The Influence of Charge Dilution and Injection Timing on Low-Temperature Diesel Combustion and Emissions. *SAE International 2005-01-3837.*

Kubo T., Kawada Y., Zukeran A., Ehera A., Takahashi T., Hawakami H. and Takamatsu T. (1999) Reduction of Particles and NOx Exhausted from Diesel Engine by Barrier Discharge Type ESP. *J. Aerosol Sci, Vol. 30, Suppl. 1, pp S793 – S794.*

Lakkireddy V.R., Mohammed H., Johnson J.H. and Bagley S.T. (2006) The Effects of a Diesel Oxidation Catalyst and a Catalyzed Particulate Filter on the Emissions form a Heavy Duty Diesel Engine. *SAE 2006-01-0875.*

Laskowski E.L. and Donoghue J.F (1981) A Model of a Mercury Arc Lamp's Terminal V-I Behaviour. *IEEE Transactions of Industry Applications, Vol. IA-17, No. 4, pp 419 – 426.*

Law M.C., Clarke A. and Garner C.P. (2004) The effects of soot properties on the regeneration behaviour of wall-flow diesel particulate filters. *Proc. Instn. Mech. Engrs. Vol. 218 Part D: J. Automotive Engineering, pp. 1513 – 1524.*

Law M.C., Clarke A., Garner C.P. and Williams A.M. (2008) A finite-volume-based two-dimensional wall-flow diesel particulate filter regeneration model. *Proc. Instn. Mech. Engrs. Vol. 222 Part D: J. Automotive Engineering, pp. 829 – 857.*

Leach A.G. (1993) The thermal conductivity of foams. I: models for heat conduction. *Journal of Physics D: Applied Physics, Vol. 26, pp 733 – 739.*

References

Longbao Z., Hewu W., Deming J. and Zuohua H. (1998) Study of Performance and Combustion Characteristics of a DME-Fueled Light-Duty Direct-Injection Diesel Engine. *Society of Automotive Engineers, Paper No. 1999-01-3669*.

McAdams R. (2001) Prospects for non-thermal atmospheric plasmas for pollution abatement. *Journal of Physics D: Applied Physics, Vol. 34, pp 2810 – 2821.*

Miller A.L., Stipe C.B., Habjan, M.C. and Ahlstrand G (2007) Role of Lubrication Oil in Particulate Emissions form a Hydrogen-Powered Internal Combustion Engine. *Environ Sci Technol, 41(19):6828-6835.*

Mizuno A. (2007) Industrial applications of atmospheric non-thermal plasma in environmental remediation. *Plasma Physics and Controlled Fusion, Vol. 49, A1-A15.*

Moon K. S., Choi H. D., Lee A.K. (1999) Dielectric Properties of Epoxy-Dielectrics-Carbon Black Composite for Phantom Materials at Radio Frequencies. *Journal of Applied Polymer Science Vol. 77, 1294-1302.*

Neeft J.P.A. (1995) Catalytic Oxidation of Soot: Potential for the Reduction of Diesel Particulate Emissions. *PhD Thesis, Delft University of Technology*, *ISBN 90-9008768-0.*

Nikolas S.G. and White A.D. (2006) Engine Tests of an Active Diesel Particulate Filter Regeneration Sysem. *SAE Paper 2006-01-1089.*

Ning Z. and He Y. (1999) Experimental Study on Microwave Regeneration Characteristics of Diesel Particulate After-Treatment System. *Society of Automotive Engineers, Paper No. 1999-01-1470*.

Nixdorf R.D. Green J.B. Story J.M. Wagner R.M. (2001). "Microwave-Regenerated Diesel Exhaust Particulate Filter." *SAE 2001-01-0903.*

References

_____

Nozaki T., Miyazaki Y., Unno Y. and Okazaki K (2001) Energy distribution and heat transfer mechanisms in atmospheric pressure non-equilibrium plasmas. *Journal of Physics D: Applied Physic. 34, pp 3383 -3390.*

Okubo M., Miyashita T., Kuroki T., Miwa S. and Yamamoto T. (2004) Regeneration of Diesel Particulate Filter Using Nonthermal Plasma Without Catalyst. *IEEE Transactions on Industry Applications, Vol. 40, No. 6, pp 1451 – 1458.*

Palma V., D'Amore M., Russo P., D'Arco A. and Ciambelli P. (2002) Regeneration of a soot-trap ceramic foam by a single-mode microwave cavity. *Combust. Sci. and Tech., 174 (11&12), pp 295 – 308.*

Park D.S., Kim J.U., Hyeon B.Y. and Kim E.S. (1996) Considerations on the Temperature Distribution and Gradient in the Filter During the Regeneration Process in Burner Type Particulate Trap System. *Society of Automotive Engineers, Paper No. 961978*.

Paschen F. (1889) "Ueber die zum Funkenübergang in Luft, Wasserstoff und Kohlensäure bei verschiedenen Drucken erforderliche Potentialdifferenz". *Annalen der Physik 273 (5): 69–75.*

Pavon S., Dorier J.L., Hollenstein C., Ott P. and Leyland P. (2007) Effects of high speed airflows on a surface dielectric barrier discharge. *Journal of Physics D: Applied Physics, Vol. 40, pp 1733-1741.*

Poppel M.V. and Lenaers G. (2005) Real life evaluation of the emission reduction potential of a city bus retrofitted with a continuous regenerating trap. *Atmospheric Environment, Vol. 39, pp 2451 – 2457.*

Proctor J.W. (2007). "Investigation and Development of the Diesel Particulate Filter Autoselective Regeneration System" *PhD thesis Loughborough University.*

References

Rajanikanth B.S., Das S. and Srinivasan A.D. (2004) Unfiltered Diesel Engine Exhaust Treatment by Discharge Plasma: Effect of Soot Oxidation. *Plasma Science & Technology, Vol. 6, No. 5, pp 2475 – 2480.*

Richter H. and Howard J.B. (2000) Formation of polycyclic aromatic hydrocarbons and their growth to soot - a review of chemical reaction pathways. *Progress in Energy and Combustion Science, Vol 26*, pp.565-608.

Ricoult D. (2005) Materials Engineering and New Designs for Robust Cordierite Diesel Particulate Filters. *SAE Paper 2005-26-024*.

Roth J.R. (1995) "Industrial Plasma Engineering Volume 1". IOP Publishing Ltd, *ISBN 0750303182.*

Roth J.R. (2001) "Industrial Plasma Engineering Volume 2". IOP Publishing Ltd, *ISBN 0750305452.*

Rypos Inc. (2009) Product data published and available at *www.rypos.com.*

Saha B.P., Johnson R., Ganesh I., Rao G., Bhattacharjee S and Mahajan Y (2001) Thermal anisotropy in sintered cordierite monoliths. *Materials Chemistry and Physics. 67, pp 140-145.*

Salvi S., Blomberg A., Rudell B., Kelly F., Sandstorm T., Holgate S.T.,and Frew A. (1999) Acute Inflammatory Responses in the Airways and Peripheral Blood After Short-Term Exposure to Diesel Exhaust in Healthy Human Volunteers. *American Journal of Respiratory and Critical Care Medicine, Vol. 159,* pp. 702 – 709.

Seo J.M., Chang H.S. and Kim S.K (2006) Control of a Catalyzed Diesel Particulate Filter System III (Engine Bench Accelerated Aging Test Development for a Passenger Car Catalyzed Particulate Filter System). *SAE Paper 2006-01-0422.*

References

Setiabudi A., Makkee M. and Moulijn J.A. (2003) An optimal NOx assisted abatement of diesel soot in an advanced catalytic filter design. *Applied Catalysis B: Environmental 42,* pp 35 – 45.

Singh P., Thalagavara A.M., Naber J.D., Johnson J.H. and Bagley S.T. (2006) An Experimental Study of Active Regeneration of an Advanced Catalyzed Particulate Filter by Diesel Fuel Injection Upstream of an Oxidation Catalyst. *SAE Paper 2006-01-0879*.

Son G.S., Gwak C.S., Choi E.R. and Hwang C.W. (2006) PM Reduction in Diesel Exhaust Gases with a Photocatalytic DPF Reactor. *SAE Paper 2006-01-0876*.

Song J., Alam M., Wang J. and Boehan A. (2004) Fuel Impacts on Soot Nanostructure and Reactivity. *The Energy Institute 2004 Diesel Engine Emissions Reduction Conference.*

Song I.H., Kim M.J., Kim H.D. and Kim Y.W. (2006) Processing of microcellular cordierite ceramics from a preceramic polymer. *Scripta Materialia 54, pp. 1521 – 1525.*

Staack D., Farouk B., Gutsol A. and Fridman A. (2005) Characterization of a DC atmospheric pressure normal glow discharge. *Plasma Sources Sci. Technol. Vol. 14 pp 700 – 711.*

Stein H.J. (1996) Diesel oxidation catalysts for commercial vehicle engines: strategies on their application for controlling particulate emissions. *Applied Catalysis B: Environmental 10, pp 69 – 82.*

Takesa K., Uchiyama T and Enamito S. (1991) Development of Particulate Trap System with Cross Flow Ceramic Filter and Reverse Cleaning Regeneration. *SAE Paper 910326.*

References

Thomas S.E., Martin A.R. Raybone D., Shawcross J.T., Hg K.L. and Beech P. (2000) Non Thermal Plasma Aftertreatment of Particulates – Theoretical Limits and Impact on Reactor Design. *SAE Paper 2000-01-1926.*

Uman M.A., Orville R.E. and Sletten A.M. (1968) Four-Meter Sparks in Air. *Journal of Applied Physics, Vol. 39, No. 11, pp 5162 – 5168.*

Tikhomirov K., Krocher O., Elsener M., Wokaun A., (2005). "MnOx –CeO$_2$ mixed oxides for the low-temperature oxidation of diesel soot." *Elsevier. Applied Catalysis B: Environmental 64 (2006) 72-78.*

Verderber R.R., Morse O., Rubinstein F. M. (1985) Life of fluorescent lamps opperated at high frequencies with solid-state ballasts, *IEEE-IAS LBL-19778.*

Verma D.K., Finkelstein M., Kurtz L., Smolynee K. and Eyre S. (2003) Diesel Exhaust Exposure in the Canadian Railroad Work Environment. *Applied Occupational and Environmental Hygiene, Vol 18(1), pp 25 – 34.*

Voitenko A.E. and Model I.S. (1963) Production of strong shock waves during electricaldischarges in gaps. *Soviet Physics Jetp, Vol. 17, No. 6, pp 1180 – 1182.*

Waples D.W. and Waples J.S. (2004) A Review and Evaluation of Specific Heat Capacities of Rocks, Minerals, and Subsurface Fluids. *Natural Resources Research, Vol. 13, No. 2, pp. 97 – 122.*

Weisstein E.W. (2010)
http://mathworld.wolfram.com/FourierSeriesTriangleWave.html
MathWorld.com freely available mathematical reference material.

Westbrook C.K. and Pitz W.J (2002) Motor Fuels: Energy Efficiency and Emissions in Transportation, *Washington DC, Oct 2002.*

References

Williams A.M. (2007). "Autoselective Regeneration of Gelcast Ceramic Foam Diesel Particulate Filters" *PhD thesis Loughborough University.*

Winter J., Lange H. and Golubovskii Y.B. (2008) Gas temperature in the cathode region of a DC glow discharge with a thermionic cathode. *Journal of Physics D: Applied Physics, Vol. 41, 085210.*

Wright J. and Kukla P. (2003) A Novel Electrostatic Method of Ultrafine PM Control Suitable for Low Exhaust Temperature Applications. *SAE Paper 2003-01-0771.*

Yaakov S.B. and Shvartsas M (2001) An Electronic Ballast for Fluorescent Lamps with No Series Passive Elements. *IEEE 0-7803-6618-2/01.*

Yamamoto T., Okubo M. and Kuroki T. (2003) Nonthermal Plasma Regeneration of Diesel Particulate Filter. *SAE Paper 2003-01-1182.*

Yang L.C. (1981) Diesel Particulates Destruction by Electrical Discharge Technique. *State California Air Resources Board under Contract AO-047-32.*

Zhang, Y A 2-D Diesel Particulate Regeneration Model. *Private communication.*

Zelenka P., Schmidt S. and Elfinger G. (2001) An Active Regeneration Aid as a Key Element for Safe Particulate Trap Use. *SAE Paper 2001-01-3199.*

Zelenka P., Telford C., Pye D. and Birkby N. (2002) Development of a Full-Flow Burner DPF System for Heavy Duty Diesel Engines. *Society of Automotive Engineers, Paper No. 2002-01-2787.*

Zikoridse G., Velji A. and Heidrich E. (2000) Particulate Trap Technology for Light Duty Vehicles with a New Regeneration Strategy. *SAE Paper 2000-01-1924.*

10. Appendices

Appendix I

This appendix contains details about the electronic power supplies that were designed and built during the project.

10.1 Switching Inverter

The switching inverter is used as a method of converting DC into AC. The output of the inverter is a square wave and contains a continuous spectrum of frequency components of odd multiples of the switching frequency. One application of the inverter is to allow power conversion using transformers. The main limitation of this type of inverter is that output currents out of phase with the switching waveform produce significant switching losses. This limits the maximum operating frequency when driving reactive loads such as transformers.

The circuit in Figure 10.1 is a half-bridge inverter driving a high voltage transformer, it can operate up to 40 kHz. The key components are the transistor driver, the MOSFET half-bridge and the high voltage transformer. This sub circuit is labelled the power electronics since it is responsible for the power conversion.
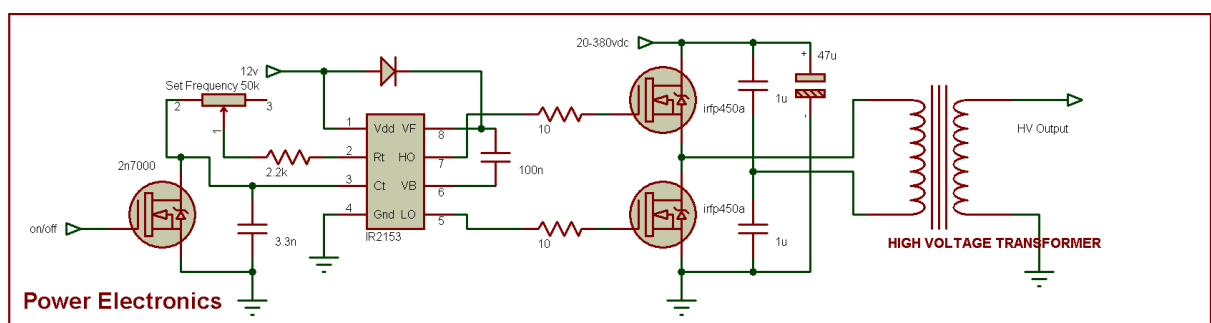
Figure 10.1 Medium frequency inverter, high voltage AC output

The supply electronics shown in Figure 10.2 provides the initial power conditioning required before each stage of the power supply. In this circuit, the supply electronics

provides a low voltage output for the timing generation and drive electronics as well as a medium current, higher DC voltage for the inverter.
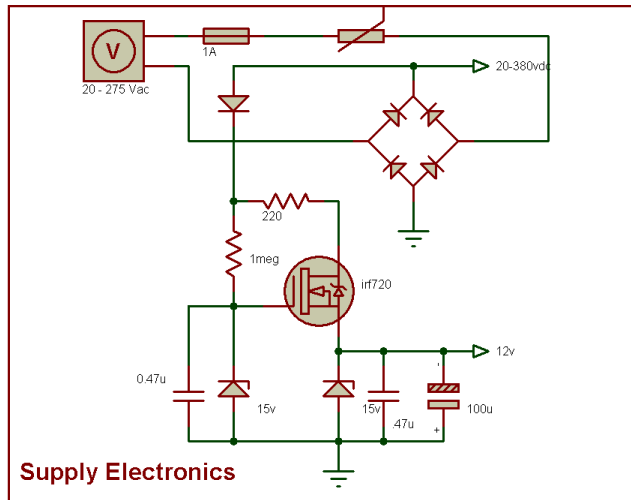

Figure 10.2 Supply electronics

The final stage of this power supply is the timing generation circuit shown in Figure 10.3 which provides the signals that turns the inverter on and off. The on- and off-time generator uses a timing integrated circuit (555 timer). This stage could also be termed the control electronics since it controls the behaviour of the power electronics. Most of the schematics in this appendix have been divided into these three categories where possible to clarify the purpose of the components used.
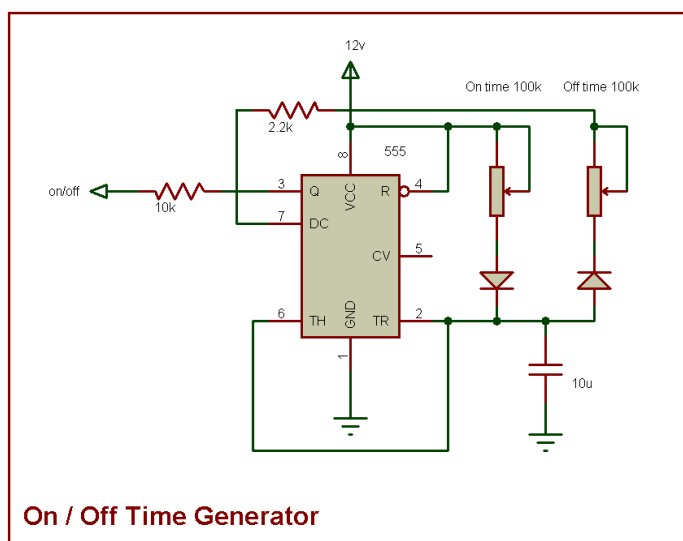
Figure 10.3 On- and off-time generation circuit

10.2 High Voltage DC Power Supply

The DC plasma used in parts of this research was powered by an adaptation of the previous inverter circuit. The DC output inverter circuit shown in Figure 10.4, it does not have the on- and off-time generation section. The output of the high voltage transformer is rectified using a bridge rectifier to produce a DC voltage that is current limited by the transformer. The diodes of the high voltage rectifier must be have high enough voltage and current ratings as well as being fast enough to rectify the 20 kHz voltage waveform.
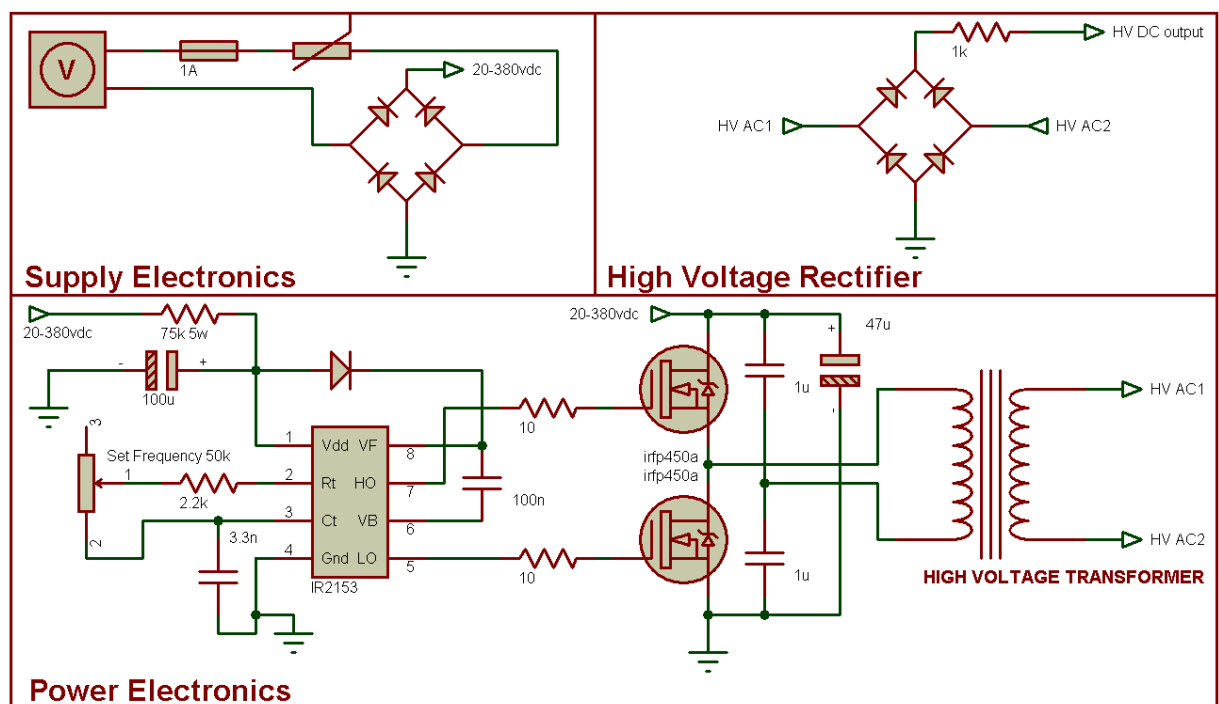
Figure 10.4 High voltage DC power supply

10.3 Low Frequency High Voltage Sine Wave Generation

A power supply was designed to produce a high voltage sine wave to power a low frequency atmospheric discharge. A simple square wave inverter output was unsuitable for this application since the resulting plasma was observed to draw more current at the harmonics of the drive frequency than at the fundamental and would not have provided useful results. A PWM method was used to create the waveform since this method was most efficient. The PWM waveform was a high frequency square wave was modulated with a low frequency sine wave, this was achieved

digitally using a microcontroller. For the modulating frequency of 1 kHz, a transformer was designed to step up the low voltage sine wave to a high voltage suitable for stabilising a discharge. A series capacitance was used to limit the current and multiple series capacitors were used to power several discharges simultaneously. The transformer frequency response was limited to 10 kHz by using stacked windings to control the transformer coupling. The switching frequency of the PWM was chosen to be much higher than the transformer bandwidth so that the transformer did not transfer it to the high voltage output. The output of the transformer was observed to be a good approximation of a sine wave. The drive electronics was operated at low voltage to simplify the process of programming the microcontroller which was done using ICSP (in circuit serial programming). A high current MOSFET driver was used which allowed operation of the half-bridge up to 100 kHz. The circuit is shown in Figure 10.5.
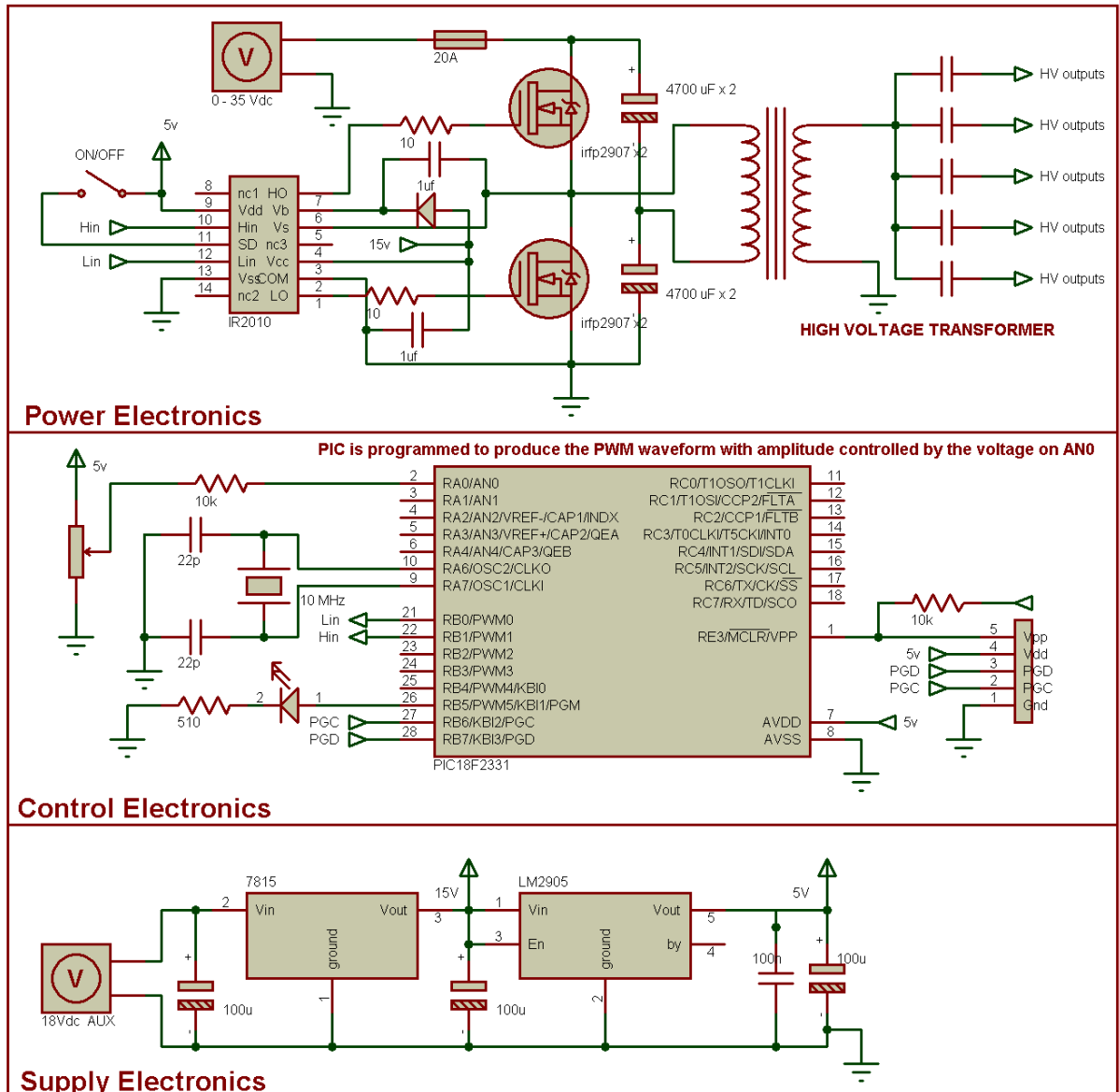
Figure 10.5 Low frequency low voltage PWM power supply

10.4 High Frequency PWM Power Supply

The low frequency power supply in Figure 10.5 was suitable for powering capacitively stabilised discharges up to 5 kHz. The Autoselective discharge normally operated from 10 kHz to 30 kHz using inductively stabilised discharges in order to keep the high voltage transformers small. In order to gain the benefits of the microcontroller controlled PWM drive strategy, a half-bridge was needed that operated at up to 300 kHz to ensure sufficient margin between the switching and modulating frequencies. Driving the transformers with a digitally synthesised PWM waveform allowed the

discharge current to be controlled quickly and accurately by the microcontroller. Since the microcontroller would be directly controlling the discharges, the Variac normally used to control the discharge is eliminated reducing weight and cost. A high frequency MOSFET based inverter was designed initially, this proved to be unreliable due to the high current transients. The MOSFET were replaced by the latest technology IGBTs recently developed for high frequency operation. The IGBTs were able to survive high current transients reliably. A power supply was built that could power twenty discharges using an array of parallel high frequency inverters, it is shown in Figure 10.7. The circuit for this supply is shown in Figure 10.6.
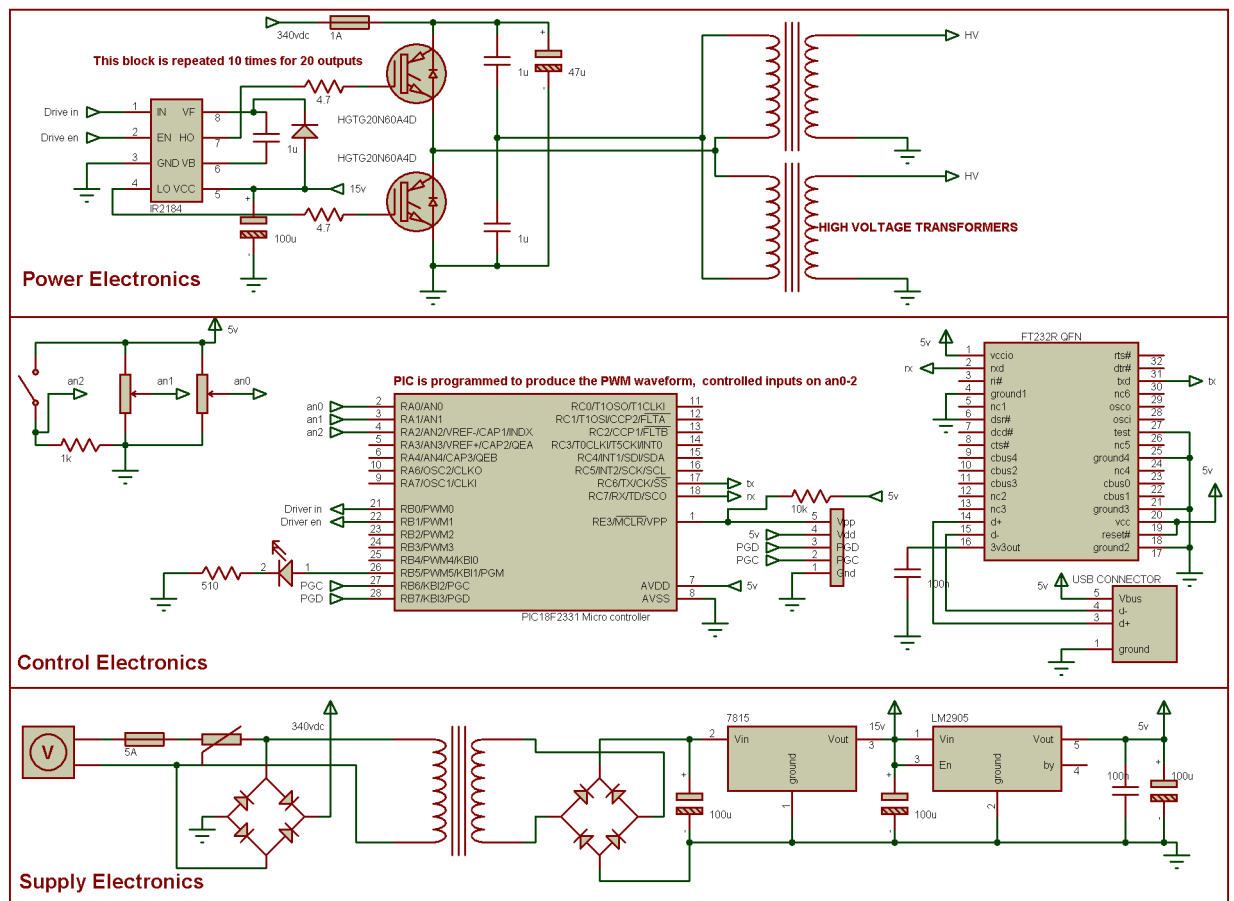
Figure 10.6 High frequency PWM power supply

Figure 10.7 Photos of the high frequency PWM supply

10.5 High Frequency Push Pull Discharge Power Supply

A power supply was designed to operate a discharge up to 1 MHz to test the effect of higher frequencies. Operation of a half-bridge at high frequencies above about 400 kHz is not achievable using conventional drive electronics, a push pull topology was therefore chosen. A microcontroller was used to synthesise the drive waveforms, this allowed stable waveforms with variable dead times to be produced. Dead time is the time added between the waveform transitions to allow the transistors to switch completely. At high frequency, accurate dead time control is essential to control switching losses. The push pull topology is often used for wide bandwidth RF (radio frequency) amplifiers up to approximately 1 GHz. RF design techniques were used to keep losses as low as possible. The circuit for the push pull amplifier is shown in Figure 10.8. Different high voltage transformers were wound to cover the frequency range 20 kHz to 1 MHz.
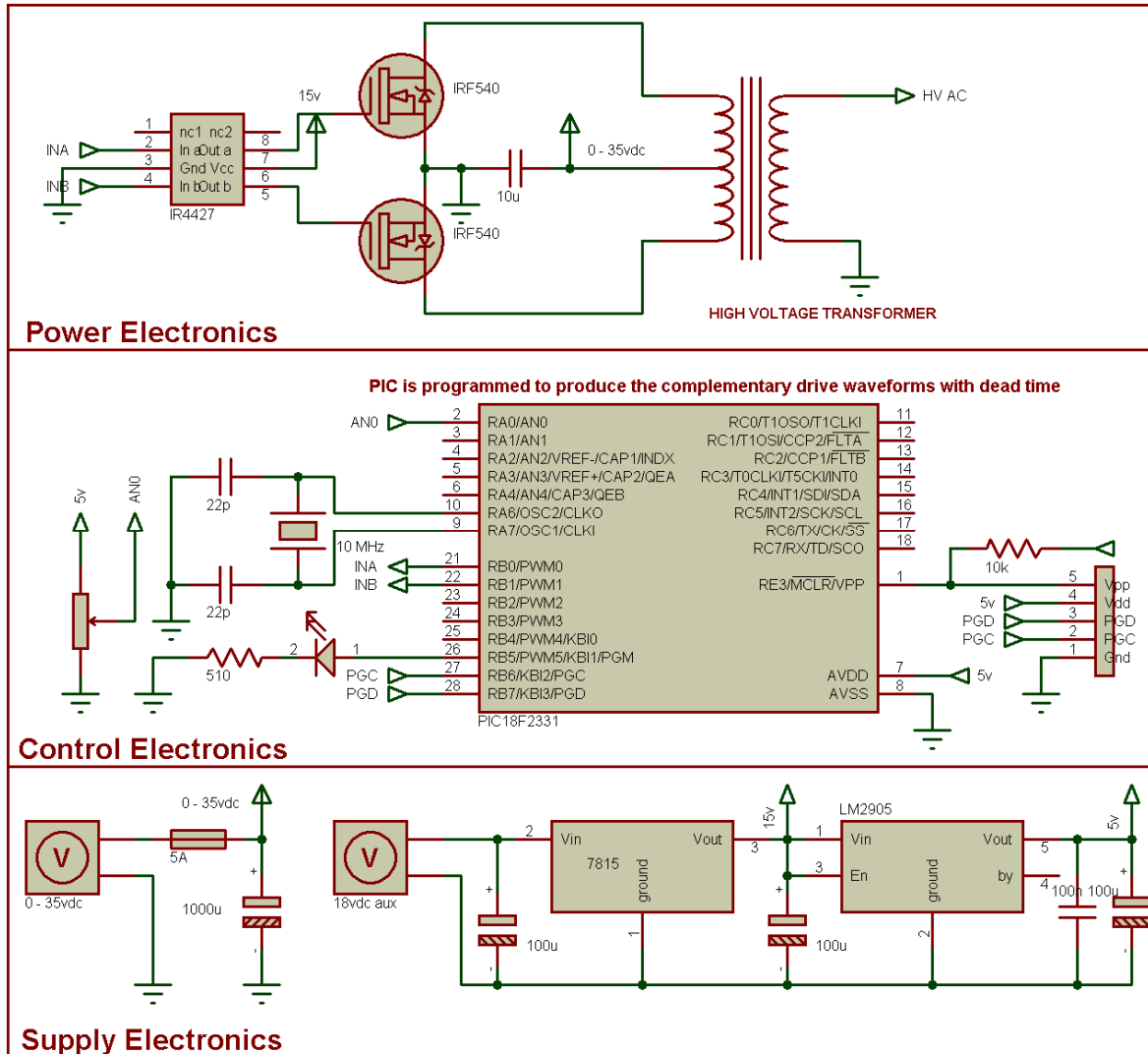
Figure 10.8 High frequency push pull discharge power supply

10.6 Class E Amplifiers for High Voltage High Frequency Discharges

A class E amplifier is a topology that can be used to efficiently power discharges above 1 MHz without significant cost or complexity. This design was used to generate discharges at 4 MHz at up to 300 W. The same topology was used to power discharges at 300 kHz and 1 kW for the discharge penetration tests into a full filter. The wide range of loads that the class E amplifier can supply makes it perfect for resonating loosely coupled air cored resonant transformers. A transformer coupling coefficient of 0.5 to 0.05 was tested with maximum efficiency occurring around 0.25. The class E driver circuit can be seen in Figure 10.9.
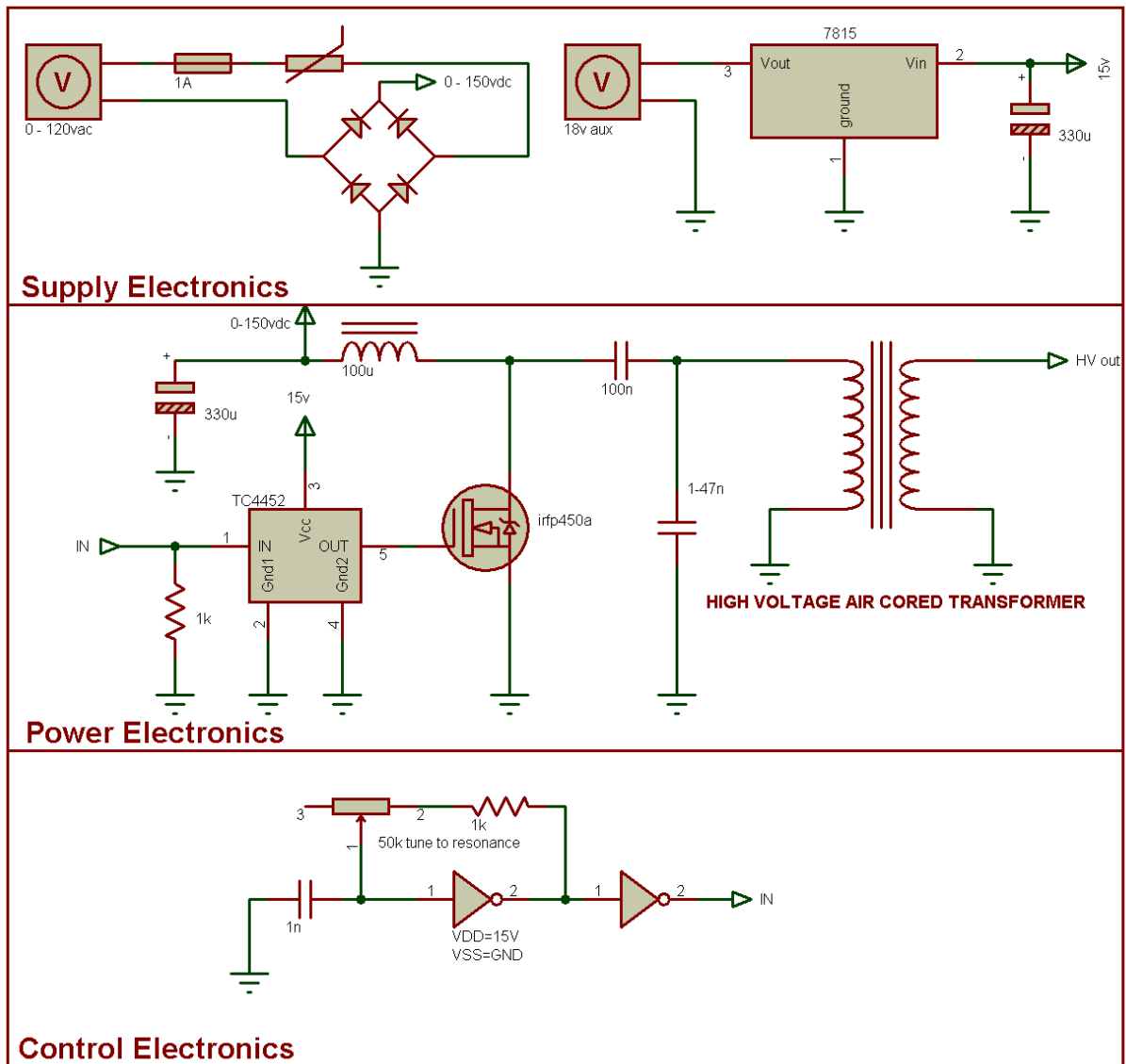
Figure 10.9 Class-E plasma power supply

The component values in the power electronic section need to be chosen for optimum efficiency at the chosen frequency. During correct class E operation, the transistor (MOSFET) is biased in class C mode (no bias current) and the input is over driven to saturate the transistor. The output network is designed so that when the transistor turns off, the output voltage (MOSFET drain voltage V_{ds}) rings and returns to zero at the instant that the transistor switches back on again for the next cycle. If this occurs, the device incurs little switching losses and the efficiency can be well over 90%. Class E amplifiers require careful tuning to achieve optimum power transfer, it is however possible to make self tuning designs. These are often the types of circuit chosen for low cost plasma applications such as plasma globes and low

voltage tube light drivers. Figure 10.10 shows such a circuit utilising a close coupled high voltage transformer. If the coupling is high (>0.8), class E operation can be achieved over a wide range of loads at the expense of output power and efficiency. The circuit shown was used to power the Autoselective discharge before a more controllable power supply was developed.
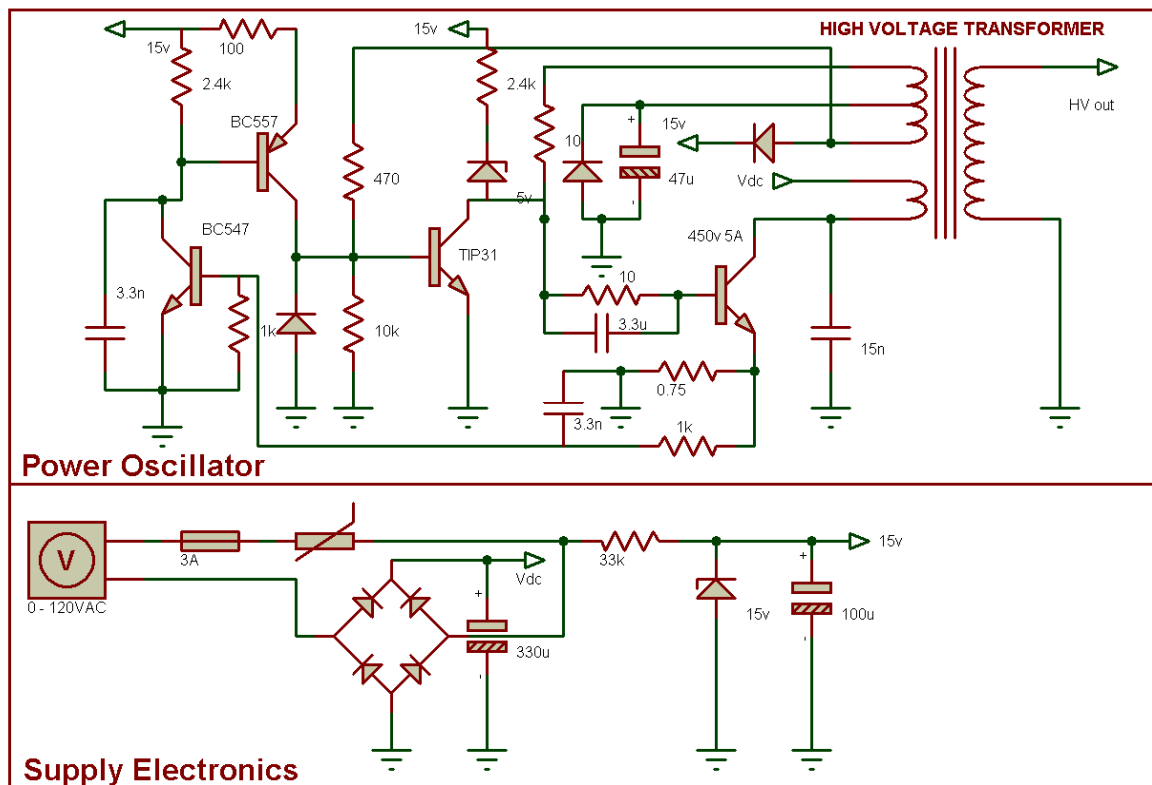

Figure 10.10 Self oscillating Class-E discharge driver

Appendix II

Wall flow filters were sectioned extensively during this research to allow inspection of the channels and to produce smaller samples of filter for experimentation. This section explains how the filter was sectioned. This information is included to make the diagrams and photographs of filter sections less ambiguous and also to ensure the research is repeatable.

10.7 The Wall Flow Filter

The wall flow filter consists of hundreds of parallel channels made from a ceramic substrate. All the channels are plugged at one end so that for the exhaust gas to flow through the channel it must pass through the porous ceramic wall, see Figure 10.11. The plugs are arranged alternately on each side of the filter so that the filter has a chess board like appearance.
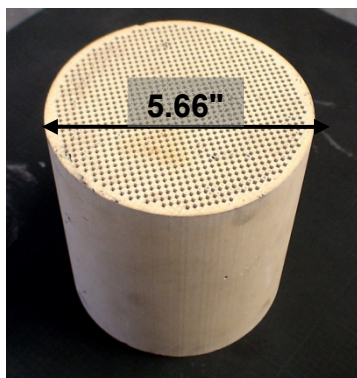
(a)
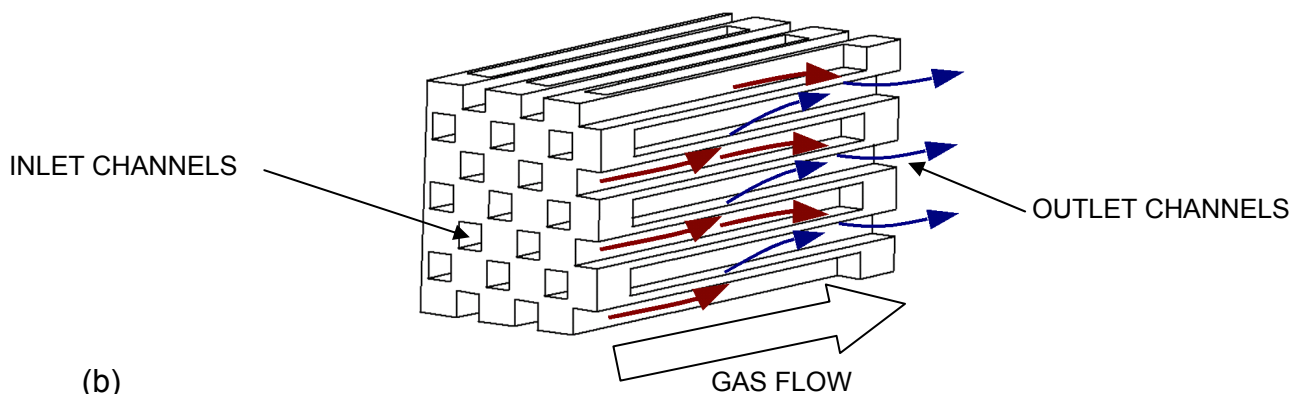
(b)

Figure 10.11 (a) A 5.66" diameter, 6" long 100 cpsi wall flow filter. (b) The wall flow filter concept, inlet airflow is forced to flow through the walls to reach the outlets

10.8 Cutting the Filter

The filter can be cut with a fine tooth metal hacksaw by hand, see Figure 10.12. The steel blade was quickly dulled by the abrasive ceramic. The sectioning produces harmful ceramic power and particulates that must not be breathed.
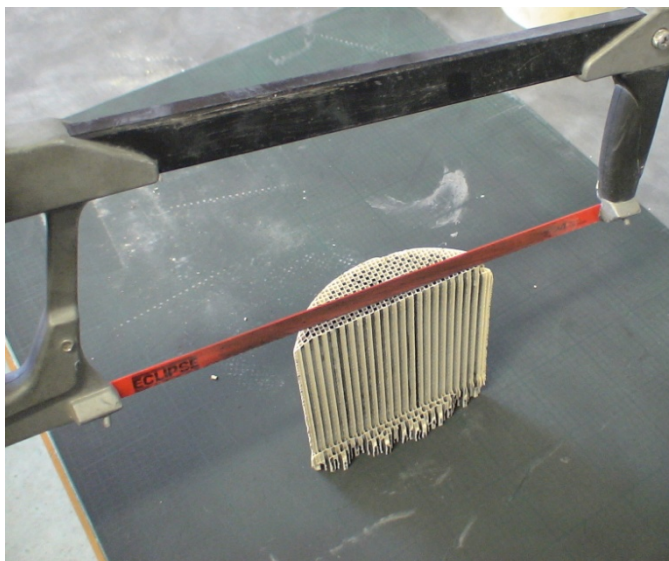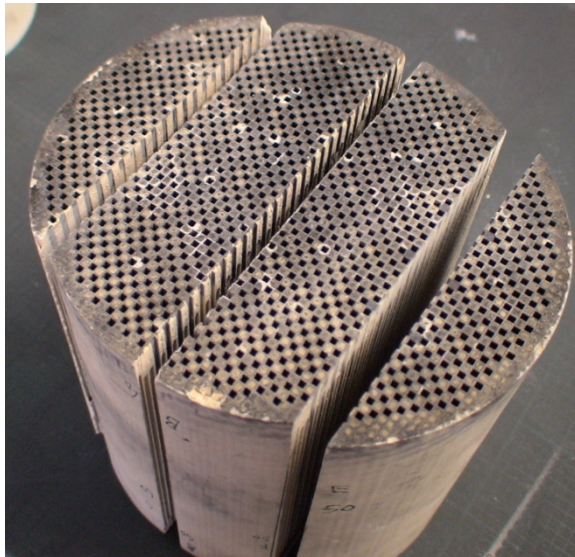

Figure 10.12 Sectioning a wall flow filter with a saw

The cement plugs at the end of the filter present the most resistance to the saw blade and were often removed leaving only the matrix of filter walls behind, see Figure 10.13. This filter section was often used when no flow is required for a test since it allowed good optical access to the inside of the filter.
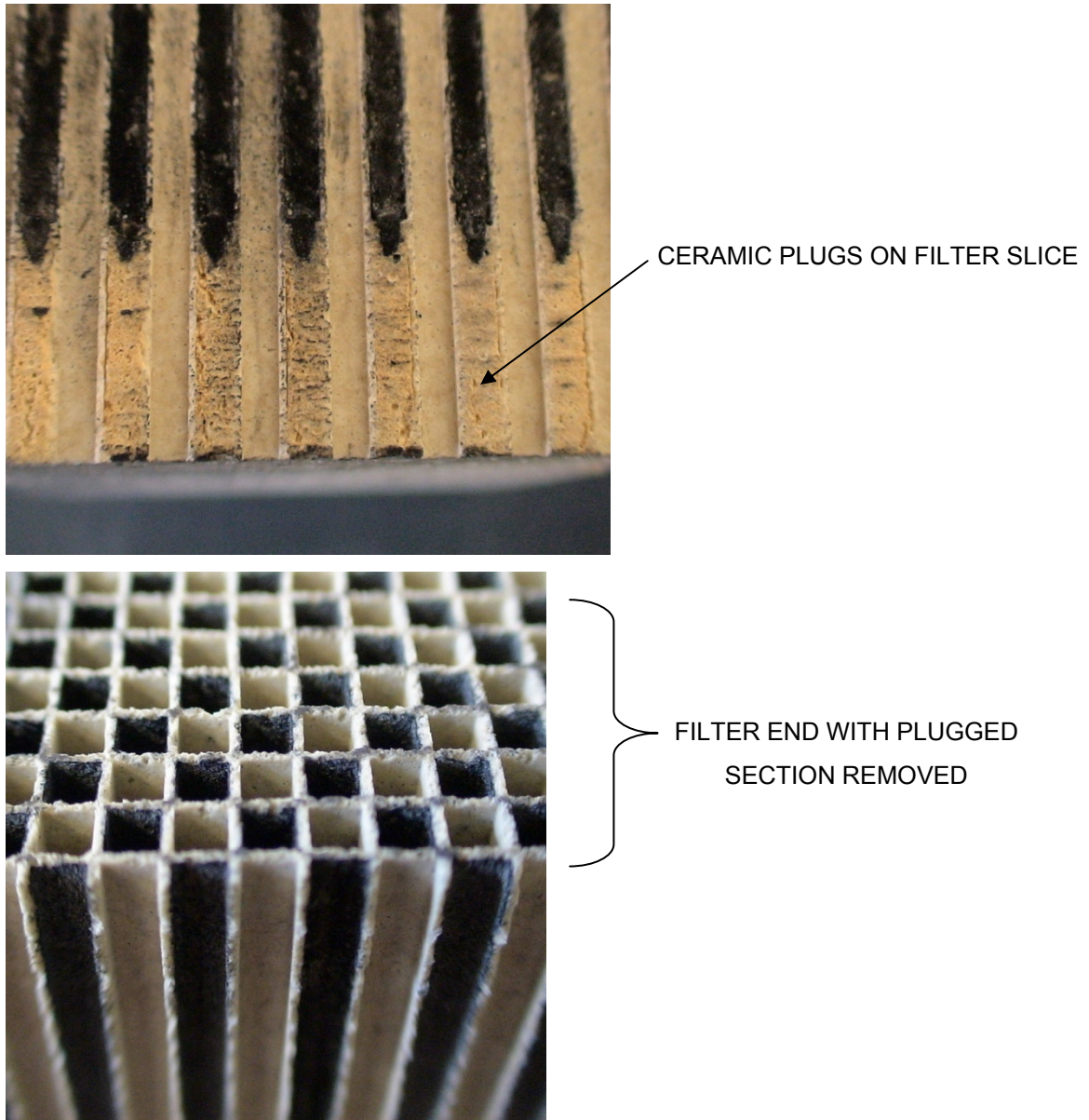
CERAMIC PLUGS ON FILTER SLICE

FILTER END WITH PLUGGED
SECTION REMOVED

Figure 10.13 Filter end plugs (left) and without end plugs (right)

10.9 Producing Useful Samples and Sections

The filter can be sliced to produce thin sections of the wall. The wall has a striped appearance due to the alternating up and downstream channels, see Figure 10.14. The thin sections of filter wall are useful for damage analysis work.
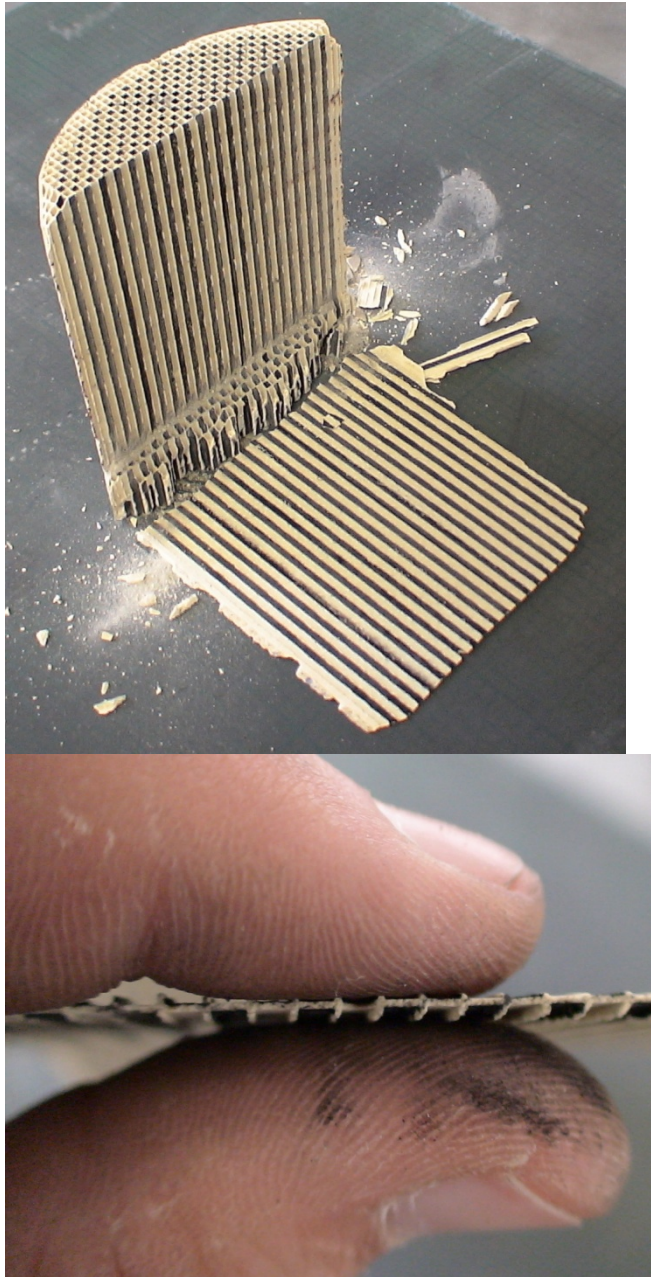
Figure 10.14 Slices of filter wall

Finally, a section can be taken perpendicular to the channel length in order to provide better optical access to the inside of the filter; see Figure 10.15. This type of section is useful when observing a discharge with the filter; the one shown is 10 mm thick.
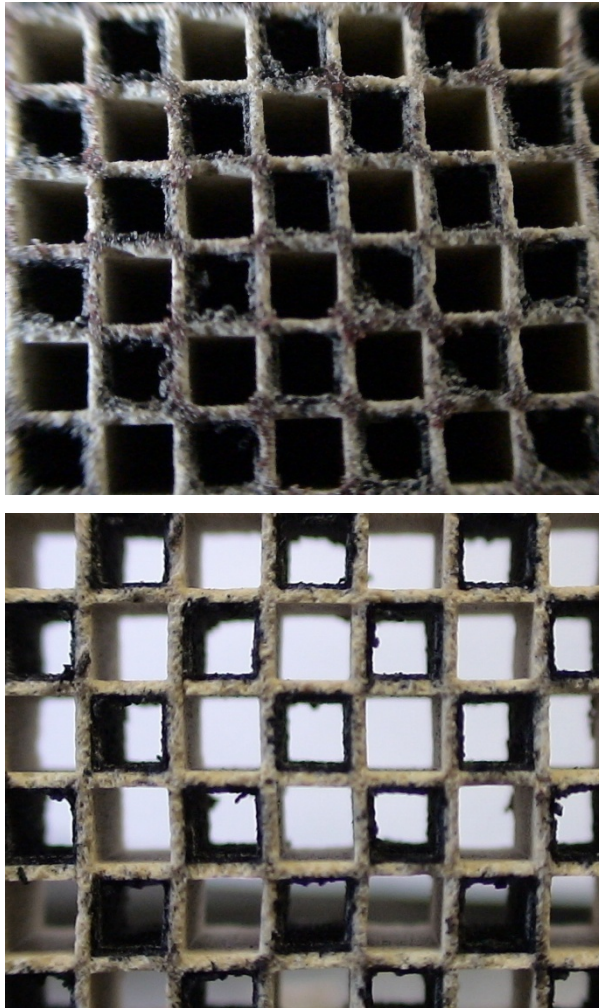
Figure 10.15 Filter sections showing improved optical access with perpendicular cut

Appendix III

This appendix presents the derivation of the equations given in the main thesis. Only the more complex derivations are shown since most of the equations are obvious.

10.10 Equation 3.3

This equation shows that the minimum inductance to achieve a stable steady state operating point for a plasma is

$$X_L \geq \sqrt{Rp \cdot Rn}$$
$$X_L = 2 \cdot \pi \cdot f \cdot L$$

where R_p and R_n are the magnitudes of the positive and negative resistances respectively as detailed in section 3.3.

Taking a voltage source with amplitude V_s at angular frequency ω driving a series combination of a discharge load and inductance L each with a voltage V_p and V_L respectively, the current I can be seen to be

$$V_s = Ij\omega L + V_d$$

and the steady state magnitude of V_s can be written as

$$V_s^2 = (I\omega L)^2 + V_d^2$$

where the discharge voltage and current are in phase at the angular frequency ω.

If a deviation to the discharge operating point occurs it can be represented as

$$V_{s\text{-new}} = (I+dI)\omega L + V_d + dV_d$$

where dI and dV_d are the changes in the current and voltage respectively. For stability to occur, increases in current (positive dI) must result in increases to V_s. I.e. The negative resistance is cancelled out such that

$$V_{s\text{-new}}^2 \geq V_s^2$$

or

$$V_{s\text{-new}}^2 - V_s^2 \geq 0$$

$V_{s\text{-new}}^2$ can be found by expanding the equation

$$V_{s\text{-new}}^2 = ((I + dI)\omega L)^2 + (V_d + dV_d)^2$$
$$V_{s-new}^2 = (I\omega L)^2 + (dI\omega L)^2 + 2dI \cdot I(\omega L)^2 + V_d^2 + dV_d^2 + 2V_d dV_d$$

which simplifies to

$$V_{s-new}^2 = (I\omega L)^2 + 2dI \cdot I(\omega L)^2 + V_d^2 + 2V_d dV_d$$

by ignoring the d^2 terms. The stability criteria is now

$$((I\omega L)^2 + 2dI \cdot I(\omega L)^2 + V_d^2 + 2V_d dV_d) - ((I\omega L)^2 + V_d^2) \geq 0$$

$$2dI \cdot I(\omega L)^2 + 2V_d dV_d \geq 0$$

$$(\omega L)^2 + \frac{2V_d dV_d}{2dI \cdot I} \geq 0$$

$$X_L^2 \geq -\frac{V_d dV_d}{dI \cdot I}$$

$$X_L \geq \sqrt{-\frac{dV_d}{dI} \cdot \frac{V_d}{I}}$$

$$X_L \geq \sqrt{R_n \cdot R_p}$$

10.11 Equation 3.6

This equation describes the required stabilising capacitance C_s required for a discharge of effective resistance R_e in parallel with a capacitance C_e and voltage supply voltage V_s and angular frequency ω. The voltage source is firstly transformed to have a single series capacitor and resistor combination where the new voltage is

$$V_{trans} = \frac{V_s C_s}{C_s + C_e}$$

and the value of the new capacitor is

$$C_{trans} = C_s + C_e$$

The load current then becomes

$$I = V_{trans} \left(R_e + \frac{1}{j\omega(C_s + C_e)} \right)$$

which expands to

$$I = \frac{V C_s j\omega}{1 + j\omega R_e(C_s + C_e)}$$

and if solved for C_s gives

$$\frac{V}{I} = \frac{1 + j\omega R_e(C_s + C_e)}{j\omega C_s}$$

$$\left| \frac{V}{I} \right|^2 = \left(\frac{1}{j\omega C_s} \right)^2 + \left(\frac{C_s + C_e}{C_s} \right)^2 R_e^2$$

$$= \left(\frac{1}{j\omega C_s}\right)^2 + R_e{}^2 + \left(\frac{C_e R_e}{C_s}\right)^2$$

$$\left|\frac{V}{I}\right|^2 - R_e{}^2 = \frac{1}{C_s}\left(\frac{1}{\omega^2} + (C_e R_e)^2\right)$$

$$C_s{}^2 = \frac{\frac{1}{\omega^2} + (C_e R_e)^2}{\left|\frac{V}{I}\right|^2 - R_e{}^2}$$

$$C_s = \frac{1}{\omega}\left(\frac{1 + (\omega C_e R_e)^2}{\left|\frac{V}{I}\right|^2 - R_e{}^2}\right)$$

Where V is the supply voltage, I is the load current, R_e is the equivalent discharge resistance, C_e is the electrode lumped sum capacitance and ω is the angular frequency.

10.12 Equation 3.12

This was solved by applying the limits to the equivalent circuit shown in Figure 3.11 of infinite frequency and zero frequency (DC). As frequency tends to infinity the equivalent circuit yeilds the value for R_p which is simply R2 i.e.

$$R2 = R_p$$

For the DC case the value of R_n is found from the parrallel combination of R1 and R2 hence

$$R_n = \frac{R1R2}{R1 + R2}$$

$$R1R_n + R_p R_n = R1R_p$$

$$R1 = \frac{R_p R_n}{(R_p - R_n)}$$

The transfer function of the discharge load can be represented using Laplace to yeid the poles and zeros by finding

$$H(s) = \frac{1}{Z_L(s)}$$

$$H(s) = \frac{sL + R1 + R2}{sLR2 + R1R2}$$

This yields the pole and zero as

$$\text{Pole} = -\frac{R_p R_n}{L(R_p - R_n)}$$

$$\text{Zero} = -\frac{R_p(1 + R_n)}{L(R_p - R_n)}$$

10.13 Equation 3.26

Refer to Figure 3.16 for notations. This equation describes the resulting sinusoidal output from a resonant circuit driven at its natural frequency.

$$V_{out} = \frac{V_{in}\text{Sin}\omega_0 t}{\left(sL + R + \frac{1}{RC}\right)sC}$$

$$= \frac{V_{in}\text{Sin}\omega_0 t}{s^2 LC + sCR + 1}$$

$$= \frac{V_{in}\text{Sin}\omega_0 t}{LC\left(s^2 + \frac{sR}{L} + \frac{1}{LC}\right)}$$

$$= \frac{\omega_0^2 V_{in}\text{Sin}\omega_0 t}{s^2 + 2\alpha s + \omega_0^2}$$

where

$$2\alpha = \frac{R}{L}, \qquad \omega_n^2 = \omega_0^2 - \alpha^2$$

$$\overline{Vout} = \left(\frac{\omega_0}{s^2 + \omega_0^2}\right)\left(\frac{\omega_0^2 V_{in}}{s^2 + 2\alpha s + \omega_0^2}\right)$$

$$= \frac{As + B}{s^2 + \omega_0^2} + \frac{Ds + E}{s^2 + 2\alpha s + \omega_0^2}$$

which solves to give

$$A = -\frac{\omega_o V_{in}}{2\alpha}$$

$$B = 0$$

$$D = \frac{\omega_o V_{in}}{2\alpha}$$

$$E = \omega_o V_{in}$$

yielding

$$\overline{Vout} = -\frac{\omega_0 V_{in} s}{2\alpha(s^2 + \omega_0^2)} + \frac{\left(\frac{\omega_0 V_{in}}{2\alpha}\right)(s + \alpha - \alpha) + \omega_0 V_{in}}{(s + \alpha)^2 + \omega_n^2}$$

$$\overline{Vout} = -\frac{\omega_0 V_{in} s}{2\alpha(s^2 + \omega_0^2)} + \frac{\left(\frac{\omega_0 V_{in}}{2\alpha}\right)(s+\alpha)}{(s+\alpha)^2 + \omega_n^2} + \frac{\frac{\omega_0 V_{in}}{2}}{(s+\alpha)^2 + \omega_n^2}$$

which solves to

$$V_{out}(t) = -\left(\frac{\omega_0 V_{in}}{2\alpha}\right) Cos\omega_0 t + \left(\frac{\omega_0 V_{in}}{2\alpha}\right) e^{-\alpha t} Cos\omega_n t + \left(\frac{\omega_0 V_{in}}{2\omega_n}\right) e^{-\alpha t} Sin\ \omega_n t$$

but for high Q factor circuits where

$Q > 10$

$$Q = \frac{\omega_0 L}{R} = \frac{\omega_0}{2\alpha}$$

$$\omega_n^2 = \omega_0^2 \left(1 - \frac{\alpha^2}{\omega_0^2}\right) = \omega_0^2 \left(1 - \frac{1}{Q^2}\right)$$

then

$\omega_0 \approx \omega_n$

and

$$V_{out}(t) \approx -QV_{in} \left(1 - e^{-\left(\frac{\omega_0 t}{2Q}\right)}\right) Cos\omega_0 t + \frac{V}{2} e^{-\left(\frac{\omega_0 t}{2Q}\right)} Sin\omega_0 t$$

which for our case can be further simplified to (because the sine term decays quickly)

$$V_{out}(t) \approx -QV_{in} \left(1 - e^{-\left(\frac{\omega_0 t}{2Q}\right)}\right) Cos\omega_0 t$$

and the amplitude becomes

$$V_{out} = QV_{in} \left(1 - e^{-\left(\frac{R n \pi}{2 L \omega_0}\right)}\right)$$

where n is an integer representing the number of half cycles of the sinusoid that have elapsed and V is the approximate waveform amplitude for that cycle.